2013-03-06

Real Time Torque and Drag Analysis during Directional Drilling

Fazaelizadeh, Mohammad

UNIVERSITY OF CALGARY

Real Time Torque and Drag Analysis during Directional Drilling

by

Mohammad Fazaelizadeh

A THESIS

SUBMITTED TO FACUALTY OF GRADUATE STUDIES

IN PARTIAL FULFILMENT OF THE REQUIREMENTS FOR THE

DEGREE OF DOCTOR OF PHILOSOPHY

DEPARTMENT OF CHEMICAL AND PETROLEUM ENGINEERING

CALGARY, ALBERTA

March, 2013

Abstract

The oil industry is generally producing oil and gas using the most cost-effective solutions. Directional drilling technology plays an important role especially because the horizontal wells have increased oil production more than twofold during recent years.

The wellbore friction, torque and drag, between drill string and the wellbore wall is the most critical issue which limits the drilling industry to go beyond a certain measured depth. Surface torque is defined as the moment required rotating the entire drill string and the bit on the bottom of the hole. This moment is used to overcome the rotational friction against the wellbore, viscous force between pipe string and drilling fluid as well as bit torque. Also, the drag is the parasitic force acting against drill string movement to pull or lower the drill string through the hole. The drill string friction modeling is considered an important assessment to aid real time drilling analysis for mitigating drilling troubles such as tight holes, poor hole conditions, onset of pipe sticking, etc. In directional drilling operations, the surface measurement of weight on bit and torque differs from downhole bit measurement due to friction between the drill string and wellbore. This difference between surface and downhole measurements can be used to compute rotating and sliding friction coefficients from torque and hook load values respectively. These friction coefficients are used as indicators for real time drilling analysis.

To do this analysis, analytical and finite element approaches were used to develop practical models for torque and drag calculations for any well geometry. The reason why two different approaches were used to develop torque and drag models is that the drill string was assumed to be soft string in the analytical approach which has full contact with the wellbore. In the finite element approach, the effect of drill string stiffness was included in the model and the drill string does not have full contact with the wellbore. Also, a new method for effective weight on the bit estimation was developed using wellbore friction model. The new method only utilizes the available surface measurements such as hook load, stand pipe pressure and surface rotation. Using the new method will eliminate the cost of downhole measurements tools and increase drilling rate of penetration by applying sufficient weight on the bit.

In this research, different effects which have great contributions on torque and drag values were investigated precisely. These effects include buoyancy, contact surface due to curve surface area,

hydrodynamic viscous force, buckling, hydraulic vibrations, adjusted unit weight and sheave efficiency.

Finally, some field examples from offshore and onshore wells were selected for model validation and verification. The field data include hook load and surface torque for different operations such as drilling, tripping in/out and reaming/back reaming.

Acknowledgments

I would like to express my appreciation to Dr. Geir Hareland for his supervision, advice, and guidance from the beginning of my study as well as giving me valuable experiences all the way through my research work, with his endurance and knowledge, while allowing me the opportunity to work independently.

I wish to thank Dr. Bernt Aadnoy, University of Stavanger, and Dr. Zebing (Andrew) Wu, University of Calgary, for their help and contributions during the development of analytical and finite element method modeling.

My gratitude also extends to Dr. Raj Mehta, Dr. Gordon Moore, Dr. Larry Lines and Dr. Mesfin Belayeneh for serving on my examination committee.

I would thank Dr. Mazeda Tahmeen and Mohammad Moshirpour for programming and software development as well as Benyamin Yadali and Patricia Teicheob for editing and proofreading of my thesis.

I am really thankful of Department of Chemical and Petroleum Engineering, University of Calgary for the giving me the chance to pursue my studies in the Doctor of Philosophy program.

Finally, I would like to thank my family, particularly my wife, Mahdieh Salmasi, for their constant support and inspiration throughout my entire studies.

Table of Contents

List of Tables

List of Figures

Nomenclature

α	Inclination angle (rad)
β	buoyancy factor
γ	Specific weight ($N/m^{3)}$
η	contact surface angle(rad)
δ	pipe-wellbore ratio
ε	rotational displacement (m)
θ	dogleg angle(rad)
μ	friction coefficient
υ	Poisson's ratio
ρ	density,(kg/m^3)
φ	azimuth angle (rad)
ψ	angle between axial and tangential pipe velocities (rad)
Ω	rotary speed, (1/sec)
Δd	clearance between wellbore and drill string (m)
ΔL	length of an element (m)
A	cross sectional area of drill string (m^2)
BHA	bottom hole assembly
C_c	mud clinging constant
C_s	contact surface correction factor
d	drill string outer diameter(m)
D	wellbore diameter(m)

DL	dogleg angle(rad)
DLS	dogleg severity(rad/30m)
DWOB	downhole weight on the bit (N)
e	sheave efficiency
E	modulus of elasticity (N/m^2)
F	axial load along drill string(N)
F_D	hydrodynamic viscous drag force(N)
F_N	normal force (N)
F_{dl}	deadline tension (N)
FF	friction force(N)
{F}	generalized nodal force vector
G	shear modulus (Pa)
g_n	gravity acceleration (9.8066 m/sec^2)
HL	hook load (N)
i	number of element
I	area moment of inertia (m^4)
J	polar moment of inertia (m^4)
k	kinetic energy (J)
[K]	system stiffness matrix
L	length (m)
$\dot{m}$	mass flow rate (kg/min)
[M]	system mass matrix
n	flow behavior index
N	number of drilling lines

N_r	rotary speed (rpm)
N_{Re}	Reynolds's number
p	potential energy (N.m)
P	pressure ($N/m^{2)}$
P_g	absolute atmospheric pressure (N/m^2)
PV	plastic viscosity (cp)
Q	volumetric flow rate (m^3/min)
r	radius of tool joint (m)
R	radius of curvature (m)
R_α	radius of bend in vertical plane (m)
R_φ	radius of bend in horizontal plane (m)
ROP	rate of penetration m/sec
S	specific gravity
SWOB	surface weight on the bit (N)
t	pipe wall thickness (m)
T	torque in string (N.m)
T_{ave}	absolute average temperature (K)
T_g	absolute atmospheric temperature (K)
U	displacement (m)
$\dot{u}$	velocity (m/sec)
$\ddot{u}$	acceleration (m/sec^2)
{u}	displacement vector
{U}	generalized nodal displacement vector
V	resultant velocity (m/sec)

v_{ae}	average effective velocity (m/sec)
v_h	hoisting velocity (m/sec)
v_p	pipe velocity (m/sec)
v_r	rotational velocity (m/sec)
w	unit weight of drill string (N/m)
W	static weight of drill string (N)

Subscripts

1	bottom of element
2	top of element
g	gas
l	liquid
m	mud
mix	mixture
w	water
x, y, z	components in x, y and z directions

CHAPTER ONE: **INTRODUCTION**

"People outside the oil and gas industry believe that most oil and gas wells are drilled vertically, in a simple straight line. In reality, most oil and gas well profiles can be anything but straight vertical. Some of them are actually tangent from the vertical and then depart in a different direction. These wells are called directional wells. The primary purpose of a directional well is to reach oil or gas targets that are underneath places that are difficult to reach such as a city or a lake as well as oil companies even drill deviated wells in order to reach several targets", Discovery Channel Online, (2011).

Figure 1.1: Schematic of directional drilling (Discovery Channel Online, 2011)

One of the advantages of directional drilling is that it provides a larger producing interval length by drilling through the reservoir at an angle. It means the larger the angles in the reservoir, the more oil and/or gas can be produced through the one wellbore. Currently, the most drilled type of directional well is the horizontal well which develops into an inclination angle around 90° from vertical. As the hydrocarbon stores horizontally in some suitable formations, it becomes interesting for the oil and gas companies to drill their oil and gas wells horizontally.

Directional drillers are given a well path by the well planner and geologist. Periodic surveys are taken while drilling to provide inclination and azimuth of the wellbore. This is typically taken between every 30 and 500 ft and most commonly every 90 ft. If the current path deviates from the planned path, corrections could be made by different available techniques. If the deviation is not that severe, the well path can be corrected by changing rotational speed as well as drill string weight and stiffness. For severe cases, introducing new downhole motor with a bent sub is the solution that is more complicated and time consuming (KFUPM online, 2011).

Two important tools are used for directional drilling. The first is the mud motor which is positioned exactly above the drill bit at the end of the drill string. The mud motor not only generates additional power through the drilling hydraulic to the bit while drilling, it can bend and turn the well in different directions. The second one is the Measurement While Drilling (MWD) which is used for constant reporting on well path changes through the use of mud impulses from down hole to surface. The MWD service will be added to update survey measurements to use for real time adjustment. Accelerometers and magnetometers measure inclination and azimuth (Halliburton Online, 2011). MWD is expensive and is not always used. Instead of MWD, the wells are surveyed after drilling through the formations and the a multi-shot surveying tools run into drill string on a wireline to measure inclination and azimuth angle at the different measured depths.

With a MWD tools, the drilling crew can guide the well toward the planned target as well as receiving the following downhole information while drilling.

- rpm at the bit
- smoothness of that rotation
- type and severity of any downhole vibrations
- downhole temperature
- bit torque and weight on the bit
- mud flow volume

The measured downhole parameters are transmitted from downhole to the surface using mud pulse telemetry. The mud pulse telemetry can be divided into three general categories: positive

pulse, negative pulse and continuous wave. The positive pulse tools work by briefly restricting the mud flow within the drill string which causes a raise in surface pressure. The negative pulse tools operate by briefly venting drilling fluid from inside of the drill string out to the annulus which causes a pressure drop that can be seen at the standpipe pressure at the surface. Finally, continuous wave tools generate the sinusoidal wave through the mud within the drill string (KFUPM online, 2011).

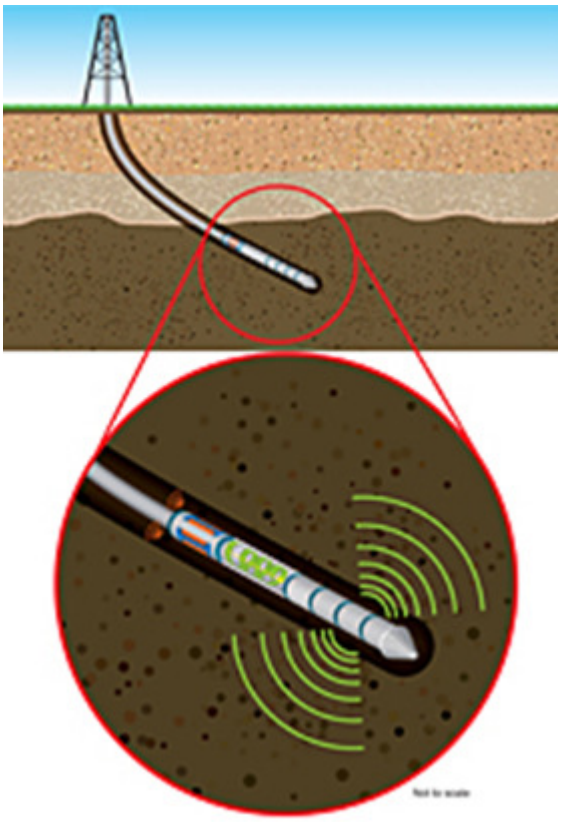

Figure 1.2: Measurement While Drilling (Soft online, 2011)

In the past decades, the reach of directional and horizontal wells has increased. Because of this evolution in directional drilling the numbers of offshore platforms to drain offshore oilfields have been significantly reduced which allows more wellheads to be grouped together on one surface location.

The friction between drill string and the wellbore which is known as torque and drag is one of the critical limitations which not allow the drilling industry to go beyond a certain measured depth. In deviated well construction, it is vital to monitor torque and drag to make sure they are in normal “acceptable” range. For this reason, the torque and drag modelling is regarded as an invaluable process to mitigate drilling problems in different stages of directional drilling. Torque and drag analysis has proven to be useful in well planning/design, real time analysis and post-analysis.

During the well planning phase the wellbore friction analysis is used to optimize the trajectory design to minimize the torque, drag and contact forces between the drill string and the borehole wall. In real time analysis, used together with monitoring of wellbore conditions during different operations, torque and drag modeling is particularly useful in diagnosing hole cleaning problems, impending differential sticking, and severe doglegs as well as determining the possibility of reciprocating casing during cementing operations. In post analysis the wellbore friction modeling helps to analyze true causes of wellbore problems that previously were unexplained or attributed to other factors such as mud weight, mud chemistry or problems related to sensitive shale formations.

CHAPTER TWO: **LITERATURE REVIEW**

To ascertain a background for this research, a study is completed in this chapter about the most important researches and studies in the area of torque and drag modeling and analysis. This chapter is divided into two different parts; one for the analytical approach which is based on the soft string theory and another is the finite element method which considers drill string stiffness in the calculations.

2.1 Analytical Modeling

In the analytical modeling the drill string is assumed to be like a cable and forces due to bending moments have not been considered to affect the normal forces as well as friction force between the drill string and the wellbore. This is fairly good assumption as it may contribute little normal forces on the overall force balance. In reality, the friction coefficient is not really a single coefficient; it is an overall factor that considers all the other different friction factors. These factors include mud system lubricity, cuttings bed, key seats, stabilizer and centralizer interaction, differential sticking, dogleg severity, hydraulic piston effect and viscous force.

For torque and drag calculation modeling, an element of the drill string is considered in the wellbore which is filled with drilling fluid. The forces acting on the pipe element are buoyed weight, axial tension, friction force and normal force perpendicular to the contact surface of the wellbore. Calculation of the normal force is the first step in calculating the friction force for an element of the drill string. The friction force is defined as an acting force against pipe movement which is equal to friction coefficient multiplied by the normal force as shown in Equation 2.1

$$FF = \mu \times F_N \tag{2.1}$$

where

FF: friction force, N

μ: friction coefficient

F_N: normal force, N

In straight inclined and horizontal sections, the normal force is equal to the normal weight of the element and there is no other contribution, but for a curved section such as build-up, drop-off, side bends and/or a combination of them, the normal force mostly depends on the tension at the bottom end of the pipe element and less on the weight of the element (Aadnoy and Andersen, 2001). The following general equation shows the force balance for an element along drill string.

$$F_2 = F_1 + Static\ Weight \pm \mu \times F_N \tag{2.2}$$

"1" and "2" represent the bottom and top locations of the drill string element where the tension force applies.

The weight and friction force of each element should be calculated and added up from bottom to the surface. In Equation 2.2, the plus and minus signs are for pipe movement either up or down. For a drilling operation, the weight on bit should be deducted from the right hand side. Fazaelizadeh et al., (2010) showed the value of weight on bit can have an effect on friction force in the curved section, which should be considered during torque and drag analysis.

Torque and drag modeling originally started by the works of Johancsik et al., (1985). Because of the simplicity and being user friendly, his work has been extensively used in the field and industry applications. Johancsik assumed both torque and drag are caused entirely by sliding friction forces that result from contact of the drill string with the wellbore. He then defines the sliding friction force to be a function of the normal contact force and the coefficient of friction between the contact surfaces based on Coulomb's friction model. He wrote the force balance for an element of the pipe considering that the normal component of the tensile force was acting on the element contributing to the normal force. This is not the case for a straight section, like in hold section. The normal force presented by Johancsik et al., (1985) is given by the Equation 2.3:

$$F_N = [\left(F_1(\varphi_2 - \varphi_1)\sin\left(\frac{\alpha_2 + \alpha_1}{2}\right)\right)^2 + \left(F_1(\alpha_2 - \alpha_1) + w\sin\left(\frac{\alpha_2 + \alpha_1}{2}\right)\right)^2]^{1/2} \quad (2.3)$$

where

F: axial force, N

φ: azimuth angle, rad

α: inclination angle, rad

w: unit weight, N/m

The above equation is then used to derive the equation for the tension increment which is applied to the drag calculations:

$$\Delta F = w\cos\left(\frac{\alpha_2 + \alpha_1}{2}\right) \pm \mu \times F_N \quad (2.4)$$

Where, the plus and minus sign allows for pipe movement direction whether running in or pulling out of the hole. Also, for the torsion increment which is used for torque calculations:

$$\Delta T = \mu \times F_N \times r \quad (2.5)$$

where

T: torque, N.m

r: tool joint radius, m

Later Sheppard et al. (1987) put the Johancsik's model into standard differential form and integrated the mud pressure that acts upward when the drill string is running inside hole. In other words he put effective tension instead of true tension and defined the effective tension as the sum of the true tension and mud pressure. He used this concept and showed that an under section trajectory could have reduced friction compared to a conventional tangent section. He also suggested that to put torque and drag into two categories separately: one caused by poor hole conditions and improper mud weight and the other associated with the well path.

Brett et al. (1989) used the Johancsik model for a field case and based on the model a well was first planned and then it was used to monitor hole conditions by back-calculating apparent friction coefficients through the whole well interval and sections with large increase in the friction factor. The friction factor can express the fact that a problem is existing in the wellbore which could be either to hole geometry (e.g., inclination and azimuth changes with dogleg) or to some other factors (e.g. problems with cuttings accumulations and hydraulics). Brett also used the model for post analysis of drilling problems by analyzing the previously drilled wells. Utilizing this information in planning gained for a better wellbore trajectory, changing of mud type and casing setting depth, raising/lowering of the kick-off point to reduce tension/torque required to drill the wellbore and changing the place of the bottom hole assembly to optimize forces in the wellbore.

In the North Sea, this development became very important not only to drain older fields more efficiently, but to reduce the number of offshore platforms in new development projects. Eek-Olsen et al. (1993) demonstrated the evolution from a 3 km horizontal reach to more than 7 km. The "Wytch Farm" project in the UK carried the length to more than 10 km horizontal reach well (Payne et al., 1995). As a quick summary this identifies the evolution within the drilling industry the past decades, from a horizontal reach of 3 km to presently approaching 12 km. The minimization of friction in the well is one of the primary issues for these extended reach wells.

Lesage et al. (1988) separated the rotating friction factor for conventional drilling or wiper trips and sliding friction factor for turbine/downhole motor drilling or tripping in/out without rotation and developed a computer model that calculates averaged axial and rotational friction factor for the complete wellbore. He and Kyllingstad (1995) discussed the relationship between torque and helical buckling in drilling.

Maidla and Wojtanowicz (1987, a) presented a method to evaluate an overall friction coefficient between the wellbore and the casing string. The computation is based on matching field data and modeling by assuming a friction coefficient. The equation for predicting surface hook loads are derived from the respective governing differential equations. Maidla and Wojtanowicz (1987, b) also presented a new procedure for wellbore drag prediction. The procedure employed iteration over directional survey points, numerical integration between the stations and mathematical models of axial loads within pipe movement in the wellbore. The model considers some new effects such as hydrodynamic viscous drag, contact surface and dogleg angle.

Maidla and Wojtanowicz (2000) used an experimental design to mimic real hole situations to measure friction factor for different mud types (i.e. oil-based or water-based) and different formation types with or without filter cake and they observed oil-based and water-based drilling fluids behave differently as the mud cake and amount of solid in the drilling fluid was changing. They observed that the presence of filter cake in water-based mud sometimes mitigates the friction by reducing the friction factor and also the solids and cuttings between pipe and borehole act as a roller bearing for string.

Luke and Juvkam-Wold (1993) investigated the effect of sheave friction in the block and tackle system of the drilling line and they concluded that hook only is a function of deadline tension, number of lines between the blocks as well as sheave efficiency and block-movement direction. It also depends on the type of deadline sheave whether active or inactive. They proposed the equations to calculate the friction from the drilling line and to modify the hook load readings. Their friction models should be used to modify the hook load measured values for torque and drag analysis.

Reiber et al. (1999) developed a computer model for on-line torque and drag analysis in which he assessed the borehole conditions based on calculation of the friction factors incrementally. The calculating routine starts by calculating the hook load and torque bottom-up at each node with the bottom-end boundary conditions to be measured downhole weight and torque on the bit. By iteratively changing the friction factor until the calculated surface load matches the measured value real time evaluations of the friction factor could be obtained. He performed the real-time calculation based on the incremental friction coefficient, in which the friction coefficient is changing during each interval and for the next interval the value from the previous interval was

assumed constant. This method starts calculations from top-hole to the bottom and this is valid if we have measured values for downhole weight and torque on the bit. He also used a single average friction factor for the entire wellbore interval which is very common in available torque and drag simulators. Wilson et al. (1992) used a torque and drag model to plan and drill two double azimuth - double S-shaped wells in Gulf of Mexico successfully by incorporating the simulated dogleg in the model properly.

Anston (1998) addressed techniques to minimize torque and drag in the wellbore including both mechanical and chemical methods. Mechanical methods are by using special equipment or tubulars in the wellbore and chemicals are for example the use of lubricants. Aarrestad (1995) discussed application of a catenary well profile in a well in the North Sea that has been introduced by Sheppard (1987) and later changed it to modified a catenary profile by Alfsen (1993) and Aadnoy (2006) which is a hyperbolic function well profile and the drill string is hanging from two fixed points. This is like an ambitious profile that almost has zero contact force with the hole wall. The modified catenary curve demands a strict adherence to low dogleg severity in the shallow part of the well and a slow increase in build rate as depth increases. Moreover Mc Clendo and Anders (1985) studied the catenary well profile and demonstrated its advantages over conventional methods. This development became very important not only to drain older fields more efficiently, but also to reduce the number of offshore platforms in new development projects. Eek-Olsen et al. (1993, 1995) and Alfsen et al. (1993) demonstrated the evolution from a 3-km horizontal well reach to more than 7 km.

Payne et al. (1998) describes concerns regarding torque and drag considerations including buckling, cuttings bed and wellbore trajectory. Lesso et al. (1989) assessed the possibility of developing nine directional wells from a single platform by analyzing previous exploration wells in a field in Canada and to minimize excessive torque in the wells which was a major concern. They planned the wells such that they have different dog-leg severity in a range that gives a reasonable torque not to exceed from its acceptable range.

Ho (1988) improved the previous soft-string model into a somehow stiff-string and showed that for most parts of the drill string the stiffness effect for drillpipe and heavy-wall drillpipe is minor and while for drillcollars is major and has to be taken into account.

Opeyemi et al. (1998) perform both well planning and drill string design by using a torque and drag analysis by considering all constrains that might be encountered during the planning phase like surface location and target coordinates, geometric specifications, casing program and geological obstacles. It also suggests that the torque and drag model which is used for planning and modeling processes should be updated with the dynamics of the field operation by performing drilling, tripping and frictional sensitivity analysis. This will ensure more precise understanding of wellbore/drill string interactions from surface to total depth. Moreover, the deployment of heavy weight drillpipe for efficient weight transfer to bit and integration into the drill string as a stiffer beam to retard drill string helical buckling was an outcome of this analysis.

Aarrestad (1990) presented a case study of effect of a steerable bottom hole assembly on torque and drag. He concluded that the crooked profile which these tools give to the well path may increase the problems associated with high torque and drag in the wellbore. An analysis of combining surface weight on the bit and bit torque and downhole measurement of these values gives a clearer picture of the drilling downhole. In this case, poor bit performance could be distinguished from other problems related to cuttings transport and differential sticking and thus the correct necessary action could be taken.

A review of design considerations and potential problems was presented by Guild et al. (1995) and later in 1996 the complete well design process had been described by Aadnoy and completed in 1998. He derived all equations for different sections of the wellbore profile including straight inclined sections and drop-off and build-up sections. He also derived the equation for a side bend to right or left in the wellbore geometry. Finally, the modified catenary profile issues had been addressed and it concluded that the developed model could be applied for a two dimensional well.

Rae et al. (2005) used a torque and drag simulator to firstly to plan a well and then used it online to calculate the hook load and torque at the surface with the model. The planned values were then compared to the field surface hook load and torque data. If the values matched it meant that the well is drilling as it was planned. Otherwise there was either a problem in the modeling or a warning to a possible problem in the wellbore was given.

Schamp et al. (2006) suggested some industrial methods to reduce torque in the wellbore during drilling. He introduced two sources of torque in the wellbore: the frictional resistance between

the rotating drill string and the casing/borehole and the bit/stabilizer torque. He proposed some methods to mitigate the frictional resistance which contained enhancing drilling fluid properties, using lubricants, adequate hole cleaning, promoting surface roughness and reducing side loads as much as possible by reducing the number of unnecessary doglegs or using rotary steerable systems which gives a smoother well path, applying a catenary well path if possible.

Mason et al. (2007) pointed out different minor effects that have to be considered in the soft-string models in order to have a more realistic model. One of these factors is hydrodynamic viscous force which is the drag force as a result of pipe movement in opposite direction of the drilling fluid flow. Another is the tortuosity effect. Although the preplanned well is a smooth path, a crooked profile will be seen in reality. For this reason the model has to take this effect into account. A crooked well path shows higher torque and drag values. The buckling of the tubulars should also be taken into account in order to have a sense of the excessive drag limit which may put the string in compression so that it buckles.

Aadnoy (2006) has extensively derived the mathematical equations for a catenary well profile. He applied the developed equations to a field case study for an ultra long well with 10 km extended-reach. Little friction reduction was observed in comparison with a conventional well profile as the entrance to the catenary profile at the top creates extra friction. Du and Zhang (1987) illustrated two field cases using catenary trajectories drilled in China. Liu et al. (2007, 2009), Han (1987, 1997) and Liu (2007) later discussed the different methods for planning a catenary profile.

Aadnoy (2008) generalized the equations for different sections of the wellbore and the status of the pipe either by the string moving up or down in order to simplify it. Kaarstad and Aadnoy (2009) also performed an experimental investigation of the friction factor dependence on temperature and they observed an increase in the friction coefficient with temperature. A temperature dependent friction coefficient model was presented. Mitchell (2008, 2009) has used the previously torque and drag model and the model has been formulated such that the stiffness of the pipe. In his mathematical model he assumed the pipe as a beam member and calculated the bending moment over this beam as a result of forces acting on the beam.

Aadnoy and Andersen (2002) developed analytical solutions to calculate wellbore friction for different well geometries. These solutions gave better insight into the frictional behavior

throughout the well, and each geometry required individual equations. Mason and Chen (2007) provided an assessment of limitations of the various torque and drag model and evaluated their validity. The torque and drag model formulation has been reviewed by Robert et al. (2007) in the context of a large displacement equilibrium analysis. Aadnoy and Djurhuus (2008) investigated the symmetry of the various friction equations, reducing them to one equation for torque and one for drag. However, these solutions were still limited to horizontal and vertical planes. It seems a practical model should be developed to compute friction for any well geometry. More recently, Aadnoy et al. (2009) modeled an entire well by two sets of equations for straight and curved sections. The curved equation is based on the absolute dogleg of the wellbore.

2.2 Finite Element Modeling

The use of Finite Element Analysis, (FEA), has its beginnings as far back as 1953 when it was employed by Richard Courant who used the Ritz Method of variation calculus to analyze vibration systems. The essential concept is to subdivide a large complex structure into a finite number of sample elements, such as beam, plate, and shaft elements. In this case, a set of n second order differential equations are obtained where n is the number of degrees of freedom (Williamson, 1980). The rapid advance of computing power and the even more magnificent reduction in computing cost would subsequently lead to more widespread use of FEA.

The Finite Element Method (FEM) has been used for a number of years in the oil and gas industry. The finite element analysis is the right choice to take into account the stiffness and the borehole/drill string clearance effectively when calculating torque and drag. It can get a solution regardless of the degree of complexity of the wellbore curvature, the drill string and the boundaries. For finite element analysis, the drill string is meshed into beam elements that each element has six degrees of freedom (three rotations and three displacements). The only shortcoming it is time consuming when the number of elements are large (Dykstra, 1996).

Yang in 2008 presented a three dimensional finite difference differential method for bottom hole assembly (BHA) analysis under static loads. The analysis was used to optimize the BHA configurations for drilling of directional well holes. The optimization of the BHA configurations ensures the controlled cruising of the drill bit to drill the hole along the planned trajectory. The model incorporated the contact response between drill string and wellbore wall, the upper

tangent point problem, stabilizer configurations, bent sub model and other considerations for numerical solutions as shown in Figure 2.1.

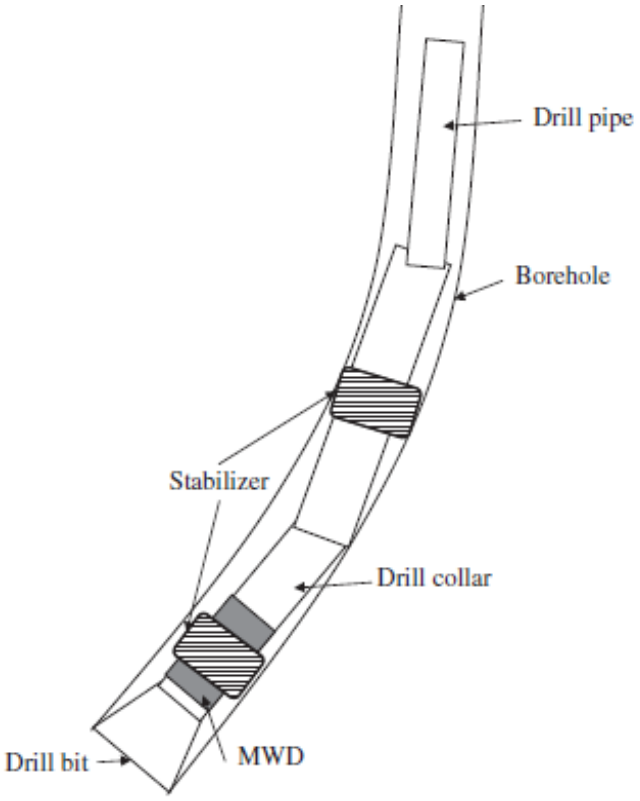

Figure 2.1: Schematic of bottom hole assembly (BHA) (Yang, 2008)

It should be mentioned that all calculations based on a local coordinate systems must be transformed to reference coordinate system for entire drill string to keep consistency in this analysis as shown in Figure 2.2.

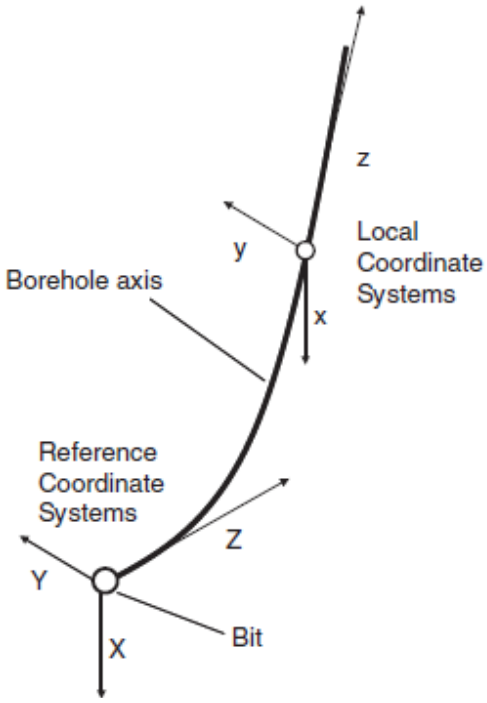

Figure 2.2: Reference and local coordinate systems (Yang, 2008)

In 2003, Schmalhorst and Neubert introduced new industry leading dynamic modeling software. Several case studies show the potential of their presented modeling software. This research model was intended for use by engineering research personnel in analyzing bottom hole assembly configurations, MWD tool design, and field tool failures in greater detail. The drill string dynamics simulation program is based on the finite element method and the drill string is modeled with geometrically nonlinear beam elements. Deformations of the drill string are measured by three nodal displacements and three rotations as shown in Figure 2.3

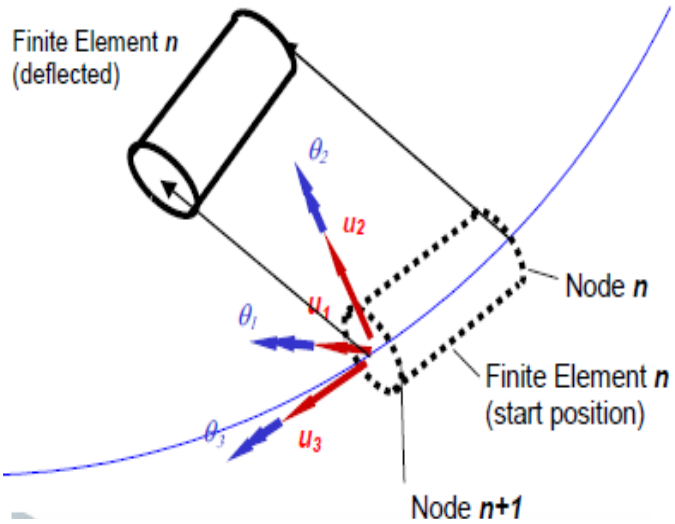

Figure 2.3: Three dimensional finite beam element (Schmalhorst and Neubert, 2003)

Bueno and Morooka in 1995 modeled the drill string as undeformed elastic beams. They proposed a methodology to estimate the contact forces generated by the drill string against the wellbore. The boundary conditions at the bit and the stabilizers are shown on Figure 2.4.

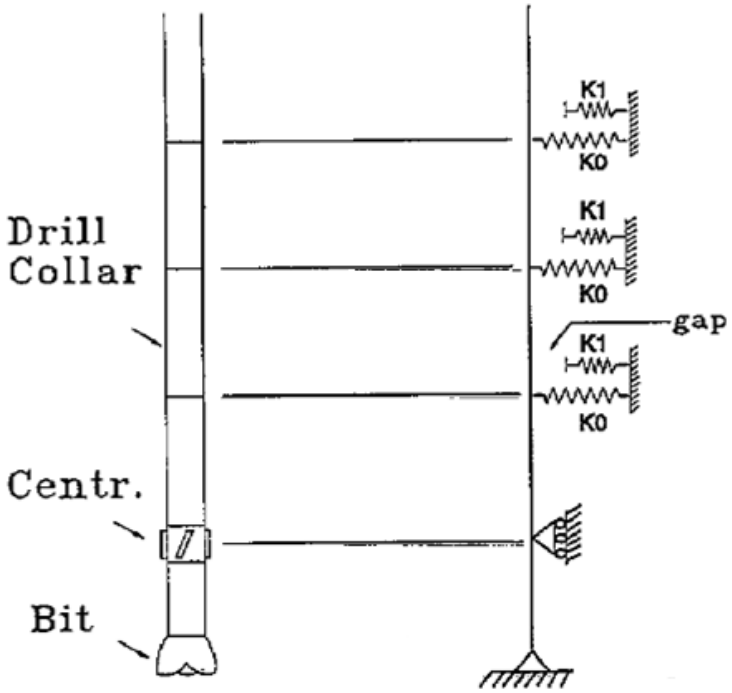

Figure 2.4: Boundary conditions (Bueno and Morooka, 1995)

It is assumed that the contact points occur only at the tool joints. The upper boundary condition (rotary table) is a full restriction of the degrees of freedom. The wellbore was divided into contact elements with specified spring stiffness.

Newman in 2005 presented a 3-D finite element model which considers the pipe bending inside the wellbore. The yielding of coiled tubing can be included in this model. The model is able to calculate the beginning of buckling during drilling operation. He presented the equations and methodology used in the development of the finite element model and compared the results with other analytical solutions which are currently in use. Also, he introduced a dynamic finite-element/ finite-difference model which is a part of a drilling software package. The model performs a 3-D finite element analysis of drill string at each specific point in time. This analysis is run repeatedly at short time steps through time using a finite-difference algorithm (Newman and Procter, 2009).

The behavior of many dynamic systems such as drill string undergoing time-dependent changes can be described by ordinary differential equations. When the solution for differential equation(s) of motion of a dynamic system cannot be obtained, a numerical method can be used. The results are approximated but at least the equation(s) have been solved, (Dukkipati, 2009).

CHAPTER THREE: **TECHNICAL APPROACH – ANALYTICAL**

In this chapter, a new analytical model for torque and drag calculations is presented. The following new developed model is a soft string model and it ignores any tubular stiffness effects. This means that the pipe is as a heavy cable lying along the wellbore. This expresses that axial tension and torque forces along drillstring as well as contact forces that are supported by the wellbore. The derived equations define the hook load for hoisting, lowering, reaming and back reaming operations and also the torque for a string in a wellbore. Two sets of equations are presented, one for the straight well sections such as straight, vertical and horizontal and one for the curved sections.

3.1 Buoyancy Factor

For torque and drag modeling, it is vital to consider effect of buoyancy force during different operations. The effective string weight or the string tension in a fluid filled well is the unit pipe weight multiplied by the buoyancy factor. The buoyancy factor is defined as:

$$\beta = 1 - \frac{\rho_o A_o - \rho_i A_i}{\rho_{pipe}\left(A_o - A_i\right)} \tag{3.1}$$

where

β: buoyancy factor

ρ: density, kg/m^3

A: cross sectional area, m^2

Subscripts “o” and “i” refer to the outside and inside of drill string. If there is equal fluid density inside and outside of the pipe, the buoyancy equation becomes:

$$\beta = 1 - \frac{\rho_o}{\rho_{pipe}} \tag{3.2}$$

Equation 3.2 is most commonly used during drilling operation, whereas Equation 3.1 is used in cases where there is a density difference between the inside of the string and the annulus like during cementing, running drill string in the hole as well as under balanced drilling operations. During well intervention operations, the wellhead may be shut in and an annular pressure applied and the same buoyancy equation applies, but one must add end reactions caused by the annular pressure. The buoyancy factor will be discussed further in Chapter 5.

3.2 Straight Sections Modeling

Characteristic of a straight wellbore is that the tension along the string is not contributing to the normal pipe force, and hence not affecting friction. Straight sections are weight dominated as only the normal weight component gives friction. Because gravity acts downwards, the wellbore inclination is used and azimuth changes do not have any contributions. Figure 3.1 shows the force balance for a straight pipe. The resulting equation uses the following sign convention:

+ means that the pipe is pulled upward

– means that the pipe is lowered downward

$$F_2 = F_1 + \beta w \Delta L \{\cos \alpha \pm \mu \sin \alpha\} \tag{3.3}$$

where

ΔL: length of the element, m

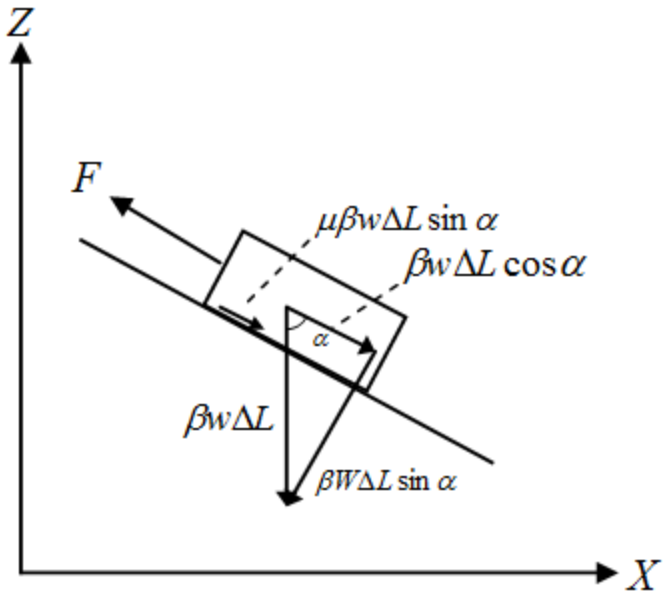

Figure 3.1: Force balance for pipe pulling along a straight surface

The first term of Equation 3.3 is referring to the weight of the element and the second term is referred to as additional frictional force required for moving the pipe element. If inclination α is equal to zero, it means the pipe section is in a vertical position and the friction term will diminish. If α becomes 90 degrees, it means the pipe section is located in a horizontal position and the weight term will diminish.

From Figure 3.2 the axial weight component is:

$$W(\alpha) = w\Delta L\cos\alpha \tag{3.4}$$

From Figure 3.2, the vertical height is:

$$\Delta z = \Delta L\cos\alpha \tag{3.5}$$

Combining Equations 3.4 and 3.5 gives:

$$W(\alpha) = w\Delta z \tag{3.6}$$

This is an important result. It says that the static axial load of a pipe is equal to the unit weight multiplied by the projected vertical height. If a vertical well has a depth *D*, and a deviated well has the same projected vertical depth, the static drill string weight will be the same for these two wells.

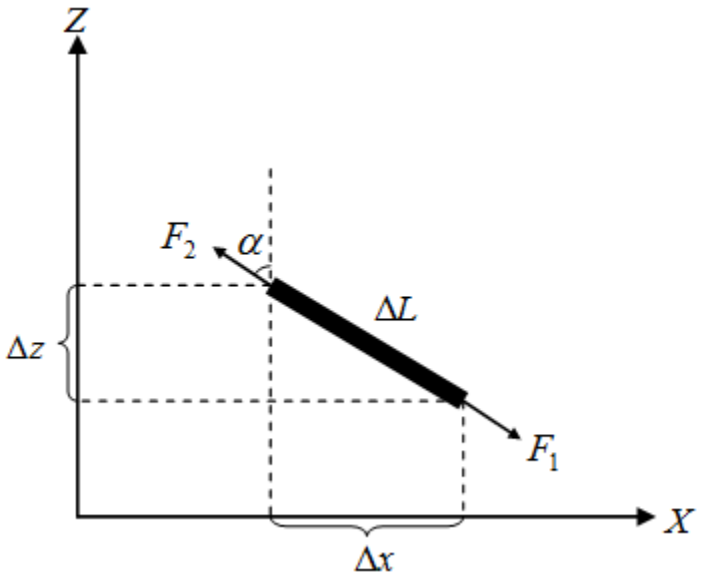

Figure 3.2: Geometry of the inclined straight pipe

Once the drill string description, the survey data, and the friction coefficient are specified, the calculation starts at the bottom of the drill string and proceeds stepwise upward. The same approach is used for the curved section.

If the string is divided to *n* elements, F_{i-1} is the force at bottom of each element and F_i is the force on top of each element which can be added up the entire wellbore section. Sometimes the well is filled with different mud weights which results in different buoyancy factor β_i in different sections. If the well is filled with only one drilling fluid with uniform density, all buoyancy factors β_i will be equal. Also, the drill string consists of different components with different unit

weights w_i such as drill pipe, heavy weight drill pipe and BHA which should all be taken in consideration in the hook load calculation.

Using the friction coefficient μ, there are two approaches for torque and drag calculations. The first is assuming one friction coefficient for entire well including both the cased and open hole sections and try to get the match between field and modeling data. The second is assuming different friction coefficient for cased and open hole. All μ_i can be equal or different depending on if we have separate open hole or cased hole friction coefficient. If the drill string is divided to n-1 elements, the general equation for entire drill string in a straight section can be written as:

$$F_n = \sum_{i=2}^{n} \{\beta w \Delta L \times (\cos\alpha \pm \mu \sin\alpha)\}_i \tag{3.7}$$

When the friction coefficient is equal to zero, Equation 3.7 shows the static weight of the drill string in a straight section for different drilling operations.

The same principle applies for the rotating friction, torque. The torque is defined as the friction coefficient multiplied by normal moment and the tool joint radius. Equation 3.8 shows the torque loss along the straight section for an element. For this case, the axial force has no contribution to the torque value. The torque can be considered independent of the direction of rotation.

$$T = \mu \times \beta w \Delta L \sin\alpha \times r \tag{3.8}$$

For inclination α equal to zero as in a vertical section; no torque loss is present due to the negligible value of the normal force. For αinclination equal to 90 degree as in a horizontal section, the maximum torque loss will be happened due to maximum normal force. The Equation 3.9 shows the torque along the drill string in straight section which divided to n-1 elements.

$$T_n = \sum_{i=2}^{n} \{\mu \times \beta w \Delta L r \sin\alpha\}_i \tag{3.9}$$

It should be mentioned that the drill string in a straight section may consist of different components which may have different tool joint radius r_i. If the bit is interacting with the rock, the bit torque should be added to all torque loses along drill string in a straight section.

3.3 Curved Sections Modeling

For the curved borehole sections, the normal contact force between string and hole is strongly dependent on the axial pipe loading. This is therefore a tension dominated process. In the derivation, it was assumed that the pipe is weightless when computing the friction, but the weight at the end of the bend is added.

During drilling the wellbore is surveyed at regular intervals. The main outputs are wellbore inclination and the geographical azimuth. These data are used to calculate depth and horizontal displacement. A short derivation of the angle change between two survey points follows. P_1 and P_2 refer to two measurements spaced along a length ΔL as shown in Figure 3.3

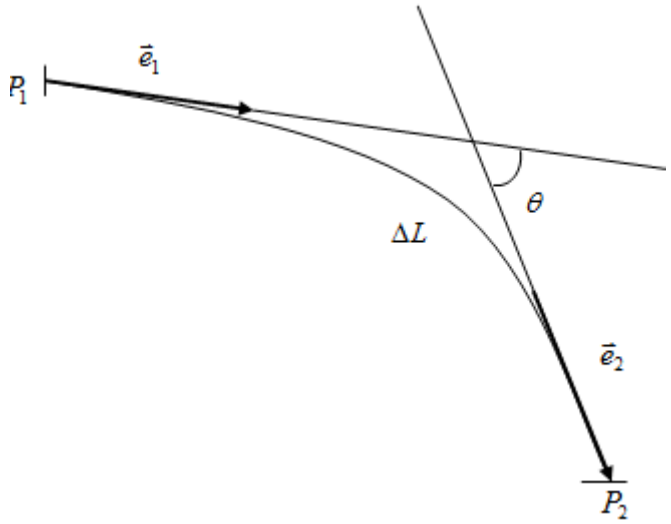

Figure 3.3: Definition of change in direction θ over a length ΔL

The angle θ enters the scalar product of the unit vectors e_1 and e_2 in the direction of the wellbore tangents at P_1 and P_2:

$$e_1.e_2 = |e_1||e_2|\cos\theta = \cos\theta \tag{3.10}$$

From Figure 3.4, the scalar product of the unit vectors may also be expressed as:

$$e_1.e_2 = e_{1x}.e_{2x} + e_{1y}.e_{2y} + e_{1z}.e_{2z} = \cos\theta \tag{3.11}$$

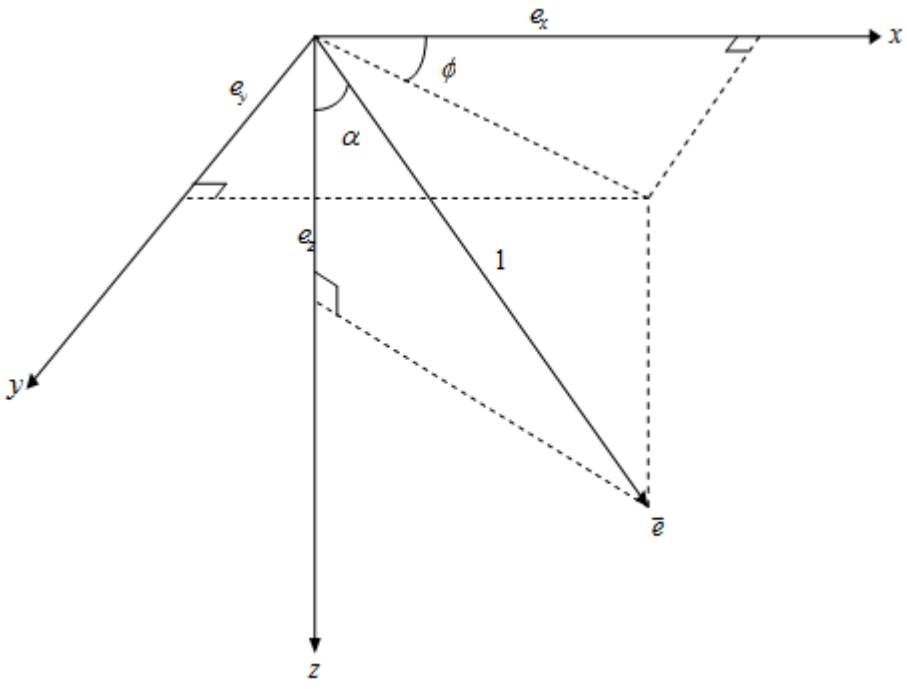

Figure 3.4: The unit vector *e* is decomposed along the x-axis, the y-axis, and the z-axis (vertical)

From Figure 3.4 the components of *e* with direction defined by the inclination and azimuth angles are:

$$e_x = \sin\alpha.\cos\varphi \tag{3.12}$$

$$e_y = \sin\alpha.\sin\varphi \tag{3.13}$$

$$e_z = \cos\ \alpha \tag{3.14}$$

Inserting Equations 3.12, 3.13 and 3.14 into Equation 3.11, the change of angle is related to the Cartesian coordinates as follows:

$$\cos\ \theta = \sin\ \alpha_1 \sin\ \alpha_2 \cos\left(\varphi_1 - \varphi_2\right) + \cos\ \alpha_1 \cos\ \alpha_2 \tag{3.15}$$

The angle θ is the total directional change. If both inclination and azimuth are changed, the plane that θ acts in is not constrained to the horizontal or vertical plane. It is therefore a fully three dimensional representation of the directional change.

Although the inclination α is measured in a vertical projection and the azimuth φ in a horizontal projection, the dogleg θ is measured in an arbitrary plane, as shown in Figure 3.5. Inspection of Equation 3.15 reveals that it depends on both inclination and azimuth. These properties will be used in the following equations when we present the new friction models and are not restricted to a specific plane.

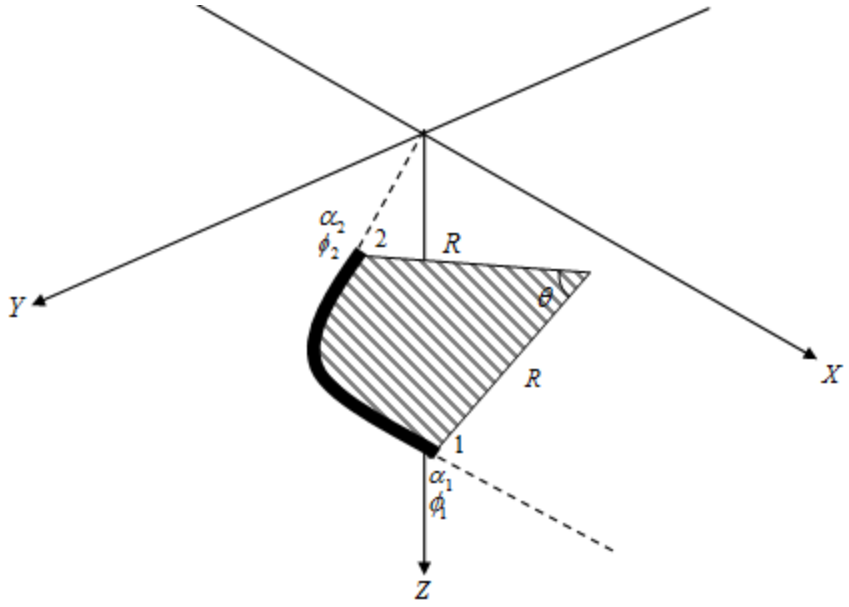

Figure 3.5: The dogleg in 3-dimensional space

The oil industry commonly uses the expression dogleg to describe this directional change. We may define this in degrees rather than radians:

$$DL(^\circ) = \frac{180}{\pi}\left|\theta(rad)\right| \tag{3.16}$$

The derivative or the slope change is called dogleg severity, and is commonly defined as angle change per 30 m hole:

$$DLS\left(^\circ/30m\right) = \frac{DL}{\Delta L}30 \tag{3.17}$$

Knowing the azimuth and inclination at two wellbore positions, the displacements in different directions will be defined by assuming a curved shape between the two positions. Figure 3.6 shows a vertical projection of the well path.

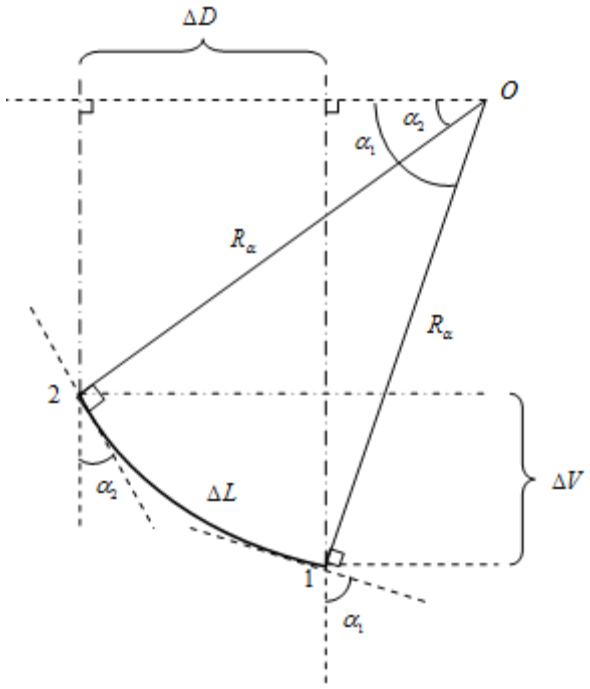

Figure 3.6: Projection of a wellbore in a vertical plane

The relationship between the wellbore, the radius of the circular segment and the angle is:

$$\Delta L = R_\alpha(\alpha_1 - \alpha_2) \tag{3.18}$$

It should be noted the above inclination angles are in radians. The vertical projected height is:

$$\Delta V = R_\alpha \sin\alpha_1 - R_\alpha \sin\alpha_2 = \frac{\Delta L(\sin\alpha_1 - \sin\alpha_2)}{\alpha_1 - \alpha_1} \tag{3.19}$$

The vertical projected height will be used to compute the axial pipe weight. To find the changes in the north and east coordinate, the wellbore trajectory is projected onto a horizontal plane, as shown in Figure 3.7:

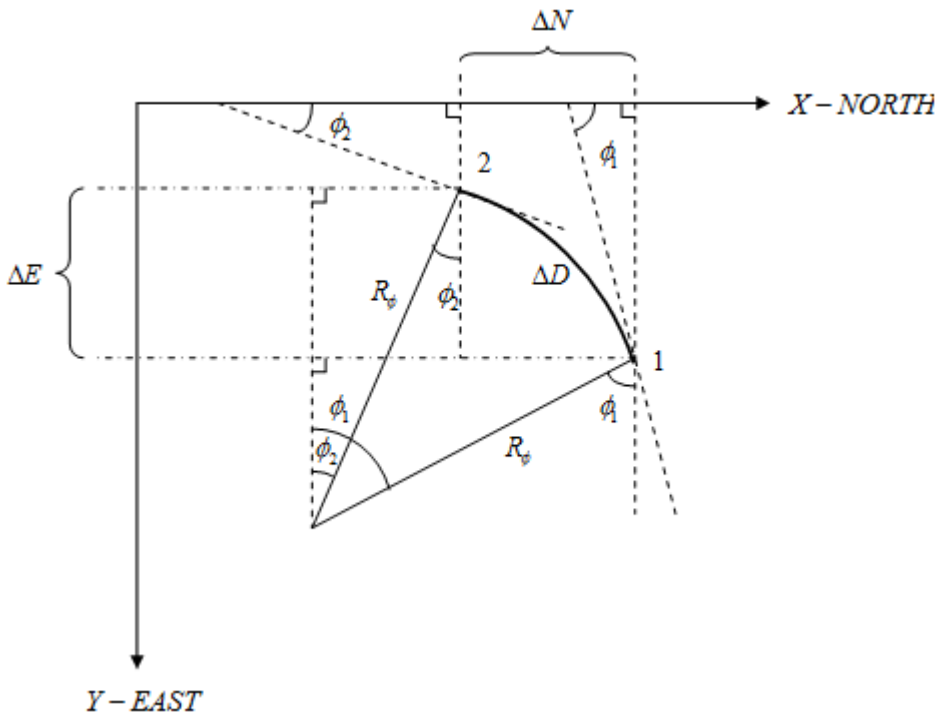

Figure 3.7: Projection of wellbore in a horizontal plane. In this projection the wellbore is assumed to be circular.

From the horizontal projection in Figure 3.7, the circular segment can be expressed as:

$$\Delta D = R_{\varphi}\cos\alpha_2 - R_{\varphi}\cos\alpha_1 \tag{3.20}$$

This is the distance of the circular projection of the wellbore in the horizontal plane, and is connected to the radius $R_{\varphi}$and azimuth angles by the relation:

$$\Delta D = R_{\phi}(\varphi_1 - \varphi_2) \tag{3.21}$$

The changes ΔN and ΔE now follow from Figure 3.7:

$$\Delta N = R_{\varphi}(\sin\varphi_1 - \sin\varphi_2) \tag{3.22}$$

and

$$\Delta E = R_{\varphi}(\cos\varphi_2 - \cos\varphi_1) \tag{3.23}$$

The complete expressions obtain from inserting for R_{ϕ} and ΔD are;

$$\Delta N = \Delta L \frac{(\cos\alpha_2 - \cos\alpha_1)(\sin\varphi_1 - \sin\varphi_2)}{(\alpha_1 - \alpha_2)(\varphi_1 - \varphi_2)} \tag{3.24}$$

and

$$\Delta E = \Delta L \frac{(\cos\alpha_2 - \cos\alpha_1)(\cos\varphi_2 - \cos\varphi_1)}{(\alpha_1 - \alpha_2)(\varphi_1 - \varphi_2)} \tag{3.25}$$

Equations 3.24 and 3.25 will not be used in this derivation. They are given for the sake of completeness, and are used to compute the geographical position of any point of the wellbore.

With reference to Figure 3.4, we may assume that the x-axis points north and the y-axis points east. Defining the unit vector to have a length ΔL, the displacements for a straight section can be defined as:

Vertical projection (to compute axial pipe weight):

$$\Delta V = \Delta L \cos\alpha \tag{3.26}$$

Horizontal projections in the northern and eastern directions are:

$$\Delta N = \Delta L \sin\alpha \cos\varphi \tag{3.27}$$

and

$$\Delta E = \Delta L \sin\alpha \sin\varphi \tag{3.28}$$

Again, the horizontal projections are not used in the derivation, but presented to define the complete set of equations to define the geographical positions of the borehole.

For the curved borehole sections, the normal contact force between the drill string and wellbore is strongly dependent on the axial pipe loading. This is therefore a tension dominated process. In e.g. a short bend, the tension is often much larger that the weight of the pipe inside the bend. In the following derivation we will assume that the pipe element is weightless when we compute the friction, but we add the weight at the end of the bend. Figure 3.8 shows an element that is pulled along a curved surface. Performing a force balance in the Z- and X- directions results in:

Z-direction:

$$dN = F \times d\theta \tag{3.29}$$

X-direction:

$$dF = \mu \times F d\theta \tag{3.30}$$

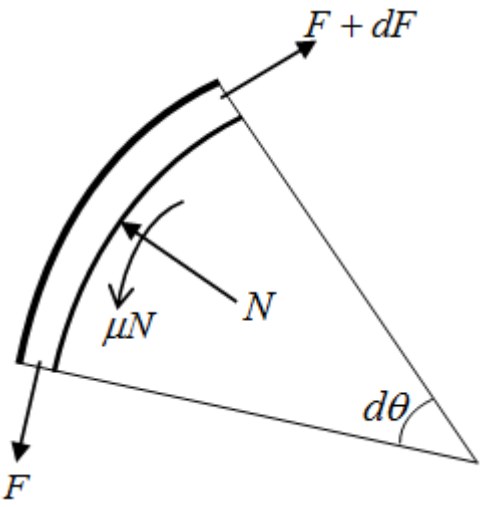

Figure 3.8: Element pulled along curved surface

Integrating the force equation between the upper and lower position gives:

(Defining $\theta = \theta_2 - \theta_1$):

$$F_2 = F_1 e^{\pm \mu |\theta|} \tag{3.31}$$

The following sign convention applies:

+ means that pipe is pulled upwards

- means that the pipe is lowered

For a rotating string, the same contact force applies, only friction direction is tangential. The torque for the pipe that is not pulled or lowered is simply:

$$T = \mu r N = \mu r F_1 |\theta| \tag{3.32}$$

Furthermore, the dogleg angle θ depends both on the wellbore inclination and the azimuth. Because the pipe will contact either the high side or the low side of the wellbore, its contact surface is given by the dogleg plane.

For build-up, drop-off, side bends or combination of these, the axial force becomes:

$$F_2 = F_1 e^{\pm\mu|\theta|} + \beta w \Delta L \left\{ \frac{\sin\alpha_2 - \sin\alpha_1}{\alpha_2 - \alpha_1} \right\} \tag{3.33}$$

where + means hoisting and – means lowering of the pipe.

The torque for the bend is defined in Equation 3.34 as:

$$T = \mu r N = \mu r F_1 |\theta| \tag{3.34}$$

Friction for any wellbore shape can thus be computed by dividing the well into straight and curved elements. The forces and torques are summed up starting from bottom to top of the well.

For the entire curved section the axial force can be calculated as follow:

$$F_n = \sum_{i=2}^{n} \left\{ F_{i-1} \times e^{\pm\mu_i|\theta_i|} + \beta_i w_i \Delta L_i \times \left[\frac{\sin\alpha_i - \sin\alpha_{i-1}}{\alpha_i - \alpha_{i-1}} \right] \right\} \tag{3.35}$$

Equation 3.36 shows torque losses for the entire curve section

$$T_n = \sum_{i=2}^{n} \mu_i \times r_i F_{i-1} |\theta_i| \tag{3.36}$$

3.5 Combined Axial Motion and Rotation

The solutions presented in sections 3.3 and 3.4 must be modified if a combined motion takes place. Aadnoy and Andersen (2001) showed how the frictional capacity is decomposed into the two directions, axial motion and rotation. The effect of combined motion is well known, for example when rotating a liner for running easier into the hole. A high rotational speed reduces axial drag considerably. During tripping operations an overpull may occur due to tight hole conditions. The remedy action is typically to rotate the drill string while pulling or lowering. In the oilfield, the considerable difference can be observed between measured hook loads while tripping in/out and the reaming/back reaming operation.

Aadnoy and Andersen (2001) showed how the frictional capacity is disintegrated into the two directions, axial and rotational movements. Figure 3.9 shows a pipe section with weight of $w\Delta L$. If it is pulled along a surface, the drag will be equal to the normal force, $w\Delta L$ multiplied with the coefficient of friction $\mu w \Delta L$. If the pipe is rotated instead, the torque ratio, *T/r* is also equal to $\mu w \Delta L$. Thus, the weight and friction coefficient results in the same frictional resistance regardless of whether the movement is axial or rotational.

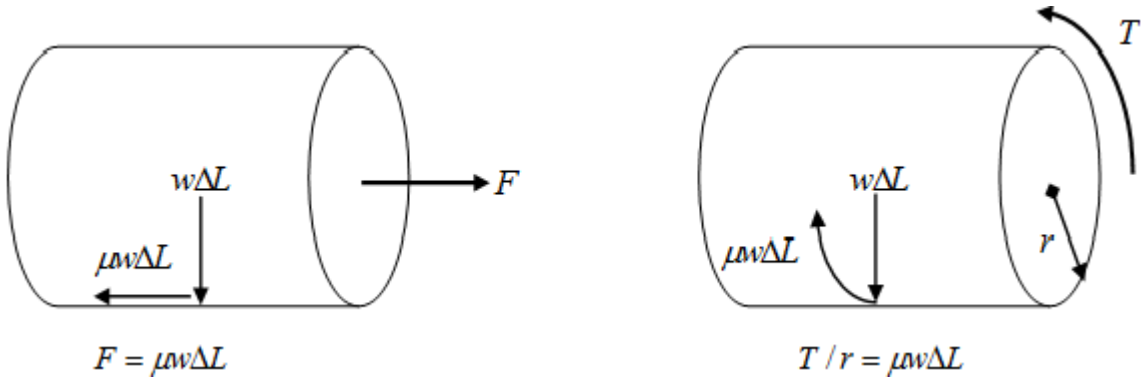

Figure 3.9: Drag and torque for a pipe element

In the following a simple model for combined motion is developed which shows the effect of rotation and axial movement on well friction as a function of tripping velocity and rotary speed. It can be multiplied by friction coefficient in sine and cosine form which results in a reduction in the value of the friction force.

During combined motion, the axial velocity is V_h, and the tangential pipe speed is V_r. As derived in following, these give a resultant velocity V. The angle between the two velocities is defined in Figure 3.10 below.

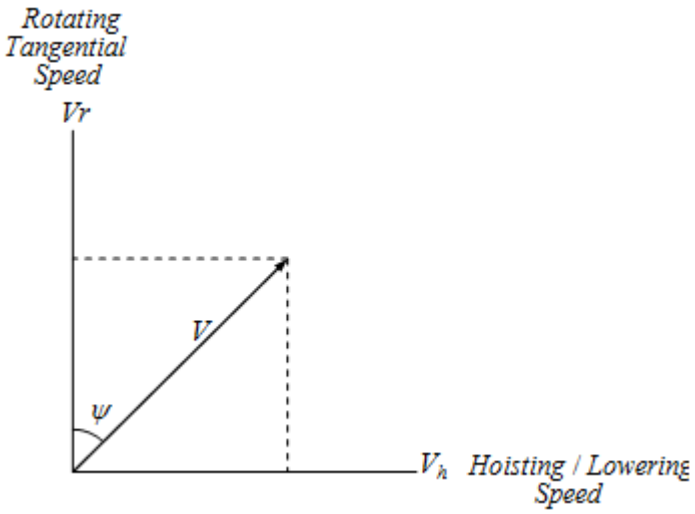

Figure 3.10: Relationship between hoisting/lowering and rotational speed

Figure 3.10 shows the velocities on the pipe surface for combined motion. They are given by the following Equations:

$$V_h = hoisting/lowering \quad speed(m/s)$$
$$V_r = \tan gential \quad speed \quad due \quad to \quad rotation(m/s)$$
$$or: \qquad (3.37)$$
$$V_r = \frac{2\pi \times r(m)}{60} N_r(rpm)$$

We assume that the amount of friction axially/tangentially is proportional to the relative velocities. The angle of the friction vector is:

$$\psi = \tan^{-1}\left(\frac{V_h}{V_r}\right) \tag{3.38}$$

For a straight pipe section, the axial and the tangential friction forces are:

$$\begin{aligned} FF_{axial} &= \mu \times \beta w \Delta L \sin\alpha \\ \frac{T}{r} &= \mu \times \beta w \Delta L \sin\alpha \end{aligned} \tag{3.39}$$

For pure hoisting/lowering or pure rotation, the frictional forces are the same for axial drag and rotation. For combined motion, the resultant frictional force is constant. Figure 3.11 shows this.

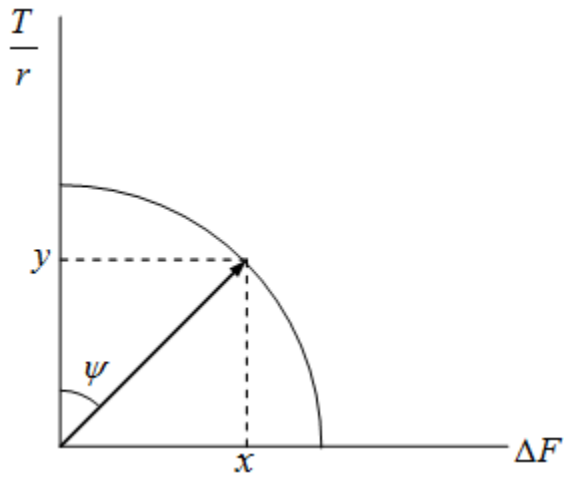

Figure 3.11: Relationships between torque and drag for straight pipe sections

First determine the hoisting/lowering speed, the rotational speed, and compute the angle ψ. Then compute the resulting torque and drag as follows:

$$F_2 = F_1 + \beta w \Delta L \cos\alpha \pm \mu \beta w \Delta L \sin\alpha \sin\psi$$
$$T = r\mu\beta w \Delta L \sin\alpha \cos\psi \tag{3.40}$$

The frictional forces for a curved section can be expressed as:

$$\Delta F = F_1 (e^{\pm|\theta|} - 1) \tag{3.41}$$

and

$$\frac{T}{r} = \mu F_1 |\theta| \tag{3.42}$$

For this case the frictional force is no longer constant for combined motion. This is due to the exponential effect, or the "capstan" effect. Figure 3.12 visualize this. The resultant frictional force vector now describes an ellipse where:

$$\left(\frac{y}{T/r}\right)^2 + \left(\frac{x}{\Delta F}\right)^2 = 1 \tag{3.43}$$

The hoisting/lowering forces and the torque for combined motion can be expressed as:

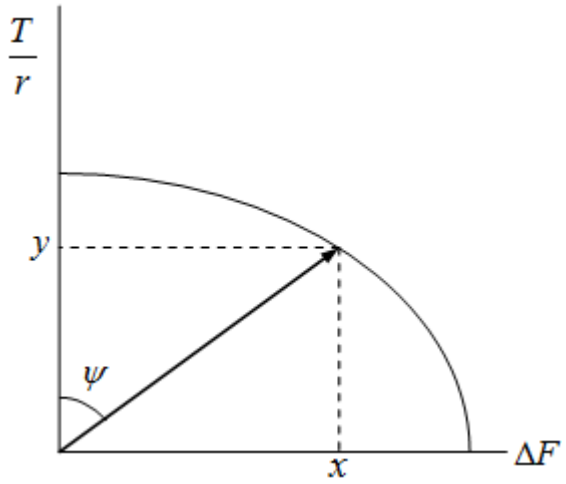

Figure 3.12: Relationship between torque and drag for bend

$$F_2 = F_1 + F_1(e^{\pm\mu|\theta|} - 1)\sin\psi + \Delta L\beta w\left\{\frac{\sin\alpha_2 - \sin\alpha_1}{\alpha_2 - \alpha_1}\right\} \tag{3.44}$$

$$T = \mu r N = \mu r F_1|\theta|\cos\psi \tag{3.45}$$

When ψ is equal to *90* degree, it means there is no rotation during axial movement, and when ψ equal to 0 degree means there is no axial movement during rotation.

The torque and drag equations can be written for combined motion as follow:

For entire straight section:

$$F_n = \sum_{i=2}^{n}\{\beta w\Delta L\cos\alpha\}_i \pm \sum_{i=2}^{n}\{\beta w\Delta L\sin\alpha\times\mu\times\sin\psi\}_i \tag{3.46}$$

and

$$T_n = \sum_{i=2}^{n} \{\mu \times \beta w \Delta L r \sin\alpha \times \cos\psi\}_i \tag{3.47}$$

For entire curved section:

$$F_n = \sum_{i=2}^{n} \left\{ F_{i-1} \times \left(e^{\pm\mu|\theta_i|} - 1 \right) \times \sin\psi_i + \beta_i w_i \Delta L_i \times \left[\frac{\sin\alpha_i - \sin\alpha_{i-1}}{\alpha_i - \alpha_{i-1}} \right] \right\} \tag{3.48}$$

and

$$T_n = \sum_{i=2}^{n} \mu_i \times r_i F_{i-1} |\theta_i| \times \cos\psi_i \tag{3.49}$$

3.5 Application of the New Model

The models presented can be applied both during drilling by computing the friction for each survey point, or by dividing the entire well into a number of elements. Three cases will be presented where entire wells are analyzed.

3.5.1 Case A: Analysis of a Two Dimensional S-shaped Well

This example will demonstrate the application of the model, and also identify some frictional effects.

Figure 3.13 shows an S-shaped well that is drilled in a vertical plane. The total length is 2111 m, and the drill string consist of 161 m of 8"×3" drillcollars (2.13 kN/m) and 1950 m of 5"-19.5 lbs/ft drillpipe (0.285 kN/m). The drillcollar radius is 0.1 m, and the drill string connection radius is 0.09 m. The well is filled with 1.3 SG drilling mud and the coefficient of friction is

estimated to be 0.2. The bottom-hole-assembly starts out just below the drop-off section, and is vertical. For this case there is no change in azimuth, and the dogleg of Equation 3.15 becomes equal to the change in inclination.

The buoyancy factor is calculated as follow:

Pipe density is 7.8 SG.

$$\beta = 1 - \frac{1.3}{7.8} = 0.833$$

Assuming that the drill bit is off bottom, we will compute the forces starting from bottom of the well. For simplicity, the frictional factors of the bends are:

$$e^{\pm\mu\theta} = e^{\pm 0.2\left(45\frac{\pi}{180}\right)} = e^{\pm 0.157} = \begin{cases} 1.17 \\ 0.855 \end{cases}$$

The net weight of the bottom-hole-assembly:

$$0.833 \times 2.13\frac{kN}{m} \times 161m = 286kN$$

The buoyed pipe weight:

$$0.833 \times 2.13\frac{kN}{m} = 0.237\frac{kN}{m}$$

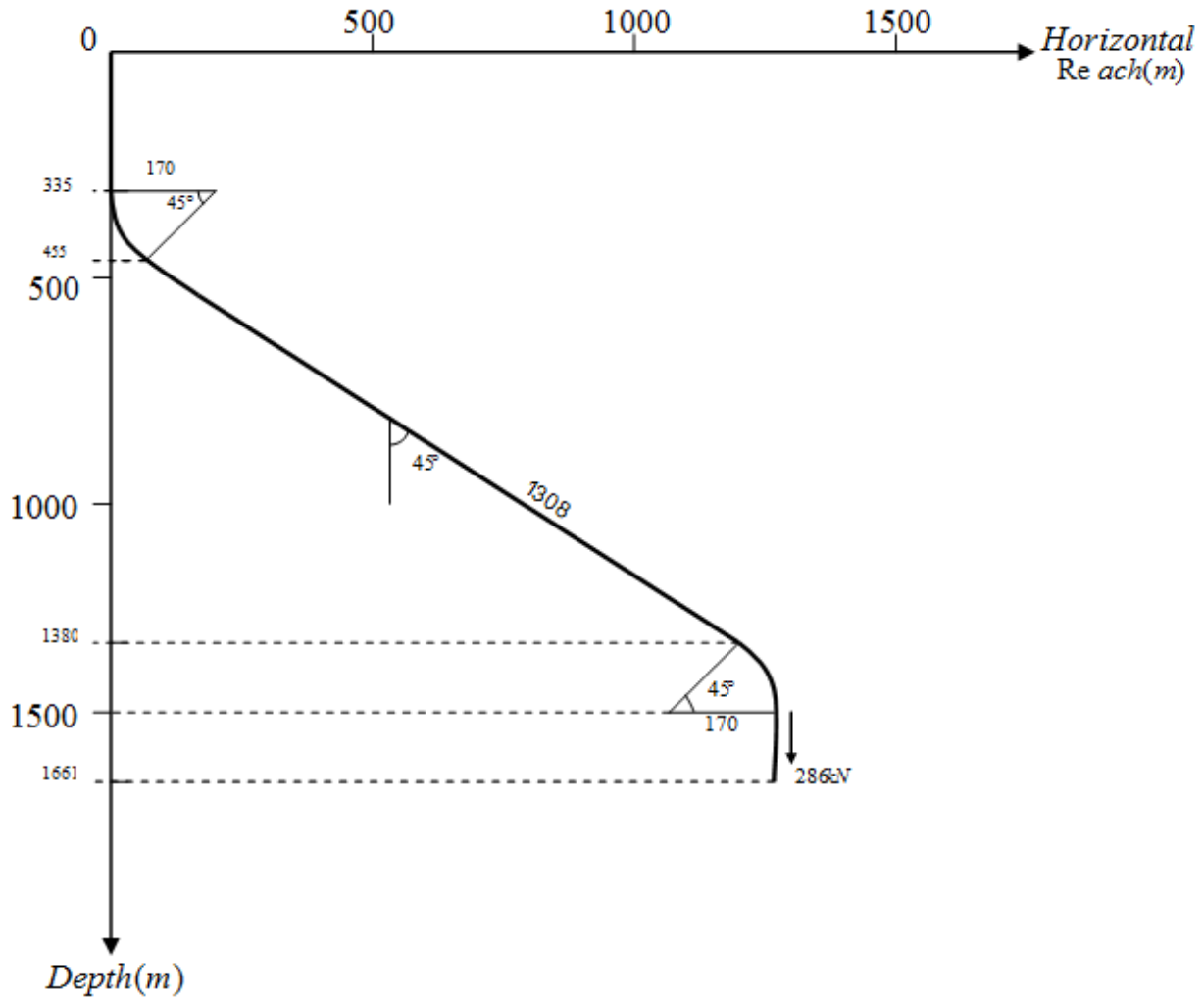

Figure 3.13: Geometry of S-shaped well

The axial forces along drill string were calculated for different points such as well bottom, bottom of drop-off section, bottom of sail section, top of sail section, top of build-up section and top well as shown in Table 3.1

Table 3.1: Forces in the drill string during hoisting and lowering

Position	***Static weight(kN)***	***Hoisting (kN)***	***Lowering(kN)***
well bottom	0	0	0
bottom drop-off section	286	286	286
bottom sail section	286+0.237×120= 315.5	286×1.17+28.5= 363	286×0.855+28.5= 272.9
top sail section	315.5+0.237×925= 533.6	363+0.237×1308(cos 55˚+0.20sin55˚)= 626	272.9+0.237×1308(cos 55˚-0.20sin55˚)= 558.3
top buildup section	533.6+0.237×120= 562	626×1.17+28.5= 760.9	558.3×0.855+28.5= 511.7
top well	562+0.237×335= 651.5	760.9+79.5= 850.3	511.7+79.5= 591.1

When calculating torque, we will use two scenarios:

1) with bit off bottom

and

2) with a weight on the bit of 90 kN

Table 3.2 shows all calculations related to all the torque for on bottom and off bottom interest points. The static weight for the second case is simply obtained by subtracting the bit force throughout the string.

Table 3.2: Torque in drill string during drilling while bit is off bottom

Position	***Static weight, Bit off bottom (kN)***	***Torque, Bit off bottom (kN.m)***	***Static weight, WOB 90 kN***	***Torque, in drill string (kNm)***	***Torque in well (kN.m)***
Well Bottom	0	0	-90	0	22-13.0 = 9
Bottom drop-off	286	0	286-90 = 196	0	9
Bottom sail	315.5	0.2×0.09×286×π/5=5.05	315.5-90 = 225.5	0.2×0.09×196×π/5 = 2.77	9+0.2×0.09×196×π/5=11.77
Top sail section	533.6	5.05+0.2×0.09×0.237×1308×sin55 = 8.0	533.6-90 = 553.6	2.77+3.95 = 6.72	11.77+3.95 = 15.72
Top build-up	562	8.0+0.2×0.09×533.6×π/5 = 15.55	562-90 =572	6.72+0.2×0.09×553.6×π/5 = 13.0	22
Top well	651.5	15.55	651.5-90 = 551.5	13.0	22

Figure 3.14 shows the axial load along drill string for different conditions. It is obvious that the build-up and drop-off bends have a dominating effect on wellbore friction. The data from Table 3.1 were used to generate Figure 3.14.

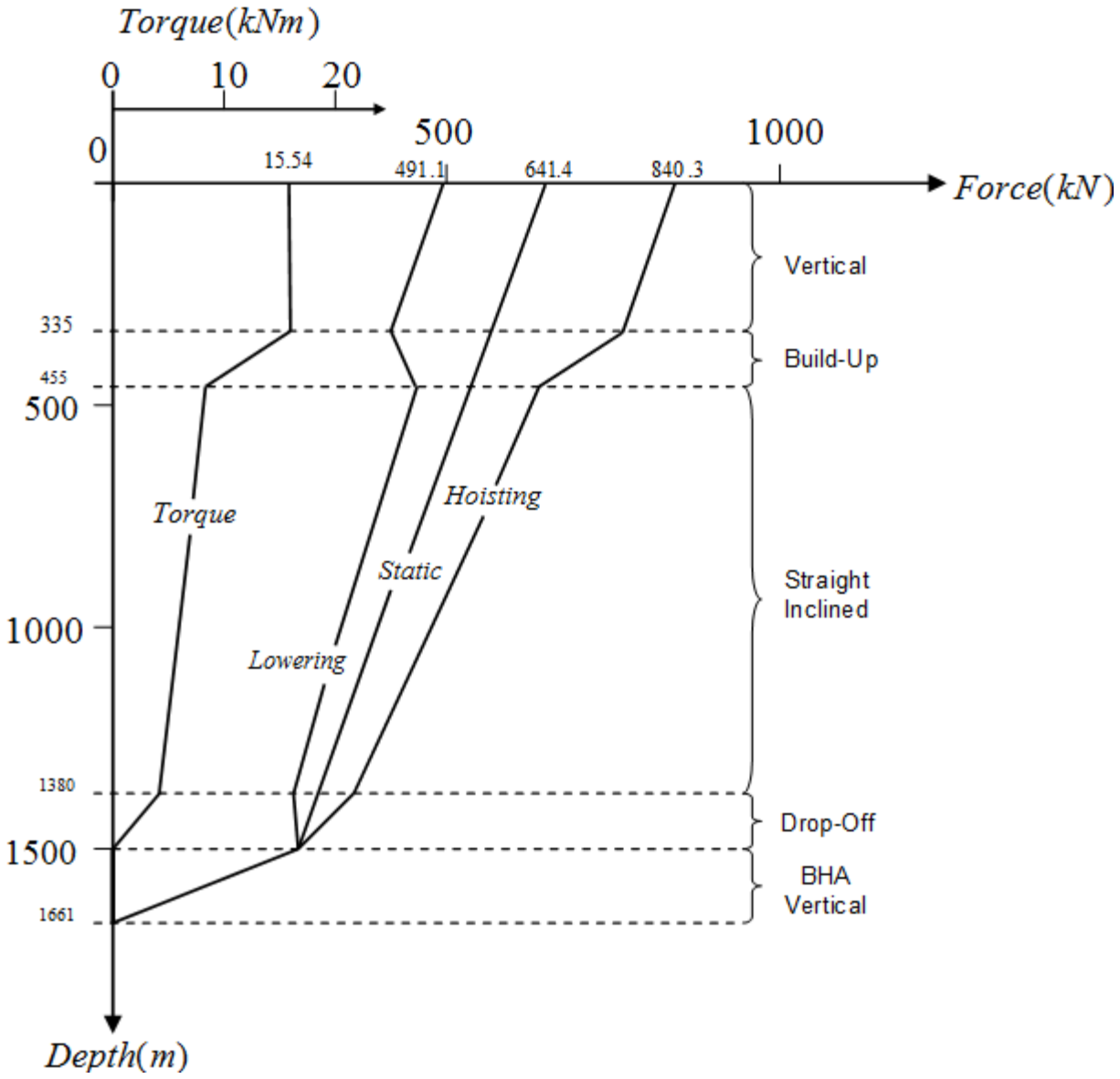

Figure 3.14: Torque and drag for the S-shaped well

This is further seen in Figure 3.15, which shows the torque calculations along drill string. When the bit force is applied, weight on the bit, the tension in the string decreases, leading to less string torque in the curved sections.

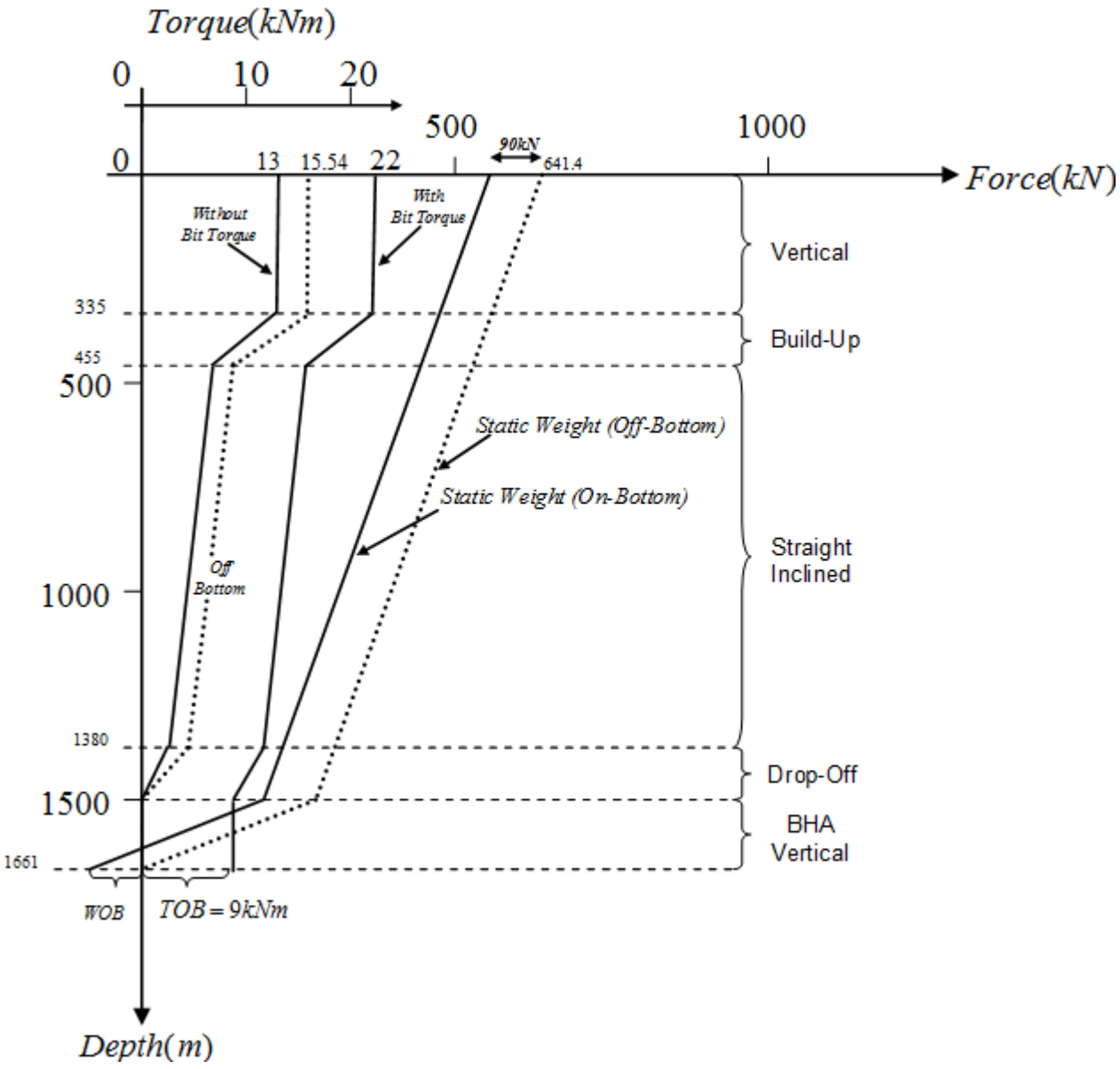

Figure 3.15: Torque along drill string during off/on bottom conditions

Figure 3.15 shows the reduction in string tension that leads to a reduced string torque. The numerical values are given in Table 3.2. When the bit force, weight on the bit, is applied, the driller observes an increase in torque of 6.56 kNm to a total value of 22 kNm. However, due to the reduction in string torque, the bit torque is actually 9 kNm. From this example it is obvious that the bit torque is always higher than the torque increase at surface for a deviated well.

3.5.2 Case B: Analysis of a 3-dimensional Well

Figure 3.16 shows this well. It is complex as its direction changes in the 3-dimensional space. The analysis is similar to the analysis of Case A, except that the bends are not restricted to a vertical plane, but in a 3-dimensional plane.

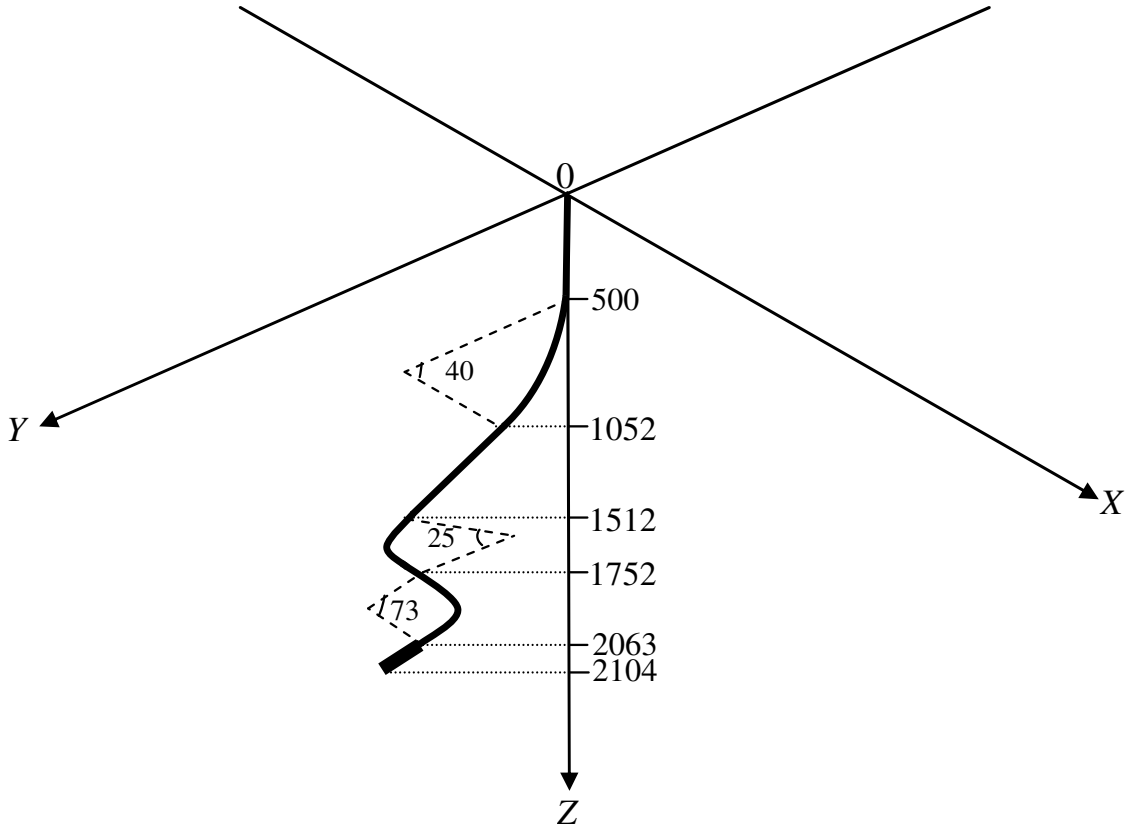

Figure 3.16: 3-dimensional well shape

The pipe data are taken the same as for Case A. Performing the analysis, the results are shown in Figure 3.17. Clearly, a different friction picture is seen in these wells which consist of 3 bends. By increasing the total angle change of a well, the friction increase significantly.

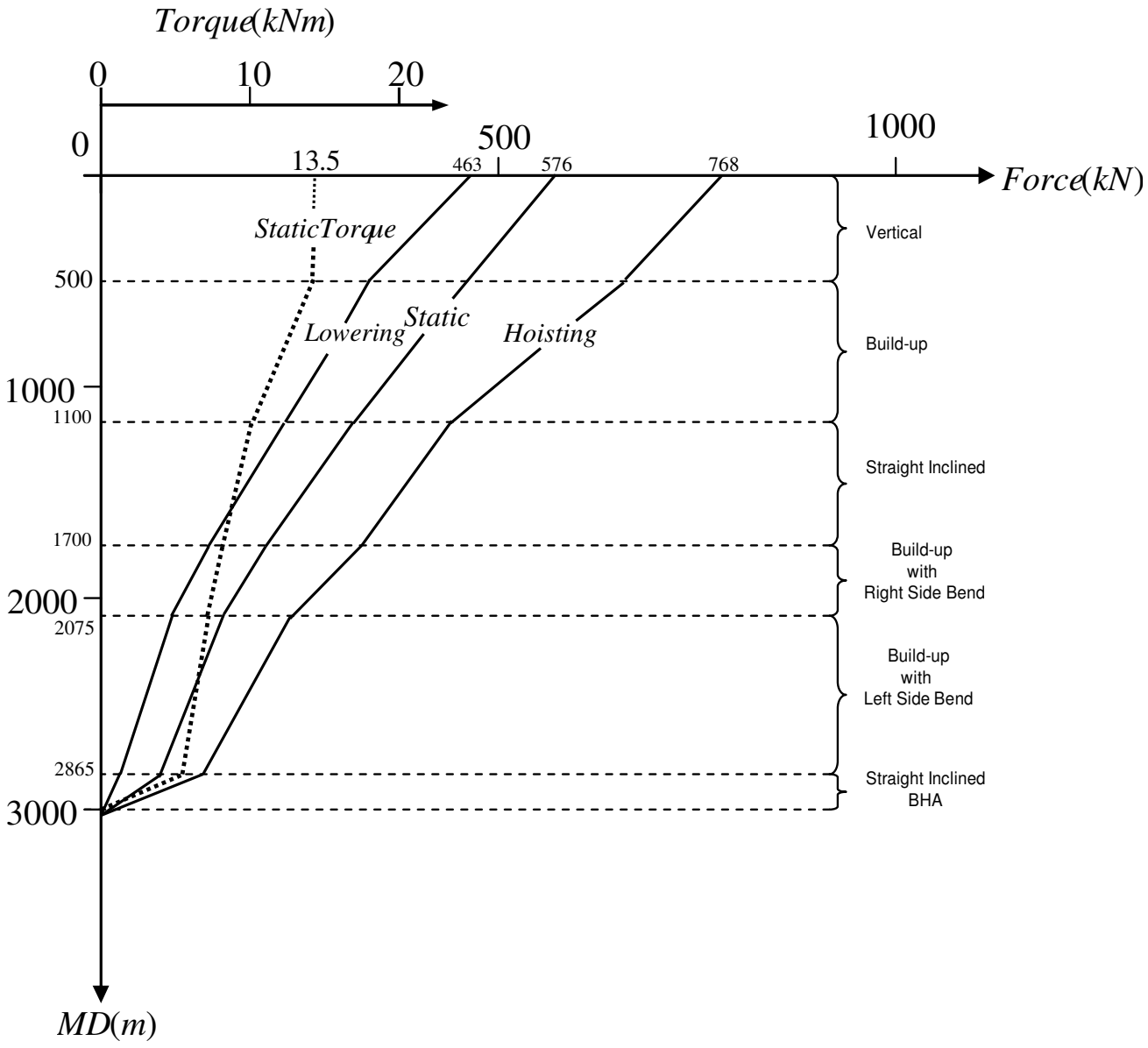

Figure 3.17: Wellbore friction for 3-dimensional well

3.5.3 Case C: Combined Motion in 3-dimensional Well

Some well operations are performed with combined motion. For high inclination wells it is common to rotate the liner in order to bring it to the desired depth. In the following we will investigate the frictional picture during such events.

Again assuming the same pipe data we will investigate the effect of combined motion in the well of Case B. The pipe is rotated at 100 rpm, and it is hoisted or lowered at 0.27 m/sec. From Equation 3.38, the angle between the axial and tangential pipe velocities becomes 30 degrees.

Using Equations 3.39 and 3.40, the friction for combined motion is computed. The results are shown in Figure 3.18, which compares pure hoisting/lowering with combined motion. A clear reduction in drag is observed.

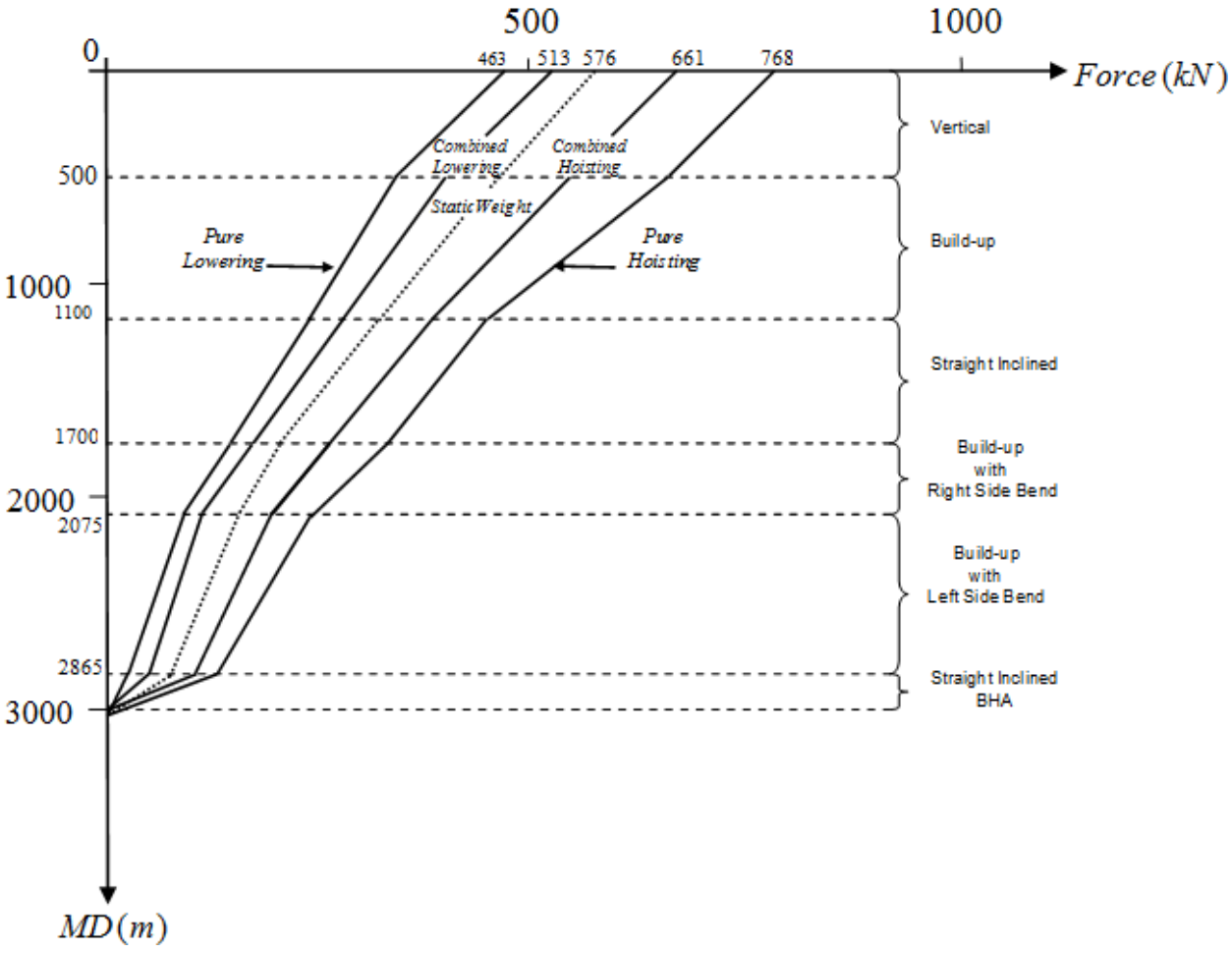

Figure 3.18: Comparison between pure hoisting/lowering and combined motion

Both when hoisting and lowering the string a reduced axial friction is seen. It is seen that the limiting value, $\psi \rightarrow 0^{\circ}$, which is obtained with low hoisting speed or high rotational speed, both

the hoisting and the lowering forces approached the static pipe weight. In other words, high rotation removes the axial friction.

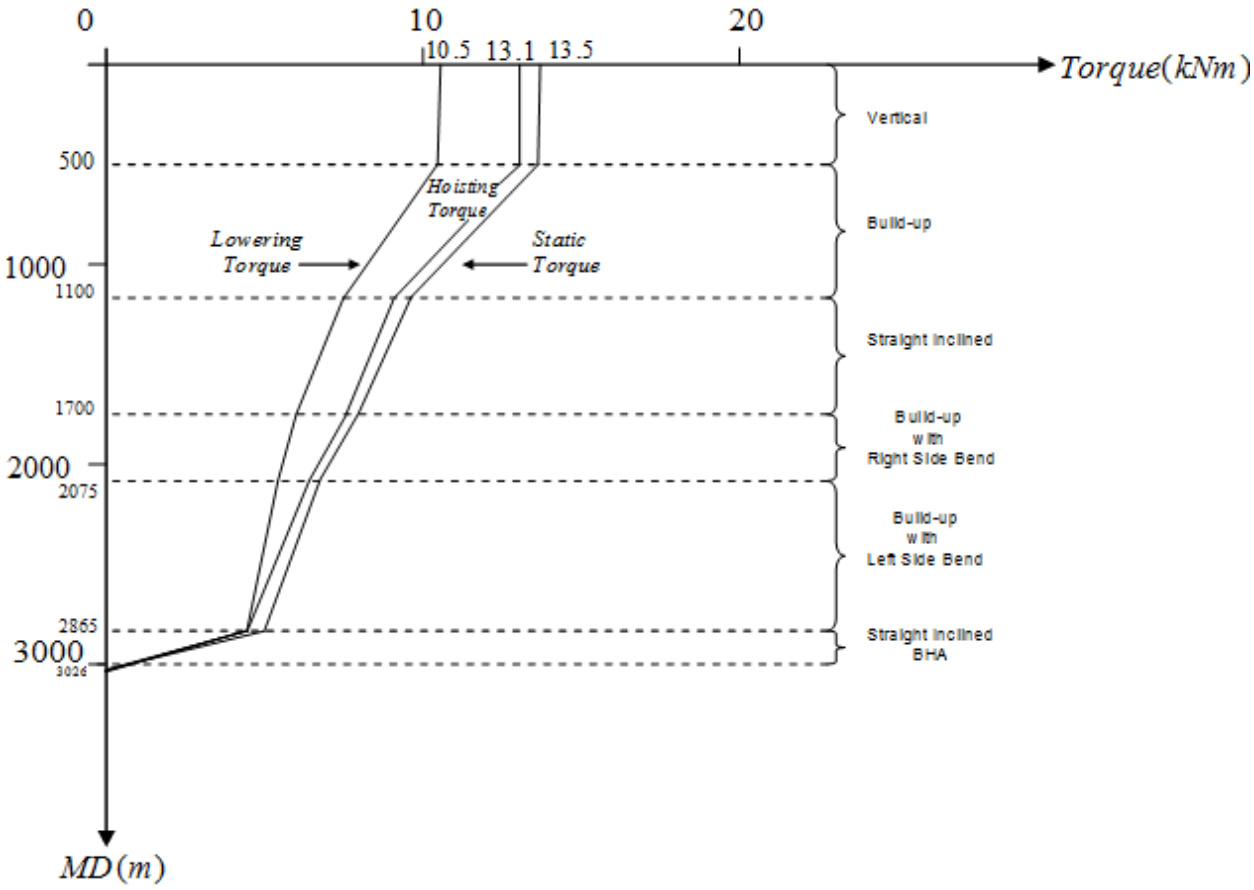

Figure 3.19: Torque along drill string with combined motion

Using equations 3.39 and 3.50, the torque during hoisting and lowering is compared to the static (bit off bottom) torque. During hoisting while back reaming the torque decreases slightly, whereas during lowering the torque decreases more as shown in Figure 3.19.

The examples above serve to show the potential of torque and drag analysis using the simple 3-dimensional models presented herein. To determine the coefficients of friction from field data, not only can the hoisting-lowering-rotation models be used, but also the models for combined motion. This should improve the determination of the frictional forces in a well, and also in application to any well operation.

CHAPTER FOUR: **TECHNICAL APPROACH- FINITE ELEMENT**

The finite element method is one of the most applied numerical methods for solving differential equations with complicated geometries (Reddy 2005). In this method problems are divided into a set of logical steps that can be implemented on a computer and solved for a wide range of input data. For example in drilling engineering, the finite element divides the entire drill string to finite number of small elements. Every smaller drill string element has simpler form to analyze and is not as complex as the entire drill string. The simulation of all the smaller elements leads to good approximation for the entire drill string analysis. At every node a polynomial expression for the equations of motion is generated which allows an accurate result at that specific point. For finite element analysis, equilibrium exist between the external applied forces and the internal forces. A compatibility of displacements and relationships between loads applied and deformations is reached (Reddy, 2005). In finite element analysis, boundary limitations are set for a given problem. If no boundary conditions are set for the system, it is treated as a rigid body floating in space. The boundary conditions have a strong effect on the solutions values. Different analysis of the same problem can be done with different boundary conditions simply by changing them. This could be done by changing the node conditions and placements or the material properties (Dukkipati, 2009).

In this research, an attempt was made to calculate the torque and drag from a generalized displacement of the drill string model which was used to predict the lateral and axial vibrations. The drill string has been thought of as a very long, unbalanced rotor of variable geometry constrained within a continuous journal bearing of variable clearance and rigidity. The dynamics of such a system is a rotor dynamic problem, so an approach that has been used effectively to solve rotor dynamics problems in other industries is also adapted for the present research. This requires developing the equations of motion beginning with Hamilton's principle, and then solving them using the finite element method for torque and drag calculations (Dykstra, 1996).

4.1 Hamilton's Principle

Hamilton's principle states that the motion of a particle is such that the kinetic and potential energies of the particle and the work done by the forces which act on it are related as shown the Equation 4.1:

$$\delta \int_{\Delta t} (k - p) + \int_{\Delta t} \delta W = 0 \tag{4.1}$$

In this expression, k is the kinetic energy which has components due to velocities of translation and rotation. p is the potential energy or strain energy and is defined in terms of stressσ and strain ε. W is the work done by forces including gravity, unbalanced mass and viscous force.δ is the variation operator in Equation 4.1 (Dykstra, 1996).

4.2 Shape Function

In finite element a beam element is defined by the two nodes being used, with six degrees of freedom (DOF) at each node; three displacements $u(x, y, z, t)$ and three rotations. This yields a total of 12 DOF for each element. A three dimensional beam model is used with six degrees of freedom for each node as shown in Fig 4.1: two transverse displacement (U2 or U8, U3 or U9), two bending rotations (U5 or U11, U6 or U12), one torsional rotation and one axial displacement (U1 or U7, U4 or U10) as shown by Wu et al., (2011).

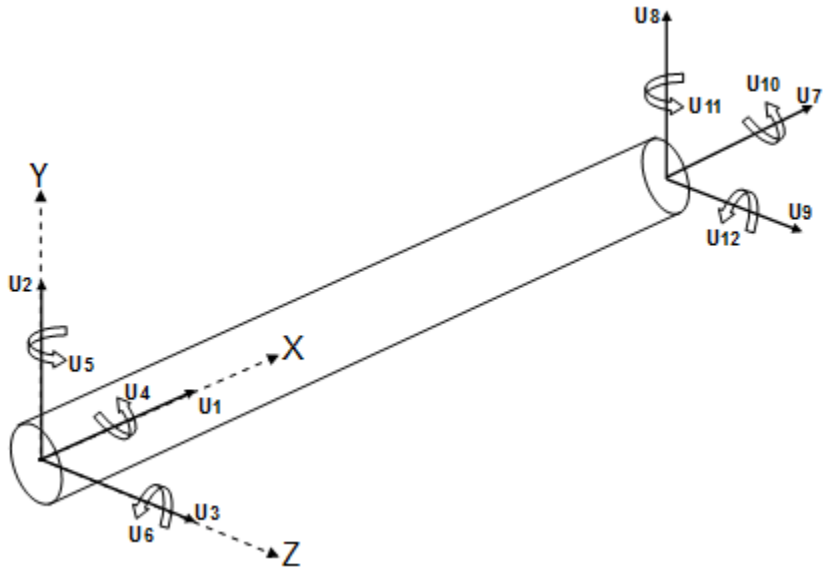

Figure 4.1: Generalized displacement for a beam element

4.3 The Dynamic Equations

The dynamic equations will be obtained by substituting the interpolation functions into the energy and work (Hamilton) expressions and evaluating the integrals. This results in the following discrete system of equations for an element which can be expressed as Equation 4.2 representing the matrix form of the equation of motion for a multi-degree of freedom system (Wu et al., 2011).

$$[M]\{\ddot{U}\}+[C]\{\dot{U}\}+[K]\{U\}=\{F\} \tag{4.2}$$

$[M]$, $[C]$and $[K]$ represents the mass, damping and stiffness matrixes respectively. If these matrixes are time independent and remain unchanged during integration, the dynamic system will be linear. For nonlinear dynamic systems, if they vary with the time, they must be modified during the integration. Also, the vectors $\{U\},\{\dot{U}\},\{\ddot{U}\}$ and $\{F\}$ represents generalized displacements, velocities, accelerations and forces acting on two nodes of an element, respectively. They can be shown in form of transpose as follow:

$$\{U\}^T = \{U_1 \quad U_2 \quad U_3 \quad U_4 \quad U_5 \quad U_6 \quad U_7 \quad U_8 \quad U_9 \quad U_{10} \quad U_{11} \quad U_{12}\} \tag{4.3}$$

$$\{\dot{U}\}^T = \{\dot{U}_1 \quad \dot{U}_2 \quad \dot{U}_3 \quad \dot{U}_4 \quad \dot{U}_5 \quad \dot{U}_6 \quad \dot{U}_7 \quad \dot{U}_8 \quad \dot{U}_9 \quad \dot{U}_{10} \quad \dot{U}_{11} \quad \dot{U}_{12}\} \tag{4.4}$$

$$\{\ddot{U}\}^T = \{\ddot{U}_1 \quad \ddot{U}_2 \quad \ddot{U}_3 \quad \ddot{U}_4 \quad \ddot{U}_5 \quad \ddot{U}_6 \quad \ddot{U}_7 \quad \ddot{U}_8 \quad \ddot{U}_9 \quad \ddot{U}_{10} \quad \ddot{U}_{11} \quad \ddot{U}_{12}\} \tag{4.5}$$

$$\{F\}^T = \{F_{11} \quad F_{12} \quad F_{13} \quad T_{11} \quad T_{12} \quad T_{13} \quad F_{21} \quad F_{22} \quad F_{23} \quad T_{21} \quad T_{22} \quad T_{23}\} \tag{4.6}$$

T in force vector represent the moment of force which means tendency of force to rotate or twist an object in different directions depends on local coordinate axis.

4.4 The Mass Matrix

The mass matrix $[M]$ is separated into two components: the matrix $[M_1]$ and $[M_2]$. $[M_1]$ Includes all three translational contributions and the axial rotation contribution, while $[M_2]$ contains contribution from rotation components, and thus provide corrections for rotary inertia (Dykstra, 1996).

$$[M] = [M_1] + [M_2] \tag{4.7}$$

The matrixes $[M_1]$ and $[M_2]$ are shown in Equation 4.8 and 4.9 for a beam element.

$$[M_1] = \rho AL \begin{bmatrix} \frac{1}{3} & 0 & 0 & 0 & 0 & 0 & \frac{1}{6} & 0 & 0 & 0 & 0 & 0 \\ 0 & \frac{13}{35} & 0 & 0 & 0 & \frac{11L}{210} & 0 & \frac{9}{70} & 0 & 0 & 0 & \frac{13L}{420} \\ 0 & 0 & \frac{13}{35} & 0 & \frac{11L}{210} & 0 & 0 & 0 & \frac{9}{70} & 0 & \frac{13L}{420} & 0 \\ 0 & 0 & 0 & \frac{I_z}{3A} & 0 & 0 & 0 & 0 & 0 & \frac{I_z}{6A} & 0 & 0 \\ 0 & 0 & \frac{11L}{210} & 0 & \frac{L^2}{105} & 0 & 0 & 0 & \frac{13L}{420} & 0 & \frac{L^2}{140} & 0 \\ 0 & \frac{11L}{210} & 0 & 0 & 0 & \frac{L^2}{105} & 0 & \frac{13L}{420} & 0 & 0 & 0 & \frac{L^2}{140} \\ \frac{1}{6} & 0 & 0 & 0 & 0 & 0 & \frac{1}{3} & 0 & 0 & 0 & 0 & 0 \\ 0 & \frac{9}{70} & 0 & 0 & 0 & \frac{13L}{420} & 0 & \frac{13}{35} & 0 & 0 & 0 & \frac{11L}{210} \\ 0 & 0 & \frac{9}{70} & 0 & \frac{13L}{420} & 0 & 0 & 0 & \frac{13}{35} & 0 & \frac{11L}{210} & 0 \\ 0 & 0 & 0 & \frac{I_z}{6A} & 0 & 0 & 0 & 0 & 0 & \frac{I_z}{3A} & 0 & 0 \\ 0 & 0 & \frac{13L}{420} & 0 & \frac{L^2}{140} & 0 & 0 & 0 & \frac{11L}{210} & 0 & \frac{L^2}{105} & 0 \\ 0 & \frac{13L}{420} & 0 & 0 & 0 & \frac{L^2}{140} & 0 & \frac{11L}{210} & 0 & 0 & 0 & \frac{L^2}{105} \end{bmatrix} \tag{4.8}$$

and

$$[M_2] = \frac{\rho I_{xp}}{L} \begin{bmatrix} 0 & 0 & 0 & 0 & 0 & 0 & 0 & 0 & 0 & 0 & 0 & 0 \\ 0 & \frac{6}{5} & 0 & 0 & 0 & \frac{L}{10} & 0 & -\frac{6}{5} & 0 & 0 & 0 & \frac{L}{10} \\ 0 & 0 & \frac{6}{5} & 0 & -\frac{L}{10} & 0 & 0 & 0 & -\frac{6}{5} & 0 & -\frac{L}{10} & 0 \\ 0 & 0 & 0 & 0 & 0 & 0 & 0 & 0 & 0 & 0 & 0 & 0 \\ 0 & 0 & -\frac{L}{10} & 0 & \frac{2L^2}{15} & 0 & 0 & 0 & \frac{L}{10} & 0 & -\frac{L^2}{30} & 0 \\ 0 & \frac{L}{10} & 0 & 0 & 0 & \frac{2L^2}{15} & 0 & -\frac{L}{10} & 0 & 0 & 0 & -\frac{L^2}{30} \\ 0 & 0 & 0 & 0 & 0 & 0 & 0 & 0 & 0 & 0 & 0 & 0 \\ 0 & -\frac{6}{5} & 0 & 0 & 0 & -\frac{L}{10} & 0 & \frac{6}{5} & 0 & 0 & 0 & -\frac{L}{10} \\ 0 & 0 & -\frac{6}{5} & 0 & \frac{L}{10} & 0 & 0 & 0 & \frac{6}{5} & 0 & \frac{L}{10} & 0 \\ 0 & 0 & 0 & 0 & 0 & 0 & 0 & 0 & 0 & 0 & 0 & 0 \\ 0 & 0 & -\frac{L}{10} & 0 & -\frac{L^2}{30} & 0 & 0 & 0 & \frac{L}{10} & 0 & \frac{2L^2}{15} & 0 \\ 0 & \frac{L}{10} & 0 & 0 & 0 & -\frac{L^2}{30} & 0 & -\frac{L}{10} & 0 & 0 & 0 & \frac{2L^2}{15} \end{bmatrix} \tag{4.9}$$

4.5 The Stiffness Matrix

The stiffness matrix is separated into linear and nonlinear contributions: $[K_L]$ and $[K_N]$.

$$[K]=[K_L]+[K_N] \tag{4.10}$$

The linear contributions to stiffness results from strain energy expression (Wu et al., 2011). The linear stiffness matrix has been shown in Equation 4.11.

$$[K_L]=\begin{bmatrix}
\frac{EA}{L} & 0 & 0 & 0 & 0 & 0 & \frac{-EA}{L} & 0 & 0 & 0 & 0 & 0 \\
0 & \frac{12EI_{zz}}{L^3} & 0 & 0 & 0 & \frac{6EI_{zz}}{L^2} & 0 & \frac{-12EI_{zz}}{L^3} & 0 & 0 & 0 & \frac{6EI_{zz}}{L^2} \\
0 & 0 & \frac{12EI_{yy}}{L^3} & 0 & \frac{-6EI_{yy}}{L^2} & 0 & 0 & 0 & \frac{-12EI_{yy}}{L^3} & 0 & \frac{-6EI_{yy}}{L^2} & 0 \\
0 & 0 & 0 & \frac{GI_x}{L} & 0 & 0 & 0 & 0 & 0 & \frac{-GI_x}{L} & 0 & 0 \\
0 & 0 & \frac{-6EI_{yy}}{L^2} & 0 & \frac{4EI_{yy}}{L} & 0 & 0 & 0 & \frac{6EI_{yy}}{L^2} & 0 & \frac{2EI_{yy}}{L} & 0 \\
0 & \frac{6EI_{zz}}{L^2} & 0 & 0 & 0 & \frac{4EI_{zz}}{L} & 0 & \frac{-6EI_{zz}}{L^2} & 0 & 0 & 0 & \frac{2EI_{zz}}{L} \\
\frac{-EA}{L} & 0 & 0 & 0 & 0 & 0 & \frac{EA}{L} & 0 & 0 & 0 & 0 & 0 \\
0 & \frac{-12EI_{zz}}{L^3} & 0 & 0 & 0 & \frac{-6EI_{zz}}{L^2} & 0 & \frac{12EI_{zz}}{L^3} & 0 & 0 & 0 & \frac{-6EI_{zz}}{L^2} \\
0 & 0 & \frac{-12EI_{yy}}{L^3} & 0 & \frac{6EI_{yy}}{L^2} & 0 & 0 & 0 & \frac{12EI_{yy}}{L^3} & 0 & \frac{6EI_{yy}}{L^2} & 0 \\
0 & 0 & 0 & \frac{-GI_x}{L} & 0 & 0 & 0 & 0 & 0 & \frac{GI_x}{L} & 0 & 0 \\
0 & 0 & \frac{-6EI_{yy}}{L^2} & 0 & \frac{2EI_{yy}}{L} & 0 & 0 & 0 & \frac{6EI_{yy}}{L^2} & 0 & \frac{4EI_{yy}}{L} & 0 \\
0 & \frac{6EI_{zz}}{L^2} & 0 & 0 & 0 & \frac{2EI_{zz}}{L} & 0 & \frac{-6EI_{zz}}{L^2} & 0 & 0 & 0 & \frac{4EI_{zz}}{L}
\end{bmatrix} \tag{4.11}$$

The components in the nonlinear stiffness matrix arise due to some terms in the strain-displacement relation presented in Equation 4.12.

$$[K_N]=[K_{NA_1}]+[K_{NA_2}]+[K_{NT}] \tag{4.12}$$

The $[K_{NA1}]$ and $[K_{NA2}]$ terms in Equation 4.12 represents coupling between axial force and flexure from different terms of strain energy (Dareing and Livesay, 1968). These terms are shown in Equation 4.13 and 4.14 respectively. These two matrixes are dependent to displacements, U_7 and U_1 which vary with the time and cause a dynamic system acts nonlinearly.

$$[K_{NA1}] = \frac{EA(U_7 - U_1)}{L^2}\begin{bmatrix}
\frac{3}{2} & 0 & 0 & 0 & 0 & 0 & \frac{-3}{2} & 0 & 0 & 0 & 0 & 0 \\
0 & \frac{6}{5} & 0 & 0 & 0 & \frac{L}{10} & 0 & \frac{-6}{5} & 0 & 0 & 0 & \frac{L}{10} \\
0 & 0 & \frac{6}{5} & 0 & \frac{-L}{10} & 0 & 0 & 0 & \frac{-6}{5} & 0 & \frac{-L}{10} & 0 \\
0 & 0 & 0 & \frac{I_x}{A} & 0 & 0 & 0 & 0 & 0 & \frac{-I_x}{A} & 0 & 0 \\
0 & 0 & \frac{-L}{10} & 0 & \frac{2L^2}{15} & 0 & 0 & 0 & \frac{L}{10} & 0 & \frac{-L^2}{30} & 0 \\
0 & \frac{L}{10} & 0 & 0 & 0 & \frac{2L^2}{15} & 0 & \frac{-L}{10} & 0 & 0 & 0 & \frac{-L^2}{30} \\
\frac{-3}{2} & 0 & 0 & 0 & 0 & 0 & \frac{3}{2} & 0 & 0 & 0 & 0 & 0 \\
0 & \frac{-6}{5} & 0 & 0 & 0 & \frac{-L}{10} & 0 & \frac{6}{5} & 0 & 0 & 0 & \frac{-L}{10} \\
0 & 0 & \frac{-6}{5} & 0 & \frac{L}{10} & 0 & 0 & 0 & \frac{6}{5} & 0 & \frac{L}{10} & 0 \\
0 & 0 & 0 & \frac{-I_x}{A} & 0 & 0 & 0 & 0 & 0 & \frac{I_x}{A} & 0 & 0 \\
0 & 0 & \frac{-L}{10} & 0 & \frac{-L^2}{30} & 0 & 0 & 0 & \frac{L}{10} & 0 & \frac{2L^2}{15} & 0 \\
0 & \frac{L}{10} & 0 & 0 & 0 & \frac{-L^2}{30} & 0 & \frac{-L}{10} & 0 & 0 & 0 & \frac{2L^2}{15}
\end{bmatrix} \quad (4.13)$$

$$\left[K_{NA2}\right] = \frac{EI_x(U_7 - U_1)}{L^4}\begin{bmatrix}
0 & 0 & 0 & 0 & 0 & 0 & 0 & 0 & 0 & 0 & 0 & 0 \\
0 & 6L^2 & 0 & 0 & 0 & 3L^3 & 0 & -6L^2 & 0 & 0 & 0 & 3L^3 \\
0 & 0 & 6L^2 & 0 & -3L^3 & 0 & 0 & 0 & -6L^2 & 0 & -3L^3 & 0 \\
0 & 0 & 0 & 0 & 0 & 0 & 0 & 0 & 0 & 0 & 0 & 0 \\
0 & 0 & -3L^3 & 0 & 2L^4 & 0 & 0 & 0 & 3L^3 & 0 & L^4 & 0 \\
0 & 3L^3 & 0 & 0 & 0 & 2L^4 & 0 & -3L^3 & 0 & 0 & 0 & L^4 \\
0 & 0 & 0 & 0 & 0 & 0 & 0 & 0 & 0 & 0 & 0 & 0 \\
0 & -6L^2 & 0 & 0 & 0 & -3L^3 & 0 & 6L^2 & 0 & 0 & 0 & -3L^3 \\
0 & 0 & -6L^2 & 0 & 3L^3 & 0 & 0 & 0 & 6L^2 & 0 & 3L^3 & 0 \\
0 & 0 & 0 & 0 & 0 & 0 & 0 & 0 & 0 & 0 & 0 & 0 \\
0 & 0 & -3L^3 & 0 & L^4 & 0 & 0 & 0 & 3L^3 & 0 & 2L^4 & 0 \\
0 & 3L^3 & 0 & 0 & 0 & L^4 & 0 & -3L^3 & 0 & 0 & 0 & 2L^4
\end{bmatrix} \tag{4.14}$$

The $\left[K_{NT}\right]$ represents coupling between torsion and flexure which is also a geometric stiffness contribution, but unlike the axial force-flexure matrices the component addresses do not coincide with those in linear stiffness matrix (Dareing and Livesay, 1968). The vectors U_{10} and U_4 represent rotation terms related to element rotations along the X-axis as shown in Figure 4.1.

$$\left[K_{NT}\right] = (1+2\nu)\frac{GI_z(U_{10} - U_4)}{L^2}\begin{bmatrix}
0 & 0 & 0 & \frac{1+\nu}{2(1+2\nu)} & 0 & 0 & 0 & 0 & 0 & -\frac{1+\nu}{2(1+2\nu)} & 0 & 0 \\
0 & 0 & 0 & 0 & -1 & 0 & 0 & 0 & 0 & 0 & 1 & 0 \\
0 & 0 & 0 & 0 & 0 & -1 & 0 & 0 & 0 & 0 & 0 & 1 \\
0 & 0 & 0 & 0 & 0 & 0 & 0 & 0 & 0 & 0 & 0 & 0 \\
0 & -1 & 0 & 0 & 0 & 0 & 0 & 1 & 0 & 0 & 0 & -\frac{L}{2} \\
0 & 0 & -1 & 0 & 0 & 0 & 0 & 0 & 1 & 0 & \frac{L}{2} & 0 \\
0 & 0 & 0 & -\frac{1+\nu}{2(1+2\nu)} & 0 & 0 & 0 & 0 & 0 & \frac{1+\nu}{2(1+2\nu)} & 0 & 0 \\
0 & 0 & 0 & 0 & 1 & 0 & 0 & 0 & 0 & 0 & -1 & 0 \\
0 & 0 & 0 & 0 & 0 & 1 & 0 & 0 & 0 & 0 & 0 & -1 \\
0 & 0 & 0 & 0 & 0 & 0 & 0 & 0 & 0 & 0 & 0 & 0 \\
0 & 1 & 0 & 0 & 0 & \frac{L}{2} & 0 & -1 & 0 & 0 & 0 & 0 \\
0 & 0 & 1 & 0 & -\frac{L}{2} & 0 & 0 & 0 & -1 & 0 & 0 & 0
\end{bmatrix} \tag{4.15}$$

4.6 The Damping Matrix

The damping matrix includes two parts: $[C_D]$ and $[C_N]$.

$$[C]=[C_D]+[C_N] \tag{4.16}$$

The matrix $[C_D]$ is a dissipative damping matrix. It means they remove energy from the system. The $[C_D]$ considered in this research is that of Rayleigh (Besaisow, et. al, 1985). It is assumed to be appropriate because the drill string is immersed in a fluid which is generally viscous. Rayleigh damping is obtained from linear combination of the mass and stiffness matrices.

$$[C_D]=\alpha[M]+\beta[K_L] \tag{4.17}$$

Where α and β are weighting parameters that allow system damping to be adjusted.

$$[C_N]=\frac{\Omega J_z}{L}\begin{bmatrix}
0 & 0 & 0 & 0 & 0 & 0 & 0 & 0 & 0 & 0 & 0 & 0\\
0 & 0 & \frac{6}{5} & 0 & -\frac{L}{10} & 0 & 0 & 0 & -\frac{6}{5} & 0 & \frac{L}{10} & 0\\
0 & -\frac{6}{5} & 0 & 0 & 0 & -\frac{L}{10} & 0 & \frac{6}{5} & 0 & 0 & 0 & -\frac{L}{10}\\
0 & 0 & 0 & 0 & 0 & 0 & 0 & 0 & 0 & 0 & 0 & 0\\
0 & \frac{L}{10} & 0 & 0 & 0 & \frac{2L^2}{15} & 0 & -\frac{L}{10} & 0 & 0 & 0 & -\frac{L^2}{30}\\
0 & 0 & \frac{L}{10} & 0 & -\frac{2L^2}{15} & 0 & 0 & 0 & -\frac{L}{10} & 0 & \frac{L^2}{30} & 0\\
0 & 0 & 0 & 0 & 0 & 0 & 0 & 0 & 0 & 0 & 0 & 0\\
0 & 0 & -\frac{6}{5} & 0 & \frac{L}{10} & 0 & 0 & 0 & \frac{6}{5} & 0 & \frac{L}{10} & 0\\
0 & \frac{6}{5} & 0 & 0 & 0 & \frac{L}{10} & 0 & -\frac{6}{5} & 0 & 0 & 0 & \frac{L}{10}\\
0 & 0 & 0 & 0 & 0 & 0 & 0 & 0 & 0 & 0 & 0 & 0\\
0 & \frac{L}{10} & 0 & 0 & 0 & -\frac{L^2}{30} & 0 & -\frac{L}{10} & 0 & 0 & 0 & \frac{2L^2}{15}\\
0 & 0 & \frac{L}{10} & 0 & \frac{L^2}{30} & 0 & 0 & 0 & -\frac{L}{10} & 0 & -\frac{2L^2}{15} & 0
\end{bmatrix} \tag{4.18}$$

The matrix $[C_N]$ is a non-dissipative damping matrix, or a gyroscopic matrix as shown in Equation 4.18 (Dykstra, 1996).

In all above matrixes, E、ν、G is drill string elastic modulus, Poisson's ratio and shear modulus respectively; I_x, I_y and I_z are on the x ,y and z-axis area moment of inertia of drill string element; Ω the drill string rotation speed; J_z is the polar moment of inertia of drill string element on z-axis . Also, ρ, A and L are density, cross sectional area and length of drill string element.

4.7 Force Vector

Dykstra in 1996 presented the external forces which include gravity, imbalanced mass and frictional interaction with the wellbore. The gravity force is the equivalent generalized force for the loading due to distributed mass. This is equivalent to setting the virtual work done on the continuous structure by the distributed loads (concentrated forces and moments) to the work done on the discrete model by the generalized nodal forces.

The contributions to the external force vectors due to imbalanced forces are obtained just as the gravity forces were. The equivalent nodal forces for the distributed imbalance loads include both forces and moments. Imbalanced force occurs when the center of gravity does not coincide with the rotary center of the drill string. In this research, the imbalanced force is neglected.

Dykstra in 1996, showed the gravity force vector as Equation 4.19. This gravity forces vector are equivalent to both concentrated forces and moments for a specific element as shown in Figure 4.2.

$$[F_{gravity}]=\left[\frac{-w_x L}{2}\quad \frac{-w_y L}{2}\quad 0\quad 0\quad 0\quad \frac{-w_y L^2}{12}\quad \frac{-w_x L}{2}\quad \frac{-w_y L}{2}\quad 0\quad 0\quad 0\quad \frac{w_y L^2}{12}\right] \qquad (4.19)$$

Where

$$w_x = w \times \cos\alpha$$
$$w_y = w \times \sin\alpha \qquad (4.20)$$

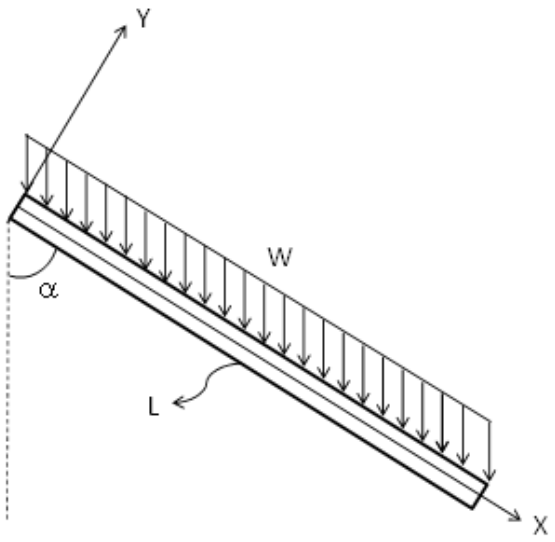

Figure 4.2: Distributed forces due to gravity on an inclined element

For friction force consideration in force vector it is necessary to estimate the normal force at each element. Figure 4.3 shows the normal force F_N acting on drill string element which is very important in torque and drag calculations.

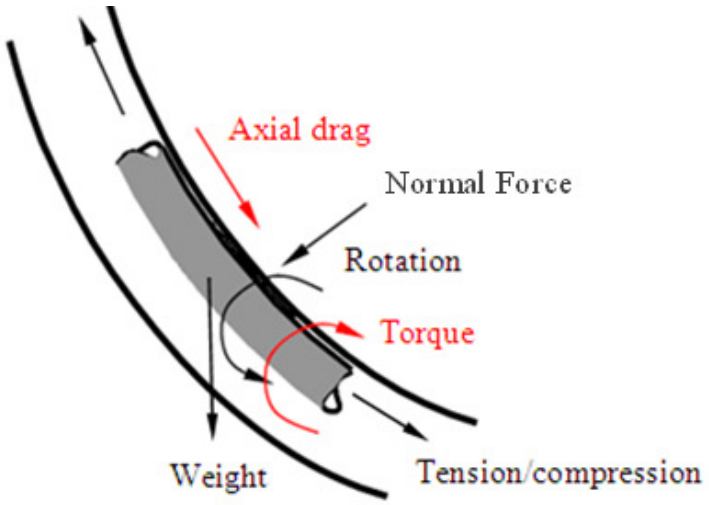

Figure 4.3: The forces applied on an element of drill string

Equation 4.21 was presented by Johancsik in 1985 as discussed in Chapter 2 is used for normal force calculation F_N.

$$F_N = [\left(F_1(\varphi_2 - \varphi_1)\sin\left(\frac{\alpha_2 + \alpha_1}{2}\right)\right)^2 + \left(F_1(\alpha_2 - \alpha_1) + \beta w \sin\left(\frac{\alpha_2 + \alpha_1}{2}\right)\right)^2]^{1/2} \quad (4.21)$$

After the normal contact force was obtained, the axial drag and torque can be obtained easily by using Equations 4.22, 4.23 for known friction coefficient.

$$FF_{axial} = \mu \cdot F_N \quad (4.22)$$

$$FF_{rotational} = \mu \cdot F_N \cdot r \quad (4.23)$$

The changes in drill string movement will change the direction of friction force. For example, if the movement of drill string is downward (tripping in, drilling), the friction force acts upwardly. Also the friction coefficient can be estimated using torque and drag model. If the measured hook load is known, the friction coefficient will be estimated using an iterative method to make the calculated hook load equal to measured one.

4.8 Transform Matrix

In different hole sections of deviated and horizontal well, each drill string element has its own coordinate which is not the same as global coordinates for the entire drill string, as shown in Figure 4.4.

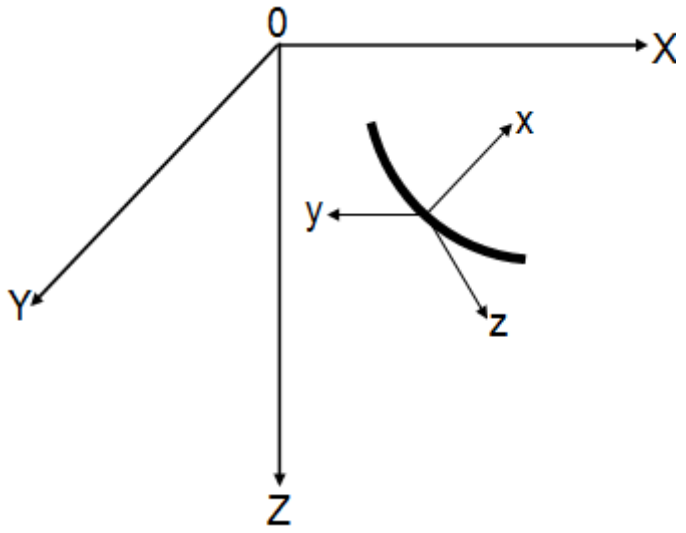

Figure 4.4: Difference between element local coordinate system and global coordinate system

To include inclination and azimuth angles in torque and drag calculations, it is required to define a matrix to transform the element coordinate system xyz to the global coordinate system XYZ. The transform matrix defined as shown in Equation 4.24 includes inclination and azimuth angles for each element. It is necessary for all matrixes such as mass, stiffness and damping as well as and vectors such as displacement, velocity, acceleration and forces to be transformed from their local coordinate to the global coordinate.

In Equation 4.25, α and φ represent inclination and azimuth, U_z, U_x, U_y, E_z, E_x and E_y are three translations and three rotations in the global system and u_z, u_x, u_y, ε_z, ε_x and ε_y are three translations and three rotations in the local system (Wu et. al., 2011).

$$\begin{Bmatrix} U_z \\ U_x \\ U_y \\ E_z \\ E_x \\ E_y \end{Bmatrix} = \begin{bmatrix} \cos\alpha & -\sin\alpha & 0 & & & \\ \sin\alpha\cos\phi & \cos\alpha\cos\phi & -\sin\phi & & 0 & \\ \sin\alpha\sin\phi & \cos\alpha\sin\phi & \cos\phi & & & \\ & & & \cos\alpha & -\sin\alpha & 0 \\ & 0 & & \sin\alpha\cos\phi & \cos\alpha\cos\phi & -\sin\phi \\ & & & \sin\alpha\sin\phi & \cos\alpha\sin\phi & \cos\phi \end{bmatrix} \begin{Bmatrix} u_z \\ u_x \\ u_y \\ \varepsilon_z \\ \varepsilon_x \\ \varepsilon_y \end{Bmatrix} \quad (4.24)$$

Also in dealing with the initial conditions and boundary conditions of work, we often need the coordinates of each element in local coordinate system. At this point it is required load, displacement, velocity column matrix to be transformed from global coordinate system to the local coordinate system. Coordinate transformation appears multiple times in a dynamic model to approach a solution.

4.9 Global Matrix

In order to get the solution of the system, the global matrix should be formed using such element mass matrix like Equation 4.25.

$$[M]^i = \begin{bmatrix} [M_{11}^i]_{6\times6} & [M_{12}^i]_{6\times6} \\ [M_{21}^i]_{6\times6} & [M_{22}^i]_{6\times6} \end{bmatrix} \tag{4.25}$$

The assembly process for entire drill string can be shown in the following Equation 4.26 taking mass matrix as an example.

$$[M] = \begin{bmatrix}
[M_{11}^1] & [M_{12}^1] & & & & & & & & & & & & & \\
[M_{21}^1] & [M_{22}^1]+[M_{11}^2] & [M_{12}^2] & & & & & & & & & & & & \\
 & [M_{21}^2] & [M_{22}^2]+\cdots & \cdots & & & & & & & & & & & \\
 & & \cdots & \cdots & \cdots & \cdots & & & & & & & & & \\
 & & & \cdots & \cdots & [M_{22}^{i-1}]+[M_{11}^i] & [M_{12}^i] & & & & & & & & \\
 & & & & \cdots & [M_{21}^i] & [M_{22}^i]+[M_{11}^{i+1}] & \cdots & & & & & & & \\
 & & & & & & \cdots & \cdots & \cdots & & & & & & \\
 & & & & & & & \cdots & & & & & & & \\
 & & & & & & & & \cdots & \cdots & & & & & \\
 & & & & & & & & \cdots & \cdots+[M_{11}^{N-1}] & [M_{12}^{N-1}] & & & & \\
 & & & & & & & & & [M_{21}^{N-1}] & [M_{22}^{N-1}]+[M_{11}^N] & [M_{12}^N] & & \\
 & & & & & & & & & & [M_{21}^N] & [M_{22}^N] & & &
\end{bmatrix} \tag{4.26}$$

For the force vector, the global vector for a single element can be written as follow:

$$\{F^i\} = \begin{Bmatrix} \{F_1^i\}_{6\times1} \\ \{F_2^i\}_{6\times1} \end{Bmatrix} \tag{4.27}$$

Where

$$\{F_1^i\}_{6\times1} = \{F_z^1 \quad F_x^1 \quad F_y^1 \quad T_z^1 \quad T_x^1 \quad T_y^1\} \tag{4.28}$$

$$\{F_2^i\}_{6\times1} = \{F_z^2 \quad F_x^2 \quad F_y^2 \quad T_z^2 \quad T_x^2 \quad T_y^2\} \tag{4.29}$$

The global vector force for entire drill string will be in the form as Equation 4.30

$$\{F\} = \left\{\{F_1^1\}^T, \{F_2^1\}^T + \{F_2^2\}^T, \{F_2^2\}^T + \{F_1^3\}^T, ..., \{F_2^n\}^T + \{F_1^{n+1}\}^T, \{F_2^{n+1}\}^T\right\} \tag{4.30}$$

4.10 Boundary Conditions

The drill string is hung on the hook during different operations and only during connections, all load goes on the slips. The derrick, drilling line and even hook by itself can be taken as suspension system. The suspension system is simplified as a spring, the stiffness coefficient of which is KH, so the hook load can be calculated as the following Equation 4.31.

$$F_{hookload} = KH \cdot U_z^1 \tag{4.31}$$

where

$F_{hookload}$: hook load, N

U_z^1: the axial translation of the first node, m

The main boundaries are at the rotary table, drill bit and stabilizers as shown in the Figure 4.5.

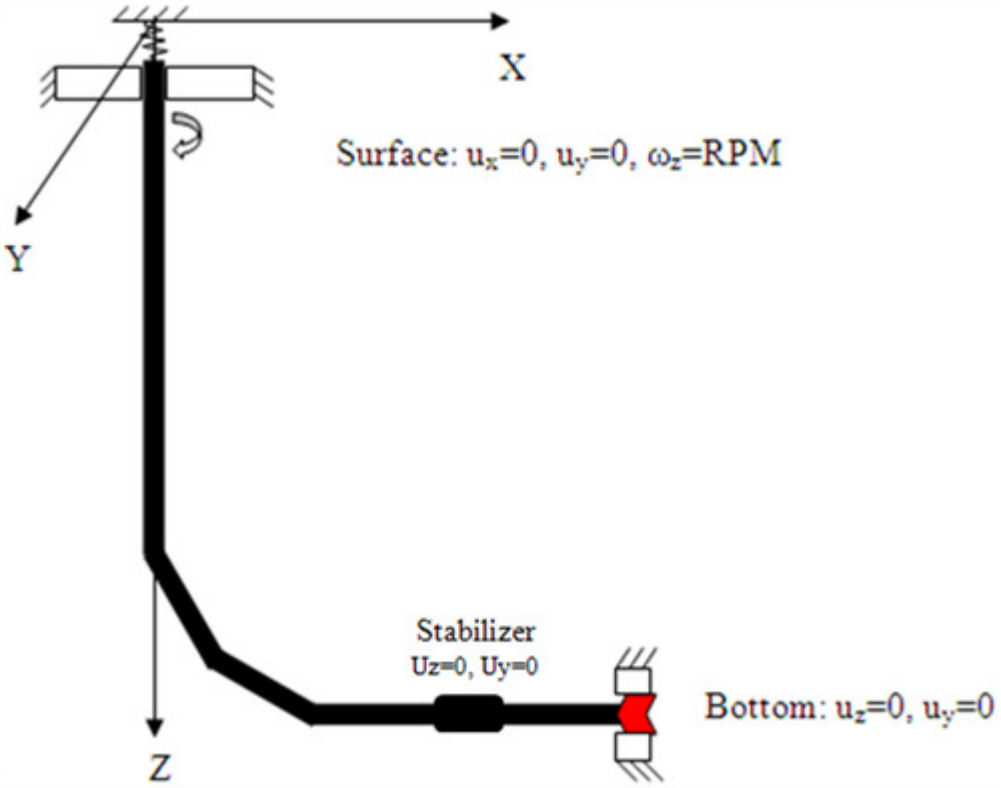

Figure 4.5: Main boundaries on the drill string in the wellbore

At the rotary table, the radial displacement is constrained but axial displacement and rotation around drill string axis are released. For the rotary table (or top drive) at surface the following boundary conditions for the different modes is considered:

(1) rotating drilling (including common rotary drilling and top drive system)

$U_x^1 = 0$

$U_y^1 = 0$

$$E_z^1 = 2 \times \pi \times rpm$$

$$T_z^1 = Torque_{surface}$$

where

rpm: rotary speed of the table

$Torque_{surface}$: torque on the table

1: 1st element

(2) sliding drilling, tripping in, tripping out

$$U_x^1 = 0$$

$$U_y^1 = 0$$

$$E_z^1 = 0$$

At the bottom hole, the radial displacement is constrained but axial displacement and rotation around the drill string axis is released. In this condition, the axial and radial forces as well as the torque around drill string are applied.

(3) rotating drilling (including common rotary drilling and top drive system) and sliding

$$U_x^n = 0$$

$$U_y^n = 0$$

$$F_z^n = WOB_{bottom}$$

$$T_z^n = Torque_{bottom}$$

(4) Sliding drilling, tripping in, tripping out

$$U_x^n = 0$$

$$U_y^n = 0$$

$$F_z^n = 0$$

$$T_z^n = 0$$

where

n: last element

At the stabilizers: radial displacement is constrained and axial displacement and rotation around drill string axis is released;

(5) For any operation mode

$$U_x^i = 0$$

$$U_y^i = 0$$

The drill string is constrained in the wellbore all the time as shown in Figure 4.6. In the local coordinate system o-xyz, lateral displacements u_x and u_y of centerline should satisfy the following Equation.

$$\sqrt{u_x^2 + u_y^2} \le \Delta d \tag{4.32}$$

Where

$\Delta D = \dfrac{(D-d)}{2}$: Clearance between the BHA components and the wellbore wall

D: diameter of the wellbore

d: outer diameter of BHA.

If the above equation is not satisfied, the BHA will contact the wellbore wall.

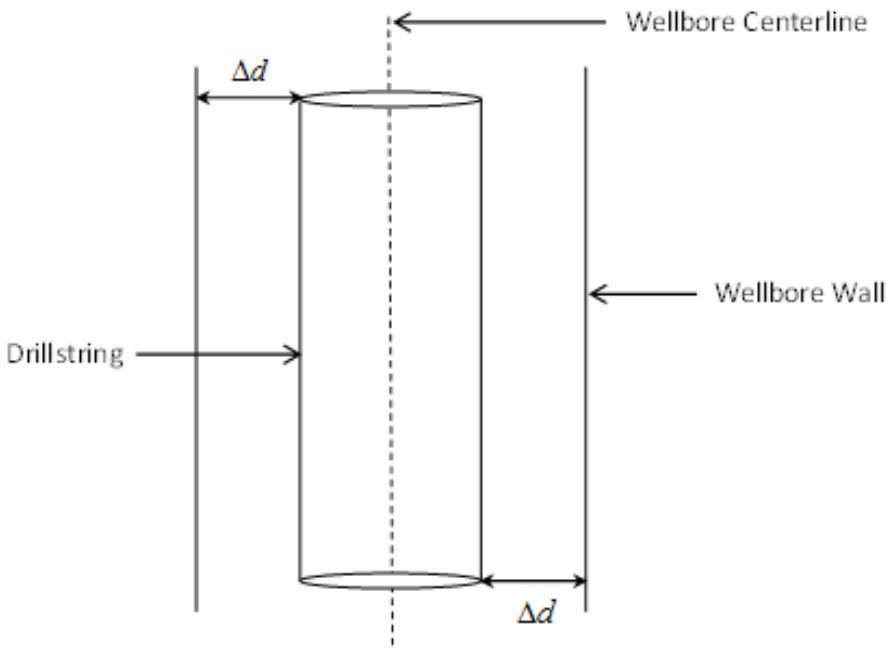

Figure 4.6: Constraint relations between drill string and wellbore

4.11 Solution Method

In this study, as solution method, the implicit method is used to get the displacement values directly as solutions from the equation of motion directly. For implicit schemes, the following solution methods are available.

- Houbolt
- Newmark Beta
- Park Stiffly stable
- Wilson-Theta

4.11.1 Houbolt Method

The Houbolt method is based on 3rd order of displacement U_t, and the multistep formulas for velocity $\dot{U}_t$ and acceleration $\ddot{U}_t$ are obtained in terms of displacement by using the backward differencesby considering a cubic curve that passes through the four successive ordinates as shown in Figure 4.7 , Dukkipati (2009).

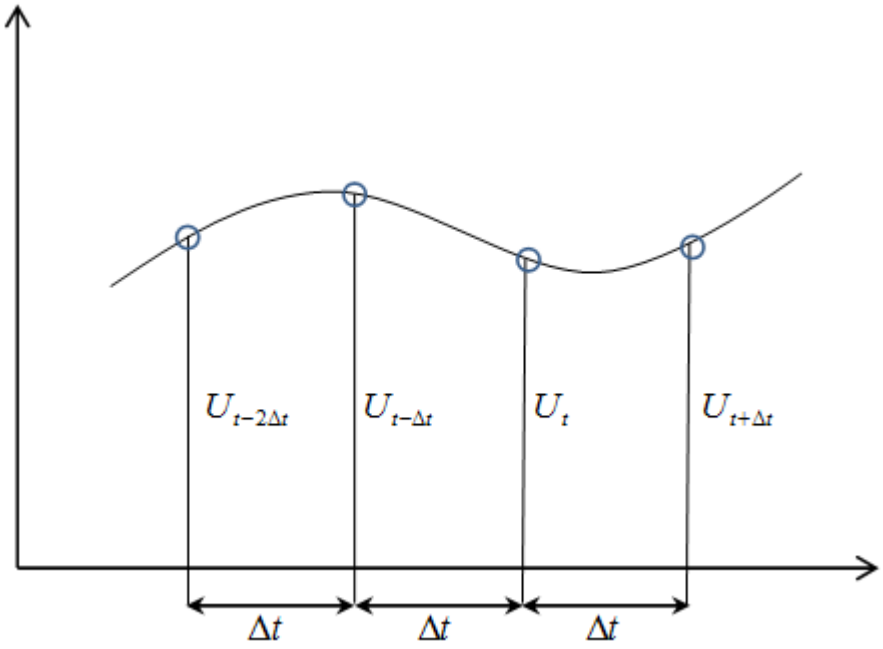

Figure 4.7: Cubic curve pass through four ordinates

The equation of motion, Equation 4.2, can be written in form of Equation 4.33 using Houbolt method as presented by Dukkipati (2009).

$$\left[\tilde{M}\right]\left\{\ddot{U}_{t+\Delta t}\right\}=\left\{FF_{t+\Delta t}\right\} \tag{4.33}$$

Where $[\tilde{M}]$, the effective mass matrix and $\{FF_{t+\Delta t}\}$ is the effective force vector as shown in following equations:

$$[\tilde{M}] = \frac{2}{\Delta t^2}[M] + \frac{11}{6\Delta t}[C] + [K] \tag{4.34}$$

and

$$\{FF_{t+\Delta t}\} = \{F_{t+\Delta t}\} + \left(\frac{5}{\Delta t^2}[M] + \frac{3}{\Delta t}[C]\right)\{U_t\} - \left(\frac{4}{\Delta t^2}[M] + \frac{3}{2\Delta t}[C]\right)\{U_{t-\Delta t}\} + \left(\frac{1}{\Delta t^2}[M] + \frac{1}{3\Delta t}[C]\right)\{U_{t-2\Delta t}\} \tag{4.35}$$

The Houbolt method has some disadvantages which does not allow this method used for drill string dynamic system. In Equation 4.35, there is no direct method to find $\{U_{t-\Delta t}\}$ and $\{U_{t-2\Delta t}\}$ initially which makes this method non-self starting. Also, it requires large computer storage to store displacement for the previous time steps (Dukkipati, 2009).

4.11.2 Newmark Beta Method

This method is based on this assumption that acceleration varies linearly between two instants of time. Two parameters of α and β are used in this method which can be changed to meet the requirements of a particular problem (Dukkipati, 2009). The effective mass matrix $[\tilde{M}]$ and effective force vector $\{FF_{t+\Delta t}\}$ are given by the following:

$$[\tilde{M}] = \frac{2}{\beta\Delta t^2}[M] + \frac{\alpha}{\beta\Delta t}[C] + [K] \tag{4.36}$$

and

$$\{FF_{t+\Delta t}\}=\{F_{t+\Delta t}\}+\left(\left(\frac{1}{2\beta}-1\right)[M]+\Delta t\left(\frac{\alpha}{2\beta}-1\right)[C]\right)\{\ddot{U}_t\}+\left(\frac{1}{\beta\Delta t}[M]+\left(\frac{\alpha}{\beta}-1\right)[C]\right)\{\dot{U}_t\}+\left(\frac{1}{\beta\Delta t^2}[M]+\frac{\alpha}{\beta\Delta t}[C]\right)\{U_t\} \tag{4.37}$$

The solution of Newmark method is $\{U_{t+\Delta t}\}$, then acceleration and velocity can be calculated at $t+\Delta t$ afterwards. For a linear system, this method is unconditionally stable if $\alpha \geq \frac{1}{2}$ and $\beta \geq \frac{1}{4}\left(\alpha+\frac{1}{2}\right)^2$ (Dukkipati, 2009). In this method α and β vary based on the nature of the dynamic system which make this method unsuitable for a drill string system that is changing during different operations.

4.11.3 Park Stiffly Stable Method

This method is an accurate method for low frequency ranges and stable for all higher-frequency components Dukkipati (2009). The effective mass matrix and force vector for this method can be written as:

$$[\tilde{M}]=\frac{100}{36\Delta t^2}[M]-\frac{10}{6\Delta t}[C]+[K] \tag{4.38}$$

and

$$\{FF_{t+\Delta t}\}=\frac{15}{6\Delta t}[M]\{\dot{U}_t\}-\frac{1}{\Delta t}[M]\{\dot{U}_{t-\Delta t}\}+\frac{1}{6\Delta t}[M]\{\dot{U}_{t-2\Delta t}\}+\left(\frac{150}{36\Delta t^2}[M]+\frac{15}{6\Delta t}[C]\right)\{U_t\}-$$
$$\left(\frac{10}{6\Delta t^2}[M]+\frac{1}{\Delta t}[C]\right)\{U_{t-\Delta t}\}+\left(\frac{1}{36\Delta t^2}[M]+\frac{1}{6\Delta t}[C]\right)\{U_{t-2\Delta t}\} \quad (4.39)$$

In the Park Stiffly Stable Method, the calculation of $\{U_{t+\Delta t}\}$ requires the displacements and velocities at t, $t-\Delta t$, and $t-2\Delta t$. Therefore a special starting procedure is needed which makes the method non-self starting. Also, the method requires large memory space to store displacements and velocities for two previous time steps (Dukkipati, 2009).

4.11.4 Wilson Theta Method

In this method, the variations of accelerations are assumed linear between two instants of time as shown in Figure 4.8. The acceleration is assumed to be linear from time t between $t_i = i\Delta t$ to time $t_{i+\theta} = t_i + \theta\Delta t$, where $\theta \geq 1.0$. Because of this reason, the method is known as the Wilson Theta method.

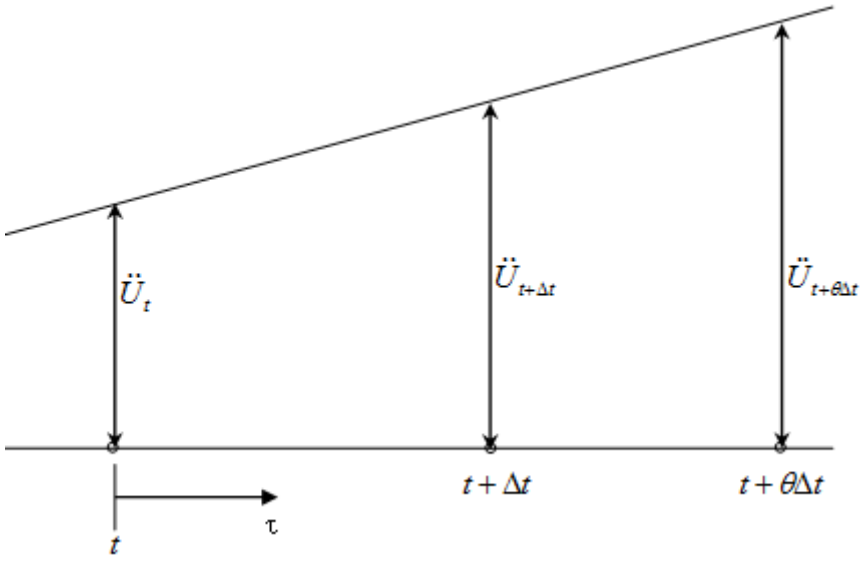

Figure 4.8: Linear changes of accelerations for a dynamic system

By using Wilson theta method, equation of motion will reform into the following format:

$$\left[\tilde{M}\right]\left\{\ddot{U}_{t+\theta\Delta t}\right\}=\left\{FF_{t+\theta\Delta t}\right\} \tag{4.40}$$

For the Wilson Theta, the effective mass matrix $\left[\tilde{M}\right]$ and the effective force vector $\left\{FF_{t+\theta\Delta t}\right\}$ are written as follow:

$$\left[\tilde{M}\right]=\left[M\right]+\frac{\theta\Delta t}{2}\left[C\right]+\frac{(\theta\Delta t)^2}{6}\left[K\right] \tag{4.41}$$

And

$$\left\{FF_{t+\theta\Delta t}\right\}=\left\{F_{t+\theta\Delta t}\right\}-\left[C\right]\times\left(\left\{\dot{U}_t\right\}+\frac{\theta\Delta t}{2}\left\{\ddot{U}_t\right\}\right)-\left[K\right]\times\left(\left\{U_t\right\}+\theta\Delta t\left\{\dot{U}_t\right\}+\frac{(\theta\Delta t)^2}{3}\left\{\ddot{U}_t\right\}\right) \tag{4.42}$$

The solution of Equation 4.40 gives $\left\{\ddot{U}_{t+\theta\Delta t}\right\}$ which is often used to substitute into the following relationship to obtain the displacements, velocities and accelerations at time $t+\Delta t$.

$$\left\{U_{t+\Delta t}\right\}=\left\{U_t\right\}+\Delta t\left\{\dot{U}_t\right\}+\frac{\Delta t^2}{6\theta}\left[\ddot{U}_{t+\theta\Delta t}\right]+(3\theta-1)\frac{\Delta t^2}{6\theta}\left\{\ddot{U}_t\right\} \tag{4.43}$$

$$\left\{\dot{U}_{t+\Delta t}\right\}=\left\{\dot{U}_t\right\}+\frac{\Delta t}{2\theta}\left\{\ddot{U}_{t+\theta\Delta t}\right\}+(2\theta-1)\frac{\Delta t}{6\theta}\left\{\ddot{U}_t\right\} \tag{4.44}$$

$$\{\ddot{U}_{t+\Delta t}\} = \frac{1}{\theta}\{\ddot{U}_{t+\theta\Delta t}\} + (1-\frac{1}{\theta})\{\ddot{U}_{t}\} \tag{4.45}$$

The method is unconditionally stable for linear dynamic systems when $\theta \geq 1.37$. The value of $\theta = 1.40$ is often used for nonlinear dynamic systems. It should be mentioned that no special starting procedures are needed, since displacements, velocities and accelerations expressed at time $t + \Delta t$ in terms of the same quantities at time t only.

In this research, Wilson Theta Method will be used for torque and drag calculations during real-time analysis.

4.12 Torque and Drag Modeling

It is important to model the interaction between the drill string and wellbore because it helps us to understand how to control and reduce the common vibrations such as axial, lateral and torsional. It also helps to calculate torque and drag more precisely. Figure 4.9 illustrates the spatial state of a drill string in a wellbore that shows the contacts between the drill string and the wellbore. It does worth here to mentioning that in the analytical model it is assumed that the drill string has full contact with the wellbore.

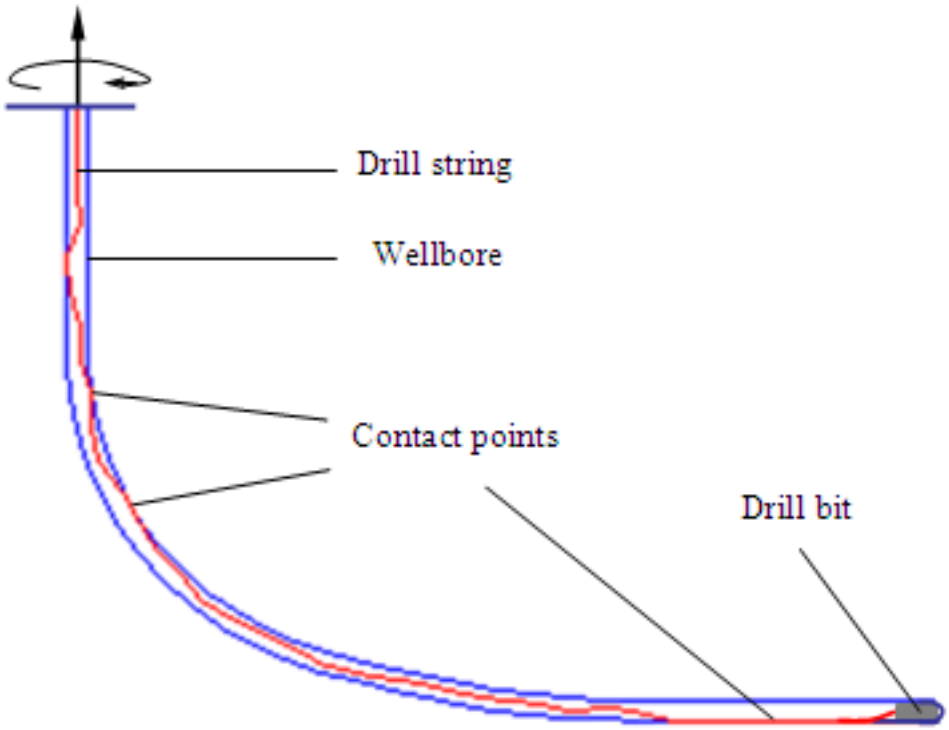

Figure 4.9: The interaction between drill string and wellbore

For this purposes, a FEA program was developed for analyzing working behavior and calculating torque and drag based on above models. The flow chart for torque and drag calculations is illustrated in Figure 4.10 it shows all the stages which are required for the torque and drag calculations. To start the program, it is necessary to provide four necessary input files. Theses input files are as follow:

The first input file is related to the drill string specifications. The file requires the specific dimensions of the pipes in the drill string including length of drill pipe, outside diameter, inside diameter, density of pipe, Young's Module, Poisson ratio and number of elements. For example, some of the values required in the file are presented as follow:

length of drill pipe, m	outside diameter, m	inside diameter, m	density of pipe, kg/m^3	Young's Module, Pa	Poisson ratio	number of elements
2793.56	0.15519	0.12136	7850	2.06E11	0.3	56

The second file is the wellbore geometry file which includes measured depth, inclination, azimuth, friction coefficient related to cased and open hole as well as the buoyancy factor which could change during different operation by changing the drilling fluid density. The following is an example of values for the well geometry file at a specific measured depth.

measured depth, m	inclination, rad	azimuth, rad	friction factor	Buoyancy factor
528.83	0.0105	2.916	0.3	0.8675

The third input file is for controlling the program and is called the control parameters file. The parameters include, time step, Wilson-theta value, total number of steps, wellbore clearance and hook stiffness. As an example, some values are listed for the control parameters below:

time step,s	theta	total steps	bit mass, kg	clearance, m	stiffness, $N.m^2$
0.005	1.5	2000	30	0.015	8.06E6

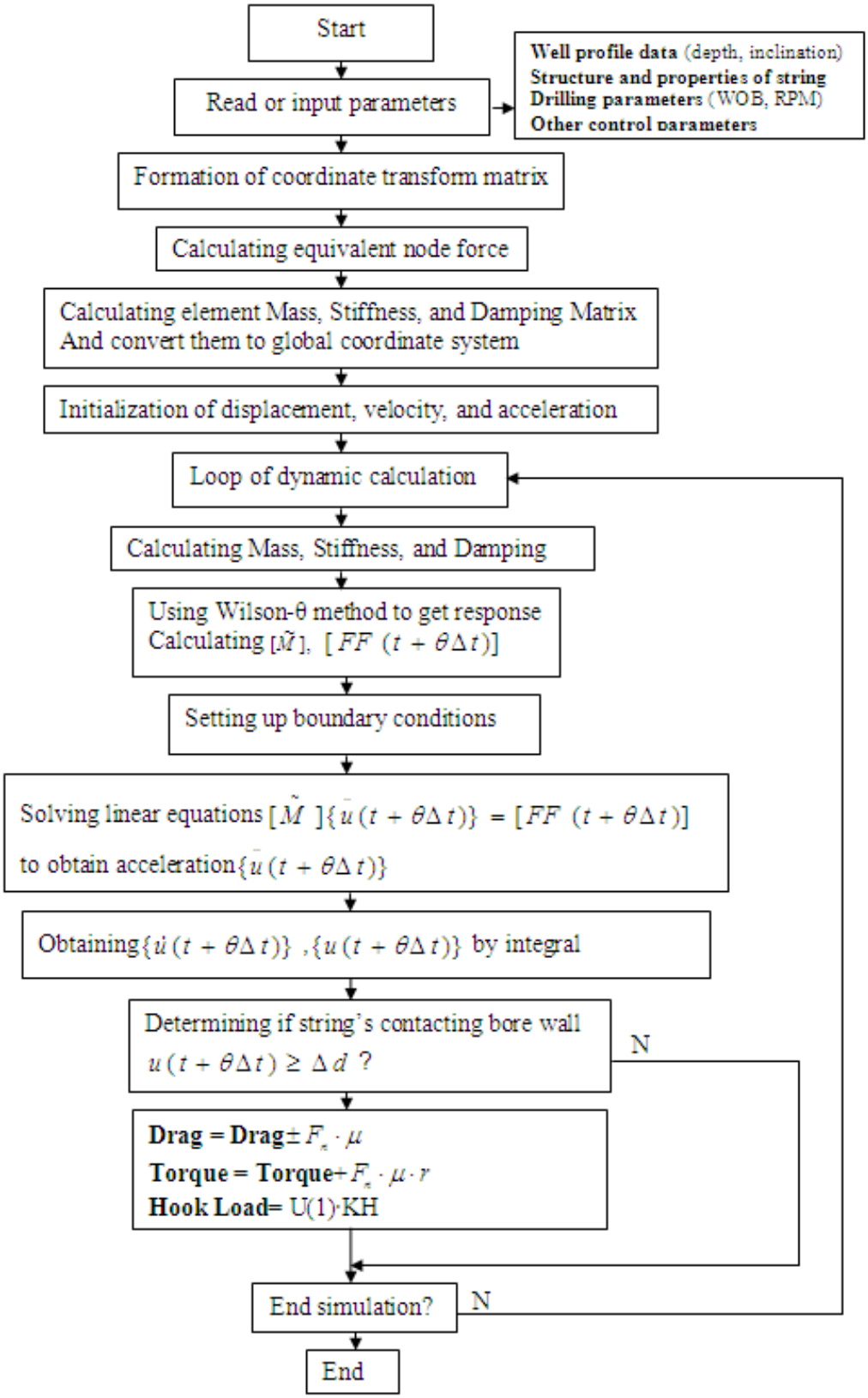

Figure 4.10: Flow chart of the FEA program for torque and drag analysis

The last file is related to drilling operating parameters which have great influence on field values of hook load and surface torque. The parameters include bit depth, measured depth, weight on the bit, hook load, surface torque, stand pipe pressure, surface rotation, tripping velocity.

After preparing the input data, the matrixes should be generated for each element and then assembled in the global matrixes. From the wellbore geometry file, the coordinate transformation matrix is formed and the equivalent node forces are calculated for each element. The accelerations, velocities and displacement are initialized with the zero values. Using the Wilson-θ method the effective mass matrix and force vector can be estimated based on the initial values. By setting the boundary conditions, the global acceleration vector at time $t+\theta\Delta t$, $\{\ddot{U}_{t+\theta\Delta t}\}$ will be found. Then the global velocity and displacement vector at time $t+\theta\Delta t$, $\{\dot{U}_{t+\theta\Delta t}\}$ and $\{U_{t+\theta\Delta t}\}$ can be obtained by integration.

When displacement vector at time $t+\theta\Delta t$, $\{U_{t+\theta\Delta t}\}$ have been found, it will be compared with clearance between drill string and the wellbore for entire system as shown in Equation 4.46.

$$\{U_{t+\theta\Delta t}\} \geq \Delta d \tag{4.46}$$

With this comparison, the contact area and the contact locations between the drill string and the wellbore can be determined. After this stage, the torque and drag can be calculated for each element. The acceleration, velocities and displacement values obtained for first run are used as initial guess for the second run and the procedure is repeated until it satisfies the Equation 4.31. After satisfying the Equation 4.31, the parameters such as length/ location of contact area of the drill string, the torque and drag along the wellbore is determined.

Figure 4.11 showed a simple example of a rod which is hung and divided into three elements. In the force vector, no friction or imbalanced forces are included.

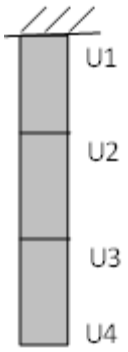

Figure 4.11: FEA of a rod with one end fixed

The rod is divided into 3 elements, which gives four nodes. The comparison between the exact value and the FEA is shown in Table 4.1. The difference between the exact value and FEA is due to the approximation nature of the finite element method.

Table 4.1: Comparison of Exact value with FEA of the rod

Nodes	***Exact value, N***	***FEA, N***
U1	0	0
U2	0.563835	0.553915
U3	0.752136	0.726339
U5	0.835903	0.817175

Another example in which the drill string is located in a vertical well is shown in Figure 4.12. The drill string is hung with a hook and rotates with a constant speed at the surface. The bottom of the string is applied with a reactive load and the weight on the bit as 525 kN. Using the FEA program, the hook load and displacements including rotation at any node can be obtained.

The input parameters are as follow:

n =60 rpm

$\varepsilon=2\pi n/60=6.28$(rad/s)

total elements=200

length of the string=2000m

total weight of the string=659.73KN

WOB=525KN

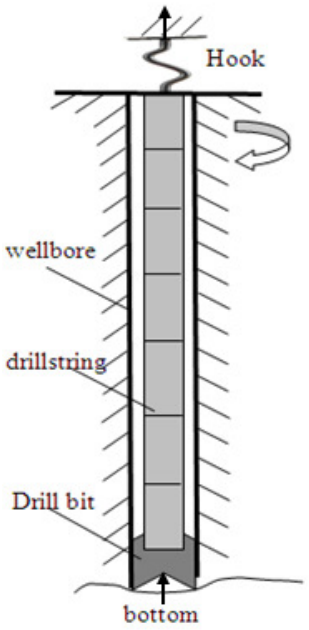

Figure 4.12: FEA of vertical well drilling

The calculated parameters using the FEA are as follow:

hook load=251.56KN

actual value=659.73-525=235.73

relative error= (251.56-235.73)/235.73=2.87%

The error is acceptable and refers to the nature of finite element solution which is an approximation as well as the stiffness of a virtual spring as taken for hook assembly.

Figure 4.13 shows the axial displacement at four different nodal locations such as surface (hook), 700 m, 1400 m, and bottom (bit). Figure 4.13 shows by increasing the depth, the displacements will be decreased. For the displacement of the hook at the surface, it can be seen that the displacement is less than those at 700 m and 1400 m due to larger stiffness coefficient of the hook than drill string at 700 and 1400 m.

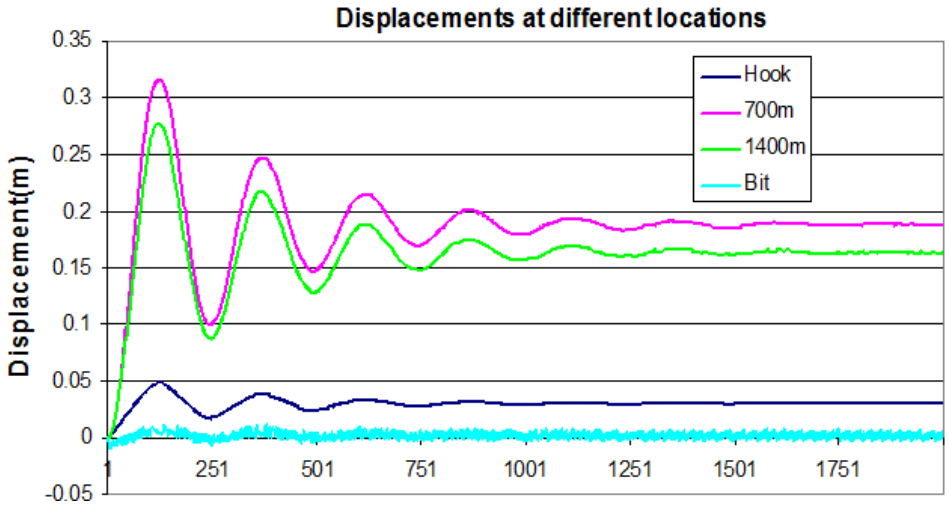

Figure 4.13: The axial displacement of four different locations

Figure 4.14 shows the rotary speed at three different locations 700m, 1400m, and drill bit. At the beginning, the rotary speed of the drill bit responds slower and the speed at the 700m location responses faster as shown in the plot. This delay is due to transmission of torsion from the surface to the bit which is proportional to the distance between the surface and point of interest. Here, the points of interest are 700 m, 1400 m and the bit.

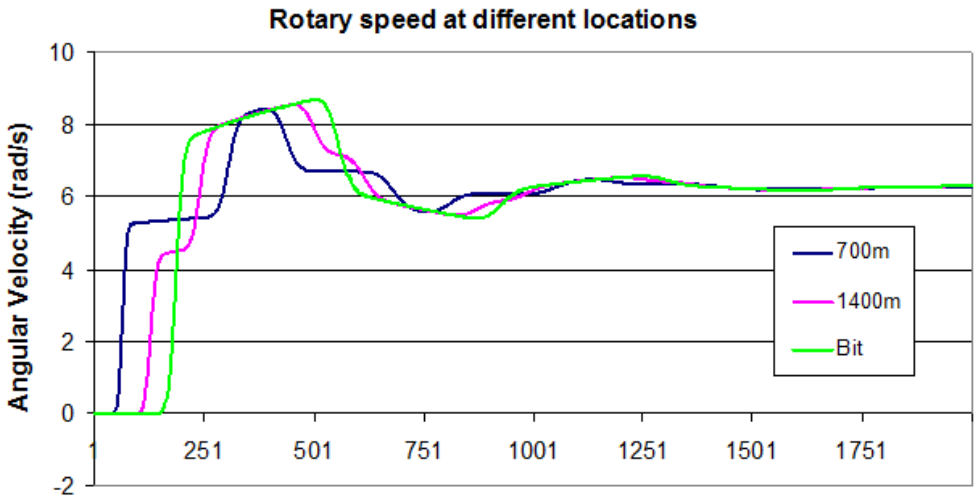

Figure 4.14: The rotary speed at three different locations

CHAPTER FIVE: **MODELING CONSIDERATIONS**

Friction coefficient plays an important role in torque and drag modeling calculations and may in some cases be a cause of confusion. It is defined as the roughness between the drill string and wellbore wall, but there are always some unwanted contributions that influence the true value of measured torque and drag. In this chapter, these effects have been investigated to get a more reasonable value for the friction coefficient for real time torque and drag analysis.

5.1 Buoyancy

The principle of Archimedes is used in buoyancy calculations. The principle says when a body is submerged into a fluid; the buoyancy force is equal to the weight of displaced fluid. Aadnoy et al. (2010) showed the drill string tension in a wellbore when filled with a drilling fluid is the unit pipe weight *w* multiplied by the buoyancy factor β. Equation 5.1 is valid for vertical and deviated boreholes if the inside and outside of the pipe are submerged into the same fluid.

$$\beta = 1 - \frac{\rho_{mud}}{\rho_{pipe}} \tag{5.1}$$

Equation 5.1 gives a good estimation of buoyancy factor when the drilling fluids are incompressible and the effect of temperature and cutting concentration can be ignored. This equation can be used for over-balanced drilling operations unless tripping in, which is discussed in following paragraph.

If there is a fluid density difference between the inside of the drill string and in the annulus, like during cementing and tripping in operations, the following equation should be used for local buoyancy factor calculations, Aadnoy et al., (2006).

$$\beta = 1 - \frac{\rho_o d_o^{\,2} - \rho_i d_i^{\,2}}{\rho_{pipe}\left(d_o^{\,2} - d_i^{\,2}\right)} \tag{5.2}$$

Equation 5.2 can calculate the buoyancy factor locally for each drill string element. In tripping-in operations, during running-in, the annulus is completely full but the inside of the string is initially empty. The reason why the drill string is empty is because the drilling crew does not typically fill the drill string during connections. Considering the collapse pressure of drill string and possible risk of blowout, the crew will typically schedule to fill the drill string after running-in every few hundred meters. This means the drill string will be partially full for a period of time and then will be completely full after running the desired length of drill string. When the drill string is full of mud the Equation 5.2 will turn into Equation 5.1 but when it is partially full and some portion of drill string is empty the Equation 5.2 will be used.

For tripping out, the mud level in the annulus does not drop quickly due to large surface area of annulus. Also the drilling crew fills the hole up using an auxiliary pump through fill-up line as a part of their routine jobs on the rig for having sufficient hydrostatic pressure for kick prevention. Therefore, the changes in buoyancy factor during tripping out are negligible.

5.1.1 Underbalanced Drilling

For underbalanced drilling specially in foam and aerated mud drilling, the density of the drilling fluid is not constant and changes along the circulating system. Drilling fluids have different compositions inside and outside the drill string. Inside the drill string, the drilling fluid is only a mixture of incompressible fluid and injected gas which flows under a two-phase condition. In the annulus the generated drill cuttings and formation influx fluid which may be a liquid or a gas, will be added and the fluid mixture and the mixture is now three phases. In this condition, the density depends on the following parameters:

- injected gas or air flow rate into circulating system
- pressure along drill string and annulus
- average temperature
- rate of penetration
- rate of influx
- nature of influx

- back pressure
- bottom hole pressure

All aforementioned parameters are subjected to change and should be recorded as real-time data during different underbalanced operations and then considered in the buoyancy calculations. In the following paragraph, the practical way of considering these parameters in the buoyancy calculations is discussed.

Equation 5.2 is used to calculate the buoyancy factor at any measured depth. This equation will give the local buoyancy factor and it should be multiplied by the unit weight of each element at that particular depth. To calculate the local buoyancy factor, it is required to have density of drilling fluid inside and outside of drill string versus measured depth.

Density inside Drill string

In aerated mud drilling, drilling fluids which are essentially incompressible are injected with atmospheric air or other gases. To develop a practical equation for the drilling fluid inside the drill string, assume the following (Lyons, et. al., 2009):

- The compressible gases could be approximated by ideal gas law.
- The mixture of compressed gas and incompressible drilling fluid is uniform and homogeneous.

Considering these assumptions, the general equation for density of the mixture inside the drill string can be written as follow

$$\rho_{mix} = \frac{\dot{m}_{gas} + \dot{m}_{mud}}{Q_{gas} + Q_{mud}} \tag{5.3}$$

where $\dot{m}$ and Q represent mass and volumetric flow rate respectively.

Lyons, et. al., (2009) presented the Equation 5.4 for calculation of mixture density inside the drill string. “g” and “m” represents gas and drilling mud in this two phase system.

$$\rho_{mix} = \frac{1}{g_n} \times \frac{\frac{P_g S_g}{R_e T_g} Q_g + \gamma_m Q_m}{\frac{P_g}{P} \times \frac{T_{ave}}{T_g} Q_g + Q_m} \tag{5.4}$$

Where

$g_{n:}$ acceleration gravity, 9.8066 m/sec^2

P_g: absolute atmospheric pressure, N/m^2

S: specific gravity

γ: specific weight, N/m^3

R_e: engineering gas constant, 29.31 N.m/N.K

T_g: absolute atmospheric temperature, K

P: pressure at any depth, N/m^2

T_{ave}: absolute average temperature, K

Density inside Annulus

Drilling fluid in the annulus is subjected to change. The generated drilling cuttings and influx is added to the drilling fluid which comes out of bit nozzles. The drilling fluid no longer is two-phase and the solid phase will be added to it. The density equation can be written for the annulus as follow:

$$\rho_{mix} = \frac{\dot{m}_{gas} + \dot{m}_{mud} + \dot{m}_{solid} + \dot{m}_{\inf lux}}{Q_{gas} + Q_{mud} + Q_{solid} + Q_{\inf lux}} \tag{5.5}$$

In comparison with volumetric flow rate of gas and liquid, the volumetric flow rate of drilling cuttings is negligible. But due to much higher density of drilling cuttings compared to gas and liquid, the mass flow rate of solid should be considered in the density calculation (Lyons, et. al., 2009).

$$\dot{m}_{solid} = \frac{\pi}{4} D^2 ROP \times \rho_{solid} = \frac{1}{g_n} \times \frac{\pi}{4} D^2 ROP \times (\gamma_w \times 2.7) \tag{5.6}$$
$$Q_{solid} \cong 0$$

For influx, there are two scenarios which should be distinguished for different cases. The influx could be gas or liquid, thus different equations should be used to calculate their mass and volumetric flow rates. For the liquid case, influx could be saline or liquid hydrocarbons which could be assumed to be incompressible. The mass and volumetric flow rate will not change by change in pressure and temperature as shown in Equation 5.7.

$$(\dot{m}_l)_{\inf lux} = (\rho_l \times Q_l)_{\inf lux} = \frac{1}{g_n} \times (\gamma_l Q_l)_{\inf lux} \tag{5.7}$$

If the influx is gas, the same formula for injected compressed gas will be used to calculate its mass and volumetric flow rate. Equations 5.8 and 5.9 can be written in following formats for liquid and gas influx. For liquid and gas influxes, Lyons, et. al., (2009) presented the followings:

$$\rho_{mix} = \frac{1}{g_n} \times \frac{\frac{P_g S_g}{R_e T_g} Q_g + \gamma_m Q_m + \frac{\pi}{4} D^2 ROP \times \gamma_w (2.7) + (\gamma_l Q_l)_{\inf lux}}{\frac{P_g}{P} \times \frac{T_{ave}}{T_g} Q_g + Q_m + (Q_l)_{\inf lux}} \tag{5.8}$$

and

$$\rho_{mix} = \frac{1}{g_n} \times \frac{\frac{P_g S_g}{R_e T_g} Q_g + \gamma_m Q_m + \frac{\pi}{4} D^2 ROP \times \gamma_w (2.7) + \left(\frac{P_g S_g}{R_e T_g} Q_g\right)_{\inf lux}}{\frac{P_g}{P} \times \frac{T_{ave}}{T_g} Q_g + Q_m + \left(\frac{P_g}{P} \times \frac{T_{ave}}{T_g} Q_g\right)_{\inf lux}} \tag{5.9}$$

5.2 Viscous Drag Force

The viscous drag force is the effect of the moving pipe on the annular mud velocity. The moving pipe walls transport mud in the direction of motion of the pipe, and at the same time the volume of the pipe displaces mud in an opposite direction of the pipe's motion. The annular mud velocity to calculate viscous pressure gradient depends on factors such as:

- ❖ the nature of the fluid (whether Newtonian or non-Newtonian)
- ❖ flow regime (laminar or turbulent)
- ❖ the pipe velocity
- ❖ open ended or close ended string (check valve (float) present in the string)

Maidla and Wojtanowicz, (1987, a) showed the hydrodynamic viscous force effect is considered by calculating surge or swab pressure associated with drilling mud flow caused by pipe movement in the wellbore. They presented a viscous pressure gradient for each pipe element. The calculation procedure for the viscous pressure gradient is based on the theory of viscous drag force for Bingham-plastic and Power-Law fluids in the wellbore. These equations presented by Maidla and Wojtanowicz, (1987, a) are applicable only for close end strings. The calculation procedure includes the following steps:

Step 1: Calculation of mud clinging constant, C_c

The value of effective mud velocity due to the moving pipe wall is related to the pipe velocity by proportionality constant C_c. The value of C_c depends upon the ratio of pipe and hole diameters, δ.

For the laminar flow

$$C_c = \frac{\delta^2 - 2\delta^2 \ln \delta - 1}{2(1-\delta^2)\ln \delta} \tag{5.10}$$

and for the turbulent flow

$$C_c = \frac{\sqrt{\frac{\delta^4 + \delta}{1+\delta}} - \delta^2}{1-\delta^2} \tag{5.11}$$

Step 2: Calculation of the average effective annular velocity, v_{ae}

It is the mud velocity that produces the viscous drag component of surge pressure. Its frame of references is the wellbore wall which was defined by Burckhardt, (1961).

$$v_{ae} = v_p \times \left(\frac{\delta^2}{1-\delta^2} + C_c \right) \tag{5.12}$$

where

V_p: pipe velocity, m/sec

Step 3: Calculation of Reynolds number N_{Re} for annular flow:

The Reynolds number can be calculated using Equation 5.13.

$$N_{\mathrm{Re}} = \frac{\rho v_{ae}(D-d)}{PV} \tag{5.13}$$

Where

PV: plastic viscosity, N.sec/m^2

For $N_{\mathrm{Re}} \leq 2100$ and $N_{\mathrm{Re}} > 2100$ the flow is laminar and turbulent respectively.

Step 5: Calculation of the friction factor

For smooth pipe and a Reynolds numbers less than10^5, a straight line approximation of the Colebrook function for Bingham-plastic fluid yields accurate friction factor presented by Bourgoyne, et. al., (2001). It is known as the fanning friction factor. The fanning equations for Laminar flow are:

$$f = \frac{16}{N_{\mathrm{Re}}} \tag{5.14}$$

For turbulent flow:

$$f = \frac{0.0791}{N_{\mathrm{Re}}^{0.25}} \tag{5.15}$$

Step 5: Calculation of the viscous pressure gradients, ΔP/ΔL

Viscous pressure gradient for Bingham-plastic model was presented by Burckhardt, (1961).

$$\frac{\Delta P}{\Delta L} = \frac{f v_{ae}{}^2 \rho}{(D-d)} \tag{5.16}$$

After calculating viscous pressure gradient, the hydrodynamic viscous drag force can be calculated by Equation 5.17:

$$F_D = \frac{\pi}{4} \sum_{i=1}^{n} (\frac{\Delta P}{\Delta L})_i \Delta L_i d_i{}^2 \tag{5.17}$$

The calculated viscous drag force for entire drill string should be added or subtracted to the calculated hook load during tripping out and in respectively to get a more reasonable friction coefficient.

5.3 Contact Surface

Maidla and Wojtanowicz, (1987, b) presented contact surface correction factor to consider in drag calculations. The correction factor, C_s, represents an effect of the contact surface between the pipe and the wellbore due to larger curve surface contact are. They showed that when a cylinder with outer diameter d moves through a pipe with the inner diameter D with applying a normal force F_N, the drag force will be as follow:

$$FF = \frac{4}{\pi} \times \mu \times F_N \tag{5.18}$$

Equation 5.18 shows that the real drag force for curve contact surface is $4/\pi$ times larger than a flat contact surface. In this case, the correction factor is $4/\pi$. In case of pipe string and wellbore, the string outer diameter is smaller than the wellbore diameter. The drag force can be written as:

$$FF = C_S \times \mu \times F_N \tag{5.19}$$

This correction factor values varying between 1 and $4/\pi$ are dependent upon contact surface angle γ which vary between 0° and 90°. Contact surface angle γ_i mainly depends on wellbore and string outer diameters. Maidla and Wojtanowicz, (1987, a) showed how contact surface effect can be calculated for each point using Equation 5.20.

$$Cs_i = \frac{2}{\pi}\gamma_i(\frac{4}{\pi} - 1) + 1 \tag{5.20}$$

For calculating the contact surface angle, the following procedure presented by Maidla and Wojtanowicz, (1987, a) should be used:

$$\gamma_i = \left| Arc\tan(\frac{2X_i}{2Y_i - D_i + d_i}) \right| \tag{5.21}$$

Where:

$$Y_i = \frac{1}{4} \times \left| \frac{d^2{}_i - D_i^{\,2} + (D_i - d_i + 2\Delta d_i)^2}{(D_i - d_i + 2\Delta d_i)} \right| \tag{5.22}$$

$$X_i = \frac{1}{2} \times \left| {d_i}^2 - 4{Y^2}_i \right|^{\frac{1}{2}} \tag{5.23}$$

$$\Delta d_i = \frac{\pi}{24E_i} \times \left\{ (\beta w_i \cos \varphi_i)^2 + (\beta w_i \sin \alpha_i + \frac{F_{i-1}}{R_i})^2 \right\}^{\frac{1}{2}} \times \frac{d_i}{t_i} \tag{5.24}$$

The values of Δd_i are negligible due to big value of modulus elasticity of steel which is2×10^{11} Pa. Its ignorance will not effect on value of Cs_i. If the Δd_i is ignored, Cs_i will be only the function of wellbore diameter and string outer diameter and can be rewritten as follow:

$$Cs_i = \frac{2}{\pi} \times Arc\tan\left(\frac{\left({D_i}^2 - {d_i}^2 \right)^{\frac{1}{2}}}{d_i} \right) \times \left(\frac{4}{\pi} - 1 \right) + 1 \tag{5.25}$$

To include contact surface effect in the torque and drag equations, it should be multiplied by the friction coefficient. If this effect is ignored in the calculations a bigger friction coefficient should be used to match modeling data with measured data.

The important application of this factor is monitoring the wellbore conditions during tripping in and out of the drill string. When BHA, which has greater diameter than drillpipe, passes through some section with smaller diameter, the overall friction coefficient will increase due to contact surface effect and this effect can be seen in real time analysis.

5.4 Sheave Friction

On the rig, the maximum load of the drill string weight and friction is applied on the hook. For measuring hook load, a hydraulic load cell or a strain gage “turtle” is attached to the dead line. The hook load displayed by the weight indicator which is assumed to be equal to the number of lines between blocks *N*, multiplies by dead line tension F_{dl} .

$$HL = F_{dl} \times N \tag{5.26}$$

Equation 5.26 is accepted industry method to calculate the hook load. It does not account for sheave friction and does not consider the difference between static and dynamic conditions. Luke and Juvkam-Wold, (1993) showed that true hook load depends on sheave friction and direction of block movement. They proved that true line tension from dead-line tension readings does not reside with the use of deadline readings, but with how these tension readings can be used.

When tripping out, the tension gradually reduced from the fast line to the dead line. In this way, the fast line would have the highest tension and dead line would have the lowest tension. It means that the indicator will display low when the drill string is being pulled out. When tripping in, the highest line tension is the dead line and the lowest tension is in the fast line. It results in high readings by weight indicator during the running of the drill string in the hole.

Dangerfield, (1987) made a mathematical analysis of the frictional resistance on the hoisting system. In his analysis, he proposed that two type of deadline sheaves existed: active and inactive. The active deadline sheave is the sheave in crown block which the dead line passes over and back to the traveling block. It is free to rotate. It is also known as friction sheave due to differential between the tensions in the lines on either side of the sheave. For the inactive dead line sheave which is known as frictionless sheave, the tensions in the lines on both sides of the sheave are the same.

The following equations presented by Luke and Juvkam-Wold, (1993) include direction of drill string movement and type of deadline sheave for true hook load prediction. For an inactive (frictionless) deadline sheave, when tripping the drill string out, the hook load can be calculated as follow,

$$HL = F_{dl} \times \frac{e\left[1 - \left(1 / e^{N}\right)\right]}{\left(e - 1\right)} \tag{5.27}$$

When tripping in:

$$HL = F_{dl} \times \frac{(1 - e^{N})}{(1 - e)} \tag{5.28}$$

For active (friction) dead line sheave, when pulling the drill string out, the hook load will be as follow:

$$HL = F_{dl} \times \frac{(1 - e^{N})}{(1 - e)e^{N}} \tag{5.29}$$

For tripping drill string in, the hook load is:

$$HL = F_{dl} \times \frac{e(1 - e^{N})}{(1 - e)} \tag{5.30}$$

Luke and Juvkam-Wold (1993) showed the average sheave efficiency e ranged from 96% to 99% for hook load estimation. For sheave efficiency determination, it is required to raise and lower a certain weight such as drillpipe joint using the hoisting assembly and record the measured value with actual weight to estimate sheave efficiency.

5.5 Hydraulic Vibrations

Rapid shut down of a control valve or stopping of a pump produces excess pressure in a tubular. Hydraulic transient as used more recently, refers to pressure fluctuations caused by a sudden change in the flow rate. Barakat, (2005) showed that when the fluid flow is stopped instantly, it results in a pressure increase which propagates at pressure wave speed in the fluid through the

fluid which causes radial expansion of the tubular wall. Due to this radial expansion, the pipe shortens behind and elongates in front of pressure rise. The application of hydraulic transient studies will be discussed further in following sections.

5.5.1 Agitator

Based on hydraulic transient, a dynamic excitation tool, Agitator, has been designed by National Oilwell Varco, (2008). Agitator smoothly oscillates the drill string to substantially reduce axial friction force. This means improved weight transfer and reduced stick-slip and reduced stick-slip in all modes of drilling. It provides this facility to increase the length of a horizontal section by breaking the axial friction force as shown in Figure 5.1. In the figure the dynamic and static friction refer the conditions with and without using agitator in drill string.

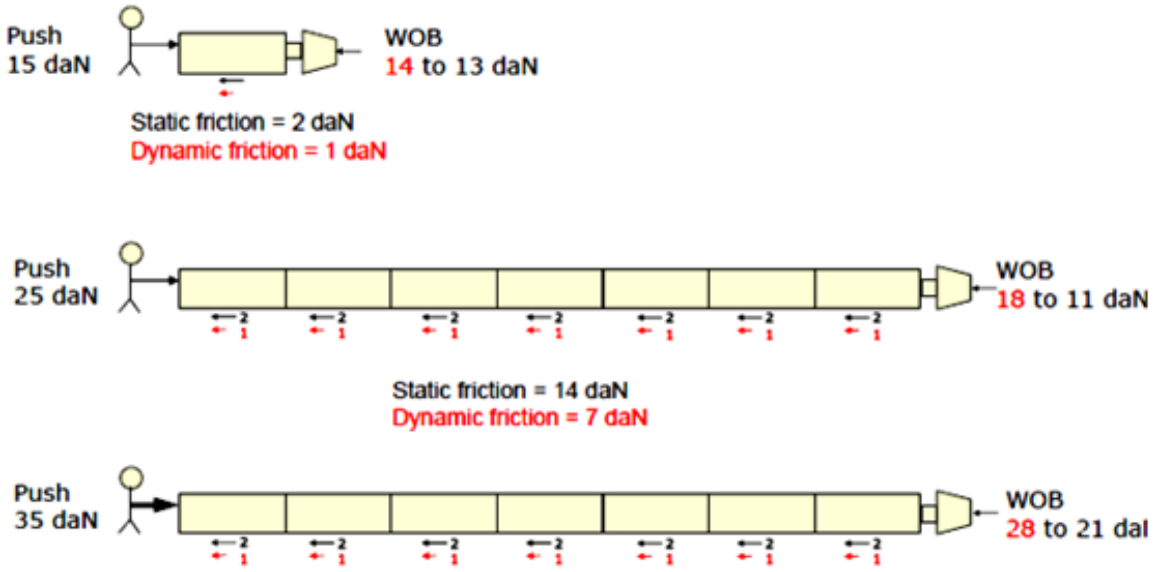

Figure 5.1: Effect of hydraulic vibration on axial friction force (Agitator Tool Handbook, 2008)

The Agitator system relies on three main *sections*.

- Power
- Valve and bearing

❖ Shock tool

The power section is short positive displacement motor which drives the valve section producing pressure pulses which in turn activate the shock tool. It is the axial motion of the shock tool which breaks static friction and converts it to dynamic.

Figure 5.2 shows the axial load along drill string when there is no agitator in the string. During long reach horizontal drilling, before and after build-up sections, the helical buckling is more probable to happen due to high compressive load as a result of axial friction and weight on the bit. This helical buckling causes additional axial friction force and lower weight on the bit.

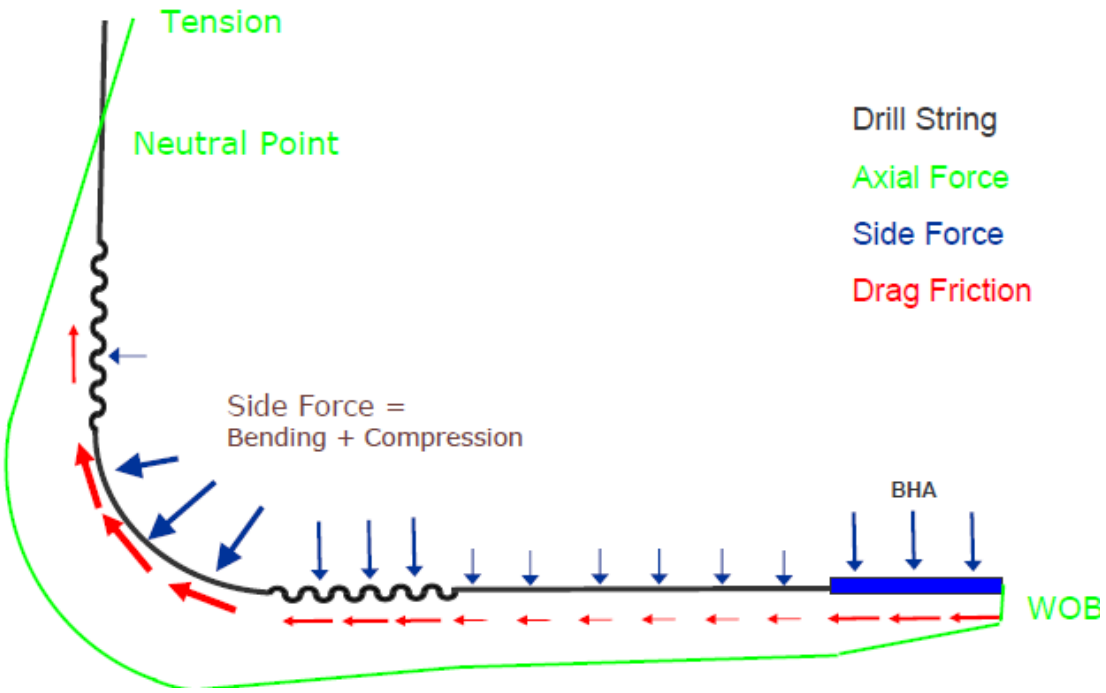

Figure 5.2: The tension-compression and axial friction forces along drill string without agitator (Agitator Tool Handbook, 2008)

Using an agitator in drill string as shown in Figure 5.3 mitigates the chance of helical buckling and reduces axial friction force along drill string. This reduction in axial friction force will improve the amount of weight on the bit in drill string slack off.

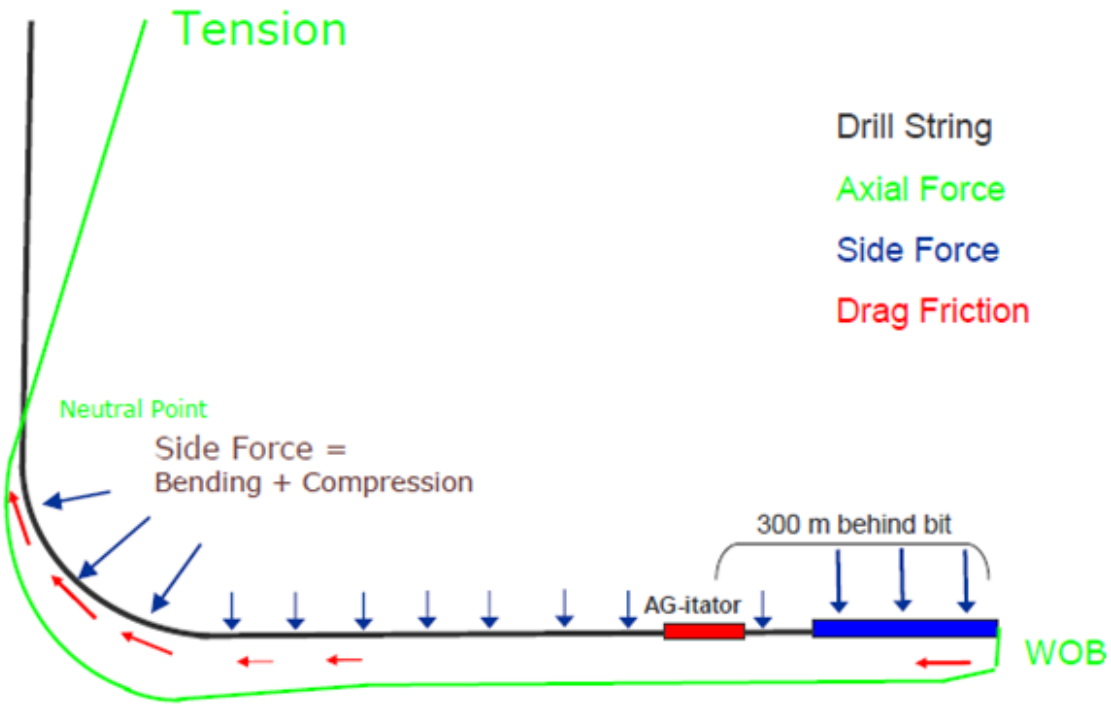

Figure 5.3: The tension-compression and axial friction forces along drill string using agitator (Agitator Tool Handbook, 2008)

Figure 5.4 (a) shows a set of field data related to a wiper trip and the drilling operations which did not use agitator. The drill string slacking off is between 18 to 27 daN and multiple pressure spikes can be seen. For the field case with the agitator as shown in Figure 5.4 (b) a constant slack off weight can be seen. The drill string slacking off value changes between 15 to 18 daN and no big pressure spikes is seen any more. Overall pressure has been increased as much as 3500 kPa due to pressure drop across agitator.

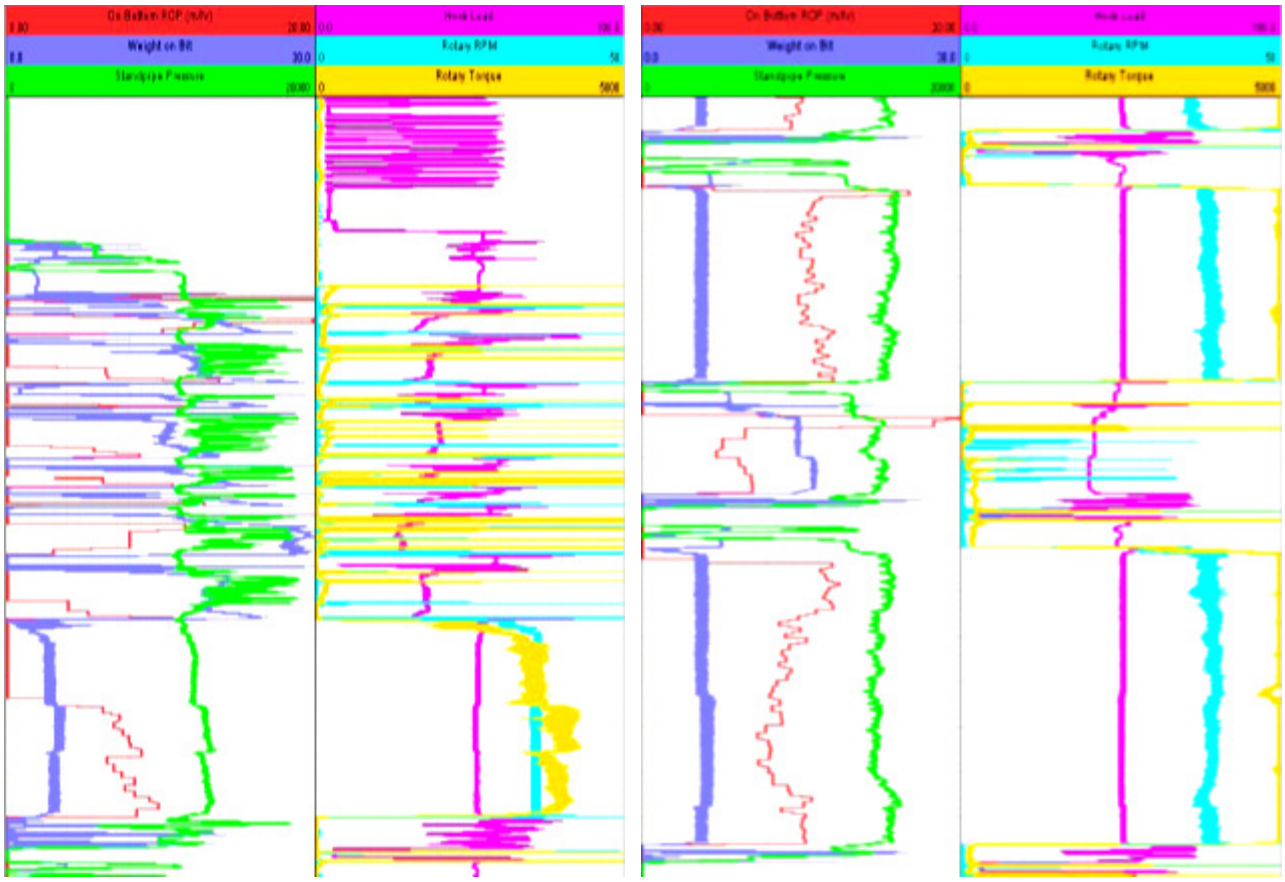

(a) (b)

Figure 5.4: Effect of using agitator on drilling parameters (Agitator Tool Handbook, 2008)

5.5.2 Surface Pressure Applied inside Drill string

Aadnoy and Kaarstad, (2006) showed effect of surface pressure on hook load measurements. They showed that the axial tension increases due to the inside applied surface pressure which is equal to the pressure increment multiplied by inner cross sectional area of drill string. The pressures in the drill string and annulus while applying surface pressure inside drill string e.g. during drilling are as follow:

$$P_{drillstring} = P_{hydrostatic} + P_{surface} - (\Delta P_{drillstring})_{loss} \tag{5.31}$$

and

$$P_{annulus} = P_{hydrostatic} + P_{surface} - (\Delta P_{drillstring} + \Delta P_{bit} + \Delta P_{annulus})_{loss} \quad (5.32)$$

Equations 5.31, 5.32 can be written for the surface drill string element which received maximum pressure and minimum pressure for inside and outside respectively. The pressure inside drillstring is taken as stand pipe pressure, SPP.

$$P_{annulus} = 0, \quad P_{drillstring} = P_{surface} = SPP \quad (5.33)$$

Equation 5.34 can be used to estimate the additional tensional force due to inside drilling fluid pressure which should be added to the hook load calculations during friction analysis.

$$F_p = SPP \times \frac{1}{4}\pi \times ID^2 \quad (5.34)$$

5.6 Buckling

A tubular can be buckled in any wellbore, but the axial compressive load to initiate buckling is different for different sections such as vertical, curved and horizontal as shown by Wu and Juvkam-Wold, (1995). The buckling may cause problems during drilling and casing running which may not transfer sufficient weight on the bit or to allow the casing to seat in right place.

5.6.1 Buckling Criteria

In a real time application, it is necessary to monitor the compressive load along drill string to find the type and beginning point and length of buckling and consider them in torque and drag analysis.

In a horizontal section, the tubulars are in compression due to axial friction, weight on the bit, and/or load on the packer. When the axial compressive load exceeds the following critical load, the tubular will buckle sinusoidally (Wu and Juvkam-Wold, 1993) as:

$$F_{Cr} = 2(EI \times \beta w / r)^{\frac{1}{2}} \tag{5.35}$$

For an inclined wellbore the Equation 5.35 can be written as follow:

$$F_{Cr} = 2(EI \times \beta w \times \sin\alpha / r)^{\frac{1}{2}} \tag{5.36}$$

The effect of sinusoidal buckling on the axial friction force is negligible and the sinusoidal tubular is treated the same as a straight one. When the compressive load exceeds the following loads the helical buckling will happen in the horizontal and inclined wellbores as discussed by Aadnoy, (2006).

$$F_{hel} = (2\sqrt{2} - 1) \times F_{Cr} \tag{5.37}$$

In vertical section, the tubular is easily buckled which adds some considerable axial friction force. Equation 5.38 calculates the critical load for sinusoidal buckling which was presented by Wu and Juvkam-Wold, (1993).

$$F_{Cr} = 2.55 \times (EI \times (\beta w)^2)^{\frac{1}{3}} \tag{5.38}$$

The helical buckling load is about 2.2 times as large as the sinusoidal buckling load in vertical wellbores as shown in Equation 5.39 presented by Wu and Juvkam-Wold, (1993).

$$F_{hel} = 2.18 \times F_{Cr} \tag{5.39}$$

5.6.2 Axial Force along Drill string

The axial load distribution will be changed when a tubular is buckled helically. When the drill string or casing buckles in a wellbore, an additional friction force will be generated. This additional friction force should be considered while estimating downhole weight on the bit. Also, this helical buckling may limit us sooner for extended reach well drilling.

In horizontal sections, when a tubular is running without helical buckling, the compressive load increases linearly due to axial friction caused by tubular weight as shown in Figure 5.5. Equation 5.40 shows the linear relationship between compressive load and length of tubular in horizontal section when no buckling happens.

$$F_2 = F_1 + \mu \beta w \times \Delta L \tag{5.40}$$

Where ΔL is the length of a non-buckled element and F_1 is the compressive force at the bottom of the element.

An additional friction force is generated due to the wellbore confinement to the helical buckling which should be considered in torque and drag analysis. Wu and Juvkam-Wold, (1993) showed that this additional friction force increases with the rate of square of axial compressive load. The axial compressive load distribution becomes nonlinear as shown in Figure 5.5 and has to be calculated by Equation 5.41 as follow:

$$F_2 = 2(EI\beta w / r)^{\frac{1}{2}} \tan\left(\mu \times \Delta L[r\beta w/(4EI)]^{\frac{1}{2}} + \arctan\left\{ F_1[r/(4EI\beta w)]^{\frac{1}{2}} \right\} \right) \quad (5.41)$$

Where, ΔL is now measured for the element in the helically buckled portion of the tubular.

For inclined and curved sections, Equation 5.41 can be written as:

$$F_2 = 2(EI\beta w \sin\alpha / r)^{\frac{1}{2}} \tan\left(\mu \times \Delta L[r\beta w \sin\alpha/(4EI)]^{\frac{1}{2}} + \arctan\left\{ F_1[r/(4EI\beta w \sin\alpha)]^{\frac{1}{2}} \right\} \right) \quad (5.42)$$

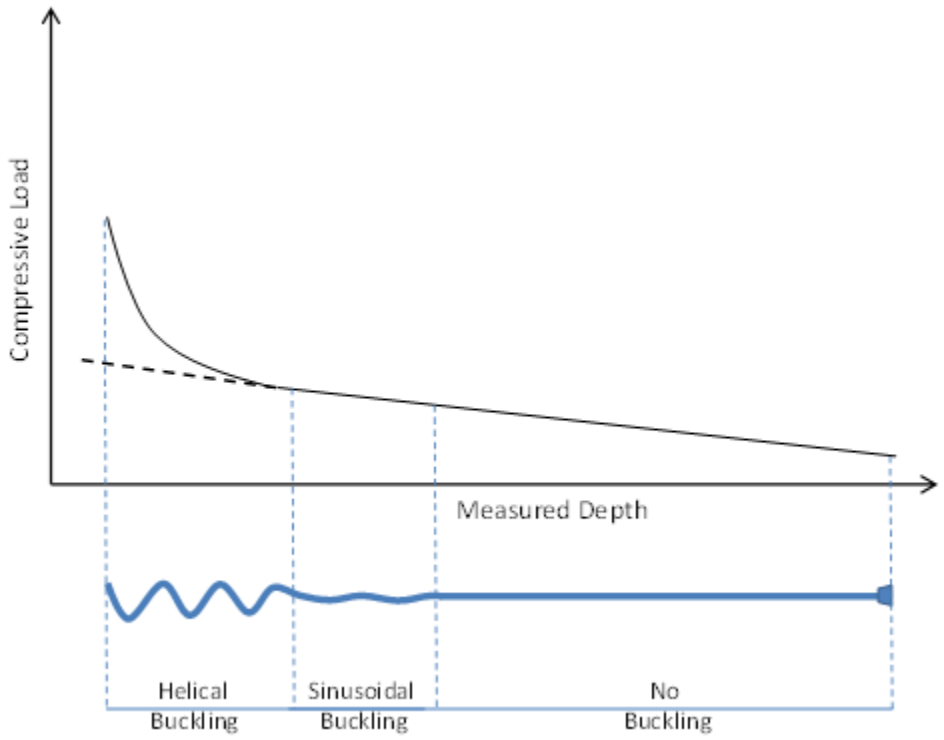

Figure 5.5: Schematic of tubular buckling in horizontal section

Theoretically, there is no axial friction force in vertical wellbore and compressive force along drill string can be written as:

$$F_2 = F_1 - \beta w \times \Delta L \tag{5.43}$$

Where, ΔL is measured element along the drill string and upward and F_1 is the axial compressive force at the bottom of the element. Wu and Juvkam-Wold, (1993) presented Equation 5.44 to calculate the compressive axial load distribution when helical buckling happens and causes the axial friction force in a vertical wellbore.

$$F_2 = 2\left(EI\beta w/(\mu r)\right)^{\frac{1}{2}} \tanh\left(-\Delta L \times \left[\mu r \beta w/\left(4EI\right)\right]^{\frac{1}{2}} + \arctan h\left\{ F_1 \left[\mu r/\left(4EI\beta w\right)\right]^{\frac{1}{2}} \right\} \right) \tag{5.44}$$

Where, ΔL is measured for helically buckled portion of tubular in vertical wellbore.

For torque increment during helical buckling, it should be mentioned when helical buckling happens, the pipe rotation is brutal and it should be avoided. It is a routine practice in the field when chance of helical buckling is high during oriented drilling, the weight on the bit should be released and then surface rotation should be started.

5.7 Off/On Bottom Data Selection

It is crucial to select the correct off and on bottom calibration data points for torque and drag analysis during drilling operations. When the drill string is lowered for further drilling, there are different values for the hook load which can be related to pump off force, tight hole, interaction between stabilizer and the wellbore, cutting accumulation etc. It is very important to recognize when the drill bit touch the bottom of the hole and interact with the formation.

When the bit interacts with the formation, an increase in stand pipe pressure can be observed due to increase in differential pressure across the downhole motor if a motor is used. The interaction cause more torque at the bit is provided by the downhole motor. The generated torque in downhole motor requires more pressure drop which results an increase in stand pipe pressure.

When the interaction point is found, the corresponded hook load value is taken as off bottom value and friction coefficient estimated by this value. The friction coefficient is a little over-estimated due to aforementioned effects. The friction coefficients should also be updated after each wiper trip by running the same procedure. Figure 5.6 shows recognition of off and on bottom data considering the standpipe pressure profile while the bit moving downward towards the bottom. In this figure, the bottom hole is at 2696.09 m but increase in stand pipe pressure begins at 2695.86, 25 cm above the bottom. The hook load that corresponds to this depth should be selected as off bottom data and to estimate the friction coefficient to vanish all discussed unwanted effects.

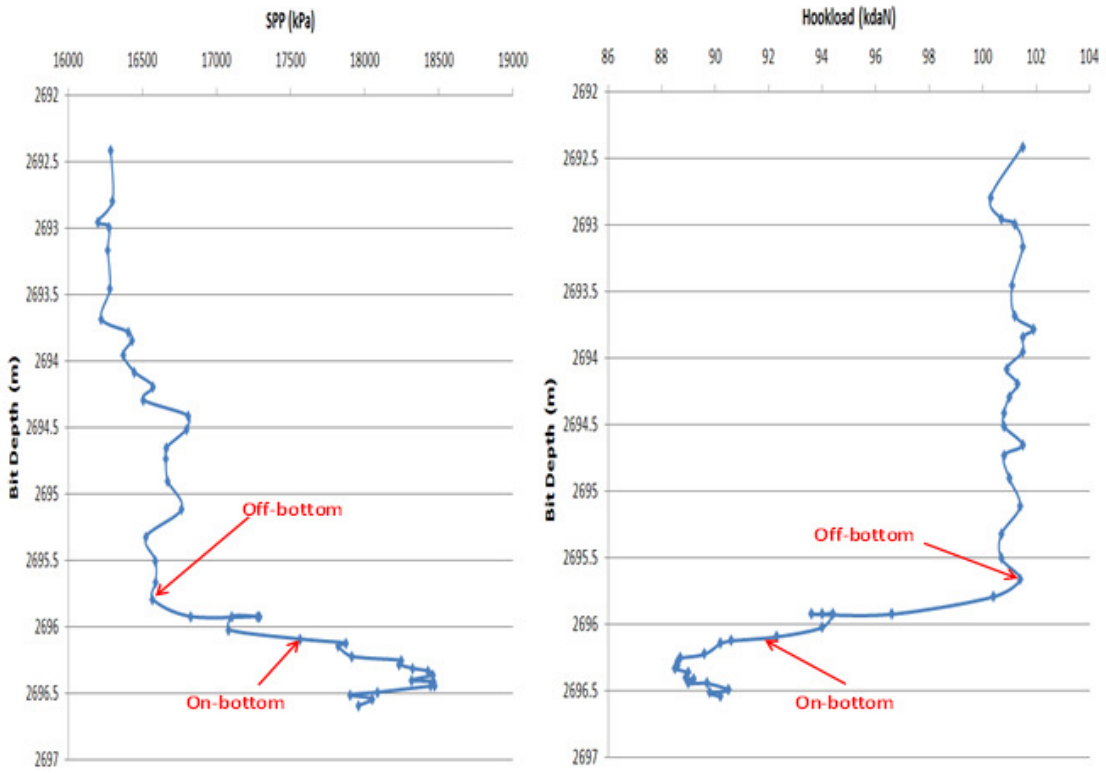

Figure 5.6: Selection of off bottom data using stand pipe pressure

5.8 Adjusted Unit Weight

The body and the tool joint of a drillpipe have different unit weights. The tool joint weight should be distributed over the unit weight of the body which is commonly known as adjusted

unit weight. The adjusted unit weight values should be given by manufacturers so more accurate values can be used in torque and drag software's and real time analysis.

Also, the drill string wears after being used for a period of time. The drill pipe should be classified according to API classification as shown in Table 5.2 presented by Samuel, (2010). The corrected outside drill pipe diameter is calculated as the following.

$$d_{Corrected} = c \times d \ + ID \times (1 - c) \tag{5.58}$$

Where c is the drillpipe class multiplier based on API classification. Table 5.1 lists the pipe class multipliers for various classes of pipe.

Where *c* and *ID* are the drillpipe class multiplier based on API classification and inner diameter of the pipe respectively. Table 5.1 lists the pipe class multipliers for various classes of pipe:

Table 5.1: The multipliers for various classes of pipes (Samuel, 2010)

NO.	***Pipe Class***	***Class Multiplier, c***
1	N: new	1.000
2	C: critical	0.875
3	P: premium	0.800
5	2: class II	0.700
5	3: class III	0.650

The following example shows how the class of the drillpipe class affects the original unit weight. Coiled tubing has been selected for this example due to the uniform nature of the tubing without any tool joints.

New:

$class = new$
$c = 1.000$
$OD = 2.375 \ \ in$
$ID = 2.063 \ \ in$
$UW = 3.7 \ \ lb / ft$

If the class of pipe changed to premium class:

$class = premium$
$c = 0.800$
$OD_{Corrected} = 2.3126 \ \ in$
$ID = 2.063 \ \ in$
$UW_{Corrected} = 2.92 \ \ lb / ft$

CHAPTER SIX: **TECHNICAL RESULTS AND DISCUSSION**

This chapter includes the field data analysis for the verification of the new models (analytical and finite element) discussed in the previous chapters. Some field cases have been selected from Canadian and North Sea wells for further discussion and evaluations. The field cases demonstrate the challenges during different operations such as drilling, tripping in/out, and reaming/back reaming. Also, a new developed method based on the friction models is presented to estimate the down hole weight on bit (DWOB) for directional drilling applications from surface hook load measurements. The application of this new DWOB method in an autodriller system is discussed in detail.

6.1 Analytical Modeling of a Two-Dimensional Well

The record of this horizontal well field case was extracted in January 2009 from an onshore rig in Alberta, Canada. The horizontal departure and vertical section of the well are shown in Figure 6.1.

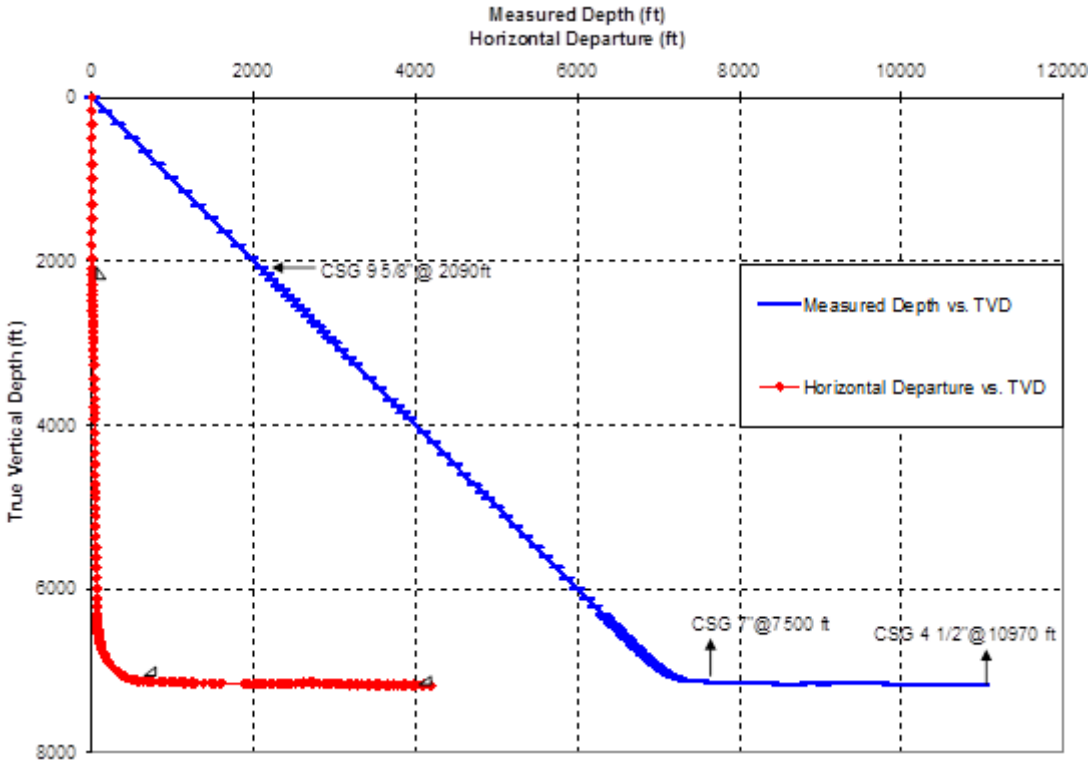

Figure 6.1: Geometry of the horizontal well in Alberta, Canada

A 9 5/8 *inch* surface casing string was run to the depth of 2090 *ft*. An intermediate 7 *inch* casing was set at 7500 *ft*. To reach the target a 6 1/8 *inch* bit was used to drill the horizontal section.

This example will demonstrate the application of the model for tripping the drill string out. The drill string total length is 10995 ft, which is shown in Figure 6.2. In this horizontal well, the drill string must be forced into the wellbore. Here, the 4 *inch* heavy weight drill pipes were placed in the vertical section to provide sufficient weight to push the drill string into the horizontal section. The entire drill string in the horizontal section is compressed during drilling. The adjusted weight for the 4 *inch* drill pipe and 4 *inch* heavy weight drill pipe are 17.71 *lb/ft* and 29.92 *lb/ft,* respectively. The adjusted diameter for the drillpipe and heavy weight drillpipe is 4.1 *inch*. The well is filled with a drilling fluid with a weight of 8.9 *lb/gallon*. For this well, there is no change in the well azimuth. As a result, the dogleg change for this well is that of the inclination.

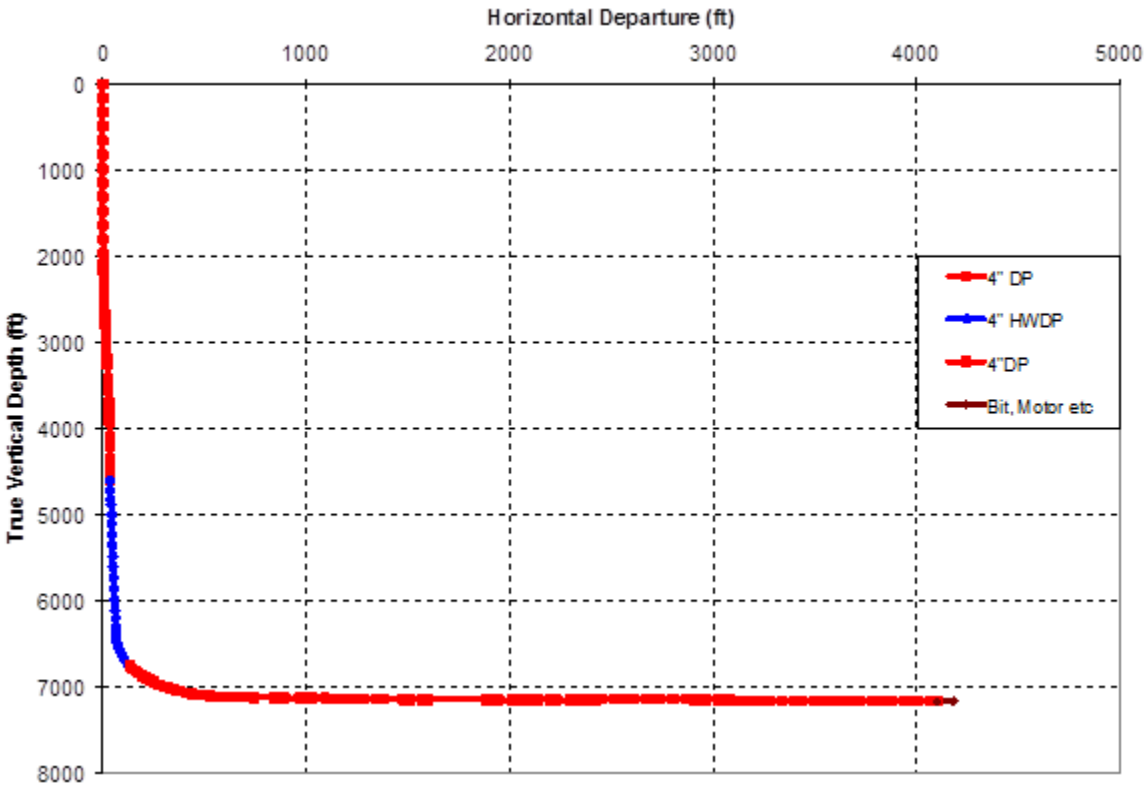

Figure 6.2: Drill string configuration for the horizontal well

6.1 .1 Tripping Out

Figure 6.3 shows the measured hook loads while tripping out. The measured hook load values are a function of drill string length, well geometry, drill string configuration and wellbore conditions. Different wellbore geometries and drill string configurations in the vertical sections show different measured hook load trends. Also, Figure 6.3 shows the hook load measurements when the entire drill string weight is on the slips during connection times. Hook load measurements during connection time represent the weight of the hoisting assembly at surface without a precise calibration. It is noted that the data recording commenced when the bit depth was 740 *ft*.

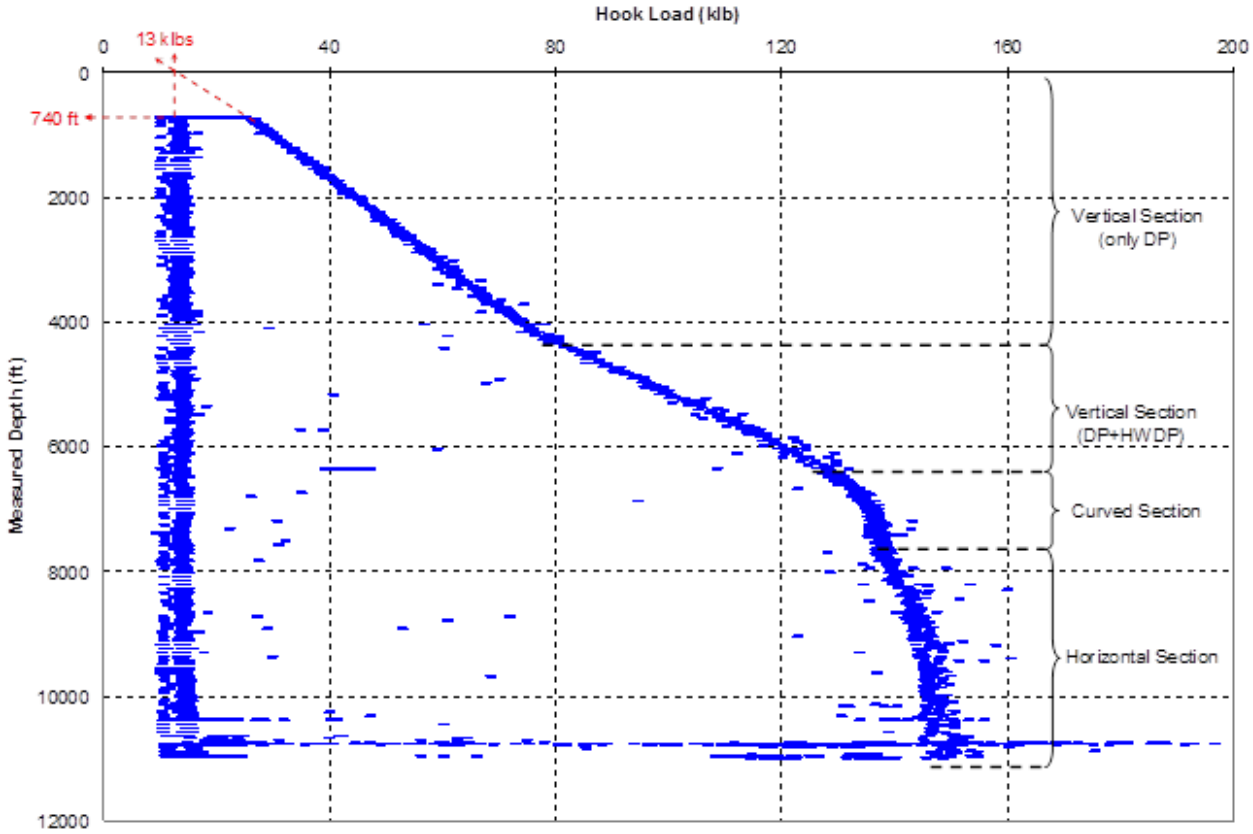

Figure 6.3: Measured hook load versus measured depth during tripping out

The friction coefficients usually vary from 0.1 to 0.4 to match the normal field data. Figure 6.4 illustrates a comparison between the measured and calculated hook load values for different

friction coefficients. This comparison shows that even with a low value of the friction coefficient (e.g., friction coefficient of 0.1), there is still a maximum of 6 percent deviation from the field data at the depth of 7700 *ft*.

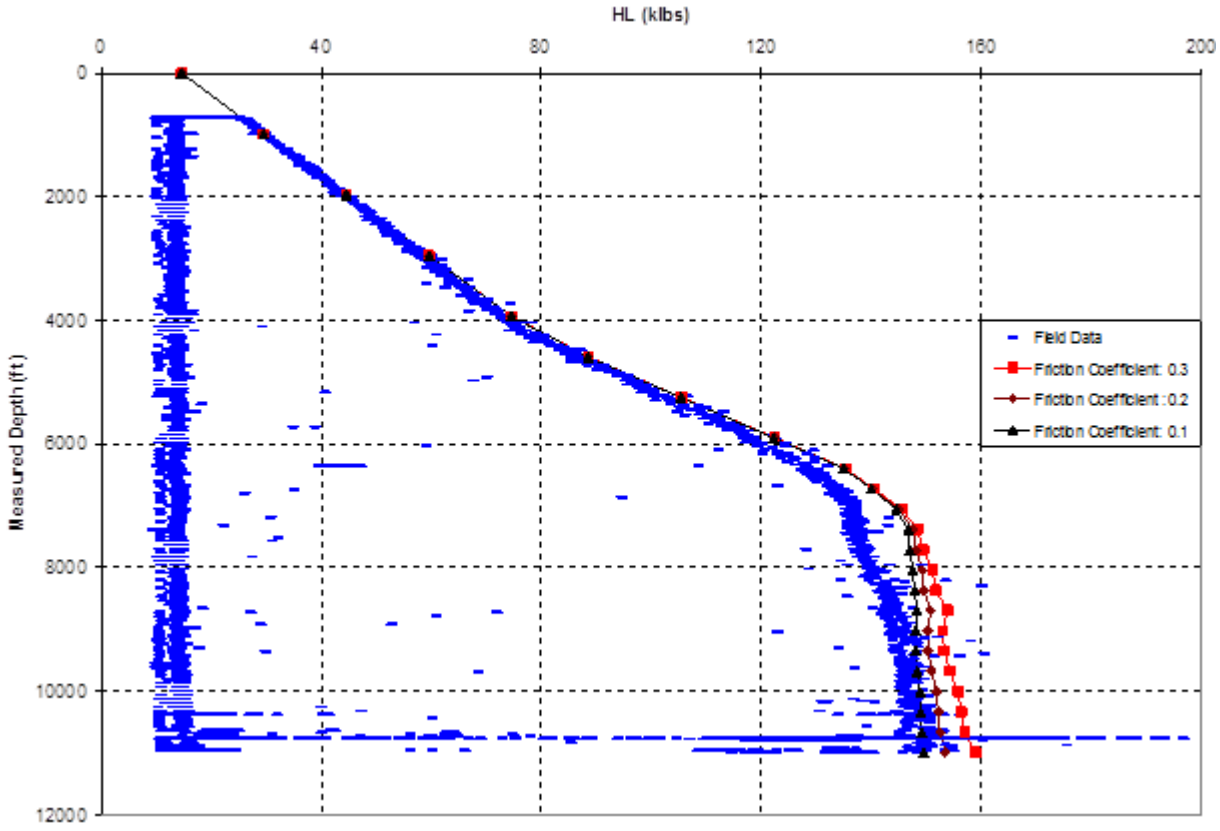

Figure 6.4: Comparison between the measured and calculated hook loads during tripping out

For quality control of the field data, the tripping data should be compared with the static weight of the drill string. Here, the static weight means the weight of drill string when there is no friction during drillstring movement. Figure 6.5 indicates that the measured hook loads have smaller values than static weight data. The latter is impossible. The field data related to tripping out should always be greater than static weight as the friction force between the drill string and wellbore is added to the static weight of the drill string. It is noted that the hook load data have been recorded based on Equation 5.26. This equation is the widely accepted industry method,

which does not include the effect of friction between the drilling lines and pulleys in a block and tackle system.

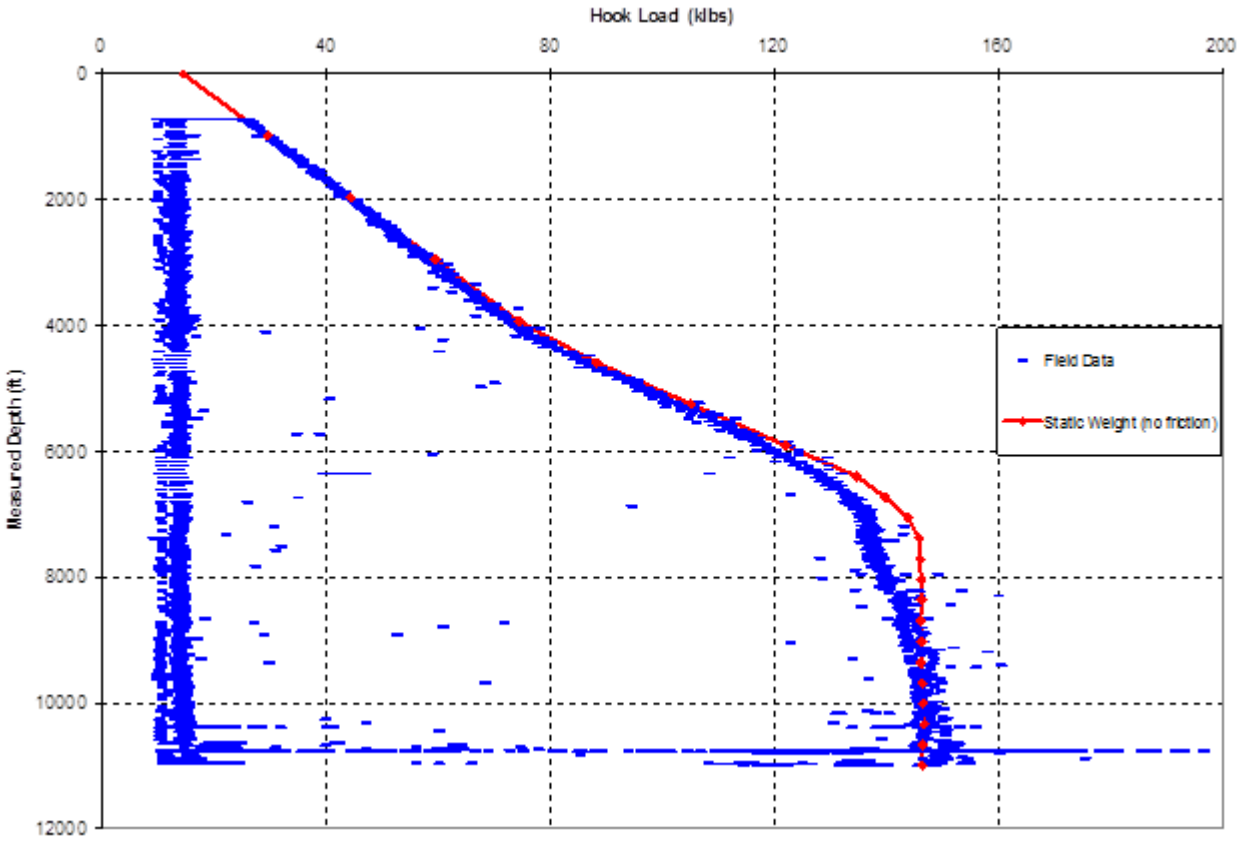

Figure 6.5: Comparison between the measured hook load and the static weight of the drill string during tripping out

As was discussed in Chapter 5, the industry's standard method measures the lower dead line tension during tripping out ignoring the sheave friction. For a sheave efficiency of 99% and 10 drilling lines, the corrected field data are shown in Figure 6.6. The error between the field data and the modeling results is reduced to 2%. This error can be attributed to the simplifying assumptions made while deriving the equations like uneven surface of the wellbore and some other possible unwanted effects.

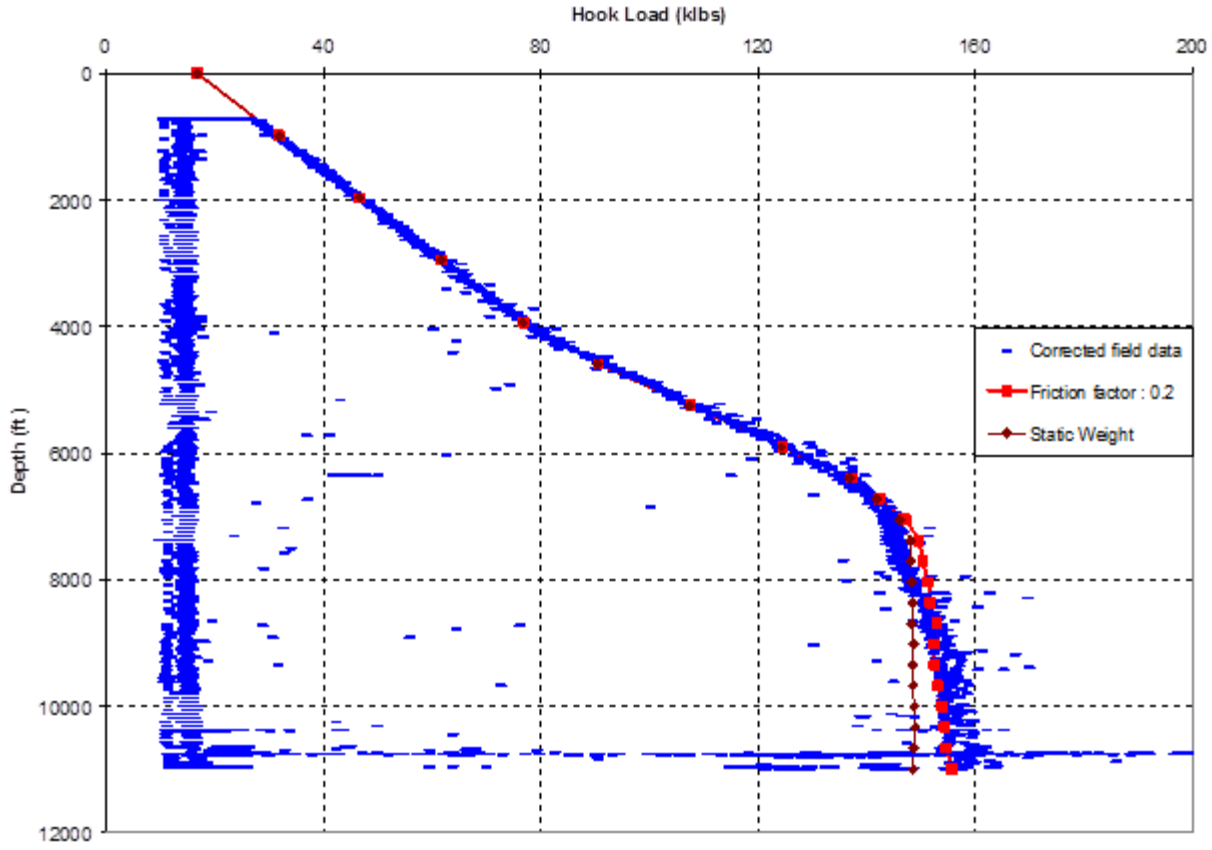

Figure 6.6: Comparison between the corrected field data and modeling results for tripping out

In order to ensure the quality of the measured data, field data should be compared with the static weight data. In doing so, using different friction models can be helpful in checking data quality. Figure 6.7 shows two subsequent hook load records during tripping out, which was due to troubleshooting of the MWD tool. This comparison illustrates how important the weight indicator calibration and quality of recorded data are for the real-time torque and drag analysis.

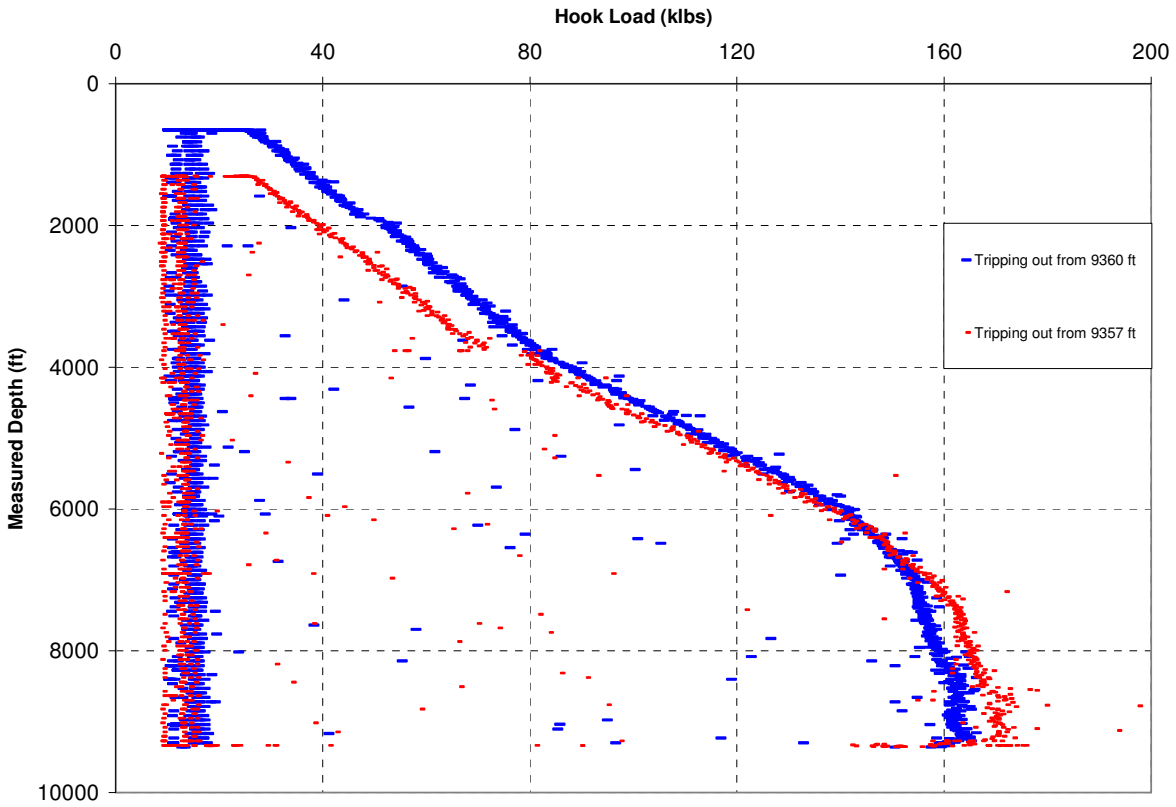

Figure 6.7: Comparison between two subsequent measured hook loads during tripping out

6.1.2 Tripping In

Figure 6.8 shows hook load data for tripping in from the surface to depth of 10760 *ft*. The well geometry is the same as that depicted in Figure 6.1. Similarly, the drill string configuration is shown in Figure 6.2. The 4 *inch* heavy weight drill pipes were placed in the vertical section to push the drill string into the horizontal section. The well is filled with the same drilling fluid with a weight of 8.91 *lb/gallon*. The field data in Figure 6.8 were treated by assuming a sheave efficiency of 99% for the 10 drilling lines between the pulleys.

Figure 6.8 shows a perfect match between the calculated and measured hook loads during tripping in from the surface to a depth of 9100 *ft*. At the interval of 9100 to10400 *ft*, there is a big reduction in measured hook loads, which is more than the expected values. This reduction can be attributed to many factors such as the effect of buckling and ledging. These factors cause greater friction coefficient for tripping in as opposed to that of tripping out. A remedy for minimizing the adverse effects of buckling and ledging is the reaming and back reaming operations, which

make a smoother path with a lower friction coefficient. A hydraulic agitator can also be used to release the compression force along the drill string in the horizontal section.

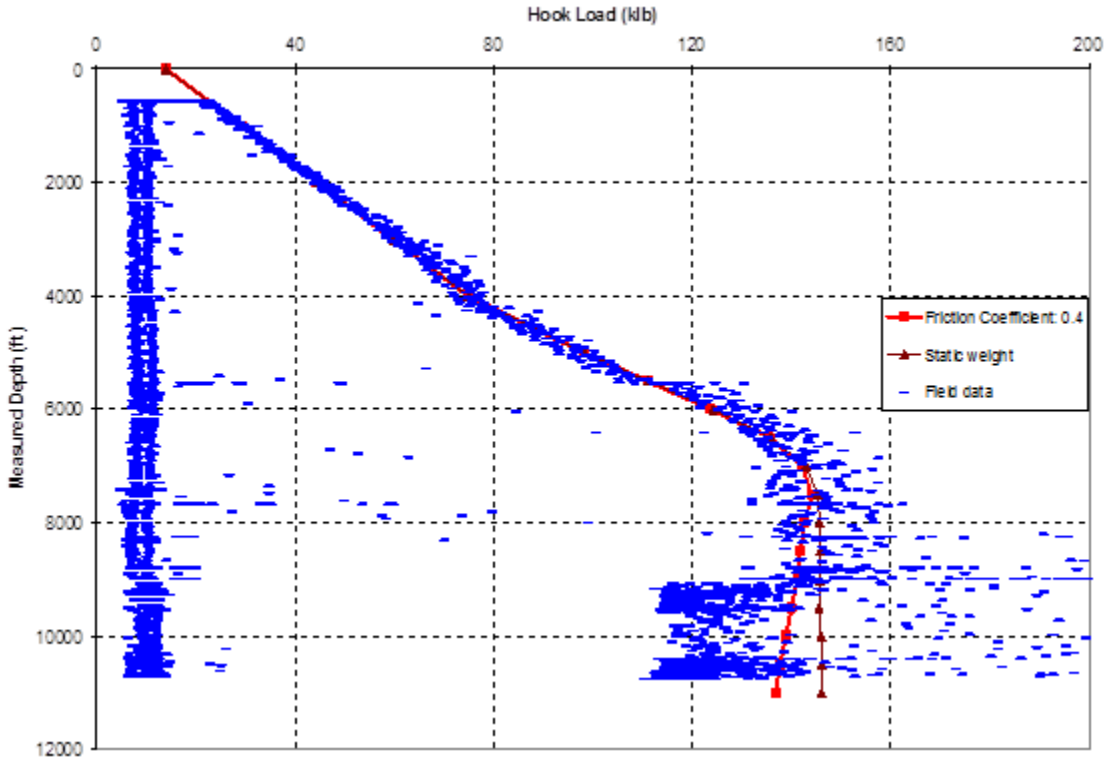

Figure 6.8: Comparison between measured and calculated hook loads while tripping in

A sensitivity analysis of the friction coefficient can be helpful in this scenario. In other words, one should try to obtain an exact match between the measured and calculated hook load values by inserting any value of the friction coefficient. Once the difference between two subsequent friction coefficients gets very small, the drill string is then moving under normal conditions. On the other hand, if the difference is considerable, a remedial action should be taken. Therefore, sensitivity analysis of the friction coefficient could be helpful to predict any problem during drilling operations. An example of finding trouble interval sections using sensitivity analysis of friction coefficient during tripping in is given in Figure 6.9.

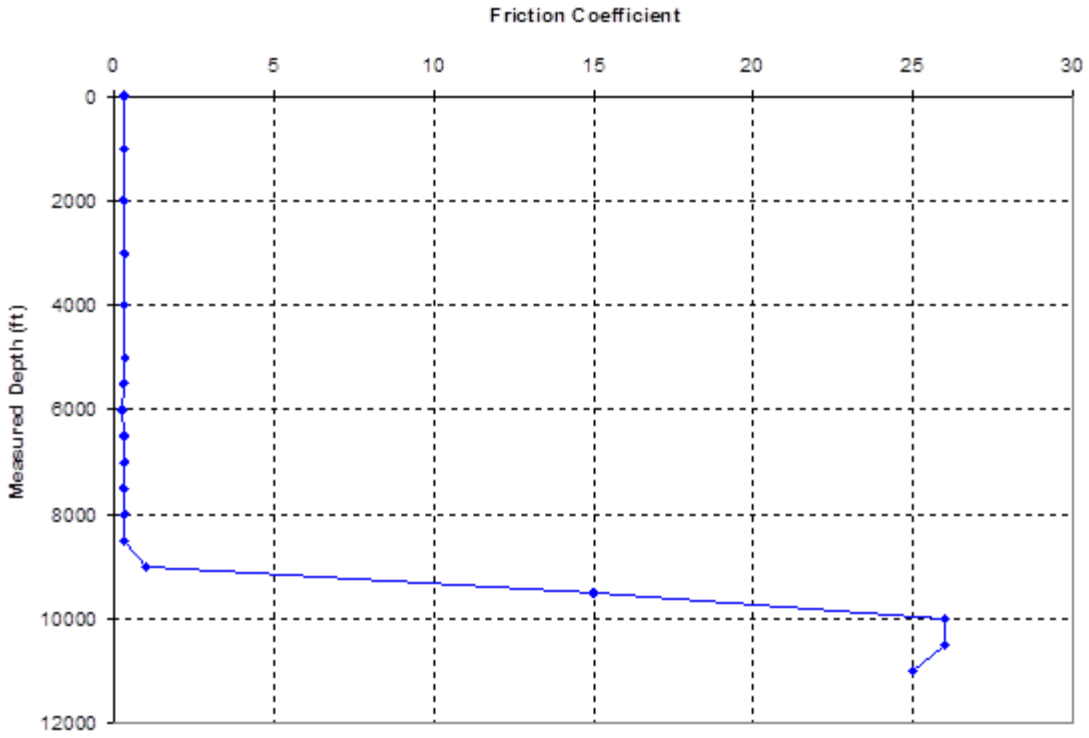

Figure 6.9: Sensitivity analysis of friction coefficient vs. measured depth while tripping in

6.1.3 Reaming/ Back Reaming

The surface torque is recorded during drilling with surface rotation, reaming and back reaming operations. As it was discussed in *tripping in*, there was some resistance against the string movement during running the drill string from the depth of 9100 *ft* to the target. To reduce this resistance against axial movement, the drill string was rotated at the surface. Therefore, surface torque was recorded during reaming and back reaming operations for this interval.

Figure 6.10 compares the measured and calculated surface torque during reaming and back reaming operations. During the reaming operation, tripping and rotary speeds were 0.5 ft/sec and 55 rpm, respectively. The majority of the field data lie between the reaming and back reaming calculated data, as shown in Figure 6.10. The measured torque data shows high fluctuations, which reflect the nature of drill string rotation dynamics such as slip/stick, restoring moment, torsional resistance and axial and lateral vibrations. It is usually difficult to compare the calculated torque with the measured data with significant fluctuations. To make this comparison easy, the measured data should be averaged over a short interval (see Figure 6.10).

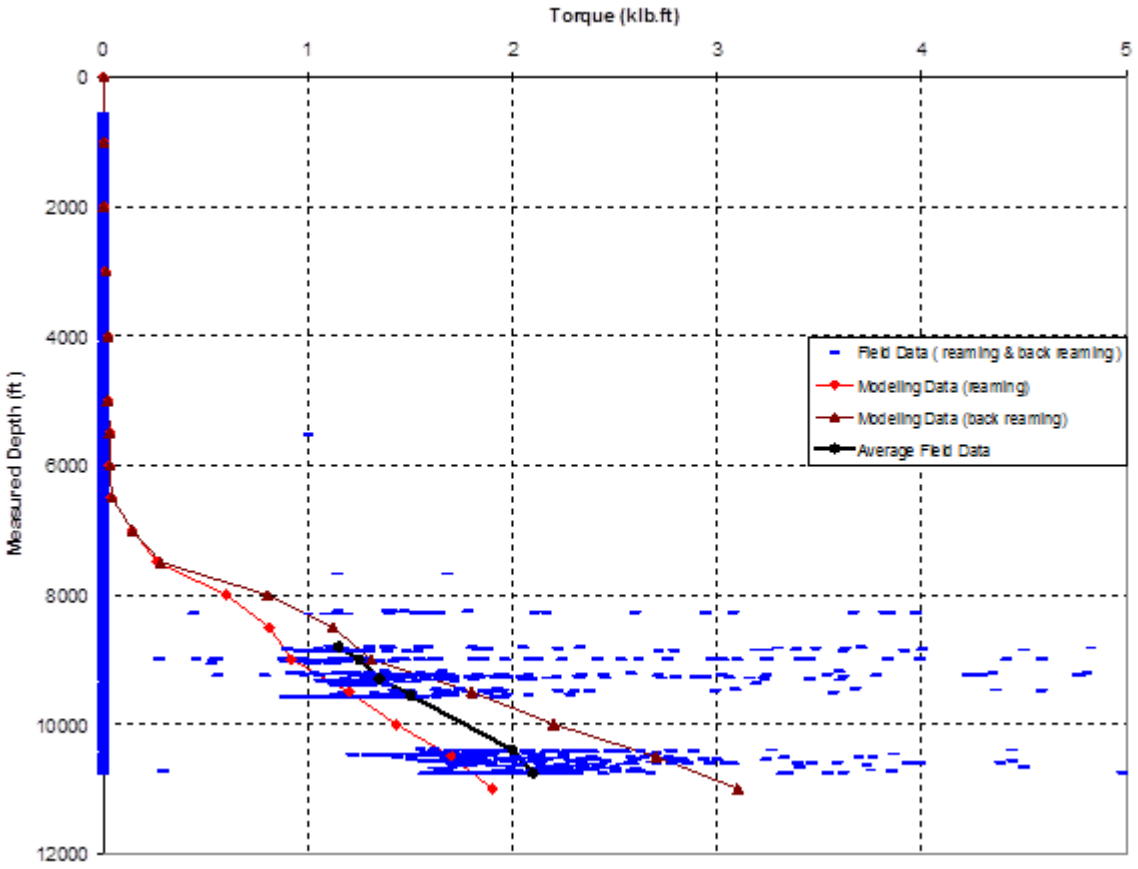

Figure 6.10: Comparison between the measured and calculated surface torque during reaming and back reaming

The first remedial action for over pull during tripping the drill string out is to rotate the drilling string at surface. As it was discussed in Chapter 3, the model for the combined motions is used to show the effect of rotation on the drag force reduction in the well. The drilling rig weight indicators show a considerable difference between the drag force generated by tripping in/out and reaming/back reaming operations. Figure 6.11 shows the effect of pipe rotation on the calculated hook load during reaming and back reaming operations.

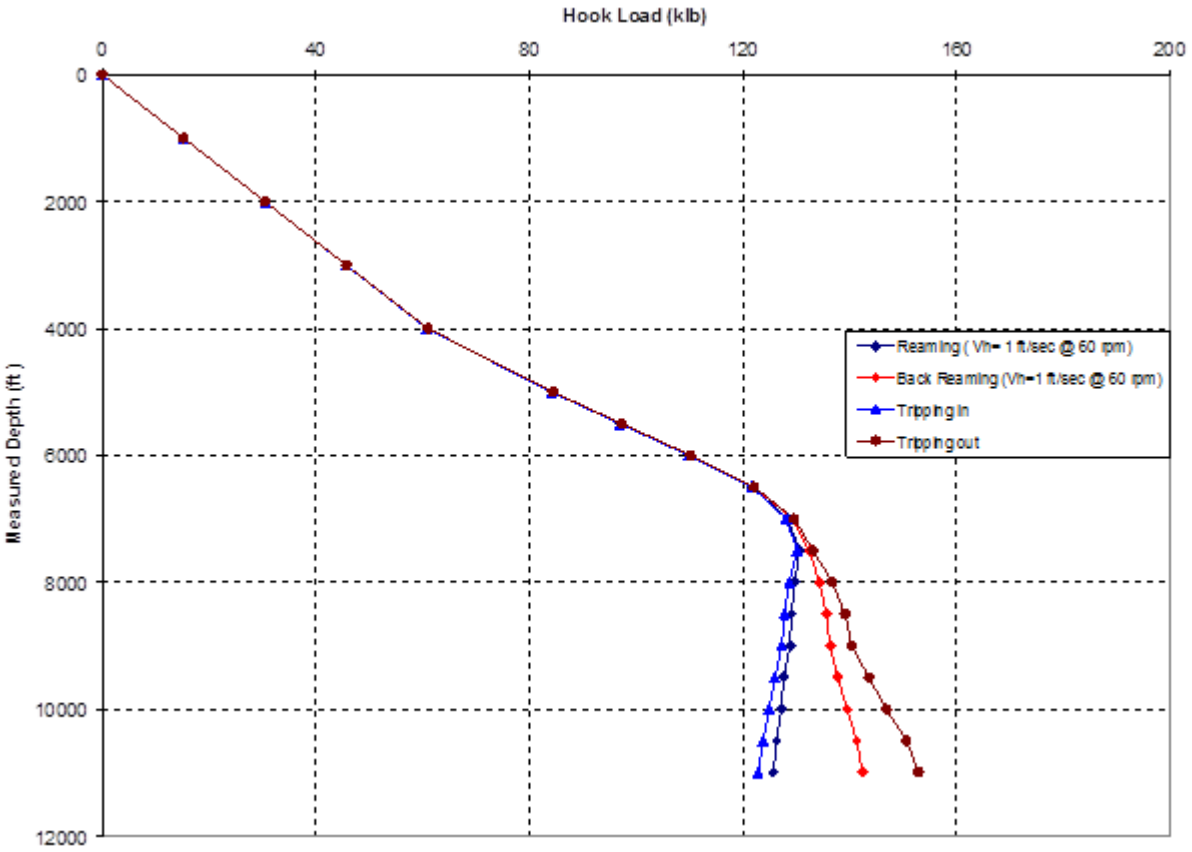

Figure 6.11: Effect of pipe rotation on the calculated hook load during tripping in/out

As was discussed in Chapter 3, the wellbore friction is divided into rotational and axial frictions. By increasing either of them, the other one will decrease. For example, at a constant pipe surface rotation speed, the torque values will decrease due to the increase of tripping speed, which leads to an increase in axial friction. The effect of tripping speed on the calculated torque at a constant rpm is shown in Figure 6.12.

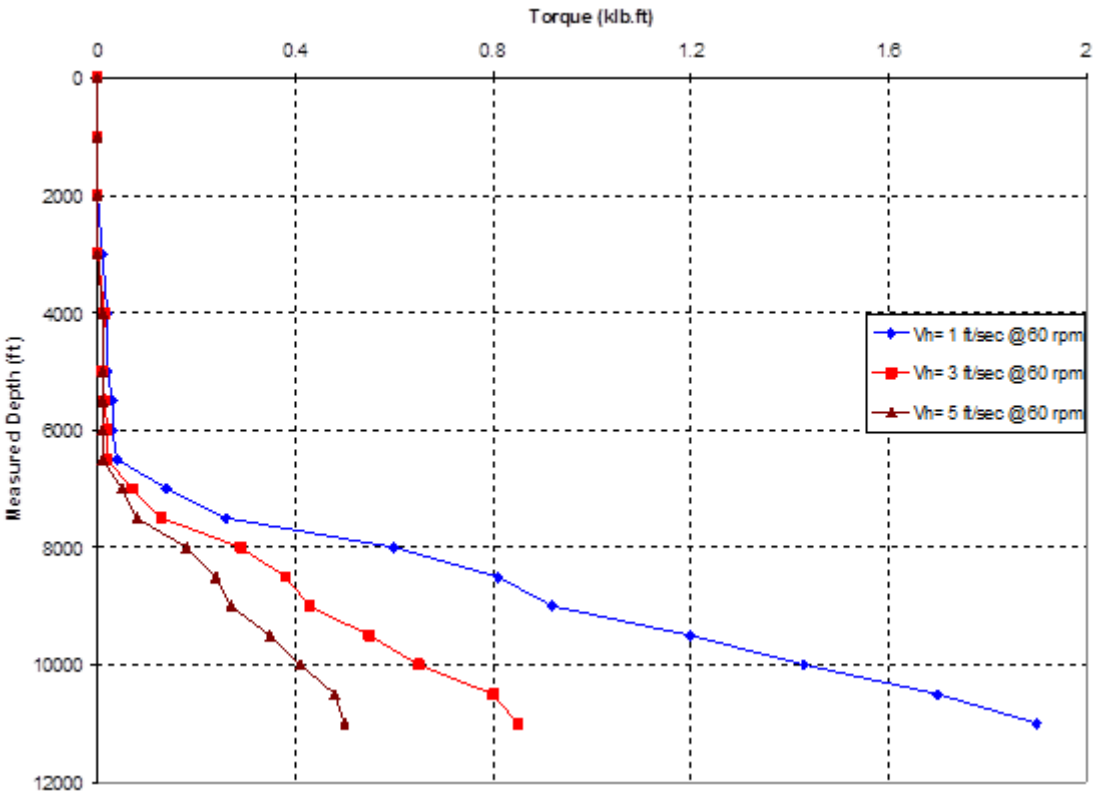

Figure 6.12: Effect of tripping speed on the calculated torque during reaming operation

Additionally, if the pipe rotation speeds up at a constant tripping speed during the reaming operation, it will result in higher torque values (see Figure 6.13). In this case, the major portion of the friction force will be the rotational friction, which will trigger an decrease in the torque along the drill string at the surface.

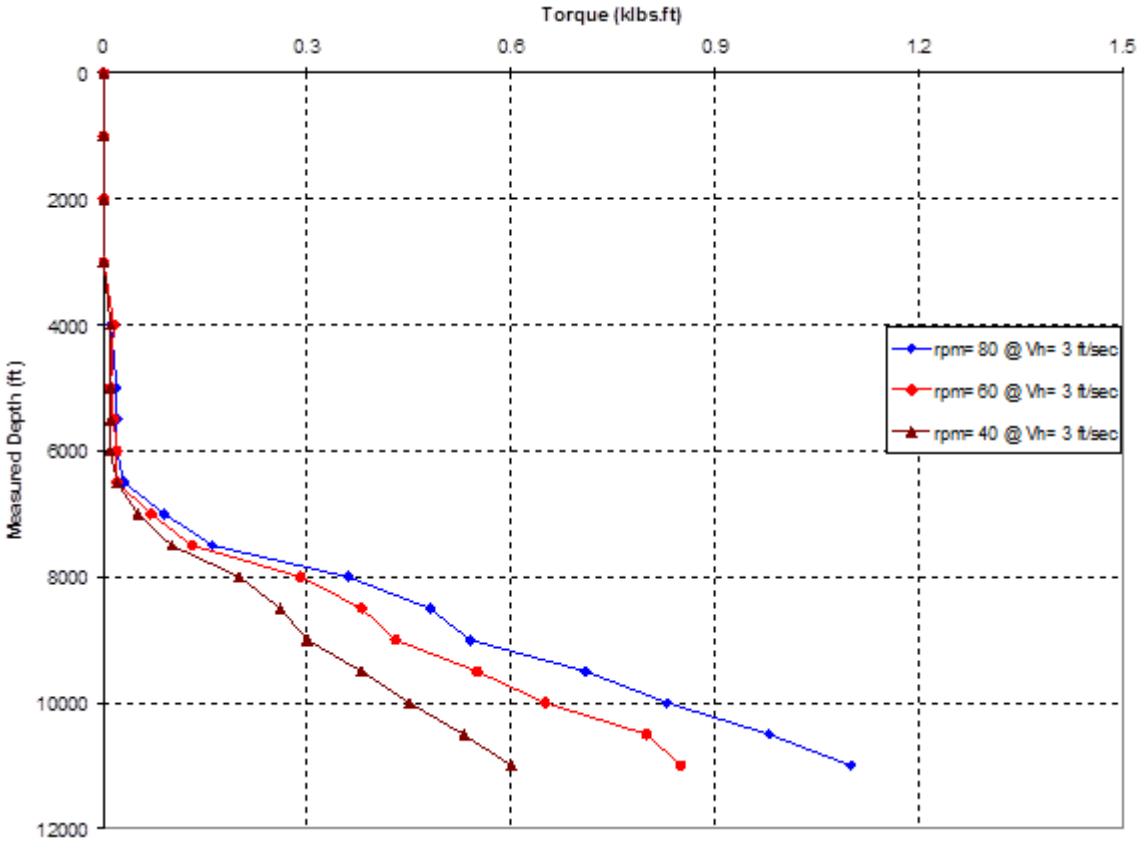

Figure 6.13: Effect of pipe rotation on the calculated torque values during reaming operation

6.1.4 Effect of Contact Surface

In this section, the effect of contact surface C_S on the torque and drag calculations is investigated. As it was discussed in Chapter 5, the data required to include this effect are the wellbore diameter and pipe string outer diameter. In this case, a 7 *inch* casing was set at the depth of 7500 *ft* and then the horizontal section was drilled by 6 1/8 *inch* bit size. Both the 4 *inch* drillpipe and 4 *inch* heavy weight drillpipe have the same adjusted outer diameter of 4.1 *inch*. The *Cs* calculated for the open hole and cased hole are 1.16 and 1.15, respectively. These values should be multiplied by the friction coefficient. If the hole has some collapsing or tightening problems, the contact surface value might approach a very big number. The latter can be used for monitoring wellbore conditions.

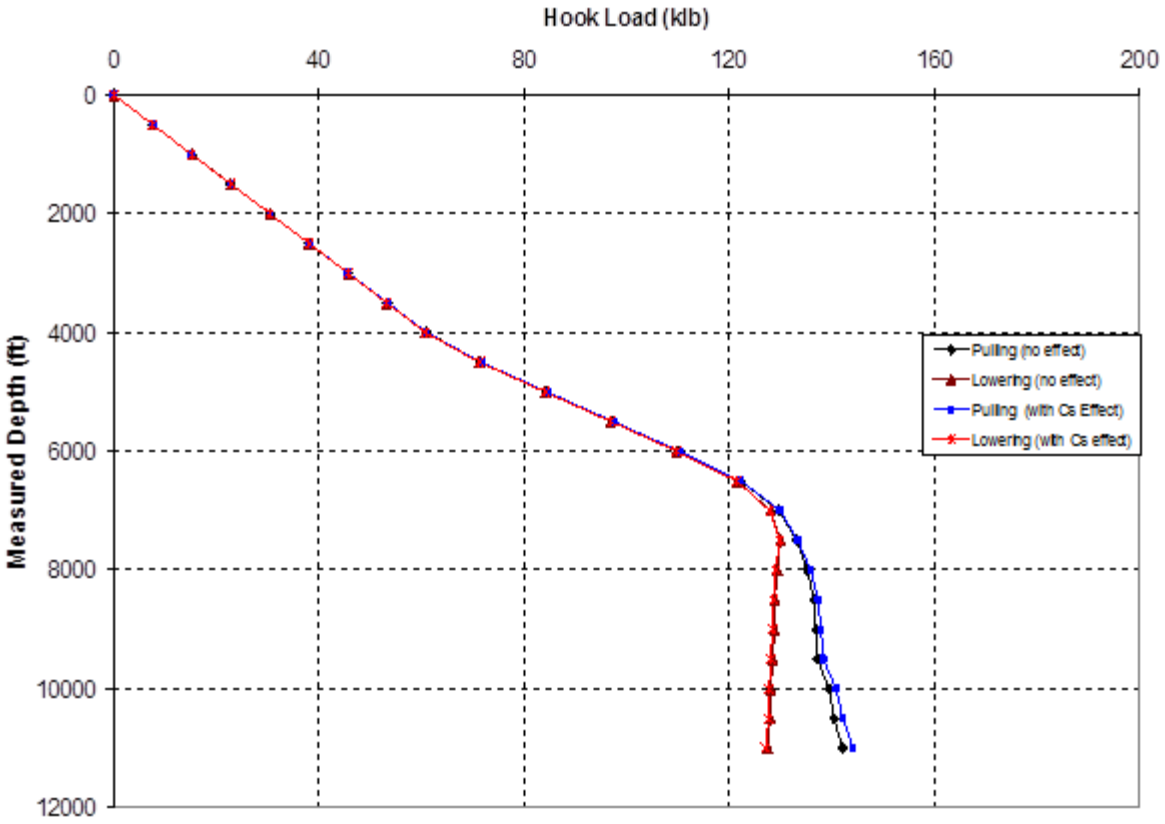

Figure 6.14: Effect of contact surface on the calculated drag values during tripping in/out

Figure 6.14 shows the effect of contact surface on the calculated hook loads during tripping in/out. When drill string is at the bottom of the well, the effect of contact surface on the hook load value during tripping in/out is 0.3% and 1.5%, respectively. The effect of contact surface on the torque calculations is more noticeable as the torque values pertinent to tripping in/out have been increased to 5% and 20%, respectively. Figure 6.15 compares the torque values before and after considering the effect of contact surface for torque calculations.

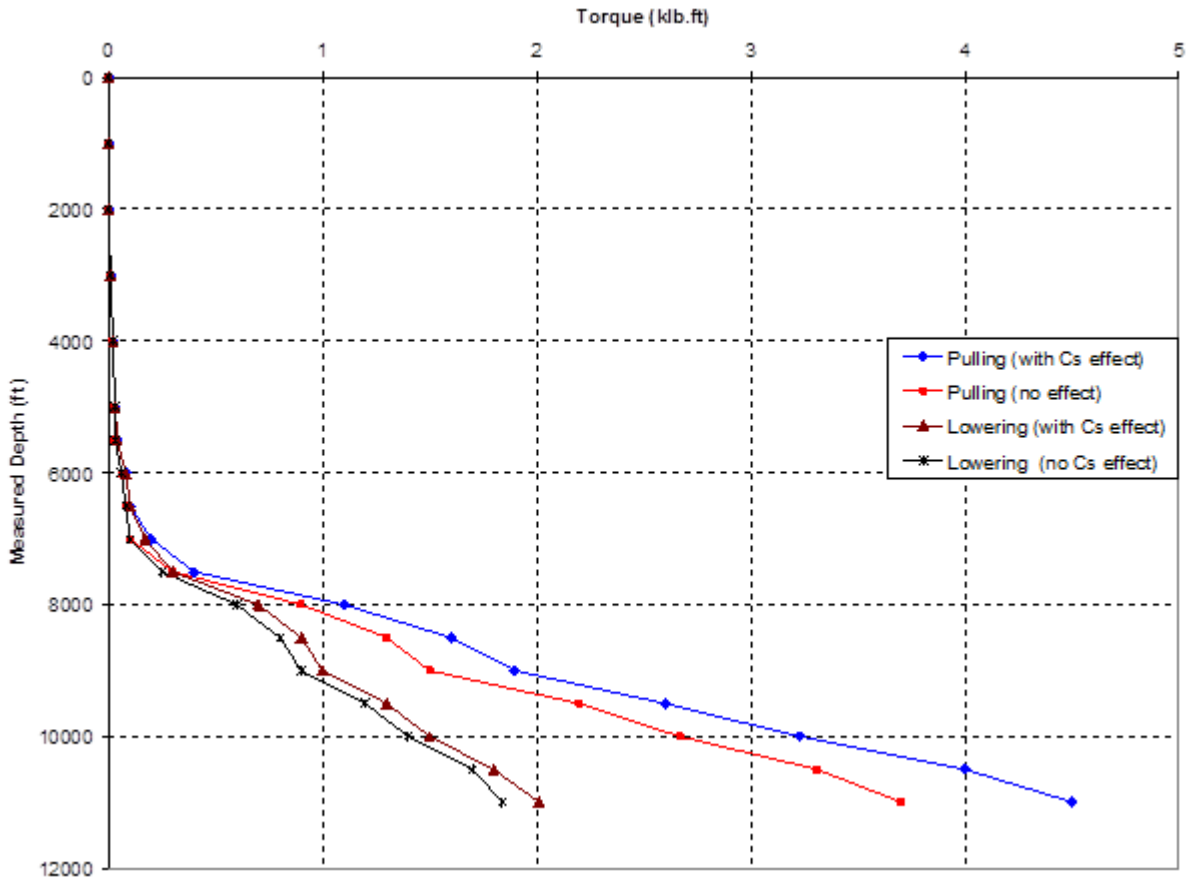

Figure 6.15: Effect of contact surface on the calculated torque values during tripping in/out

6.1.5 Effect of Hydrodynamic Viscous Force

Hydrodynamic viscous drag force is defined as the friction force between the pipe string and drilling fluid, which creates a resistance against the pipe movement. This was comprehensively discussed in Chapter 5. Viscous drag force depends on the drilling fluid properties, tripping velocity, flow regime, pipe outer diameter and the wellbore diameter. Here, the drill string configuration and the well specifications are the same as those given in the previous horizontal well. For instance, the effect of drilling fluid rheological properties on the hydrodynamic viscous drag force is shown in Figure 6.16.

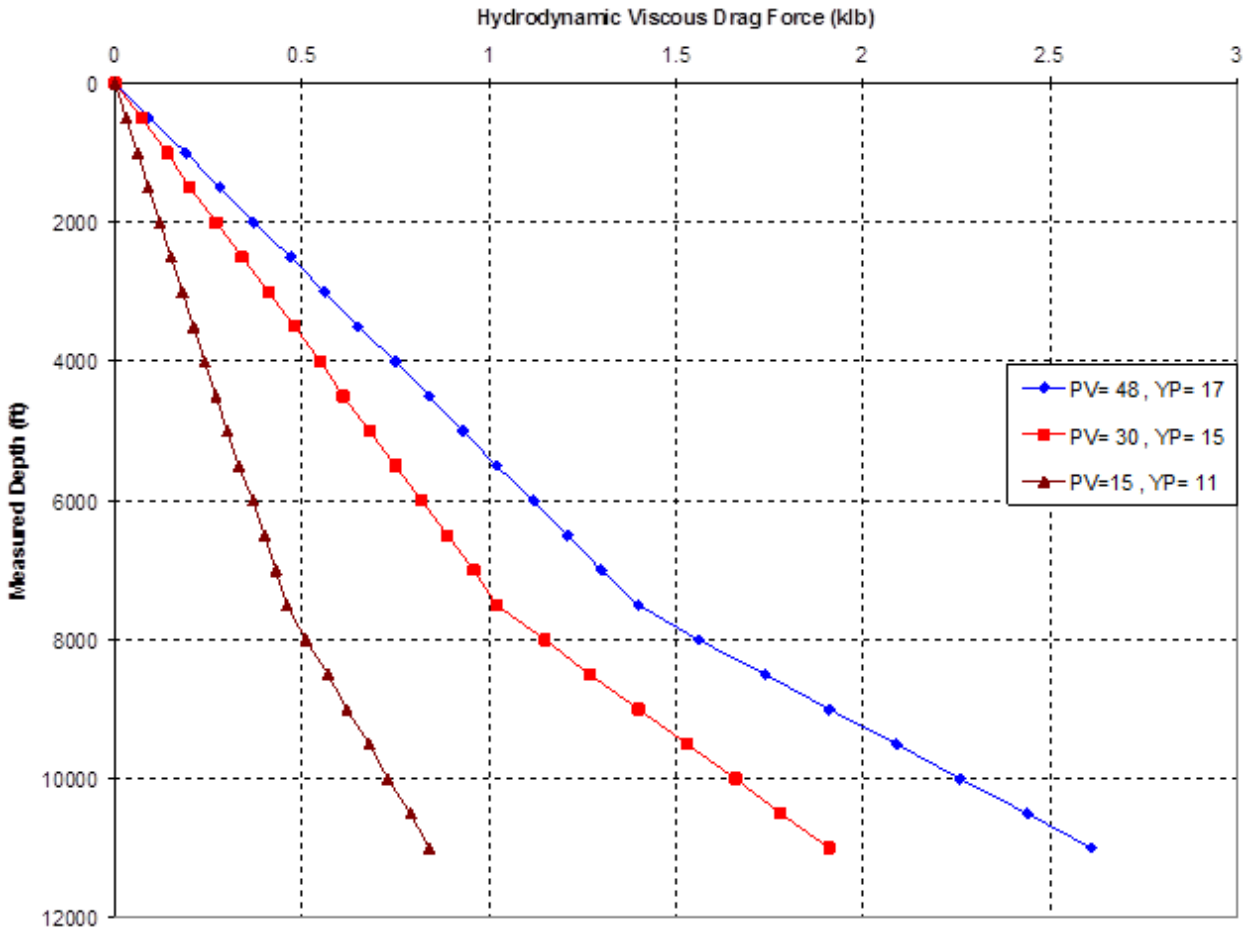

Figure 6.16: Effect of mud rheology and clearance on the hydrodynamic viscous drag force

A higher viscous drilling fluid results in a higher viscous drag force. Also, this figure shows the inverse relationship of clearance between the string and the wellbore and the viscous force. Figure 6.16 can also be used to describe the effect of flow regime on the viscous drag force. At a velocity of 1 *ft/sec*, the flow regime is laminar. When tripping speed is less than 4.5 *ft/sec*, the flow regime is laminar in both cased and open holes. At a tripping speed of 5 *ft/sec*, due to smaller clearance, the flow regime changes to transient flow in the open-hole section while it remains laminar in the cased-hole section. Table 6.1 shows different flow regimes at different tripping speeds.

Table 6.1: Flow regimes for different drill string position at different tripping speed

Tripping speed, ft/sec	*Drill string position*	*Flow Regime*
< 4.5	Cased Hole	Laminar
< 4.5	Open Hole	Laminar
5	Cased Hole	Laminar
5	Open Hole	Transient

Figure 6.17 shows how tripping speed affects the flow regime and the hydrodynamic viscous drag force. By increasing tripping speed, the flow regime approaches turbulent mode. This increases the viscous drag force drastically. Hydrodynamic viscous force should be added/ subtracted to/from the calculated hook load during tripping out/tripping in.

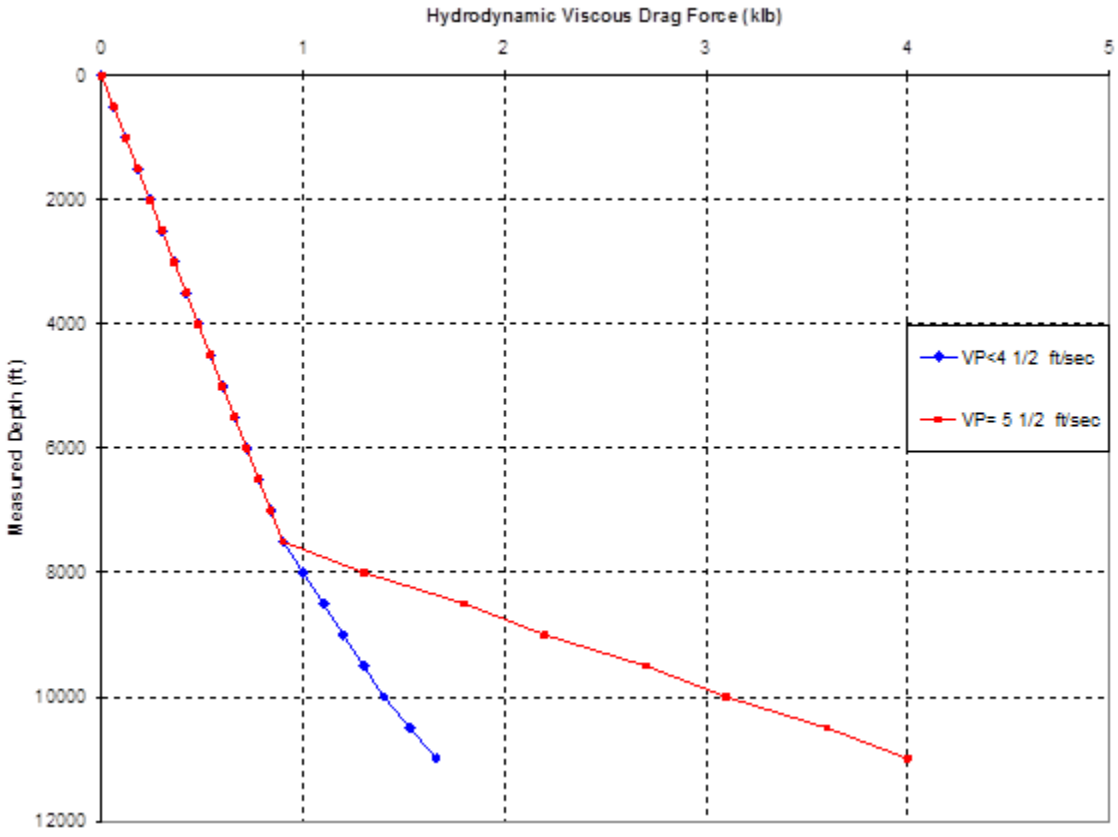

Figure 6.17: Effect of tripping speed and flow regime on hydrodynamic viscous drag force

6.2 Three Dimensional Well-Analytical Modeling

The well that has been considered for the friction analysis is located offshore in the North Sea. The well starts vertically with a kick-off point of 350 m and a first build-up section to a depth of 1200 m. Then, the angle of this build-up section is held at 30º±2º inclination until a depth of 2750 m. At this depth, the second build-up section starts from an angle of 30º±2º to 90º. The horizontal section starts from 4500 m to the final target. This well profile is a good candidate for friction analysis as different sections of the well geometry (including straight inclined, curved and horizontal sections) are present (see Figure 6.18). The 9 5/8" casing is set at a depth of 3207 m with an open-hole section to 5247 m.

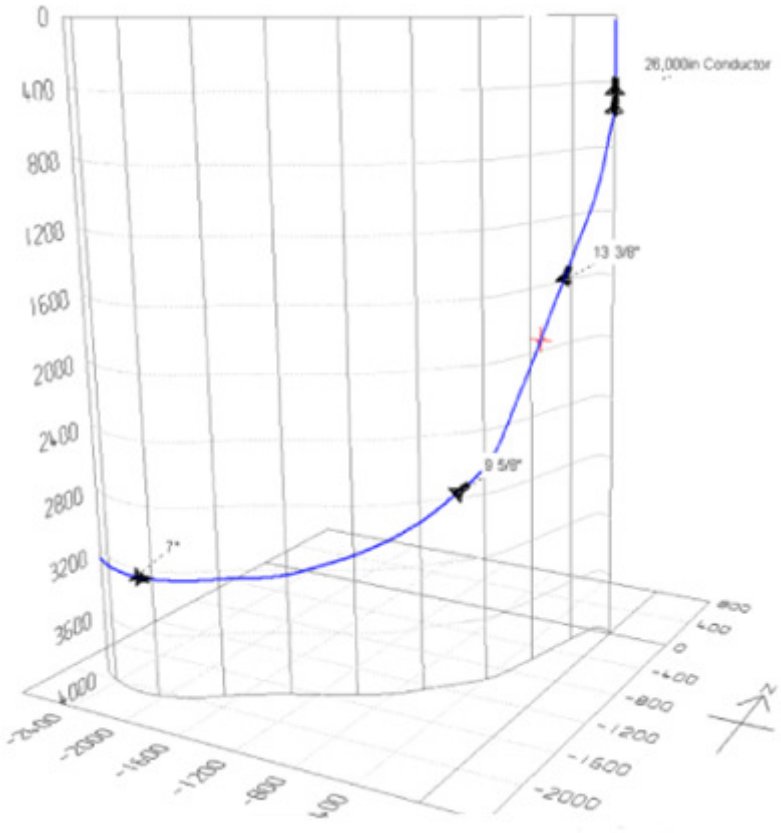

Figure 6.18: Well geometry with casing shoe depths

6.2.1 Tripping out

Figure 6.19 shows the hook load values for the tripping out operation. The calculations started from the bottom to the surface using 100 m elements. This calculation is repeated for different friction coefficients. Two different friction coefficients are considered. First, a single value is used for the friction coefficient for the entire well including the open and cased hole sections. The friction factor value is changed stepwise as 0.2, 0.3 and 0.4. For the second case, different friction factors are considered for the open-hole and cased-hole sections. The friction factor is maintained for the cased hole at a constant value of 0.2; for the open-hole sections it is changed to 0.2, 0.3 and 0.4. In this section, three models have been used for analysis. The Exxon model is the model which developed by Johancsik in 1984. The Texas A&M model is the simple accepted industry model which is modified by using the dogleg angle concepts instead of average inclination between two subsequent survey data points.

As is shown in Figure 6.19, the three models (including the newly developed analytical model) match the field data reasonably. However, the three models do not match the field data in a hump existing at an interval of 2180 m to 3140 m. This section is the build-up section, which starts with an inclination of 30º and ends at 55º. These three models cannot predict the local increase in hook load due to several factors. One factor is the well geometry. In this interval there is a build-up section with an angle of 25º over a 960 m interval. Once the three soft string models are applied (all of which assume the pipe as a cable which completely contacts the borehole wall), the estimation of friction force is inaccurate. This is allotted to the fact that in reality the drill string should be considered as a stiff string that could tolerate a bending moment in either of the bending sections. The other reason could be due to cuttings accumulation. It means that any time that the pumps are off and cuttings begin to settle, the cuttings will not be stable until they land in the lower part of the intermediate build-up section. In this section, the problem is that after getting to the casing shoe (i.e., where there are already extra cuttings accumulated due to the increased annular diameter), the well has been circulated, but only one bottoms-up. One bottoms-up circulation will not remove the cuttings from a cased hole at these inclinations. Thus, after one bottoms-up, the annulus is still full of cuttings. The result is an avalanche of cuttings down onto the top of the BHA. Although this amount of cuttings is not enough to pack off the annulus, it may be sufficient to increase the friction (as can be seen in first hump section).

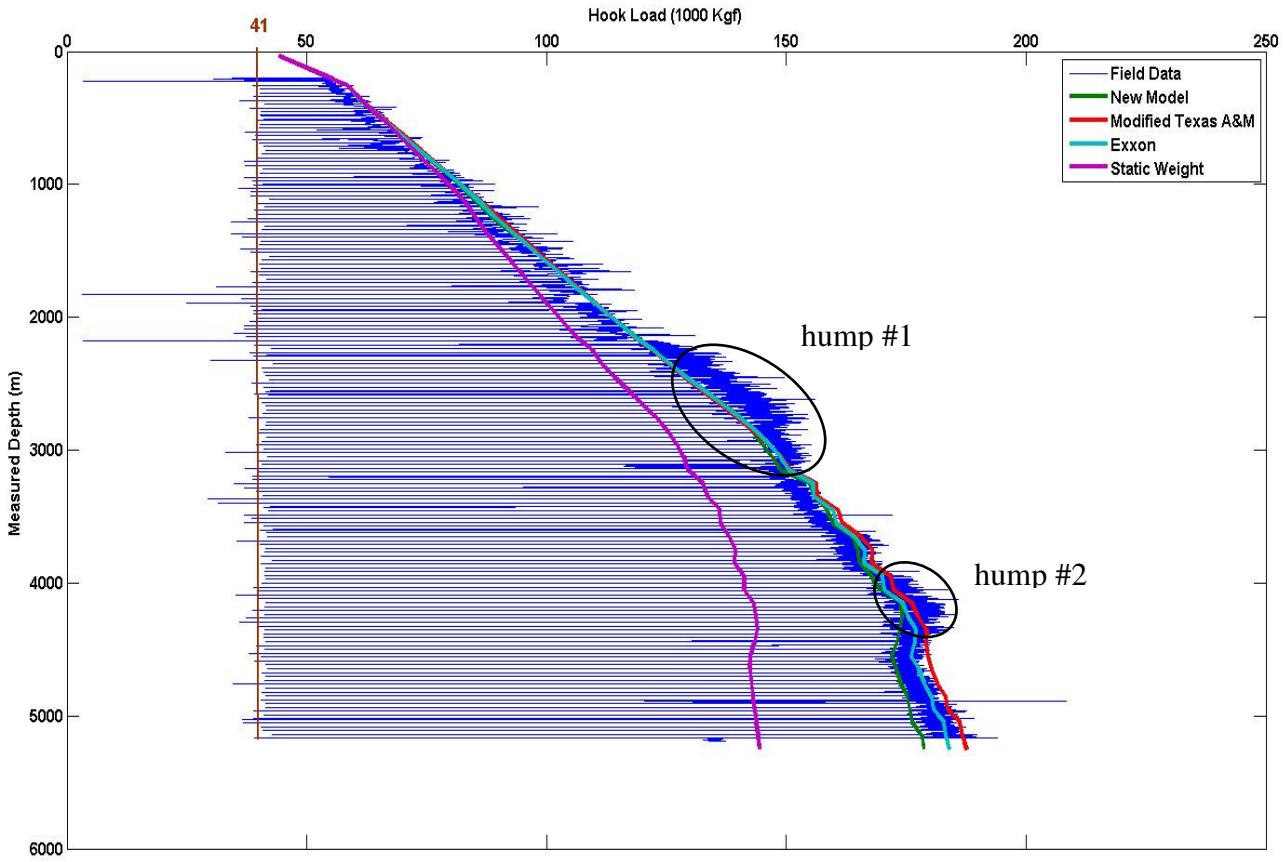

Figure 6.19: Comparison between the field and models hook load data using friction coefficient of 0.2 during tripping out

Also, Figure 6.20 depicts the tripping out procedure in terms of flow rate and drill string rotation.

The second small hump could be predicted by models. The second hump here is near the heel section and the cuttings bed (which could be removed by a single bottom-up circulation). The models cannot predict the effect of the cuttings bed formation which is related to the friction coefficient.

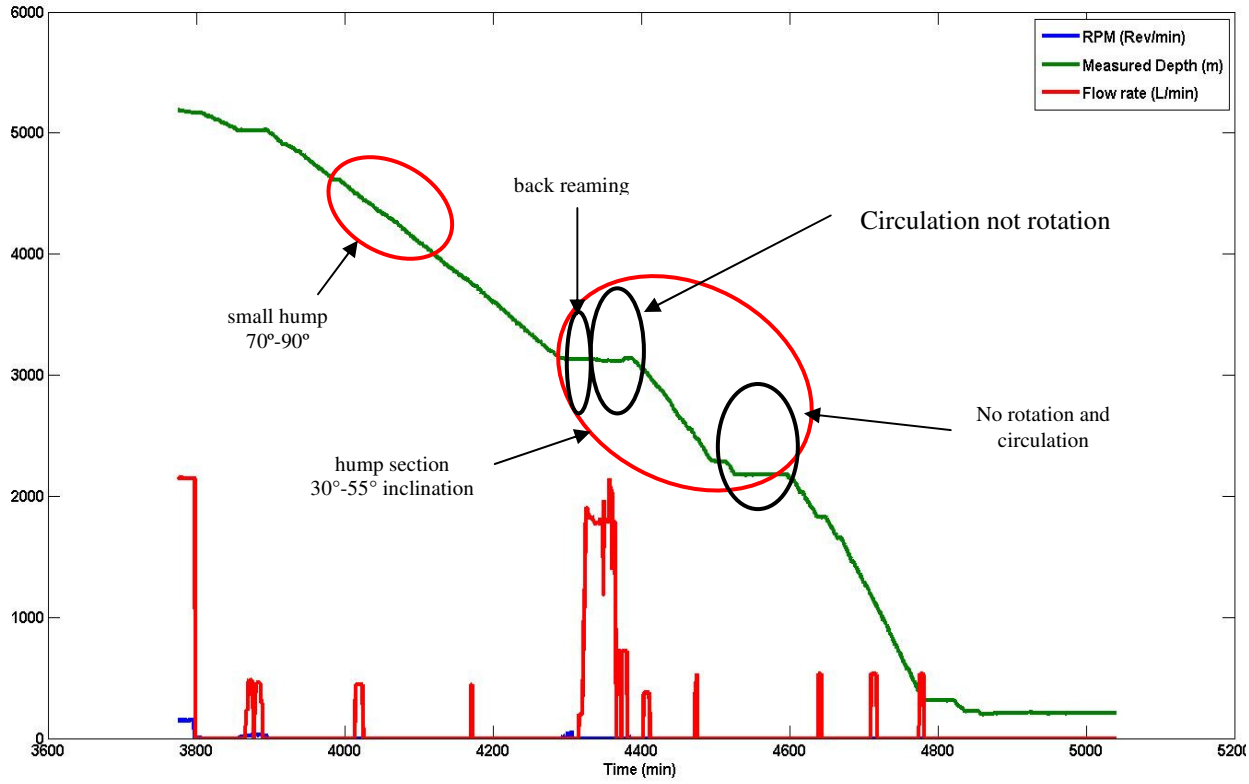

Figure 6.20: The tripping out procedure for North Sea candidate well in terms of flow rate and drill string rotation

The torque plots for the comparison of the models prediction versus the field data are shown in Figure 6.21. In this case, as the pipe is being pulled out of the hole, in most parts of the well there is no torque because there is no pipe rotation. The drill string rotation from surface only happens in two sections. A small section below the casing shoe as the hole wall is being reamed and circulated to be cleaned. Another section is the last 360 m of the well, which is related to the drilling operations.

Figure 6.21 shows the torque prediction by the three selected models versus the field data. The results reveal that the models developed by Exxon and Texas A&M University work well for the friction coefficient as high as 0.20 whereas the new model needs a larger value for the friction coefficient.

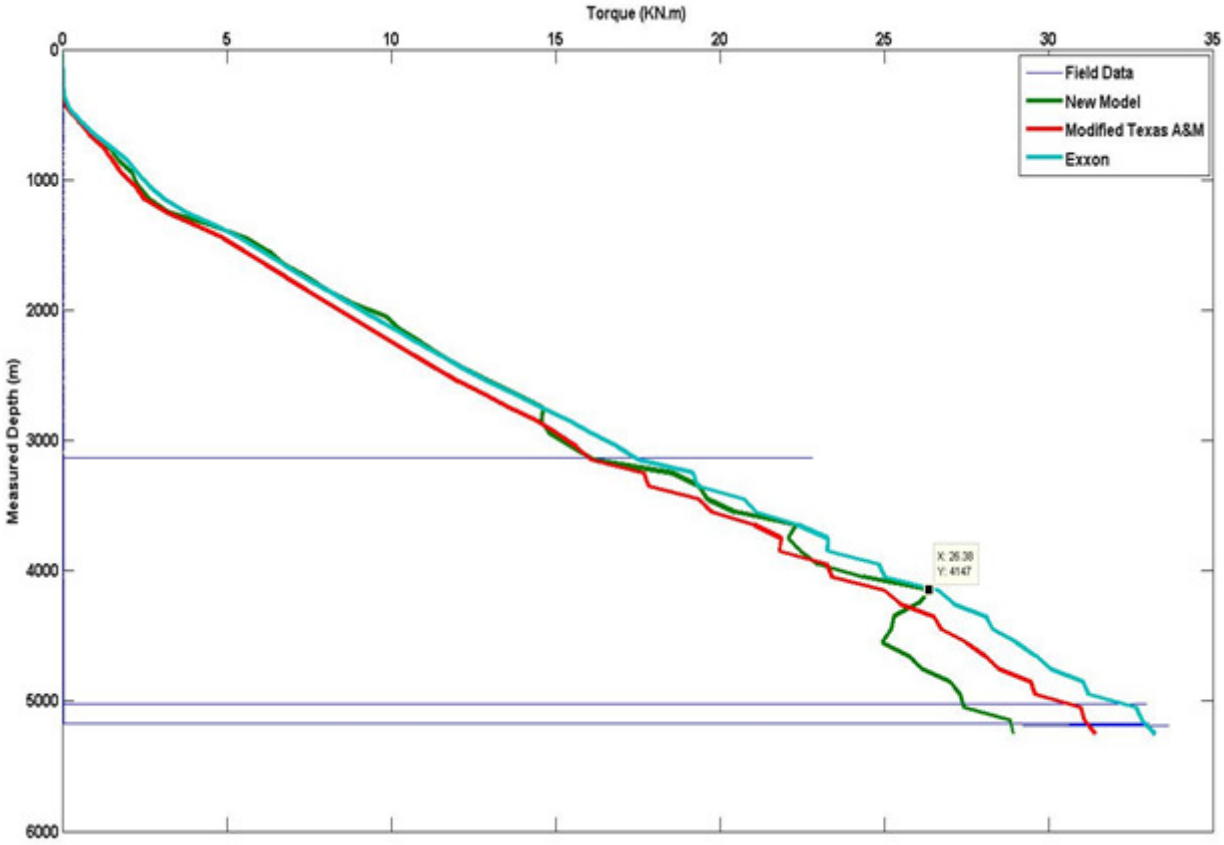

Figure 6.21: Comparison between the field and models torque data using a friction coefficient of 0.2 for tripping-out

6.2.2 Tripping In

For the case of tripping in, if the models with the same conditions are used in the tripping out, they produce inaccurate results. In the case of tripping in, usually the float valve is used above the drill bit. In this case, the drill string will be filled up with the drilling fluid a few times throughout the entire well interval. The time of fill-up depends on the collapse strength of the pipe. In this candidate well, the pipes are filled almost every 1000 m of running in. As Figure 6.23 demonstrates, in each filled up section, there is a jump in the hook load data. This jump is equal to the weight of the mud that has filled up the drill string.

Whenever a float valve is used, and drill string is not completely filled up with mud, the local buoyancy factor has to be applied. A single buoyancy factor in the case of tripping out should be

replaced by the buoyancy factor profile. This will greatly influence the buoyed weight of the string in the wellbore, hook load, and torque. Therefore, the following buoyancy profile has been calculated in order to use it in the models from which one could generate the hook load during tripping in. Figure 6.22 shows the buoyancy profile during tripping in for the candidate well. Equation 5.2 has been used for generating the buoyancy factor profile. This buoyancy profile is included in torque and drag equations in order to analyze the tripping in operation.

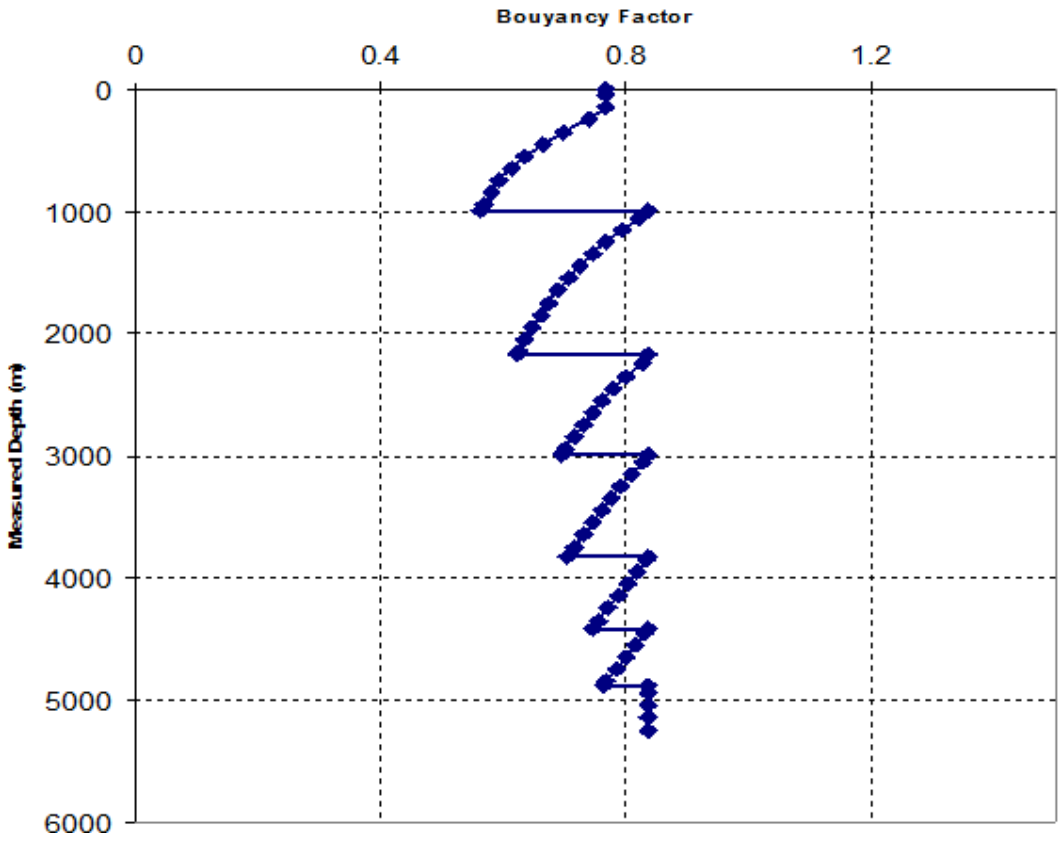

Figure 6.22: Buoyancy factor profile during tripping-in

As is shown in Figure 6.23, the step changes in the hook load data are the results of change in the buoyed weight of the pipe (while it is empty or filled with the mud). This demonstrates the importance of handling the buoyancy effect correctly.

This plot consists of two stages. The first stage is from the surface to the depth of 4990 m and the second one is from 4990m to the bottom. Hook load analysis for tripping out produced a good

match between the measured data and the models results using a friction coefficient of 0.2. Using the same friction coefficient for tripping in results in a good match in the first 3000 m. Beyond 3000m, however, a discrepancy between the field data and the models results is observed. This discrepancy is due to drill string rotation from the surface, which reduces the axial friction.

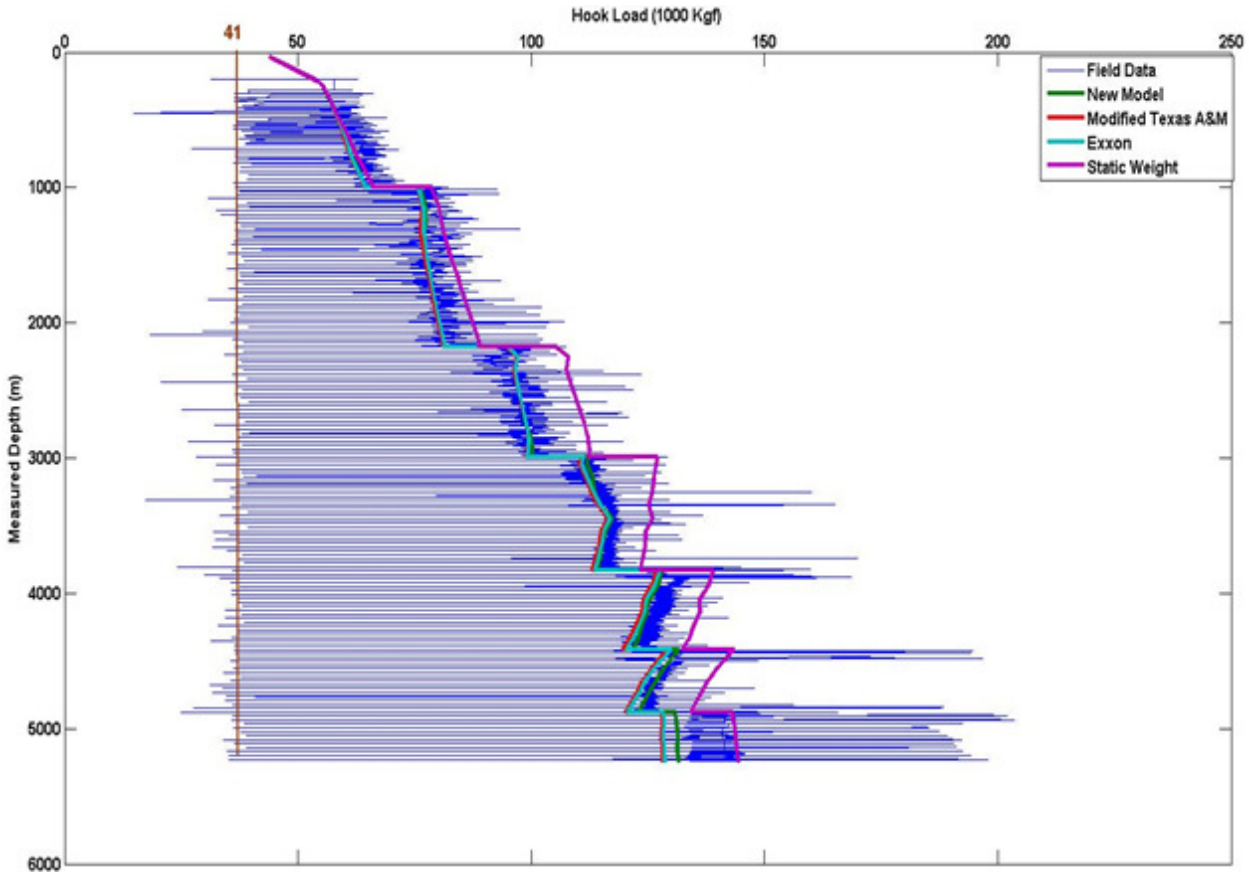

Figure 6.23: Comparison between the field and models hook load data using a friction coefficient of 0.2 for tripping in

The back calculation of friction coefficient from the hook load data is shown in Figure 6.24. The tripping out friction factor is approximately 0.2 everywhere except in the hump interval (Figure 6.19). The tripping in graph shows that the friction factor is close to 0.2 in the upper interval above 3000 m. For the interval between 3000 m and 3500 m, the friction factor starts to decrease gradually from 0.2 to 0.1. From the depth 3500 m to the 4890 m, the friction coefficient is almost 0.1.This trend is not observed in the tripping out analysis. This indicates the importance of

assessing the axial forces on the pipe whether the pipe is in tension or compression. The tripping out data shows that the drill string is in tension as it is tripping throughout the wellbore. This means that in tripping out the pipe is fully contacted on the low side of the wellbore and the assumption made in the soft string models is valid.

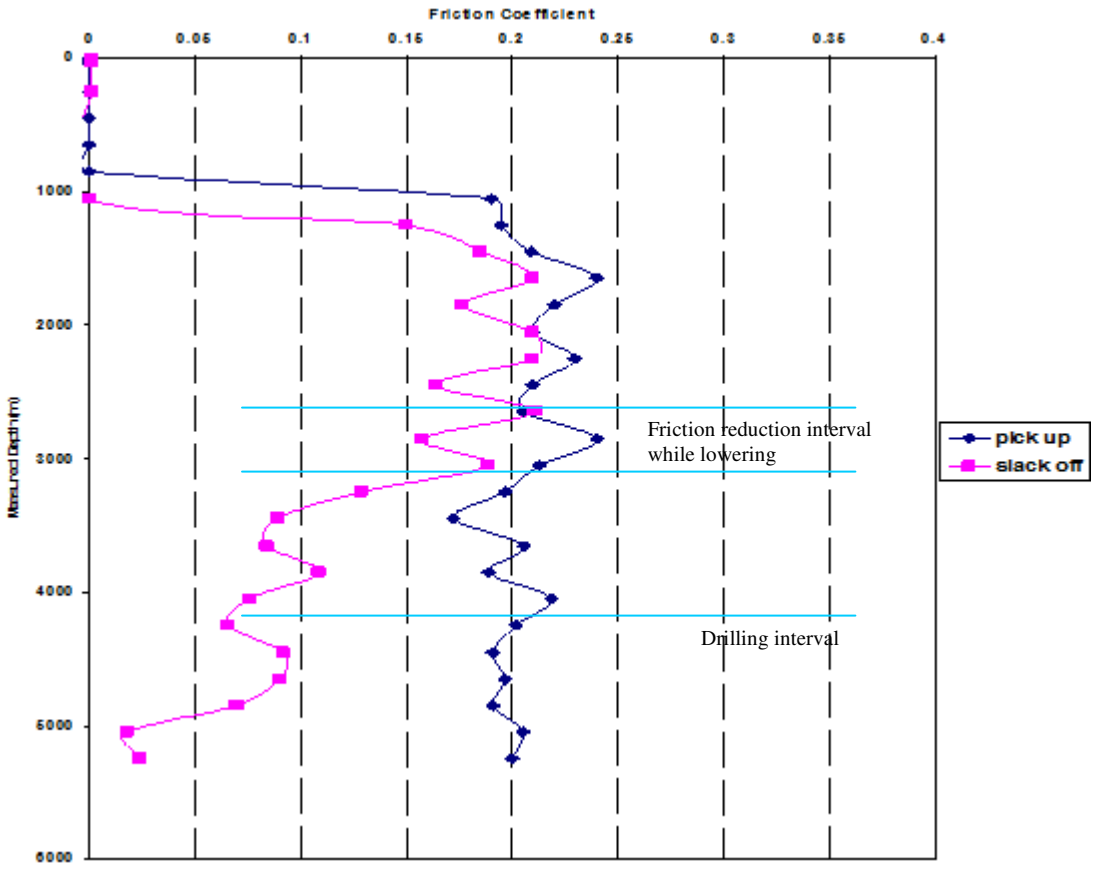

Figure 6.24: Friction coefficient versus the measured depth during tripping in and out

The tripping in pipe conditions is more complex. As it was analyzed, the section from 3200 m is in compression while the interval above this depth is in tension. Because the condition on the pipe is changing between tension and compression and the pipe is neither on the low nor high side, a pseudo-catenary profile forms and the friction is significantly reduced as the contact force is reduced. This is the case where the normal soft string models could not predict accurately. The reduction in friction force is noticeable in matching the field data with models using a friction coefficient of 0.1.

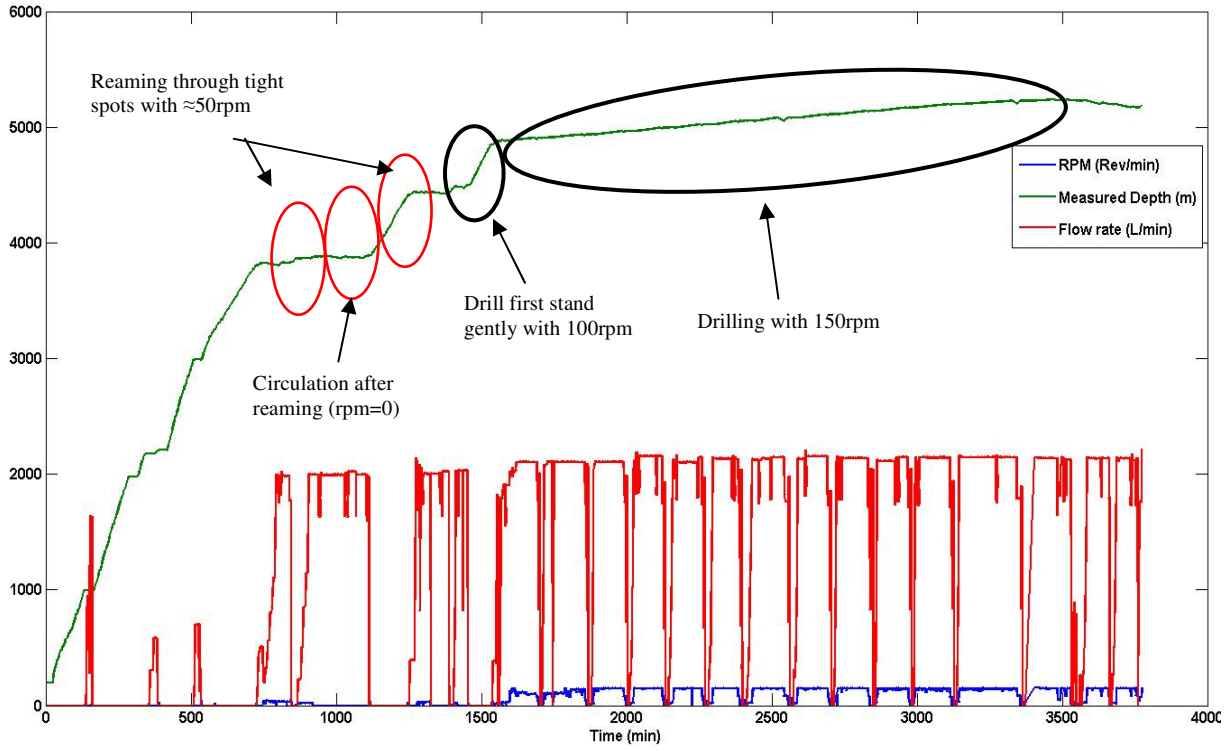

Figure 6.25: The tripping in procedure in terms of flow rate and drill string rotation

Figure 6.25 reveals that in the interval between 2990 m to 4000 m, the pipe is running in with the same axial speed of that in upper intervals. There are 3 pauses in running the pipe which occur at depths of 1000 m, 2000 m and 3000 m. These depths are the same depths possessing jumps in hook load data. These jumps occur where the pipe stops to be filled up with the mud.

Another effect that can be addressed is the acceleration of the BHA. Every time one stand is run in the hole, the string is stopped for connection. Consequently, the BHA has to decelerate before the full stop. This deceleration creates a peak in the hook load data every time the drill string is stopped for connection. Figure 6.23 shows that the peaks in the hook load occur every 30m. A comparison between Figures 6.19 and 6.23 show that the peaks for tripping in are larger than those for tripping out. This is expected considering the direction in which the deceleration of the BHA takes place.

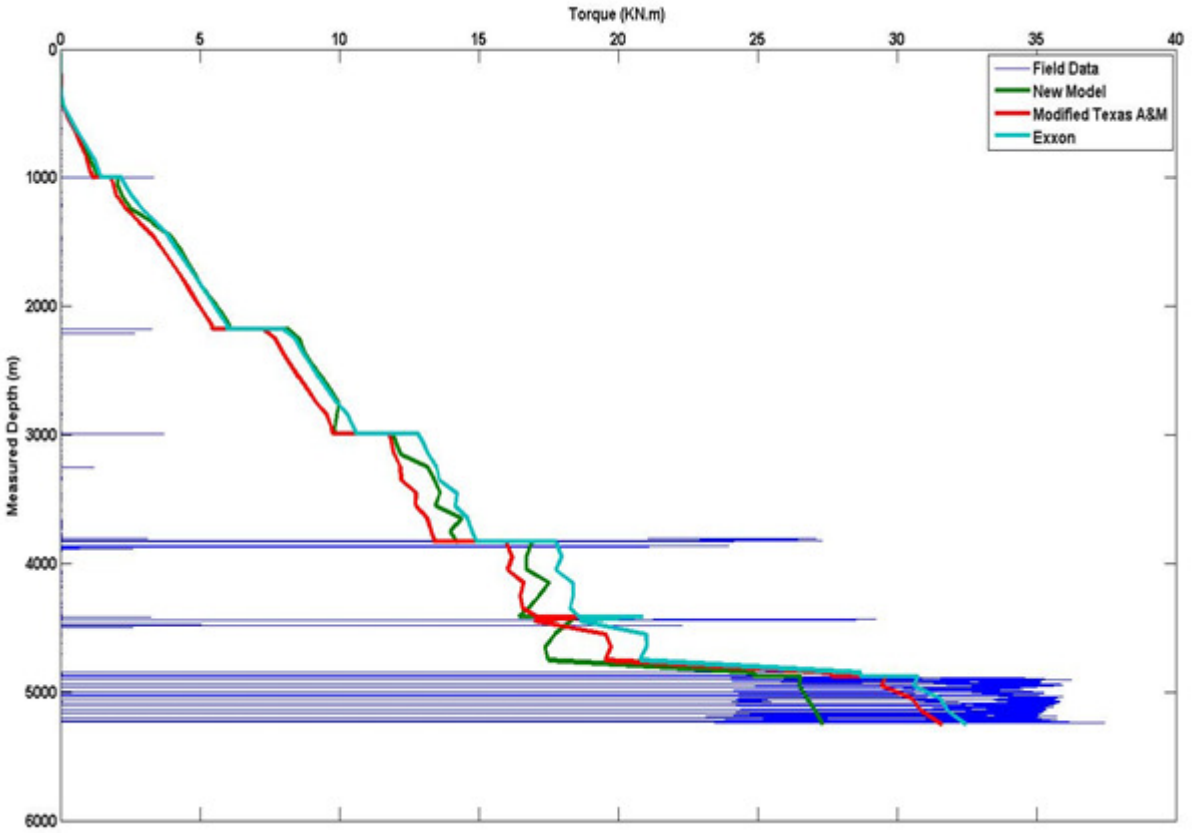

Figure 6.26: Comparison between the field and models torque data using a friction coefficient of 0.2 during tripping in

Figure 6.26 shows the corresponding torque plot during tripping in. The only sections that drill string is experiencing torque are around 3800 m, 4300 m, and the last 360 m of the well in which drilling operations has taken place. Here the bit torque is approximately 7.5 KN.m for the drilling section. The plot shows that the models and field data are quite consistent when using a friction coefficient of 0.2.

Another factor that has to be considered in the friction analysis is the sheave friction, which is the result of passing drilling lines through the sheaves. This depends on the number of drilling lines and block movement direction as well as type of deadline sheave, and whether they are active or inactive. The effect of this friction in the hook load data were considered for this field case.

6.3 Detection of Drill string Sticking - Analytical Modeling

A well drilled in western Canada is used to illustrate this type of friction analysis. The well geometry is shown in Figure 6.27. The well depth was 3251 m when the drill string got stuck during drilling operations. The well profile included a kick off point at 800 m and the heavier build-up section initiated at 2287 m. The well reached an angle of 30 degree inclination at 2700 m and drilled to a total depth of 3231m with the same inclination of 30 degrees. At this depth, the drill string was tripped out for the purpose of replacing the measured while drilling (MWD) tool. The drilling process was continued for a 20m interval after the tripping in procedure. At the depth of 3251m the drill string got stuck.

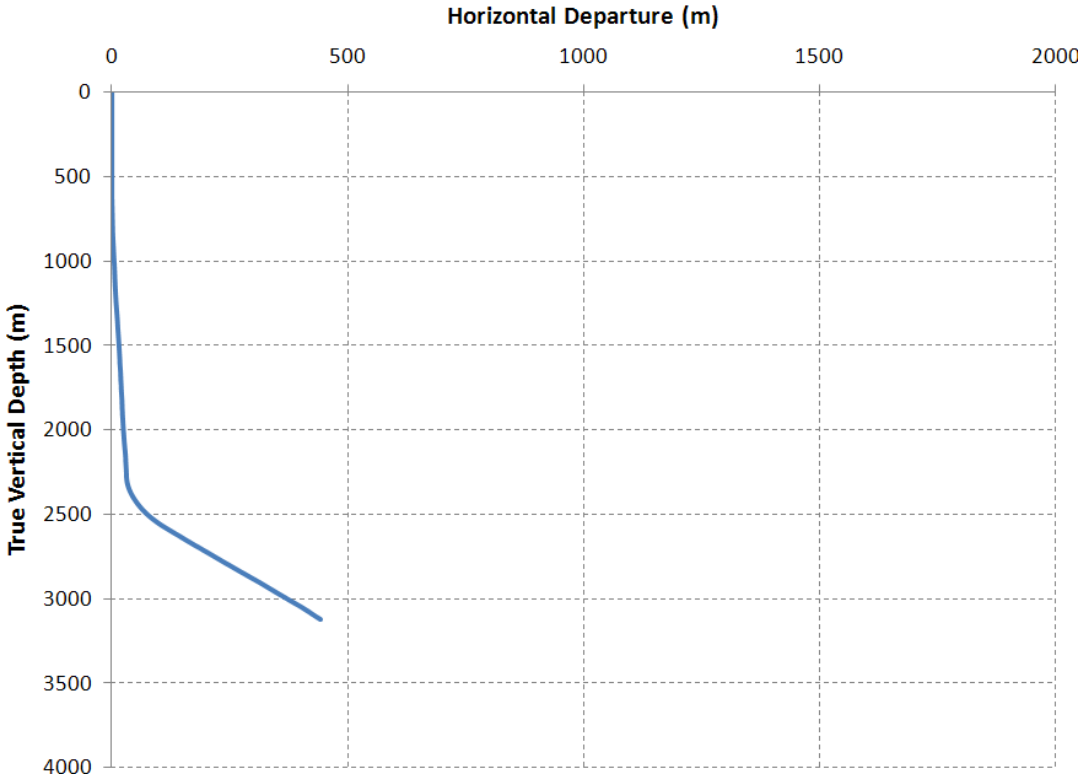

Figure 6.27: Well geometry of stuck well

The drill string configuration was not changed from 2200m to 3251 m. The BHA had a length of 290m from the bit. The BHA has a large effect on the value of friction force during tripping in and out. For example, any interval in the wellbore which has a smaller diameter (due to

formation swelling) has a greater friction force against the BHA movement. This behavior is shown in Figure 6.28.

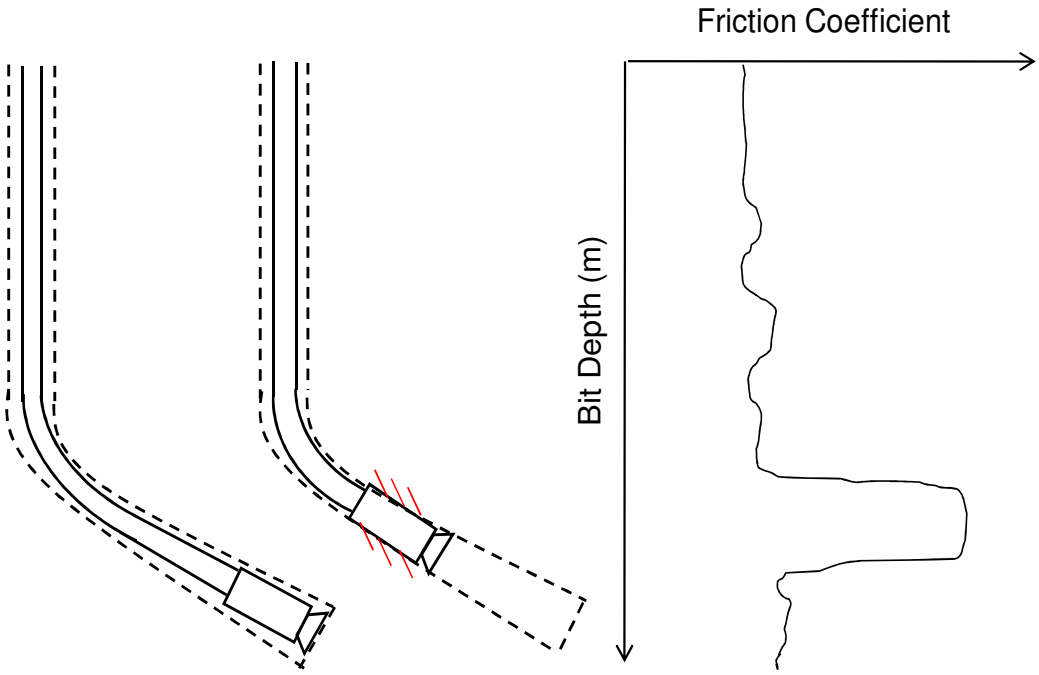

Figure 6.28: Illustration of BHA-tight hole effect on the friction coefficient

As discussed before in Chapter 5, another important factor in friction analysis is the buoyancy factor, which changes during different drilling operations. In Figure 6.29, the buoyancy factors of tripping in, drilling and tripping out modes is shown.

During the drilling process, the buoyancy factor is maintained at a constant value until the depth of 2485 m when the mud weight was increased by 300 kg/m^3 to prevent the gas inflow. This increase led to a decline in the buoyancy factor. The tripping out process exhibits a nearly constant buoyancy factor since the mud weight is kept constant and the level of mud in the annulus drops a little. The annulus is filled up periodically through the fill-up lines. The buoyancy factor during the tripping in process shows a gradual decrease due to the increasing length of the empty pipe. Since the drill string is filled periodically, some jumps in the buoyancy factor trend are observed. An increase in the level of drilling fluid inside the drill string leads to an increase in the buoyancy factor as shown in Figure 6.29.

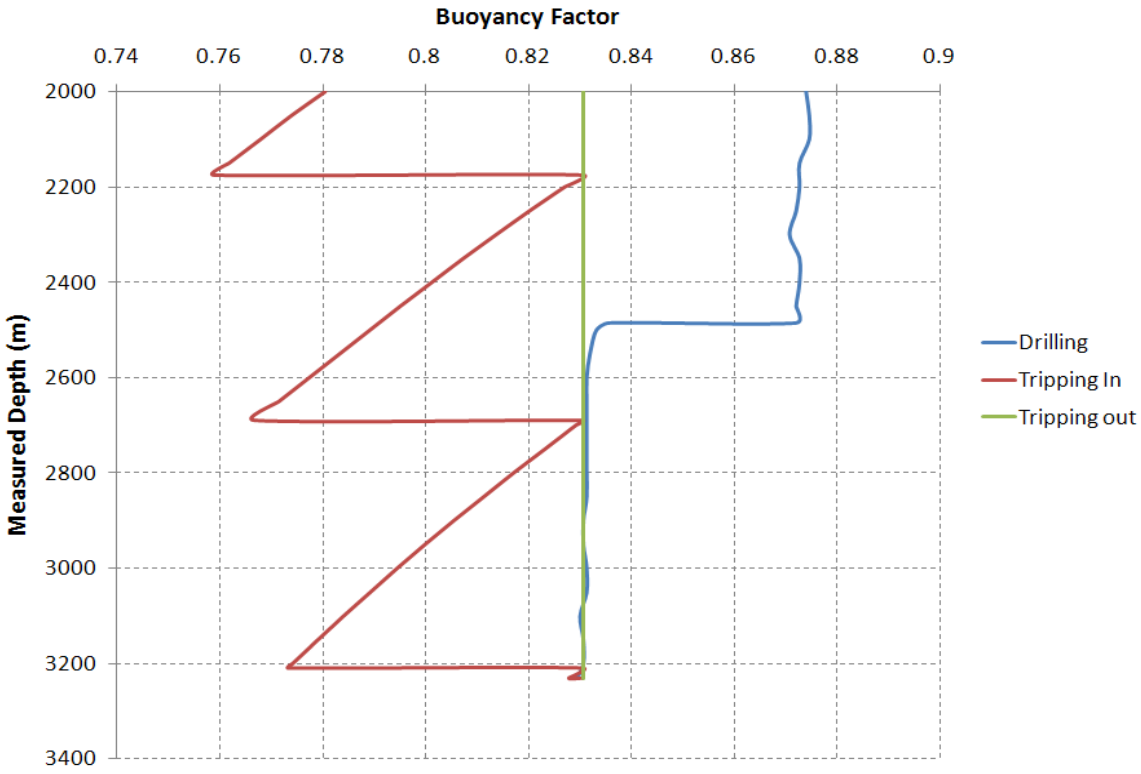

Figure 6.29: Buoyancy factor profile during different operations

The above mentioned increase in mud weight due to gas influx results in a down hole pressure rise (see Figure 6.30). This increase in the mud weight enhances the differential pressure between the drill string spots which temporarily and instantaneously stick to the formation and exerts an additional force on the pipe. Although the increase in mud weight decreases the normal force on the drill string due to a change in the buoyancy factor, the excess differential pressure has an effect with a larger magnitude, which in turn increases the frictional force in those spots. For example, in any pipe sticking problem, the first remedial action is reduction in mud weight in order to decrease the differential pressure between the drill string and the formation. In most cases, this reduction may help to release the drill string from the stuck point.

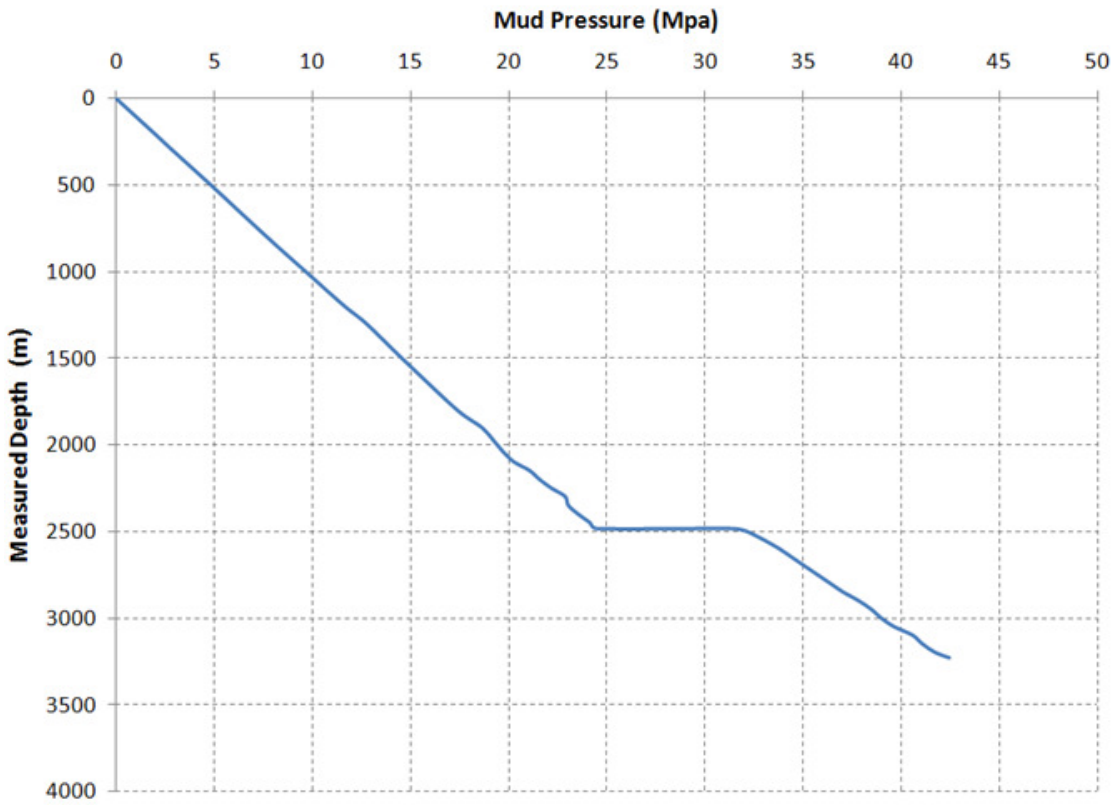

Figure 6.30: Mud pressure gradient versus measured depth during drilling operation

Figure 6.31 compares the hook load recorded during tripping in and out. These data are used to do the friction analysis for this case study. The periodical shifts in hook load values during tripping in are due to the increased buoyancy factor as the fluid fills the drill string. These jumps are not observed during tripping out because the buoyancy factor is almost constant due to filling the annulus using the fill-up lines. A deviation from the hook load trend is observed as the build-up section begins at the depth of 2287 m due to the increase in friction force in the build-up section.

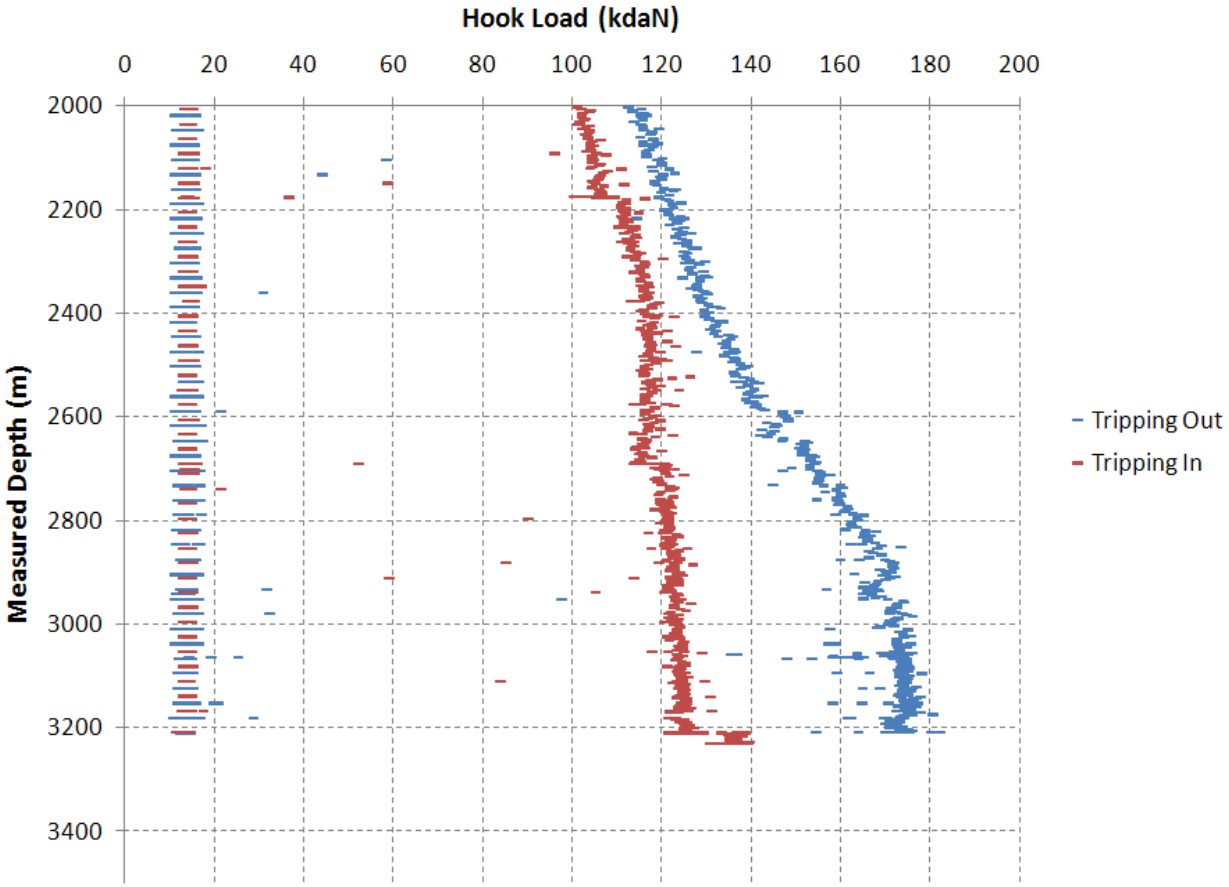

Figure 6.31: Hook load data versus measured depth during tripping in and out

Figure 6.32 presents the frictional force during the tripping out process. The friction force is calculated from the difference between the static weight of drill string and the hook load value. The friction in the curved section is tension dominated showing a rapid increase in the friction force. As the top of the BHA reaches the build-up section, an increase in the frictional force occurs at around 2900 m. As the BHA passes through the buildup section, the friction force declines.

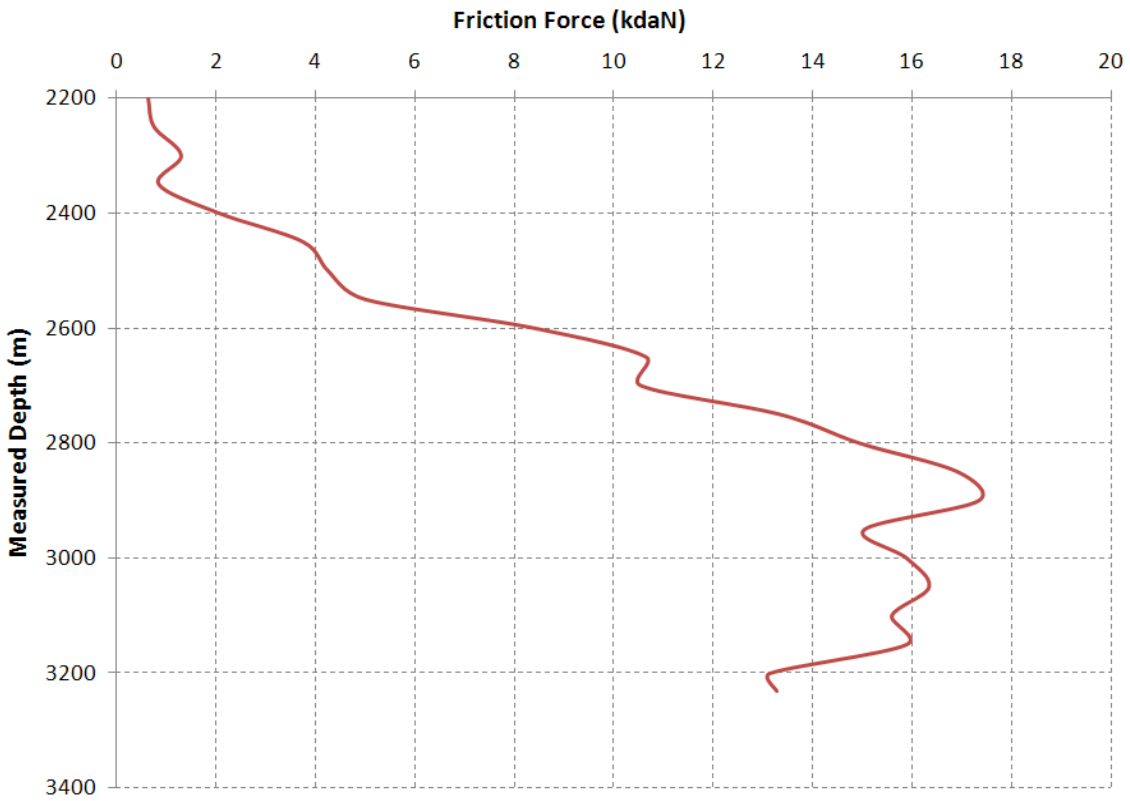

Figure 6.32: Friction force versus measured depth during tripping out

The same effect is observed in Figure 6.33 for the overall friction coefficient. The overall friction coefficient is defined as a single friction coefficient for the entire wellbore. Here, the change in friction coefficient is the effect of contact surface between the borehole and BHA. This effect vanishes gradually as the BHA passes through the build-up section.

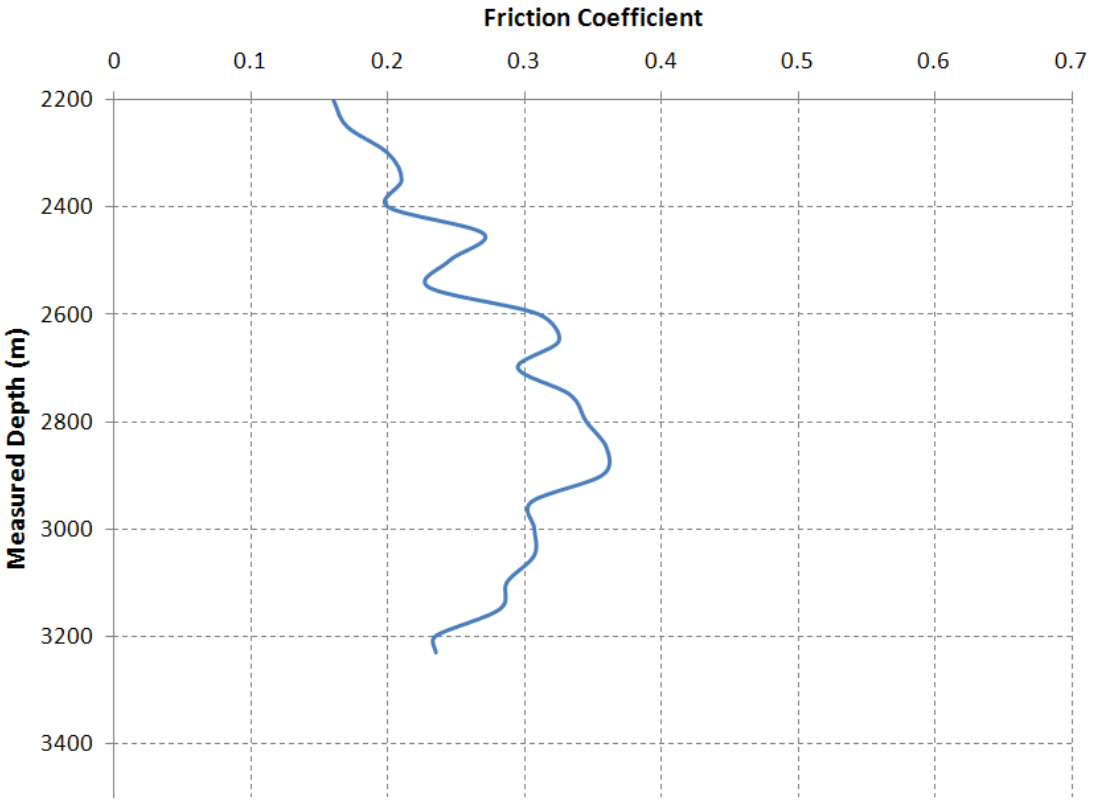

Figure 6.33: Overall friction coefficient versus measured depth during tripping out

The question that arises here is: why should the friction coefficient be calculated for the friction analysis? To be more precise, is friction coefficient required in addition to the friction force for this kind of analysis? The answer lies, in that, in some cases the friction force increases due to the change in well geometry (e.g., increase in dogleg angle). Using a wellbore friction model helps to isolate the effect of increased friction coefficient from the wellbore geometry effect.

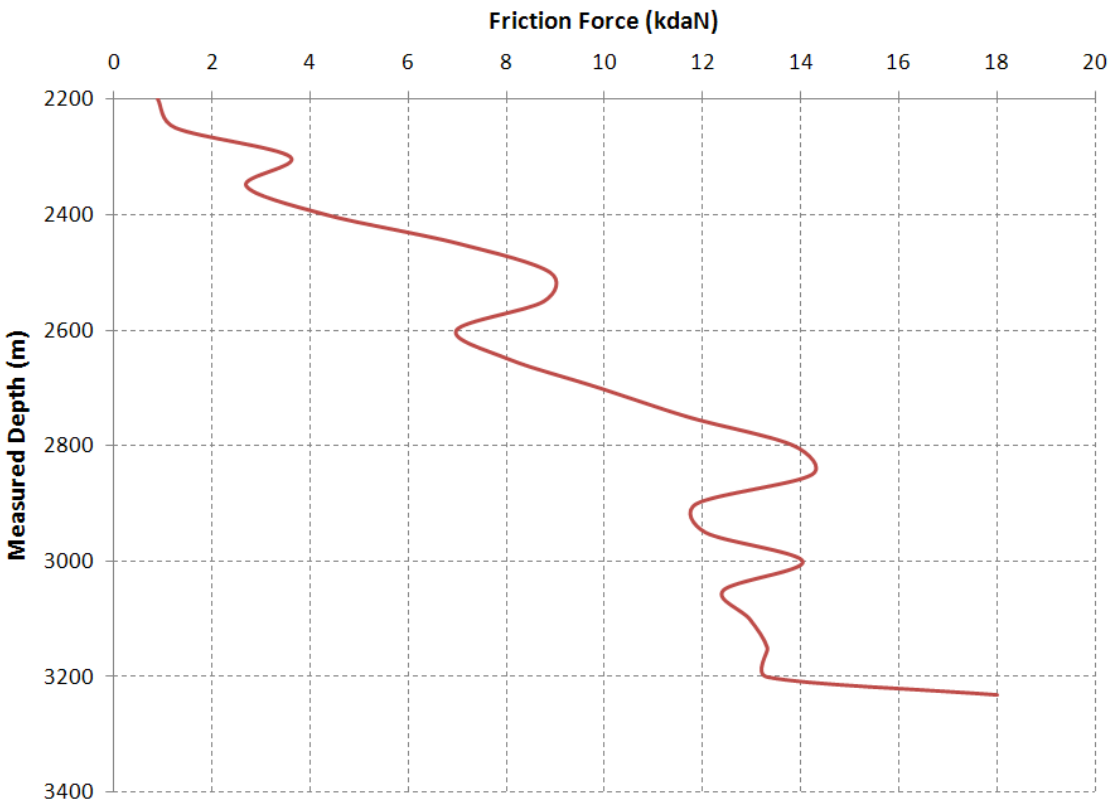

Figure 6.34: Friction force versus the measured depth during tripping in

For tripping in, the estimated friction force (Figure 6.34) and overall friction coefficient (Figure 6.35) show a significant increase as tight hole takes place during the tripping in process. Based on these two parameters, one could possibly detect the onset of pipe stuck in a well. Figures 6.32 and 6.33 do not render sufficient information in the case of occurrence of tight hole. The calculated overall friction coefficient during the tripping in process can be applied as an efficient means to detect the occurrence of a possible tight hole. A rapid increase in friction force is observed whereas the well geometry is straight inclined. One possible reason why this phenomenon is not observed during the tripping out period is because the collapse and tight hole occurred as a result of lower equivalent circulating density. Lower equivalent circulating density normally occurs due to swabbing, which occurs as a result of tripping out.

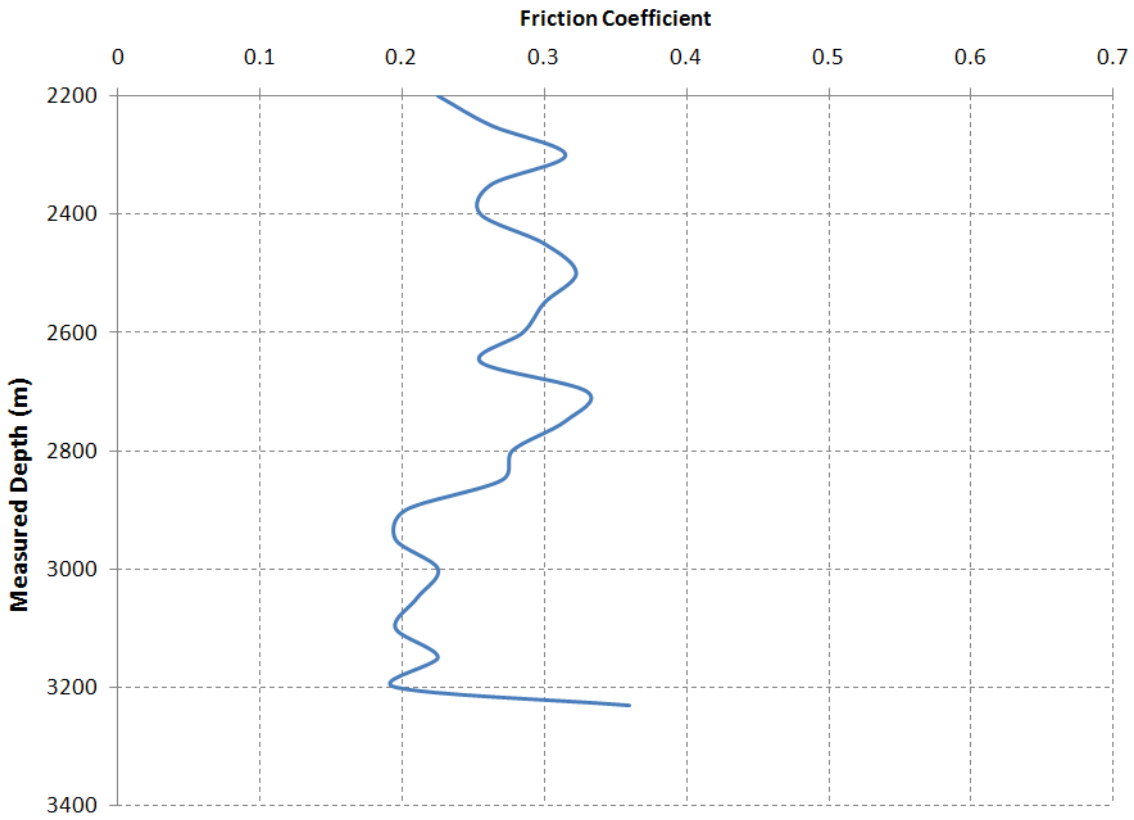

Figure 6.35: Overall friction coefficient versus measured depth during tripping in

6.4 Three Dimensional Well-Finite Element Modeling

In this section, the extended reach well in Section 6.2 is investigated by using the finite element model. Figure 6.36 shows a comparison between the hook load data for field and finite element modeling with a friction coefficient of 0.2. In this case study, the model approximately matches the field data at the bottom hump whereas the top hump is not seen in the model. As it was previously discussed (Section 6.2), this behavior is attributed to the cuttings accumulation (due to the upward dragging of the drill string) and the contact surface effect between the BHA and the wellbore. This case study verifies the analytical model developed in this research. The soft string analytical model illustrates that the discrepancies between the field and modeling data is not related to the stiffness of drill string at all. Instead, it may be related to the wellbore condition, being non-uniform during tripping out.

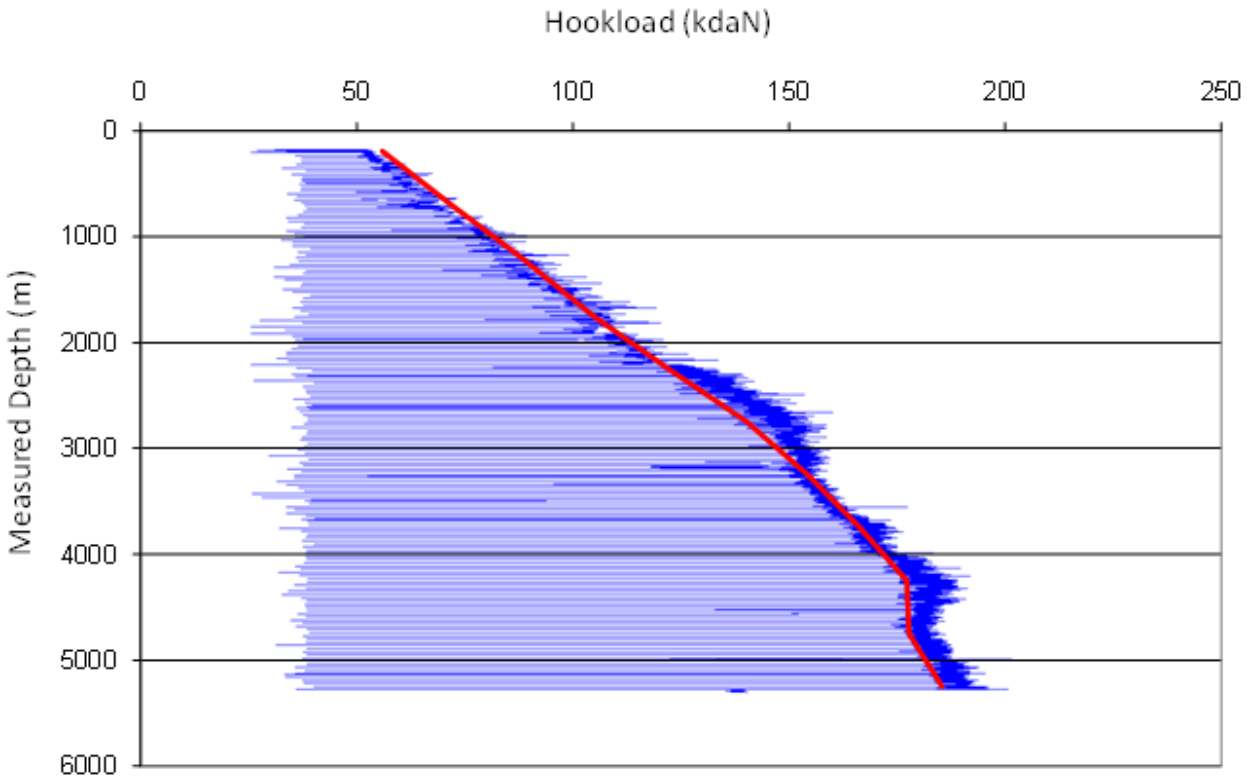

Figure 6.36: Comparison between the field and finite element hook load data using a friction coefficient of 0.2 during tripping out

For tripping in, the buoyancy profile is included during torque and drag calculations using the finite element model. A good match is observed between the field and modeling data. For the last 350 meters, the drill string was run in the well with rotation. This has a significant effect on the axial friction force. The rotation decreases the axial friction force considerably while it increases the hook load value. In this part, the friction coefficient already includes the effect of drill string rotation. Drill string rotation causes a much smaller friction coefficient then 0.20.

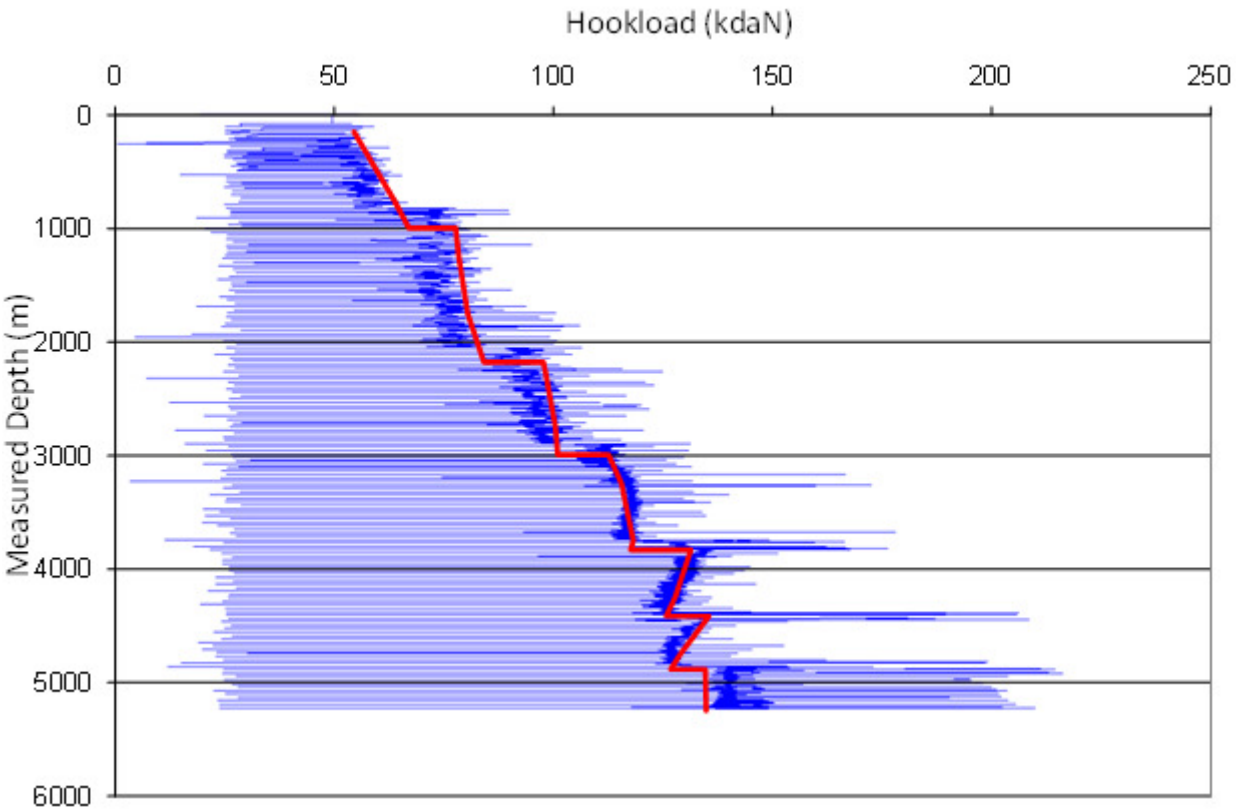

Figure 6.37: Comparison between the field and finite element hook load data using friction coefficient of 0.2 during tripping in

For the torque analysis, the data for the two dimensional well in Section 6.1 was selected. For a friction coefficient of 0.2, the modeling data lay in the middle of field data points (Figure 6.38). The field data are for both reaming and back reaming operations and the finite element modeling data is for the pure rotation without axial movement. For reaming or back reaming operations, the data trend moves to the right and left, respectively. The latter indicates the effect of combined motion and decomposing the friction force into rotational and axial components. The fluctuation of surface torque is considerably more sensitive than that of the hook load. The fluctuations in surface torque are due to stick slip of some part of the drill string (e.g., stabilizers) during pipe rotation and bit torques.

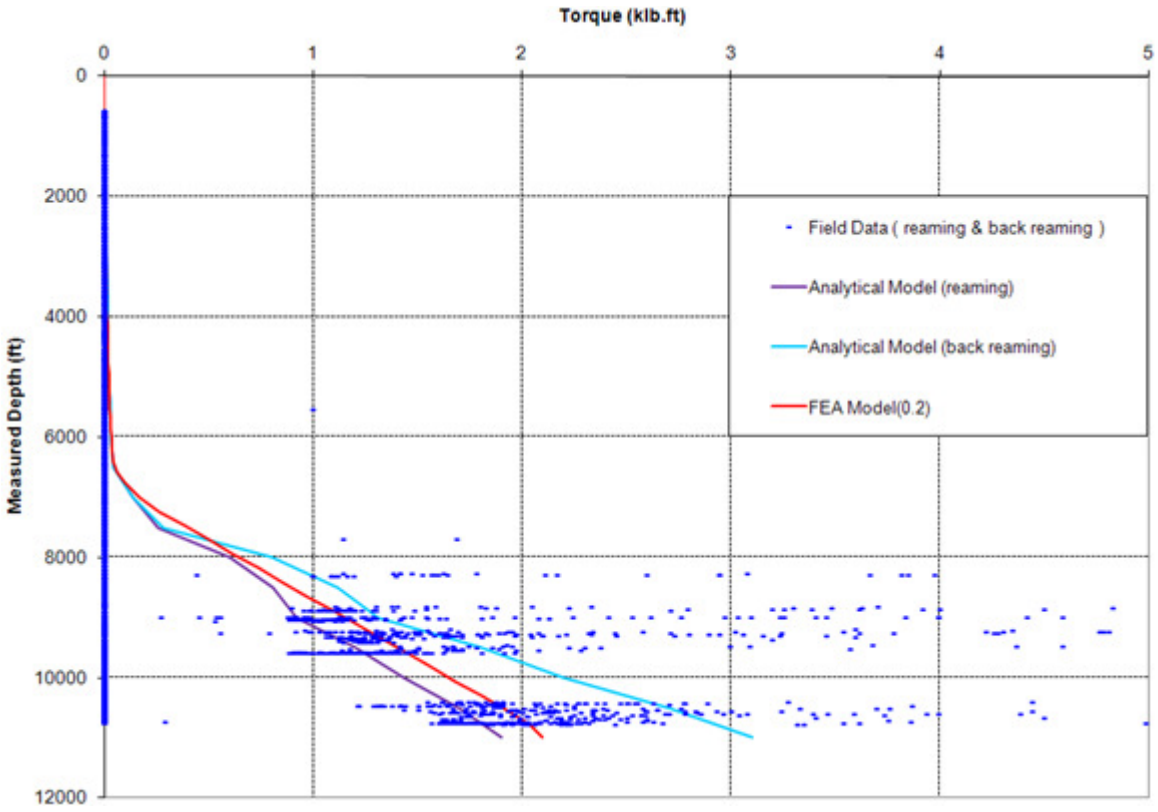

Figure 6.38: The calculated torque versus measured depth

For the third example, a drilled well in western Canada is selected (Figure 6.39). The well geometry includes two build-up sections, straight and horizontal sections. The total measured depth is 3711 m and the length of horizontal departure is almost 1000 m. For drilling the horizontal well, the hydraulic agitator was added to the drill string to reduce the axial friction (drag) resulting in sufficient WOB transfer and push pipe was added in the vertical and first build-up sections. For this well, the hook load data for drilling and tripping out are selected for torque and drag analysis using the finite element method.

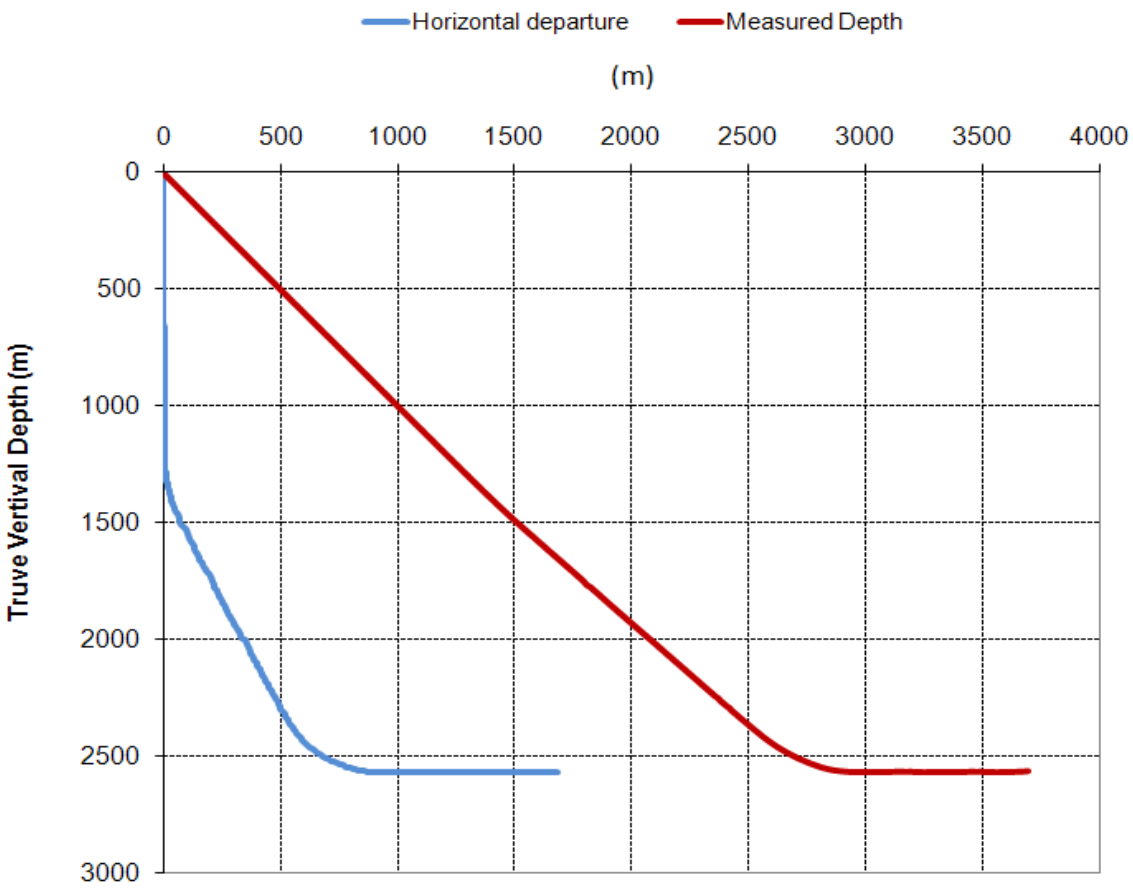

Figure 6.39: Geometry of a drilled well including vertical, build-up, straight inclined and horizontal sections

Figure 6.40 shows the hook load data during drilling. The hook load data usually has high fluctuations due to variations in weight on bit and drag forces, especially for the horizontal sections. Using the agitator from the depth of 2800 m causes a smooth transformation of the applied weight on the bit, which results in obtaining a smoother hook load data trend. A good match is observed between the field and finite element modeling data. It is worth noting that the effect of rpm is seen during hook load calculations using the finite element method. The pipe rotation (i.e., rpm) usually changes during drilling operation from sliding to high surface rotation.

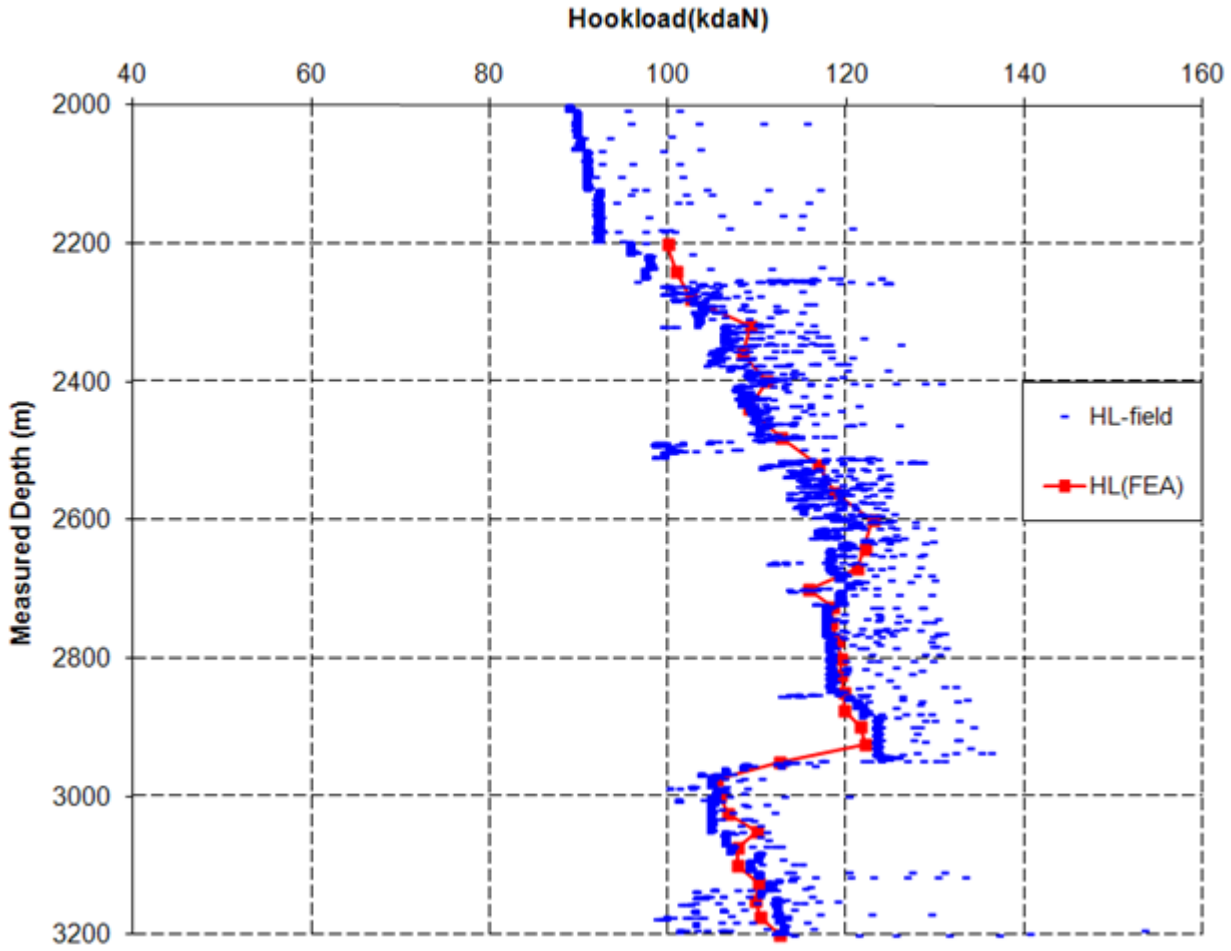

Figure 6.40: Comparison between hook load data of field and finite element modeling data during drilling

Figure 6.41 compares both analytical and finite element modeling results with tripping out data for the current well. The tripping out data related to the horizontal section has been selected for this analysis. The friction coefficient is taken as 0.2 for this analysis. The finite element results follow the field data trend better than the analytical. It is observed that the analytical result is over predicting due to full contact assumption (soft string) between drill string and the wellbore. In finite element modeling, considering the effect of stiffness helps to improve the match between the modeling and field data.

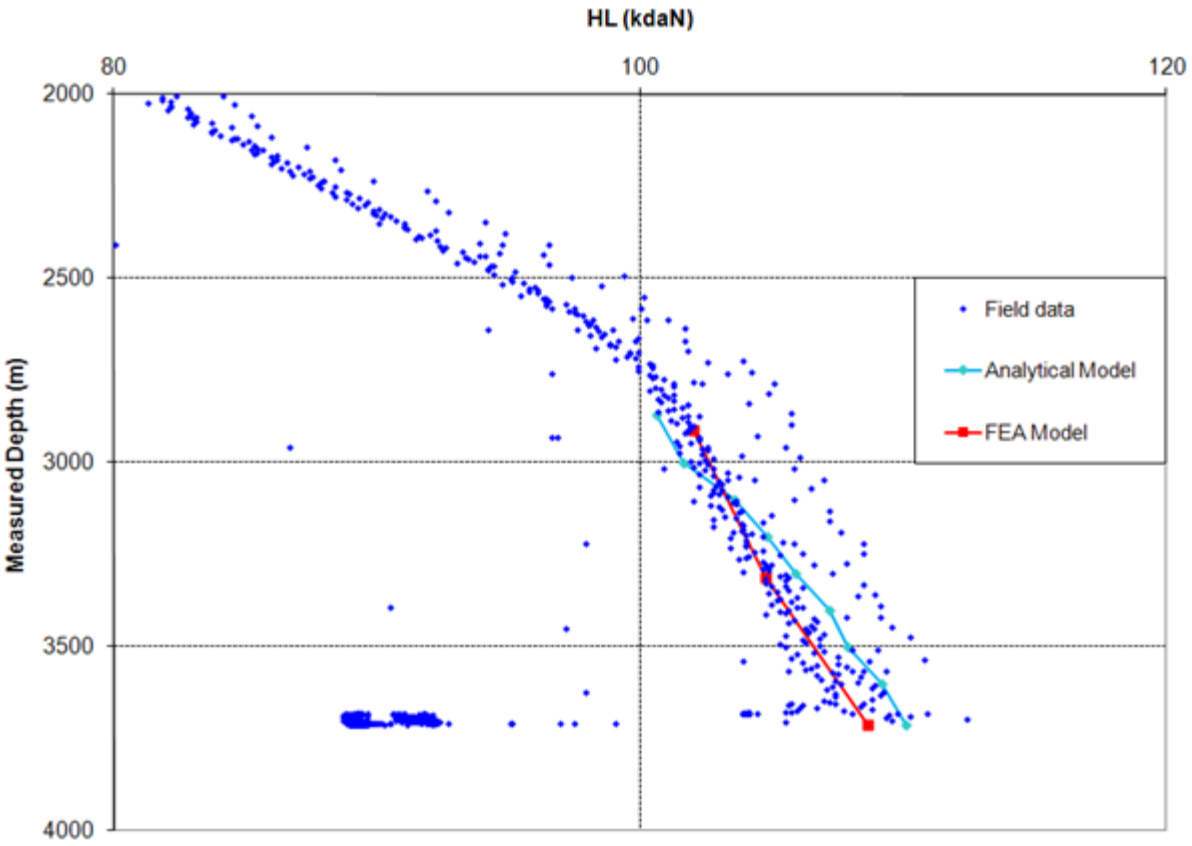

Figure 6.41: Comparison between analytical and finite element modeling result with field tripping out data

6.5 Estimation of Downhole WOB and Bit Torque

The axial and rotational friction force against drill string movement and rotation cause the difference between surface and downhole WOB and bit torque. The friction force is a function of the normal force which relates to the contact surface area and friction coefficient. As it was discussed previously, the normal force is the function of drill string unit weight, well geometry, tension and compression along drill string and the value of the weight on the bit which are changing during drilling operations. Also, friction coefficient is changing during drilling operation due to changes in drillpipe rotation, wellbore conditioning such as reaming and back reaming, hole cleaning, running casing, etc. The new developed method provides an automatic self-calibration system to predict both axial and rotational friction coefficients from the surface measurements such as hook load and surface torque while the bit is off bottom. The friction

coefficients are used to calculate the friction forces between drill string and the wellbore while the bit is on bottom during the drilling operation to estimate downhole weight on the bit and bit torque. The calculations can involve any torque and drag model using either analytical or finite element approaches.

This new method can be used for an autodriller system in directional drilling. More particularly, the autodriller system can estimate downhole weight on the bit and bit torque, from surface hook load and torque measurements during the drilling operation. Knowing downhole weight on the bit and bit torque, without running downhole measurement tools, will reduce the cost of drilling operations significantly.

6.5.1 Background

In the drilling industry, in the absence of downhole measurements, the hook load and surface torque measurements are used to calculate weight on the bit and the bit torque. Figure 6.42 shows the schematic diagram of a drilling rig. The drilling rig includes a derrick, drill string, hoisting system, rotating system, circulating system and power system. The derrick supports the hoisting system and rotating system which is operated by the power system. A drill string includes a series of drill pipe joints which are connected downwardly from surface into the borehole. A drilling bit is attached to the end of drill string. The rotating system may include the rotary table or top drive (not shown) to rotate drill string at the surface to rotate the drilling bit at the bottom. The hoisting system includes drawworks and a block and tackle system. The drawworks control the weight on the drilling bit during drilling operations and raise and lower drill string through the wellbore. The block and tackle system is comprised of crown block, travelling block and drilling line. If the number of drilling lines in the block and tackle system increases, the tension in drilling lines is decreased to provide the higher load capacity for the hoisting system.

The drilling line that is connected to the drawworks from one end, which is called fast line, and from the other end, which is called the dead line, is connected to the deadline anchor or wheel. To measure the loads applied on the hook by drill string weight and movement through the

wellbore, the hydraulic cell is connected to the deadline to measure the tension in the drilling line.

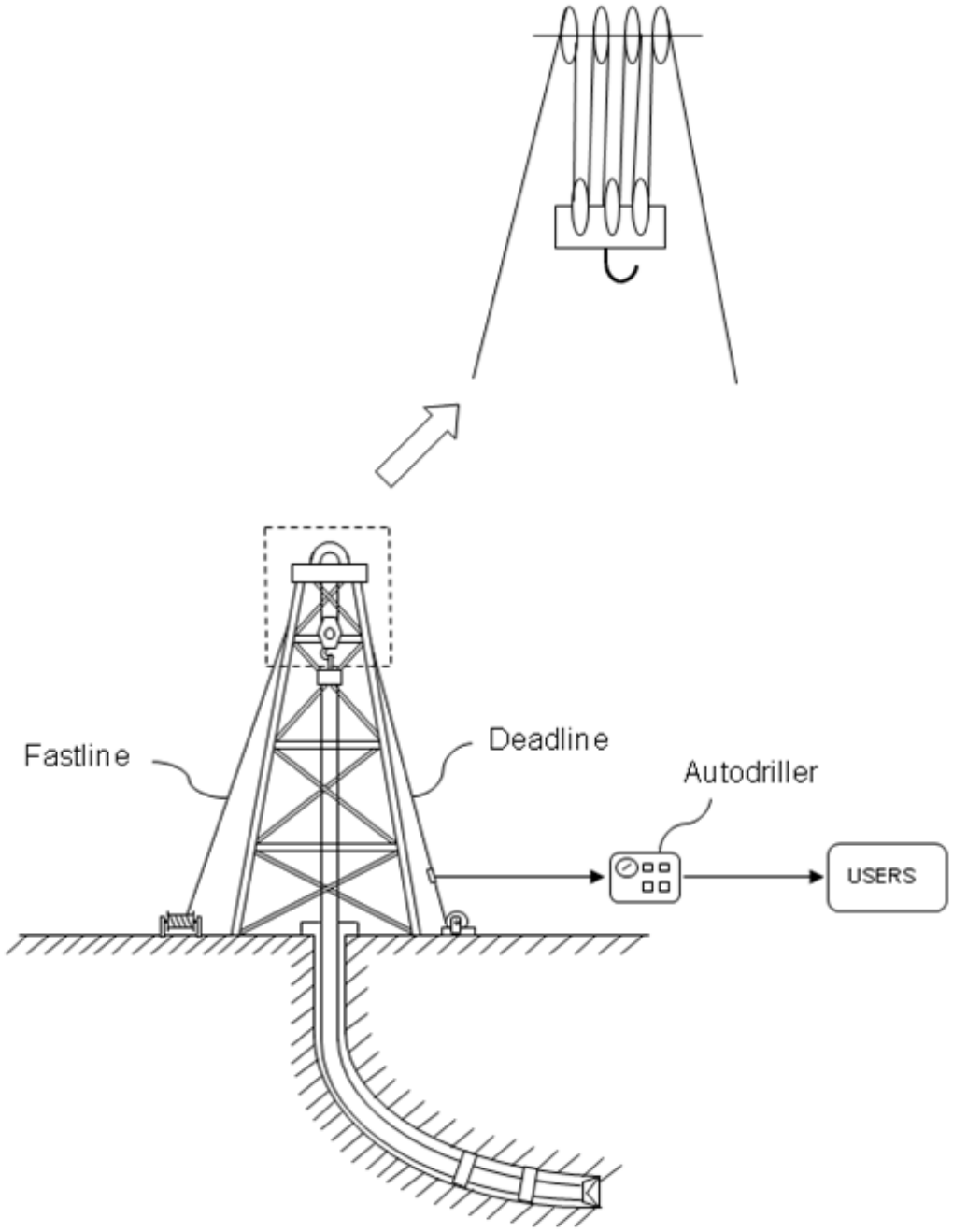

Figure 6.42: Schematic illustration of drilling rig that shows the auto driller system is connected to deadline to estimate downhole weight on the bit

For hook load measurement, the measured tension in the deadline should be multiplied by the number of drilling lines between the sheaves in the block and tackle system. The tension in the deadline is not a true value due to friction between the drilling line and the sheaves. The true value is calculated by considering the friction in the block and tackle system. When some weight of drill string is applied to the drilling bit, a reduction in deadline tension is observed. In the drilling industry, this reduction is considered as surface weight on the bit which is not usually equal to downhole weight on the bit. For downhole weight on the bit estimation, the real time hook load data should be transferred into a new autodriller system for further treatment to obtain the downhole weight on the bit. Also, the new autodriller can calculate the downhole bit torque using surface torque measurements. The real time surface torque should be sent to the autodriller system for downhole bit torque calculation. After calculating downhole weight on the bit and bit torque, they will be available for users for different purposes such as drilling optimization and real-time drilling analysis (see Figure 6.42).

Hook load and surface torque measurement values may include the following components depending on the on and off bottom positions of the drill string.

$$HL = W - Axial\ \ Friction - DWOB \tag{6.1}$$

and

$$Surface\ \ Torque = Rotational\ \ Friction + Bit\ \ Torque \tag{6.2}$$

Where W and $DWOB$ represents the static weight of drill string including buoyancy force and downhole weight on the bit respectively.

To apply weight on the bit, it is required to apply some portion of drill string weight on the bit. The surface calculated weight on bit is based on the difference between the hook load values when the drill string is off and on bottom.

The surface weight on the bit could be a true value, if the well is vertical and the axial friction force between drill string and the wellbore is negligible. When the well deviates from a vertical straight line, the surface and downhole weight on the bit could not be the same due to the axial friction force between drill string and the wellbore. A similar argument is valid for surface bit torque calculations. The bit torque is estimated from the difference between surface torque measurements while the drilling bit is off and on bottom.

The friction force is equal to the friction coefficient multiplied by the normal force which is applied on the contact surface area of the wellbore. The normal force could be the function of buoyed unit weight of drill string components, well geometry and the axial (tension and compression) force along the drill string. For straight sections such as inclined and horizontal sections, the normal force depends on the buoyed unit weight of drill string components and compressive load along the drill string. But in curved sections such as build-up and drop-off, the normal force depends on the buoyed unit weight of the drill string component and the tensile and compressive loads along the drill string in these sections.

During drilling operations, the friction force acts against drill string axial movement and rotation. In this case, when applying some weight on the bit, the tension force on drill string elements located at the curved section will be reduced and friction force will be reduced consequently. If the tensile load turns into compressive load and exceed the helical buckling, an additional friction force will be added for increased normal force due to helical buckling.

For downhole weight on bit estimation, the requirements will be the time based drilling parameters, the static weight of drill string (SWDS), which can be calculated from the vertical projection of drill string at each measured depth as well as a reliable three dimensional friction model to calculate friction forces and coefficients along drill string. All these requirements are programmed and integrated in a real-time controlling system. Downhole weight on bit and bit torque can be updated as long as surface data are being generated.

6.5.2 Vertical Well

Figure 6.43 (a) illustrates, in a schematic way, a drill string in a vertical wellbore with a hook at the top. The drill string is hung from the hook which mostly consists of drillpipe and the lower

end of the drill string called bottom hole assembly that carries a drilling bit. The borehole is being drilled and extends downwardly from the surface. In Figure 6.43 (a), the drilling bit is off bottom and the entire load of drill string applied on the hook. In this condition, the entire drill string will be in tension. The minimum tension is at the drilling bit and maximum tension will be at the surface.

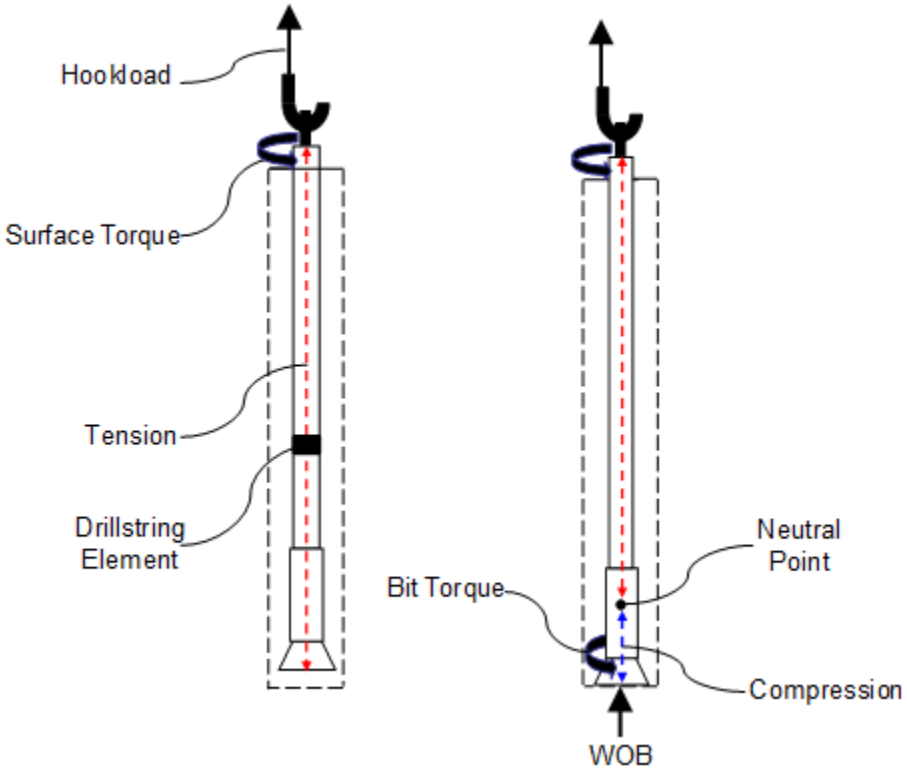

Figure 6.43: Schematic description of drill string moving downwardly in a vertical well while the bit is off and on bottom, respectively.

Also, there is a negligible contact between drill string and the vertical wellbore during drill string rotations. This means that the friction force can be neglected. For a drill string element in a vertical wellbore as shown in Figure 6.43 (a), the tension force balance can be written as follow:

$$F_{top} = F_{bottom} + W \tag{6.3}$$

To calculate the tension at the hook, drill string is divided to *n* number of elements and calculation starts from the drilling bit all the way to the surface. It is noted that in underbalanced drilling, the buoyancy factor is a dynamic parameter, which will vary along the drill string by changing the pressure, temperature, drilling cutting rate, gas influx, etc.

Figure 6.43 (b) shows the drill string in the bottom position. Once some weight of drill string is applied on the drilling bit, some length of drill string compresses beginning from bit to neutral point. At the neutral point, compression switches to tension for the rest of the drill string to the surface. Obviously, the hook load will be smaller once the drill string is on bottom; as much as the weight applied is on drilling bit. In this scenario, the weight on the bit is recorded from the difference between the hook load values when the drill bit is off and on bottom. The calculated surface weight on the bit will be the same as what is applied downhole by neglecting the minor friction in the vertical well. If helical buckling happens in vertical well drilling, it creates some additional friction force that should considered in vertical drilling for downhole weight on bit estimation. The force balance at each element can be written as follow:

$$F_{top} = F_{bottom} + W - \left[Friction_{helical} \quad or \quad 0\right] - DWOB \tag{6.4}$$

When the bit is off bottom, the surface torque value is negligible due to minor contact between drill string and the vertical wellbore. Once the bit goes on bottom for drilling and applies weight on bit, an increase in value of surface torque can be observed due to bit torque. To calculate bit torque from surface measurements, the difference between surface torques while bit is off and on bottom should be calculated.

6.5.3 Extended Reach Well

For extended reach well drilling, Figure 6.44 (a) shows a drill string in a wellbore which consist of vertical, build-up and straight inclined sections. In the build-up and straight inclined sections, there is contact between drill string and the wellbore which results in a friction force against the pipe movement. The nature of friction in these two sections is different. In this scenario, the bit is off bottom and the entire drill string is in tension. When the axial friction force calculations start from the drilling bit and upward, in the straight inclined section the tension will not have any contribution in axial friction force. But as the build-up sections begin, the tension at this point will have a great contribution in the friction force. It means, for a drill string element in the straight incline, the friction force only depends on the weight of element which applies normally on the contact area. But in the build-up section, the friction force mostly depends on the tension at the bottom of the element and also the normal weight of the drill string element.

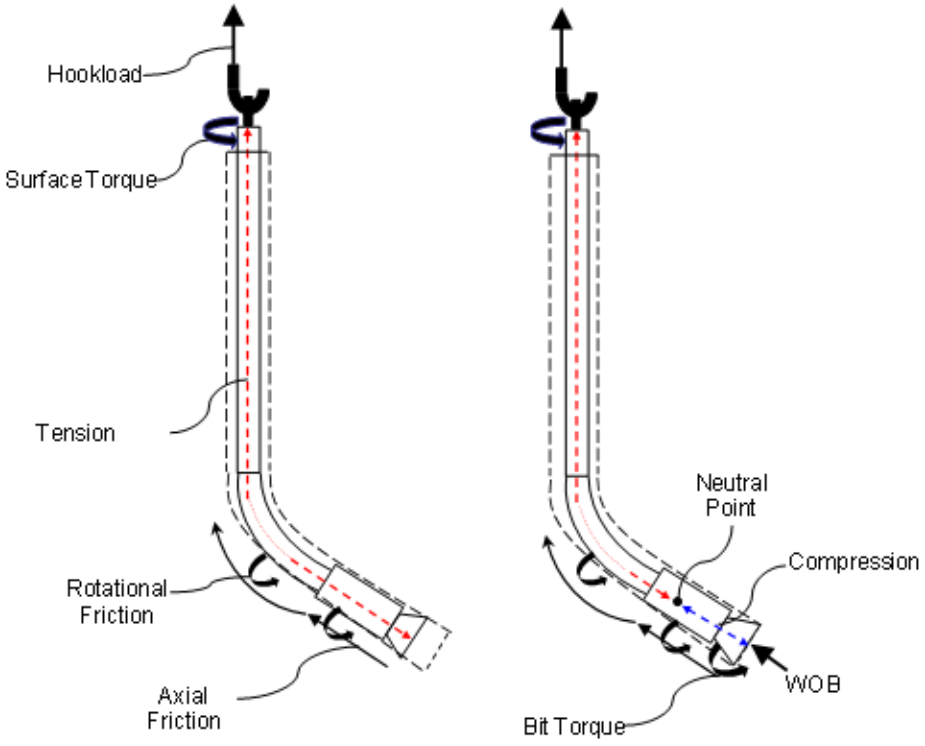

Figure 6.44: Schematic of drill string moving downwardly in a well with the geometry of vertical, build-up and the straight inclined sections

The following is the general force balance for each element along drill string for off bottom position.

$$F_{top} = F_{bottom} + W - Friction_{weight} - \left[Friction_{tension} \quad or \quad 0 \quad or\, Friction_{helical}\right] \tag{6.5}$$

In this equation, the axial friction force term related to tension will be zero if the element is in the straight section. Also, if the pipe element is placed in the vertical section both terms related to friction will vanish.

In Figure 6.44 (b), some weight of drill string applies to the drill bit which means reduction in tension along the drill string. The reduction in tension has considerable effect on the axial friction force in the build-up section but not straight inclined. If applying the weight on the bit causes the drill string to be in compression in the curved section, the axial friction force for that part will not be a function of the tension anymore and it should be treated the same as straight inclined elements. The Equation 6.6 represents the force balance when applying weight on the bit.

$$F_{top} = F_{bottom} + W - Friction_{weight} - \left\lfloor Friction_{tension\ DWOB} \quad or \quad 0 \quad or \quad Friction_{helical} \right\rfloor - DWOB \tag{6.6}$$

In Equation 6.6, the friction force in the curved section is affected by downhole weight on the bit which is subscripted by DWOB. It should be mentioned that the axial friction force changes in the curved section and will change the overall friction and surface hook load value consequently. If the downhole weight on the bit helically buckled the pipe element, then the additional friction should be considered, as discussed in Chapter 5.

The same argument is valid for the surface torque measurements. The rotational friction force between drill string and wellbore depends on the normal weight of drill string element and tension along the drill string. Applying weight on the bit reduces the tension along the drill

string, which affects the value of rotational friction force in the curved section. Equation 6.7 shows the torque for an element in drill string while the bit is off bottom and there is no weight on the bit.

$$Torque_{top} = Torque_{bottom} + Torque_{weight} + [Torque_{tension} \quad or \quad 0 \ ] \tag{6.7}$$

To calculate the surface torque, the drill string is divided into many elements; and calculation starts from the bottom to the surface. Once the element is in a straight inclined section, the torque will be the function of the element weight only. When the element is in the curved section and the drill string is in tension, the torque will depend mostly on tension and less on weight. For surface torque, when the drill string goes on bottom, the tension along drill string will change. The latter affects the value of rotational friction force in the curved section as well. Also, the value of torque on the bit will be added as shown in Equation 6.8. The rotational friction force in the straight inclined section will not change.

$$Torque_{top} = Torque_{bottom_{DWOB}} + Torque_{weight} + [Torque_{tension_{DWOB}} \quad or \quad 0 \quad Torque_{helical}] \tag{6.8}$$

6.5.4 Horizontal Well

Figure 6.45 (a) shows a horizontal well which includes vertical, build-up and horizontal sections. The drill string is off bottom and pushing toward the bottom. The axial friction force is acting against the drill string movement tendency. To push the pipe in the horizontal section, it is necessary to have some heavy drillpipes in the vertical and build-up sections to provide sufficient drive to push the drill string in the horizontal section. The axial friction force in the horizontal section is a function of the weight of drill string, which is normally applied on the wellbore contact area as well as additional friction force due to helical buckling. When the drill bit is off bottom and the drill string is pushing toward the bottom, some part of heavy drillpipe will be in compression due to axial friction force in the horizontal section. In this scenario the axial friction force in the curved section, which is in compression, is a function of the weight of drill

string element and compressive load if it exceeds the helical buckling load. Above the neutral point, the drill string will be in tension and axial friction force will depend on the normal force and tension force for each element. Equation 6.5 can be applied to horizontal well drilling for hook load calculation when the drill bit is off bottom and moving toward the bottom.

When some weight is applied on the bit (as shown in Figure 6.45 (b)), more of the drill string becomes compressed. In this case, usually most of the axial friction force in the build-up section will no longer depend on the tension. Equation 6.6 can be applied for the hook load calculations when the drill bit is on bottom and some weight is applied to the bit.

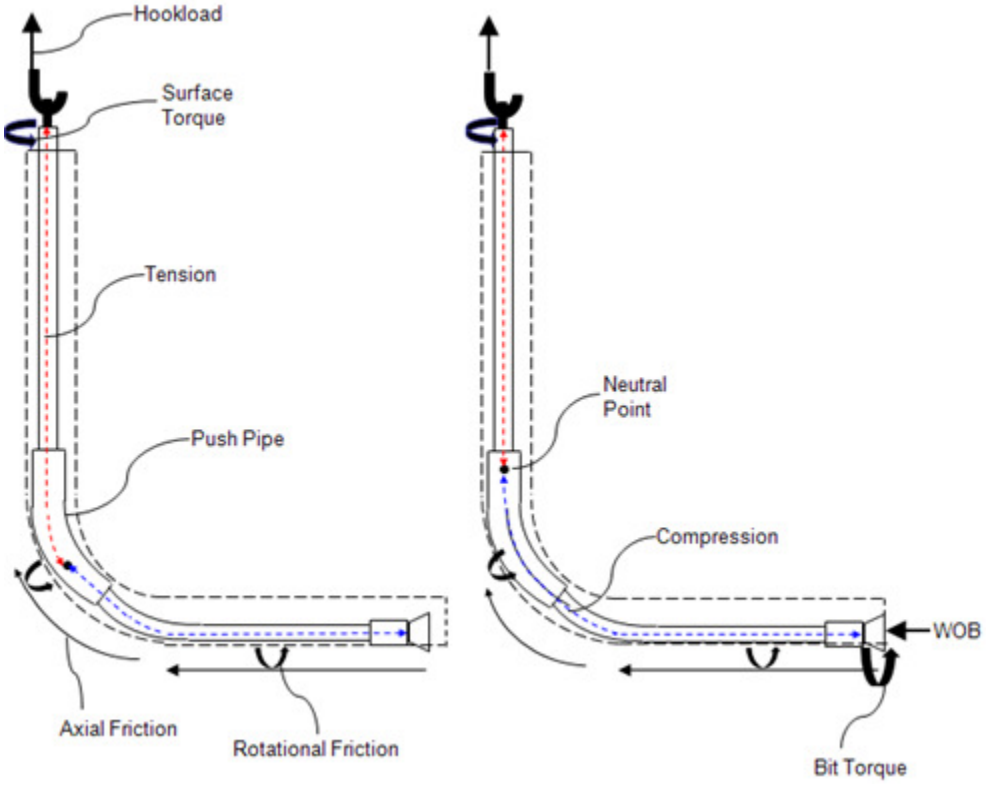

(a) (b)

Figure 6.45: The drill string along a horizontal well which is pushing toward the bottom

In Figure 6.45 (a), once the drill string is off bottom, there is no bit torque. The rotational friction force is related to build-up and horizontal sections. In the horizontal section, the rotational

friction force is the function of normal force, which is applied by the weight of drill string element as well as compressive load if the axial load exceeds the helical buckling load. In the build-up section while the drill string element is in compression, the rotational friction force is the function of weight or maybe the compressive load. However, if drill string is in tension, the rotational friction force is the function of tension and weight. Once the drill bit goes on bottom (see Figure 6.45 (b)), applying weight on drill bit causes some reduction in tension along the drill string, which affects the value of rotational friction force in the build-up section. During the drilling operation, there are some variations in bit torque and rotational friction force in the curved section. These should be estimated from surface torque measurements using the new method presented in this work.

6.5.5 Description of System

Figure 6.46 is a general flowchart showing the steps how to estimate downhole weight on the bit from surface measurements. The first step is determining the static weight of drill string, SWDS.

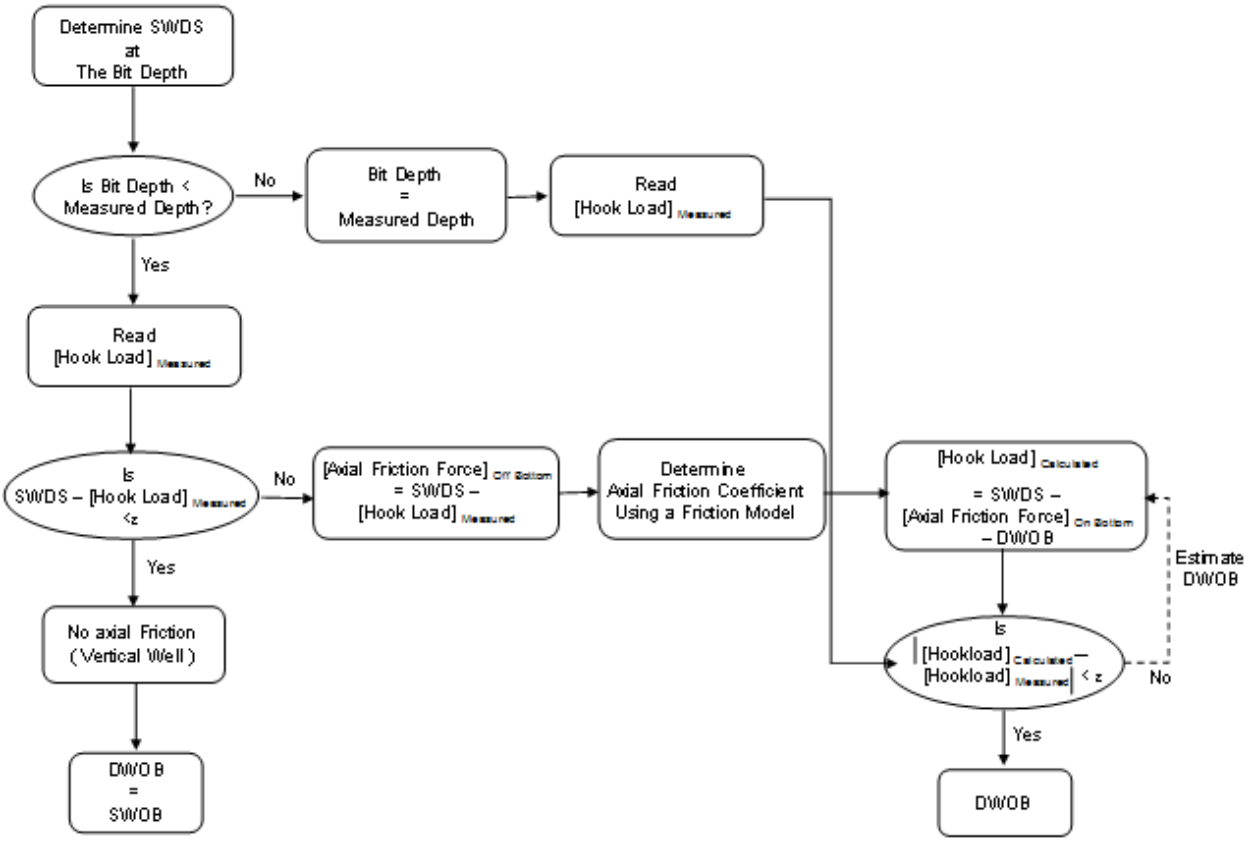

Figure 6.46: The flowchart showing the steps for calculating downhole weight on the bit using the hook load measurements

To calculate the static weight of drill string, the following information is required at any measured depth:

- Survey point data, inclination;
- Drill string components unit weights; and
- Drilling fluid density to calculate the buoyancy factor.

There are standard equations which are used to calculate the static weight of drill string. When the bit is off and then on bottom, a short length will be added to the drill string and the positions of other components will be changed as well. For this reason, it is necessary to recalculate the static weight of the drill string when the drill bit goes on bottom for further drilling. Also, in under-balanced drilling, the drilling fluid density is variable; therefore, the local buoyancy factor should be calculated for each element that is not constant anymore.

The second step is determining if the bit is off or on bottom. During drilling operations, the mud logging unit records all necessary field data. The measured depth and bit depth data will be used to know when the bit is off and on bottom and also if bit is moving upward or downward. The measured depth corresponds to final drilled depth. When the bit is off bottom and the drill string is moving downward, the measured hook load should be compared with the static weight of drill string. If the difference between values is negligible, it means there is no axial friction force and the well geometry is vertical. When the bit goes on bottom, some weight of drill string applies to the bit and a reduction in the hook load will be observed. The reduction in the hook load is taken as downhole weight on bit. Therefore, the downhole weight on bit can be calculated directly from the surface hook load measurements for a vertical well when the drill bit is off and on bottom.

If the difference between measured hook load and the static weight of drill string is not negligible, the difference between these two values provides the axial friction force between the drill string and the wellbore. It is critical to select the best measured hook load value while the bit is off bottom because the axial friction coefficient is estimated based on it. The estimated axial friction coefficient will be used for estimating the downhole weight on the bit when the well is deviated and there is considerable axial friction force between drill string and the wellbore. Therefore the following conditions are considered to select the best measured hook load value while the bit is off bottom:

- The hook load is chosen when the bit is moving downwardly very close to bottom hole. In this situation, the drill string movement is very slow similar to the on-bottom situations where the drill bit is penetrating a formation.
- The drill string rotation speed and flow rate are the same as planned ones while the bit goes on bottom for further penetration. The effect of pipe rotation is included in axial friction coefficient.

By knowing the axial friction force and having a reliable friction model, the axial friction coefficient (which includes the drill string rotation effect) will be estimated. This axial friction coefficient will be used for the estimation of downhole weight on the bit when the bit goes on bottom for further drilling.

When the bit depth and the measured depth are equal it means the bit is on bottom. In this situation, the measured hook load is known and the hook load could be calculated as well. To calculate the hook load, the static weight of drill string, axial friction force and downhole weight on the bit should be known. As discussed, the static weight of drill string is obtained directly from the aforementioned standard equations. The downhole weight on the bit is estimated and the axial friction force will be calculated based on estimated downhole weight on the bit. Here, to obtain the best value for downhole weight on the bit, some value should be estimated close to surface weight on the bit and applied to the friction model to see its effect on the value of axial friction force. If the difference between measured and calculated hook load is negligible then the value is taken as true, otherwise another value is chosen and the calculation is repeated.. This loop will be continued until the difference between the calculated and measured hook load values become negligible.

Figure 6.47 is a general flowchart showing the steps to estimate the bit torque when rotating from the surface. The procedure is similar to downhole weight on the bit. The estimated downhole weight on the bit in the previous section is used for downhole bit torque calculation. In the first step, the bit depth should be compared with measured depth to see if the drilling bit is on bottom or off bottom. When the drill bit is off bottom and the value of the measured surface torque is negligible, it means the drilling well is vertical and there is negligible rotational friction force. When the drill bit goes on bottom for further drilling, the measured surface torque almost corresponds to downhole bit torque. If the measured surface torque is not negligible while the bit is off bottom, it means the well is not vertical and there is rotational friction force against the drill string rotation. As discussed before, the best selected data for friction coefficient estimation is when the bit is off bottom and is moving downwardly close to the bottom with the same pipe rotation as planned for drilling. From the rotational friction force while bit is off bottom and using a reliable friction model, the rotational friction coefficient could be estimated for the next steps.

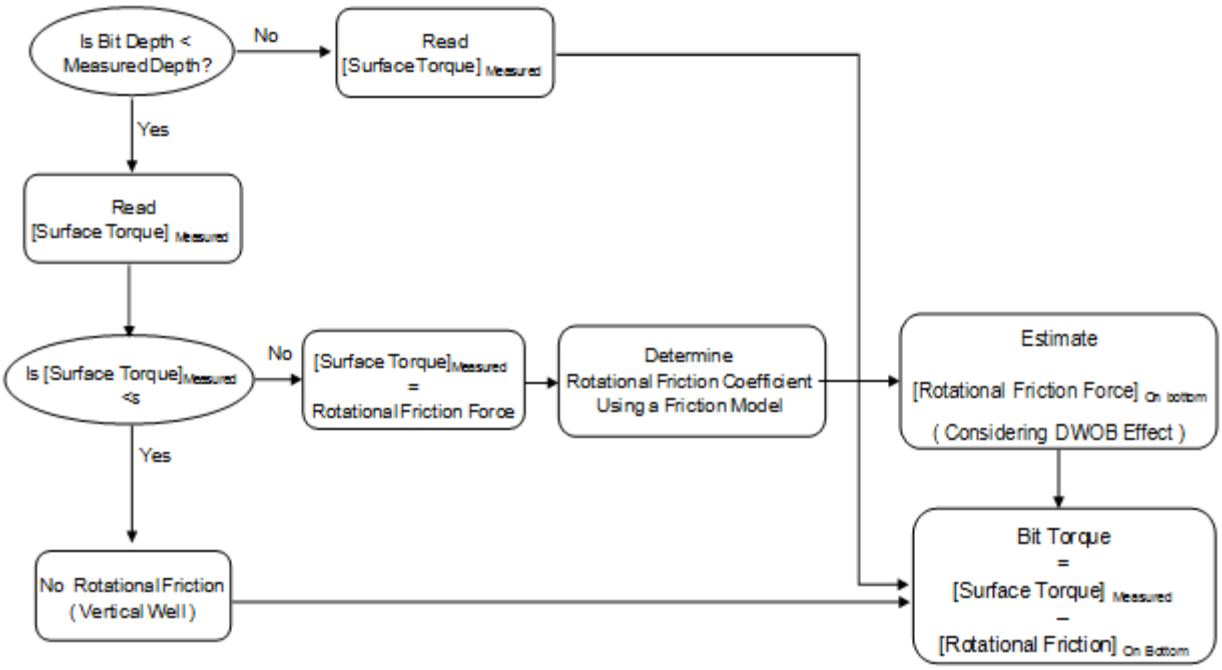

Figure 6.47: The flowchart showing the steps for the calculation of downhole bit torque by using the surface torque measurements

When the bit goes on bottom for further drilling, the measured surface torque can be read. The downhole weight on bit will affect the rotational friction force due to changes in tension along the drill string. Using the downhole weight on bit and the rotational friction coefficient in a reliable friction model yields the rotational friction force during drilling operation which changes with the changes in downhole weight on the bit. The final step is calculating the downhole bit torque due to surface rotation by subtracting the rotational friction force from surface torque measurements.

6.5.6 Example Application

To show the application of this method, a newly developed analytical friction model is used to see how the downhole weight on bit and bit torque can be calculated during drilling operations. When drill string specification, survey data and friction coefficient are specified, the calculation begins at the bottom of the drill string and continues stepwise upwardly. Each drill string element

contributes small load on hook load and surface torque. The force and torque balance on drill string element when the bit is off bottom can be written as follow:

$$F_{top} = \beta w \Delta L \left(\cos\alpha \quad or \quad \frac{\sin\alpha_{top} - \sin\alpha_{bottom}}{\alpha_{top} - \alpha_{bottom}} \right) - \mu \times \beta w \Delta L \left(\sin\alpha \quad or \quad \frac{\cos\alpha_{top} - \cos\alpha_{bottom}}{\alpha_{top} - \alpha_{bottom}} \right) \quad (6.9)$$
$$+ \left(F_{bottom} \quad or \quad F_{bottom} \times e^{-\mu|\theta|} \quad - Friction_{helical} \right)$$

For the torque at each element:

$$T_{top} = T_{bottom} + \mu \times r \times \beta w \Delta L \times \left(\sin\alpha \quad or \quad \frac{\cos\alpha_{top} - \cos\alpha_{bottom}}{\alpha_{top} - \alpha_{bottom}} \right) + \left(0 \quad or \quad \mu \times r \times F_{bottom} \times |\theta| \right) \quad (6.10)$$

and when the bit is on bottom, there is some weight on the bit which affects tension along drill string:

$$F_{top} = \beta w \Delta L \left(\cos\alpha \quad or \quad \frac{\sin\alpha_{top} - \sin\alpha_{bottom}}{\alpha_{top} - \alpha_{bottom}} \right) - \mu \times \beta w \Delta L \left(\sin\alpha \quad or \quad \frac{\cos\alpha_{top} - \cos\alpha_{bottom}}{\alpha_{top} - \alpha_{bottom}} \right) \quad (6.11)$$
$$+ \left(F_{bottom} - DWOB \quad or \quad [F_{bottom} - DWOB] \times e^{-\mu|\theta|} - Friction_{helical_{DWOB}} \right)$$

For the torque at each element:

$$T_{top} = T_{bottom\ _{DWOB}} + \mu \times \beta w \Delta L \left(\sin\alpha \quad or \quad \frac{\cos\alpha_{top} - \cos\alpha_{bottom}}{\alpha_{top} - \alpha_{bottom}} \right) + \quad (6.12)$$
$$\left(0 \quad or \quad \mu \times r \times [F_{bottom} - DWOB] \times |\theta| \right)$$

In Equations 6.9 and 6.11, the terms in order for a drill string element correspond to static weight, the axial friction force caused by the weight and axial friction force caused by the

tension and compression at the bottom. In the equations, if the inclination at the top and bottom of an element is equal, the element is considered as straight and the first term in each bracket will be used, otherwise it will be considered as a curved element and the second term will be used. When weight is applied on the bit, the effect of downhole weight on the bit can be integrated as shown in Equation 6.11, which reduces the tension along the drill string and reduces the axial friction force in the curved section. If any curved element is in compression, the effect of tension on the axial friction force will be eliminated. For friction term related to helical buckling, if the compressive load exceeds the helical limit, the equations presented in Chapter 5 should be used.

Furthermore, for bit torque calculation, it is necessary to calculate the rotational friction force from drill bit to the surface. Equation 6.10 is used to calculate the rotational friction force for each element while the drill bit is off bottom. The first term in each bracket is used when the elements are located in straight sections and the second term is used for the elements which are placed in curved sections. It should be noted that when the element is compressed in the curved section, the rotational friction force will only be a function of the weight of the element. When the drill string goes on bottom, the downhole weight on the bit causes the reduction in tension along drill string, which significantly reduces the rotational friction force.

A drilled well has been selected as shown in Figure 6.39 to illustrate how an autodriller can estimate the downhole weight on the bit and bit torque. The well geometry includes two build-up sections, straight and horizontal sections.

When the drill bit is at the depth 2700 m, the entire drill string was is in tension. Applying 11 kdaN weight on the bit causes some portion of the drill string starting at the bit to compress and reduce the tensile force for the rest, as shown in Figure 6.48.

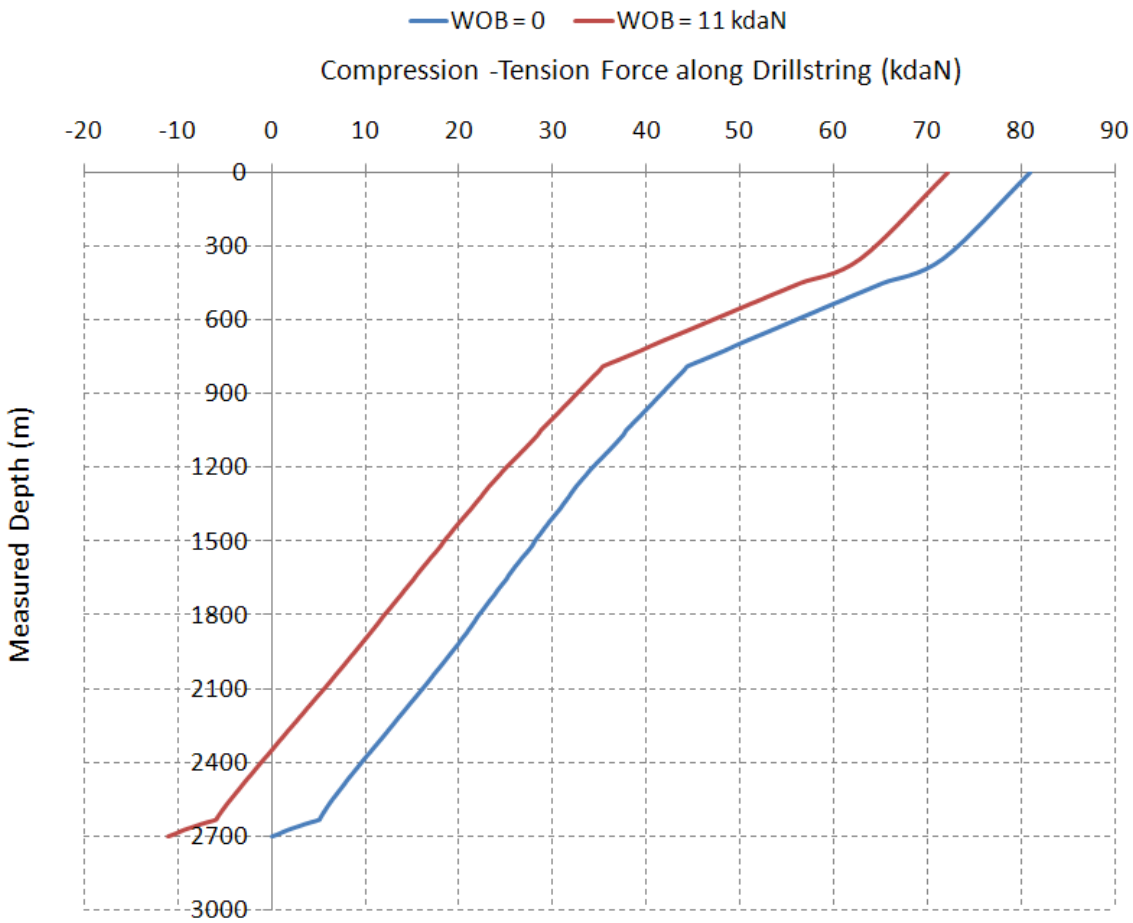

Figure 6.48: Comparison between tension and compression along drill string when 11kdan weight is applied on the bit

Figure 6.49 illustrates that the reduction in tension along the drill string has an effect on the friction force (2.15 kdaN). In the example, the downhole weight on the bit merely affects the friction force in the build-up sections. As discussed before, the weight on the bit reduces the friction force in the curved sections, which affect the axial and rotational friction force.

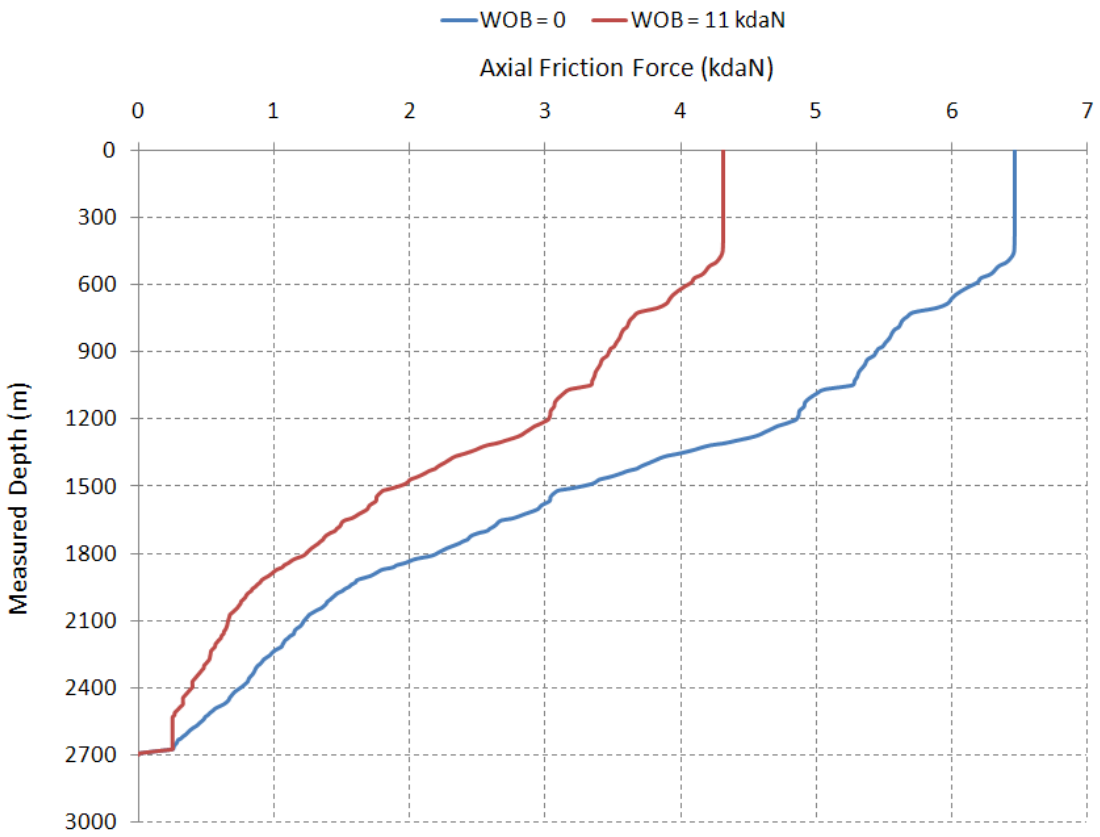

Figure 6.49 shows reduction in axial friction force along drill string when 11 kdaN weight is applied on the bit.

The sample calculation for this example is as follow:

When the bit is at the depth 2695.6 m, almost 0.4 m off bottom and moving downwardly, the axial friction coefficient including the pipe rotation effect, is estimated as follow:

$$Static\ Weight\ of\ Drill\ String = 874.4\ \ kN$$

$$Bit\ \ Depth = 2694.6\ \ m$$

$$Measured\ \ Depth = 2696.02\ \ m$$

$$Bit\ \ Depth \le Measured\ \ Depth \rightarrow \left[Hook\ \ Load_{Off}\right]_{Mesaured} = 810.2\ \ kN$$

$$\left[Axial\ Friction Force\right]_{Off\ Bottom} = 874.4 - 810.2 = 64.4\ \ kN \xrightarrow{Using\ \ Friction Model} \mu_{axial} = 0.095\ \left(\ pipe\ rotation included\right)$$

The axial friction coefficient including the pipe rotation effect is used when the drill string goes on bottom for drilling. The axial friction coefficient can be updated for each wiper trip (or in some cases connections) periodically and used for upcoming sections. The estimated axial friction coefficient is used in a friction model to calculate the hook load.

$$Bit\ \ Depth = 2696.02\ \ m$$
$$Measured\ \ Depth = 2696.02\ \ m$$
$$Bit\ \ Depth = Measured\ \ Depth \rightarrow \left[Hook\ \ Load_{On}\right]_{Mesaured} = 760\ \ kN$$
$$SWOB = 94\ \ kN$$

The different values for downhole weight on the bit should be estimated until the difference between the measured and calculated hook loads becomes negligible. When the difference is acceptable, the final estimated value for downhole weight on the bit is chosen.

$DWOB,\ \ kN$	$[Hookload]_{Calculated},\ \ kN$	$[Hookload]_{Calculated} - \left\lfloor Hookload\ \right\rfloor_{Measured} \le 1.00\ \ kN$
SWOB=94	739.5	20.50
90	742.9	17.10
85	746.9	13.10
80	751	9.00
75	745	5.00
DWOB = 70	759	1.00

Figure 6.50 compares surface and downhole weight on the bit values for a one meter drilled interval using the present invention method.

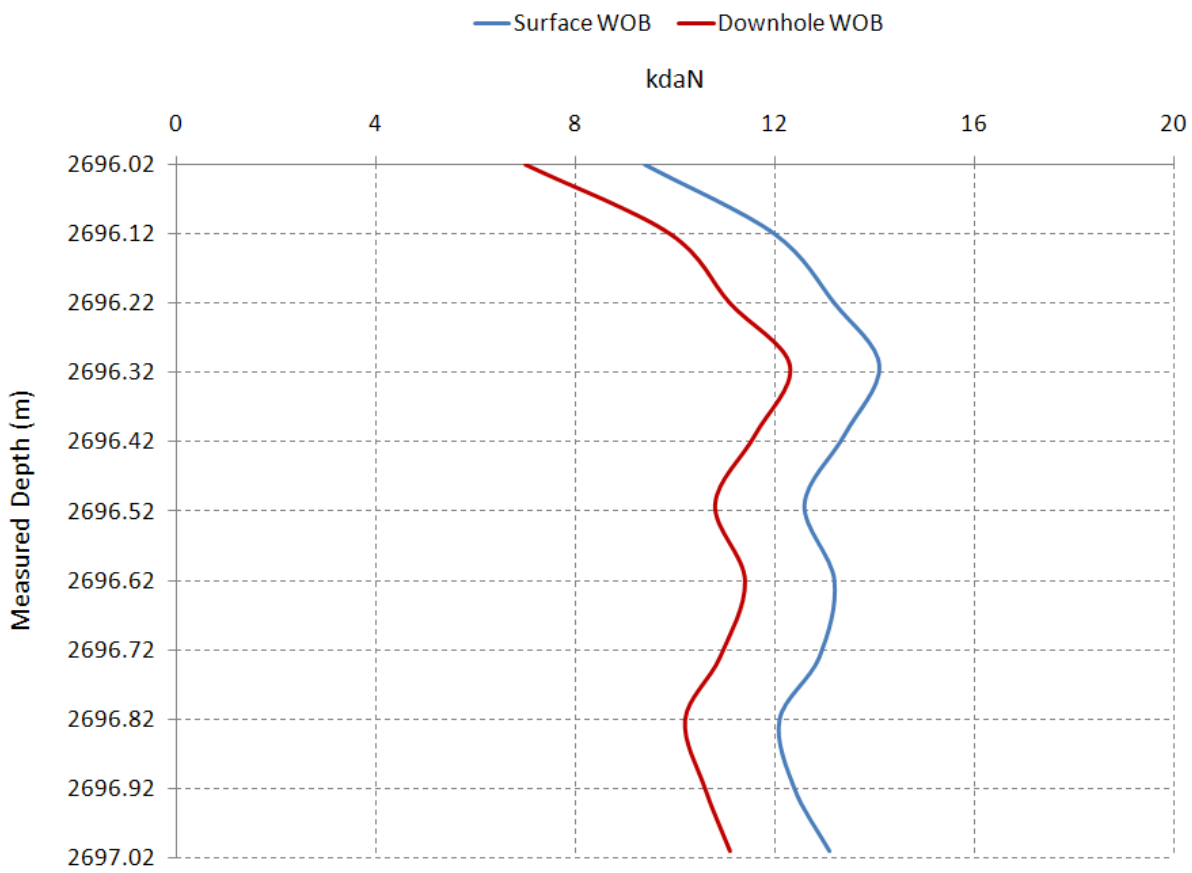

Figure 6.50 Comparison between surface and downhole weight on the bit for 1m drilled interval

For surface torque measurement, the increment in surface torque when the drill bit goes on bottom for drilling is considered bit torque. The reduction in tension has a considerable impact on the rotational friction force, which should be counted for bit torque calculations. In this field example, when the bit is off bottom and moving downwardly with the same rpm as planned for drilling, the measured surface torque is as follow:

$$Bit\ \ Depth = 2695.6\ \ m$$

$$Measured\ \ Depth = 2696.09\ \ m$$

$$Bit\ \ Depth \le Measured\ \ Depth \rightarrow \left[Surface\ Torque\ \right]_{Measured} = 13.5\ \ kN.m$$

The measured surface torque is equal to rotational friction force. By using a reliable friction model, the rotational friction coefficient can be estimated:

$$\left[Rotational\ Friction\ Force\right]_{off\ bottom} = 13.5\ kN.m \xrightarrow{Using\ Friction\ Model} \mu_{Rotational} = 0.245$$

When the drill bit is on bottom and some weight is applied to the drill bit, the surface torque measurement increases due to interaction between drill bit and rock surface. The difference between surface torque measurements for off and on bottom drilling positions, considered as surface bit torque, are shown as follow:

$$\left[SurfaceTorque_{on\ bottom}\right]_{Measured} = 14.86\ kN.m \longrightarrow SurfaceBit\ Torque = 14.86 - 13.5 = 1.36\ kN.m$$

When some weight is applied to the bit, the tension along the drill string will be reduced. The rotational friction force is reduced as well, which should be considered for bit torque measurements.

$$\left[Rotational\ Friction\ Force\right]_{on\ bottom} \xrightarrow{DWOB = 120\ kN} 12.34\ kN.m$$

The downhole torque at the bit can be estimated as follow:

$$\begin{aligned} Downhole\ Bit\ Torque &= \left[Surface\ Torque_{on\ bottom}\right]_{Measured} - \left[Rotational\ Friction\ Force\right]_{on\ bottom} \\ &= 14.86 - 12.34 = 2.52\ kN.m \end{aligned}$$

Figure 6.51 compares the surface and downhole bit torque for one meter interval by considering the effect of downhole weight on the bit on rotational friction force.

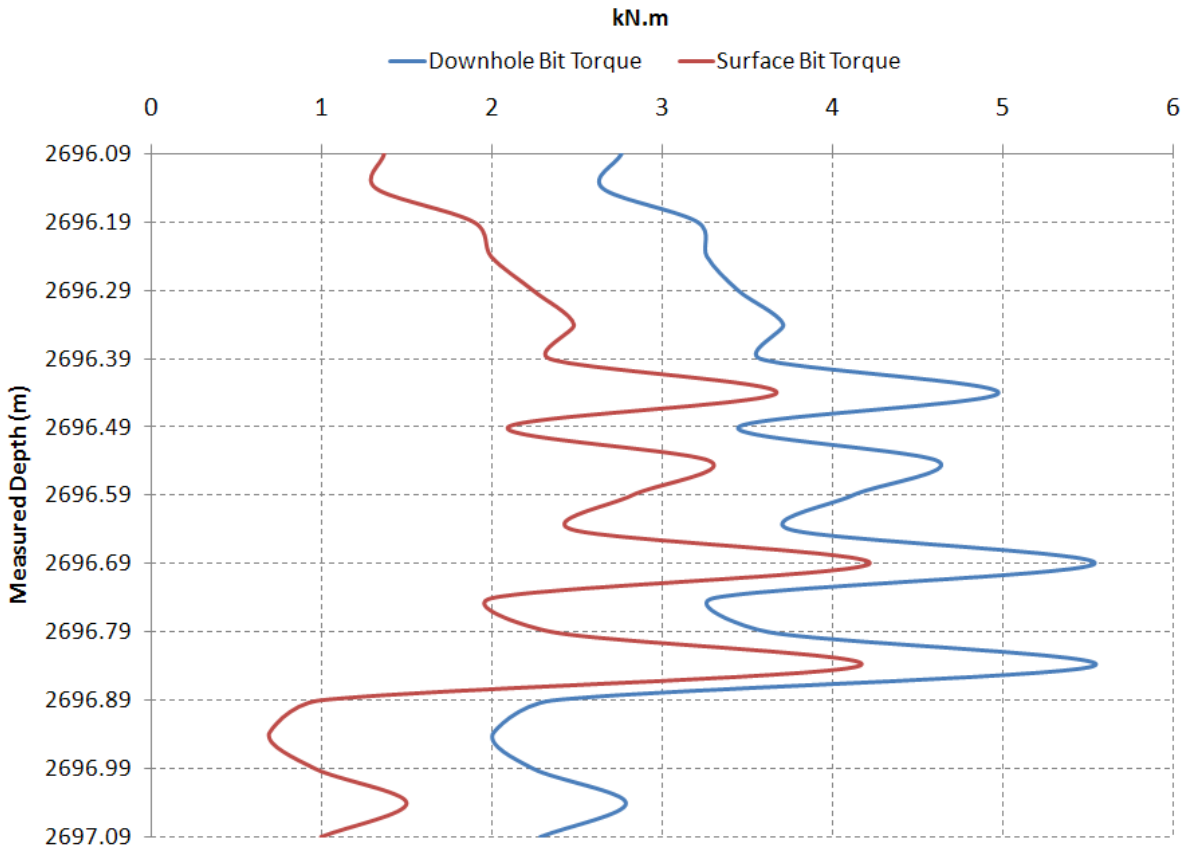

Figure 6.51: shows the surface and downhole bit torque for 1m drilled interval

6.5.7 Field Application

Figure 6.52 shows the well geometry of a field example, which verifies the application of the current method. A 350 m horizontal drilled interval was selected to estimate the downhole weight on the bit from the hook load measurements. As discussed previously, the friction coefficient should be estimated and updated during the drilling operation.

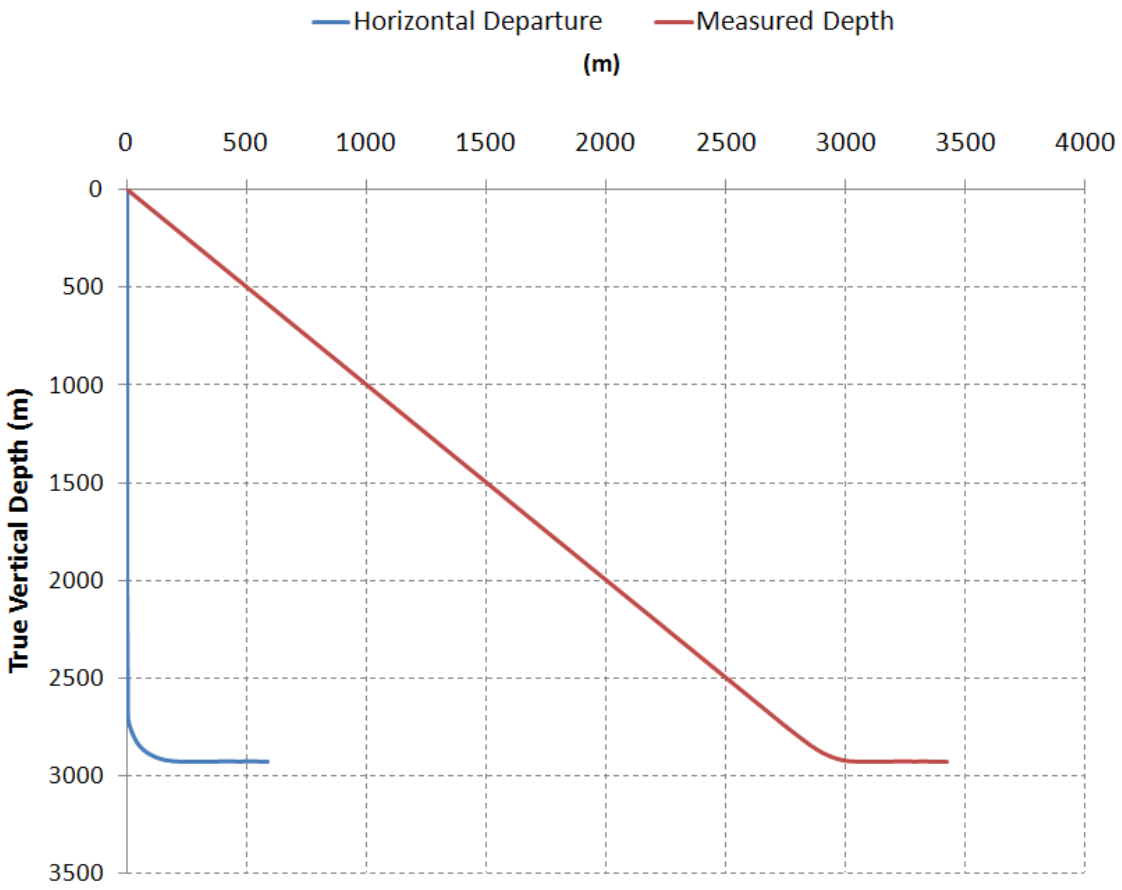

Figure 6.52: Geometry of a short bend horizontal well including vertical, build-up and horizontal sections

During drilling this 350 m horizontal interval, the drilling conditions are changed continuously. For example, the surface rotation changed from zero, sliding mode, to 30 rpm. As previously discussed, the mud rheology, cutting bed formation, and drill string positions affect the friction coefficients. Figure 6.53 illustrates the plot of friction coefficient including drill string rotation effect versus measured depth for this 350 m drilled interval used for the downhole weight on the bit estimation.

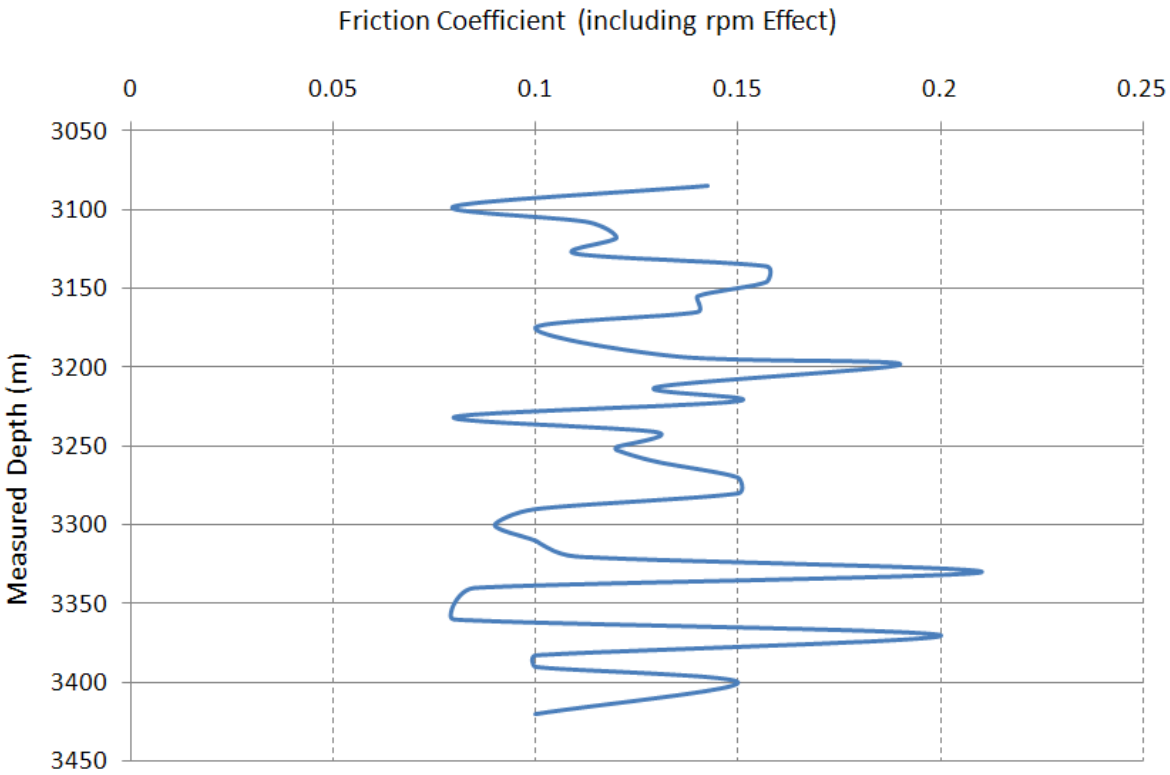

Figure 6.53: Plot of friction coefficient versus measured depth during drilling operation for the interval between 3070 m to 3420 m

Figure 6.54 compares the surface and downhole weight on bit estimated using the new designed autodriller system. It can be concluded that the effective weight on the bit is almost half of what the drilling crew thought. An autodriller system may help the drilling crew to apply the desired optimum weight on the bit to improve the drilling rate of penetration without concerns of drill string buckling and premature bit wear. Additionally, for drilling optimization that uses the offset drilling data, it is necessary to use the correct weight on the bit data as an input to this system. Using raw weight on the bit data, especially horizontal data, can show higher rock strength which would directly affect the drilling optimization output results.

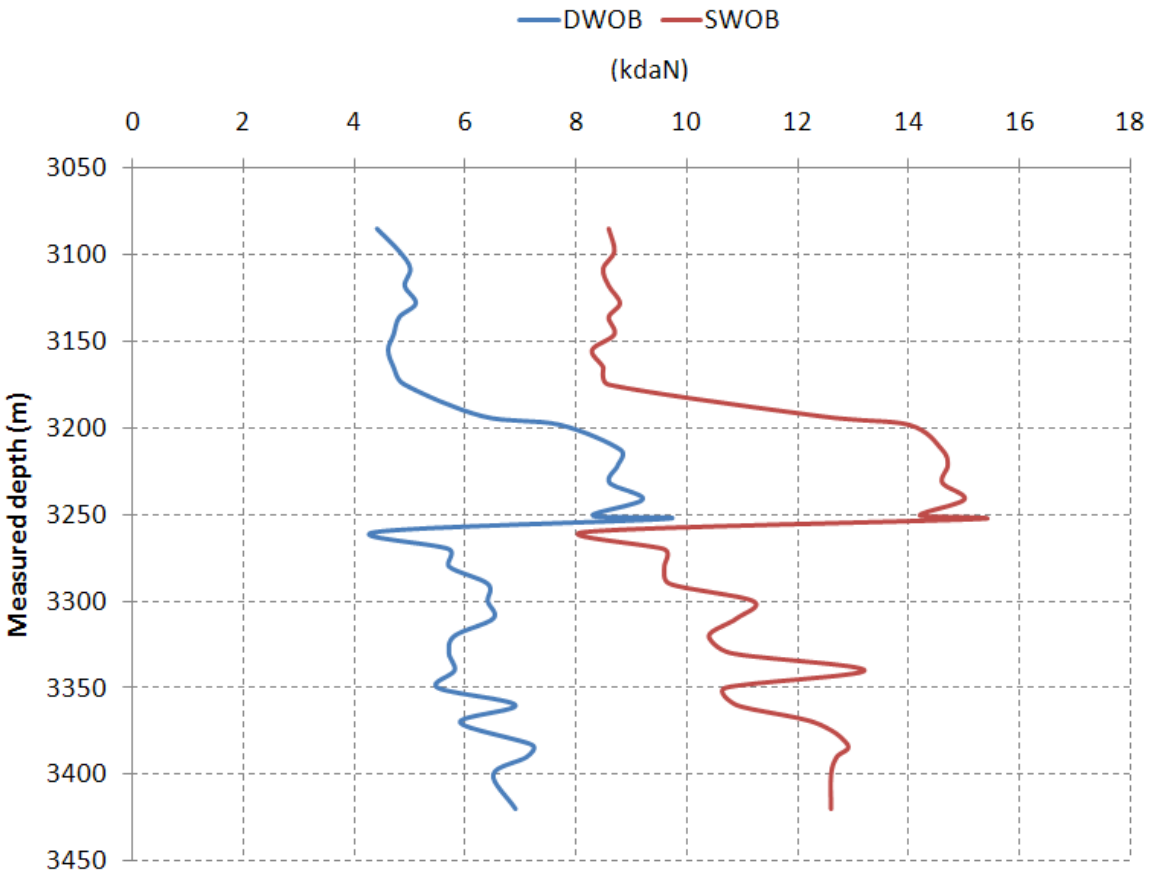

Figure 6.54: Comparison between surface and downhole WOBs for the drilled interval between 3070 m to 3420 m.

Sometimes it is desired to apply some constant weight on the bit. The autodriller system can provide this facility for the crew on the drilling rig. For this field example, by applying a constant weight on the bit as much as 10 kdaN, the autodriller estimates the value of surface weight on the bit versus measured depth (see Figure 6.55).

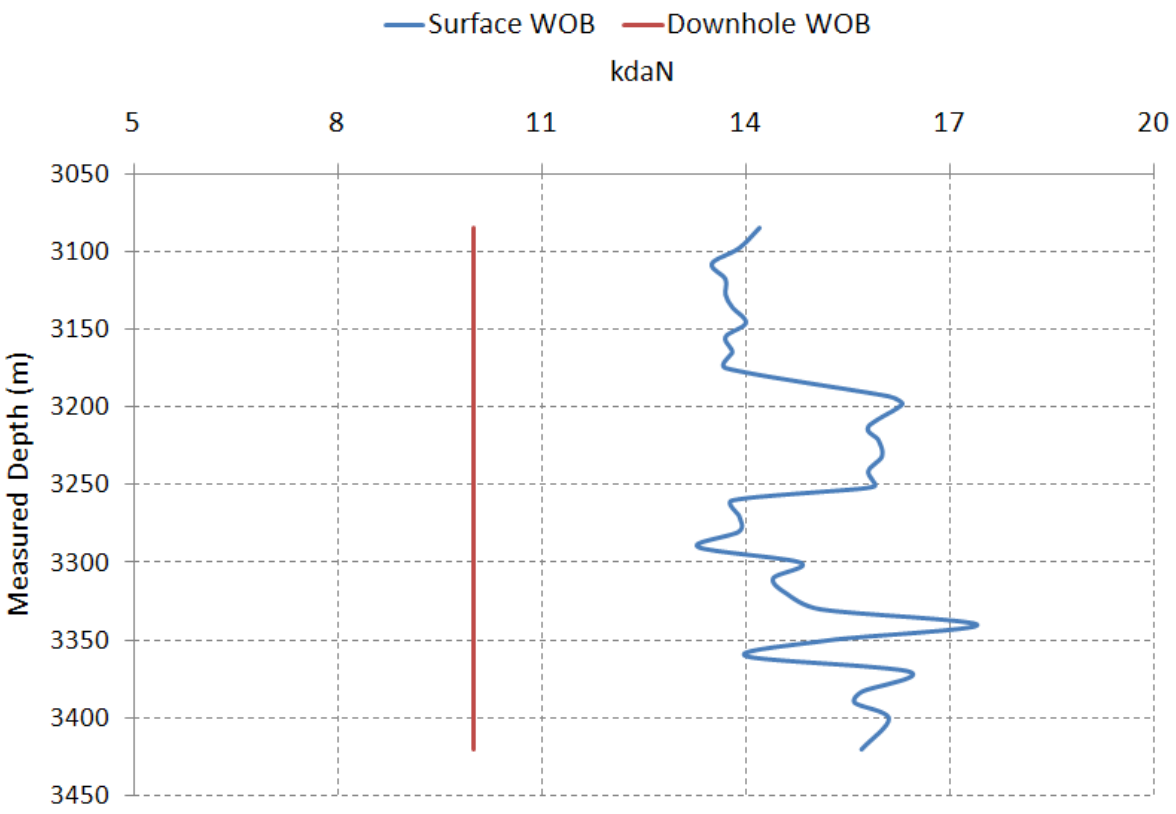

Figure 6.55: Plot of surface WOB values versus measured depth during drilling operation when keeping 10 kdaN downhole weight on the bit

This autodriller system can be also used for sliding mode drilling which is used to orient tool face in directional or horizontal drilling. The drilling bit is rotated by the mud motor instead of rotating the drill string from surface. The mud motor is powered by the fluid differential pressure. There is a certain relationship between differential pressure and downhole weight on the bit, which can be found by using the present system. Here, the "K" value is used to represent the ratio of estimated downhole weight on the bit to differential pressure which can be found during the drilling rotating time. When sliding begins, a new downhole weight on the bit can be predicted with the product of K and differential pressure. As an example, the average value for "K" is estimated during rotating time as $0.67\frac{kN}{kPa}$ for a drilled interval. The differential pressure was multiplied by "K" value to estimate the downhole weight on the bit as shown in Figure 6.56

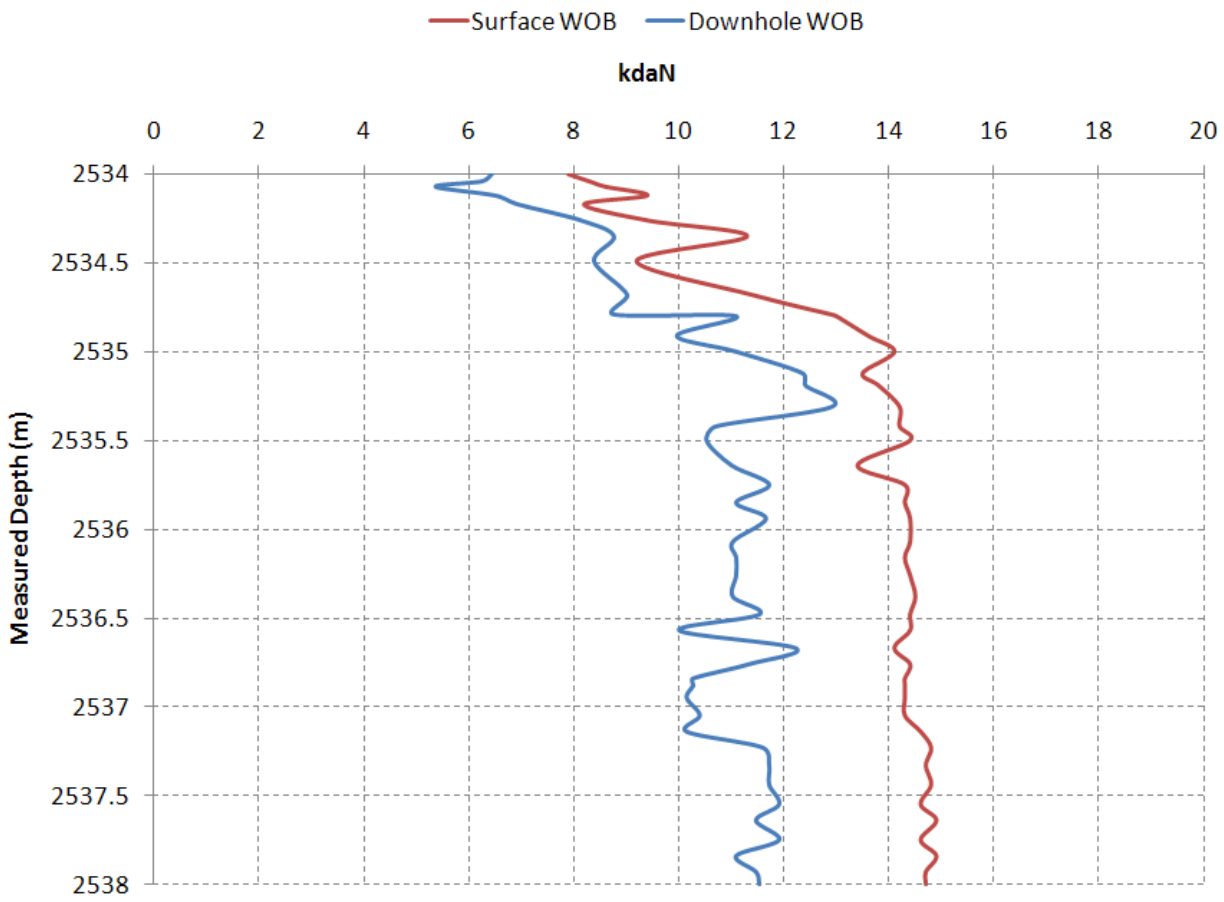

Figure 6.56: Comparison between surface and downhole weight on the bits using K value for a drilled interval from 2534m to 2538m

In all examples, the newly developed analytical model was used to calculate the axial and rotational friction between drill string and the wellbore. The model can be replaced by any other analytical and numerical models to calculate axial and rotational friction forces for downhole weight on bit and bit torque estimation.

CHAPTER SEVEN: **CONCLUSIONS AND RECOMMENDATIONS**

The two following main contributions are made as part of this thesis:

- The new models for torque and drag calculations were developed using both analytical and finite element approaches. The models are simple and practical and can be used in real time analysis. Also, all possible contributions related to torque and drag analysis were studied and the ways on how to integrate them in the modeling were proposed.

- A new method was introduced for the downhole weight on bit and bit torque estimation using torque and drag modeling. The new method uses the surface measurements such as hook load and surface torque as well as information related to drill string, well geometry and drilling fluid system.

The major conclusions that can be drawn from this thesis are summarized as follows:

- The new analytical model consists of two sets of equations for straight and curved sections. This model is three dimensional and it can consider the effects of build-up or drop-off bend combined with the side bend simultaneously.
- The new analytical model is applicable for all operations such as drilling and tripping in/out, combined motions (such as reaming and back reaming operations where the pipe is rotated and pulled or lowered at the same time).
- The hydrodynamic viscous force is considered during different operations. A procedure with a set of equations was presented for the drilling fluid model (Bingham-plastic). Ignoring this effect results in a little higher friction coefficient.
- A simple equation was presented for considering the contact surface effect. It can be multiplied with the friction coefficient and used in the modeling.
- The torque and drag analysis inside a wellbore should be carefully performed. Correct assessment of buoyancy and the effect of the well path were shown to be critical for precisely estimating the friction coefficient.
- In wellbore friction analysis, the buoyancy effect should be treated precisely. In tripping in when the drill string is partially filled with drilling fluid, ignoring this effect could result in an erroneous estimation of the overall friction coefficient.

- The friction force analysis demonstrated the difference between rotating the string and not rotating the string. Rotation not only changes the direction of friction force, it also results in a change of axial tension that may change the total friction. Proper calibration is required to determine the true value for the friction coefficient including the drill string rotation effect.
- Wellbore friction is a critical parameter not only to drill oil wells, but also during casing running and completion operations. Running the casing in long reach wells is usually one of the most critical operations.
- In real time torque and drag analysis, using the friction coefficient instead of friction force provides the possibility to exclude the effect of well geometry on the friction force.
- A finite element model was developed for the torque and drag analysis. Using the equation of motion for development of the model, the effects of drill string stiffness and vibration were considered.
- The validity of finite element model was verified analyzing examples with different complicity. The values of displacement from the finite element model matched the field data. It was shown that the result pertinent to the calculation of hook load and surface torque is convincible.
- The finite element modeling rendered a smaller friction coefficient relative to the analytical one due to the consideration of the partial contacts between the drill string and the wellbore. In the analytical modeling based on the soft string assumption, the drill string has full contact with the wellbore.
- The new method for the estimation of downhole weight on the bit was presented. The method comprised the steps of: a) determining the static weight of drill string; b) determining the axial friction coefficient including pipe rotation effect; c) determining the effect of downhole weight on the bit on value of axial friction force during drilling; d) determining downhole weight on the bit using the axial friction coefficient and surface hook load measurements.
- The new method for estimating downhole bit torque was presented. The method comprised the steps of: a) determining the rotational friction force while the drill bit is off bottom; b) determining the rotational friction coefficient including axial pipe movement effect from surface torque measurements while bit is off bottom; c) determining the effect

of downhole weight on bit on the rotational friction force during drilling; d) determining downhole bit torque using the rotational friction coefficient and downhole weight on the bit.

- The new method can be used in an autodriller as a "black box" system for the user to adjust the hook load and surface torque so that the desired downhole weight on the bit and bit torque can be obtained.
- Using the proposed new method, no downhole weight on the bit measurements is required, which can help to reduce the drilling cost.
- Using the new method, the axial friction coefficient including the drill string rotation effect can be estimated using the friction model from the best surface measured hook load. The best measured hook load is while the bit is very close to bottom moving downwardly. In this situation, the drill string rotation will be the same as the planned one for drilling a new section.
- In the new method for the downhole weight on the bit and bit torque estimation, the effect of variations in tension and compression on the friction force as well as hook load and surface torque has been considered. For example, when applying weight on the bit, the axial friction in the curved section will be reduced. This reduction cannot be recognized at the surface from surface weight on the bit.

  For the estimation of downhole weight and torque on the bit, when the weight is applied on the bit, if a drill string element in the curved section is in compression, the rotational friction force is only a function of the weight and not the tension anymore. This means the effect of tension on the rotational friction force vanishes and considerable reduction in rotational friction force occurs. If the compressive load exceeds the helical buckling load, additional friction should be estimated for this effect.

References

Aadnoy, S.A., “Friction Analysis for Long-Reach Wells”, SPE/IADC 39391 presented at SPE/IADC Drilling Conference, Dallas, Texas, March 1998.

Aadnoy, B. S., “Mechanics of Drilling”, Shaker Verlag Aachen, Germany, 2006.

Aadnoy, B.S. and Andersen, K., “Design of Oil Wells Using Analytical Friction Models”, Journal of Petroleum Science and Engineering, September 2001.

Aadnoy, B. S. and Djurhuus, J., “Theory and Application of a New Generalized Model for Torque and Drag”, SPE/IADC 114684 presented at the SPE/IADC Asia Pacific Drilling Technology Conference and Exhibition, Jakarta, Indonesia, August 2008.

Aadnoy, B.S., Fabiri, V.T. and Djurhuus, J., “Construction of Ultra-long Wells Using a Catenary Well Profile”, SPE/IADC 98890 presented at the SPE/IADC Drilling Conference, Miami, February, 2006.

Aadnoy, B.S., Fazaelizadeh, M. and Hareland, G., “A 3-Dimentional Analytical Model for Wellbore Friction”, Journal of Canadian Petroleum Technology, Volume 49, Issue 10, Page 25-36, October 2010.

Aadnoy B.S and Kaarstad, E.; “Theory and Application of Buoyancy in Wells”, IADC/SPE 101795 presented at IADC/SPE Asia Pacific Drilling Tech. Conf. and Exhibition, Bangkok, Thailand, November 2006.

Aadnoy, B. S., Larsen, K. and Berg, P.C., “Analysis of Stuck-Pipe in Deviated Boreholes”, SPE 56628 presented at the SPE Annual Technical Conf. and Exhibition, Houston, Texas, October 1999.

Aarrestad, T.V., “Effect of Steerable BHA on Drag and Torque in Wells”, SPE 20929 presented at Europec 90, The Hague, Netherlands, October 1990.

Aarrestad, T.V. and Blikra, H., “Torque and Drag- Two Factors in Extended-Reach Drilling”, Journal of Petroleum Technology, September 1994.

Anston, M.S., Hearn, P.J. and McGhee, G., “Techniques for Solving Torque and Drag Problems in Today’s Drilling Environment”, SPE 48939 presented at the Annual Technical Conference and Exhibition, New Orleans, Louisiana, September 1998.

Barakat, E. R., “An Experimental Study and Modeling of the Effect of Hydraulic Vibrations on Axial Force Transfer in Horizontal Wellbores”, Drilling Research Project for TUDRP Advisory Board Meeting, Tulsa, Oklahoma, November 14-15, 2005.

Besaisow, A. A., Jan, Y. M. and Schuh, F. J., “Development of a Surface Drill string Vibration Measurement System” SPE 14327, SPE Annual Technical Conference and Exhibition, Las Vegas, Nevada, September, 1985.

Bourgoyne, A. T. Jr., Millheim, K. K., Chenvert, M. E. and Young, F. S. Jr., “Applied Drilling Engineering”, SPE, Richardson, Texas, United States of America,1986.

Brett, J. F., Beckett, A. D., Holt, C. A. and Smith, D.L., “Uses and Limitations of Drill string Tension and Torque Models for Monitoring Hole Conditions”, SPE Drilling Engineering, September 1989.

Bueno, R.C.S. and Morooka, C.K., “Analysis Method for Contact Forces between Drill string-Well-Riser”, Society of petroleum Engineers, SPE 28723, International Petroleum Conference and Exhibition, Veracruz, Mexico, October 1994.

Burkhardt, J. E., “Wellbore Pressure Surges Produced by Pipe Movement. Society of Petroleum Engineers”, SPE 1546, Annual Conference in Denver, October 2-5, 1960.

Dangerfield, J. W., “Analysis Improves Accuracy of Weight Indicator Readings”, Oil and Gas Journal, August 10, 1987.

Dareibg, D.W and Livesay, B. J., “Longitudinal and Angular Drill string Vibration with Damping”, Journal of Engineering for Industry, Pages 1-9, 1968.

Discovery Channel Online, “Drilling in Different Direction”, Retrieved from: http://licencetodrill.ca/Articles/directional_drilling.aspx, October 01, 2011.

Dukkipati, R. V., “Matlab for Mechanical Engineers”, Tunbridge Wells: New Age Science, United States of America, 2009.

Dykstra, M. W., "Nonlinear Drill string Dynamics", Ph.D. Dissertation, The University of Tulsa, United States of America, 1996.

Eek-Olsen, J., Drevdal, K.E., Samuell, J. and Reynolds, J., "Designing Directional Drilling to Increase Total Recovery and Production Rates" SPE/IADC Drilling Conference, 27461, Dallas, Texas, February 15 – 18, 1994.

Falconer, I. G., Belaskie, J. P. and Variava, F., "Applications of a Real Time Wellbore Friction Analysis", SPE/IADC 18649 presented at the SPE/IADC Drilling Conference, New Orleans, Louisiana, February-March 1989.

Fazaelizadeh, M., Hareland, G. and Aadnoy, B. S., "Application of New 3-D Analytical Model for Directional Wellbore Friction", Journal of Modern Applied Science, February 2010.

M. Fazaelizadeh, G. Hareland, Z. Wu and M. Tahmeen; "Wellbore Friction Analysis to Detect Onset of Drill string Sticking during Extended Reach well Drilling: Case Study", Brazil Offshore Conference and Exhibition, Macae, Brazil, 14-17 June 2011.

Halliburton Online, "Measurement While Drilling" Retrieved October 07, 2011, from: http://www.halliburton.com/ps/default.aspx?navid=1754&pageid=129&prodgrpid=MSE%3a%3a1045856811401511.

He, X., Halsey, G.W., and Kyllingstad, A., "Interactions between Torque and Helical Buckling in Drilling", Annual Technical Conference and Exhibition, Dallas, Texas, October 1995.

Ho, H.S., "An Improved Modeling Program for Computing the Torque and Drag in Directional and Deep Wells", SPE 18047 presented at the Annual Technical Conference and Exhibition, Houston, Texas, October 1988.

Lesage, M., Falconer, I. G. and Wick, C. J., "Evaluating Drilling Practice in Deviated Wells with Torque and Weight Data" SPE Journal of Drilling Engineering, SPE 16114, September 1988.

Lesso, W. G., Mullens, E. and Daudey, J., "Developing a Platform Strategy and Predicting Torque Losses for Modeled Directional Wells in the Amauligak Field of the Beaufort Sea, Canada", SPE 19550, Annual Technical Conference and Exhibition, San Antonio, Texas, October 1989.

Li, Z., Liu, X., Zhou, D. and Zhang, S., "A Steady Tension-Torque Model for Drill string in Horizontal Wells", SPE 26295 presented at USMS Conference, May 1993.

Liu, X. and Samuel, R., "Catenary Well Profile for Extended and Ultra-Extended Reach Wells", SPE 124313 presented at the Annual Technical Conference and Exhibition, New Orleans, October 2009.

Luke, G. R. and Juvkam-Wold, H.C., "Determination of True Hook Load and Line Tension Under Dynamic Conditions", Journal of SPE Drilling and completion, December 1993.

Lyons, W. C., Guo, B., Graham, R. L. and Hawley G. D., "Air and Gas Drilling Manual", Third Edition, Gulf Professional Publishing is an Imprint of Elsevier, Burlington, United States of America, 2009.

Johancsik, C. A., Friesen, D. B. and Dawson, R., "Torque and Drag in Directional Wells-Prediction and Measurement", Journal of Petroleum Technology, June 1984.

Kaarstad, E., Aadnoy, B.S., "A Study of Temperature Dependent Friction in Wellbore Fluids", SPE/IADC 119768 presented at the SPE/IADC Drilling Conference and Exhibition, Amsterdam, Netherlands, March 2009.

King Fahad University of Petroleum and Minerals online, "Directional Drilling", http://faculty.kfupm.edu.sa/PET/aamajed/corses/pete%20203/directional%20drilling.pdf, Retrieved September 10, 201.

Maildla, E. E. and Wojtanowicz, A.K., "Laboratory Study of Borehole Friction Factor with a Dynamic-Filtration Apparatus", Journal of SPE Drilling Engineering, September 1990.

Maidla, E. E. and Wojtanowicz, A.K., "Field Comparison of 2-D and 3-D Methods for the Borehole Friction Evaluation in Directional Wells", Society of Petroleum Engineers, 62nd SPE Annual Technical Conference, Dallas, Texas, September 1987 (b).

Maidla, E.E., Wojtanowicz, A. K., "Field Method of Assessing Borehole Friction for Directional Well Casing", SPE 15696 presented at the Middle East Oil Show, Manama, Bahrain, March 1987 (a).

Mason, C. J., Allen, F. M., Ramirez, A. A. and Wolfson, L., "Casing Running Milestones for Extended-Reach Wells", SPE/IADC 52842 presented at the SPE/IADC Drilling Conference, Amsterdam, Netherlands, March 1999.

Mason, C. J. and Chen, D. C., "Step Changes Needed to Modernize T&D Software", SPE/IADC 104609 presented at the 2007 SPE/IADC Drilling Conference, Amsterdam, Netherlands, February 2007.

Mitchell, R., "Drill string Solutions Improve the Torque-Drag Model", SPE/IADC 112623 presented at the SPE/IADC Drilling Conference, Orlando, Florida, March 2008.

Mitchell, R.F. and Samuel, R., "How Good Is the Torque/Drag Model?" SPE Drilling and Completion, March 2009.

Newman, K. R., "Finite Element Analysis of Coiled Tubing Forces", Society of Petroleum Engineers, SPE 89502, SPE/ICoTA Coiled Tubing Conference and Exhibition, Houston, Texas, March 2004.

Newman. K.R. and Procter R., "Analysis of Hook Load Forces During Jarring", Society of Petroleum Engineers, SPE 118435, IADC/SPE Drilling Conference and Exhibition, Amsterdam, Netherlands, March 2009.

Opeyemi, A. A. and Pham, S.V., "A Robust Torque and Drag Analysis Approach for Well Planning and Drill string Design", SPE/IADC 39321 presented at SPE/IADC Drilling Conference, Dallas, Texas, March 1998.

Payne, M. L. and Abbassian, F., "Advanced Torque-and-Drag Considerations in Extended-Reach Wells", SPE Drilling and Completion, March 1997.

Paslay, P.R. and Bogy, D. B., "The Stability of a Circular Rod Laterally Constrained to be in Contact with an Inclined Circular Cylinder", Journal of Applied Mechanics. December 1964.

Rao, G., Lesso, W.G. and Sapijanskas, M., "Understanding Torque and Drag: Best Practices and Lessons Learnt from the Captain Field's Extended Reach Wells", SPE/IADC 91854 presented at the SPE/IADC Drilling Conference, Amsterdam, Netherlands, February 2005.

Reddy, J., "Solutions Manual for an Introduction to the Finite Element Method", Third Edition, McGraw-Hill, New York, 2005

Reiber, F., Vos, B. E. and Eide, S.E., "On-Line Torque and Drag: A Real – Time Drilling Performance Optimization Tool", SPE/IADC 52836 presented at the SPE/IADC Drilling Conference, Amsterdam, Netherlands, March 1999.

Samuel, R., "Formula and Calculations for Drilling Operations", Wiley – Scrivener, Houston, United States of America, 2010.

Schmalhorst, B. and Neubert, M., "Dynamic Modeling Software", American Association of Drilling Engineers Conference, AADE-03-NTCE-53, Huoston, Texas, April 2003.

Schamp, J. H., Estes, B. L. and Keller, S. R., "Torque Reduction Techniques in ERD Wells", SPE/IADC 98969 presented at the SPE/IADC Drilling Conference, Miami, Florida, February 2006.

Sheppard, M. C., Wick, C., and Burgess, T., "Designing Well Paths to Reduce Drag and Torque", SPE Drilling Engineering, 344-350, December 1987.

Soft Online, "Measurements While Drilling" Retrieved October 07, from: http://www.saftbatteries.com/MarketSegments/Oilgas/tabid/159/Language/en-US/saft/MarketSegments/Oilgas/MeasurementWhileDrilling/tabid/243/Default.aspx, 2011,

Walker, B. H. and Friedman, M. B., "Three-Dimensional Force and Deflection Analysis of a Variable Cross-Section Drill String", Journal of Pressure Vessel Technology, May 1977.

Williamson, F. Jr., "Richard Courant and the Finite Element Method: A Future Look", Historia Mathematica 7, 369-378, 1980.

Wilson, T. P. and Yalcin, O., "Two Double Azimuth-Double S-Shaped Wells Planned and Drilled Using Torque and Drag Modeling" SPE/IADC 23848 presented at the SPE/IADC Drilling Conference, New Orleans, Louisiana, February 1992.

Wu, J. and Juvkam-Wold, H.C., "Study of Helical Buckling of Pipes in Horizontal Wells" SPE25503, Production Operations Symposium, Oklahoma City, Oklahoma, 21-23 March 1993.

Wu, Z., Hareland, G. and Fazaelizadeh, M., "Torque and Drag Analysis Using Finite Element Method", Modern Applied Science, Vol. 5, No. 6, December 2011.

Yang, D., Rahman, M. K. and Chen, Y., "Bottom hole assembly Analysis by Finite Difference Differential Methods", International Journal for Numerical Methods in Engineering, Volume 74, Issue 9,1495-1517, 2008.

Zifeng, L., Xingrui, M., Wenhu, H. and Xisheng, L., "A 3-D Analysis of a Bottomhole Assembly under Large Deflection", SPE Drilling & Completion, June 1996.